Analytical and numerical studies of the dewetted bridgman process : capillarity, heat transfer and stability

Simona Epure

UNIVERSITÉ DE GRENOBLE

THÈSE EN CO-TUTELLE

Pour obtenir le grade de

DOCTEUR DE L'UNIVERSITÉ DE GRENOBLE

Spécialité : **Matériaux, Mécanique, Génie civil, Electrochimie**

Arrêté ministériel : 7 août 2006

et

L'UNIVERSITATEA DE VEST DIN TIMISOARA

Spécialité : **Mathématique appliqué**

Présentée par

Simona-Mihaela EPURE

Thèse dirigée par **Professeur Thierry DUFFAR** et
Professeur Stefan BALINT

préparée au sein du **Laboratoire SIMaP/EPM/CNRS**
dans **l'École Doctorale Ingénierie – Matériaux, Mécanique, Energétique, Environnement, Procédés, Production**

Analytical and Numerical Studies of the Dewetted Bridgman Process: Capillarity, Heat Transfer and Stability

Thèse soutenue publiquement le **« 6 Mai 2011»**,
devant le jury composé de :

M. Viorel NEGRU
Professeur à l'Universitatea de Vest din Timisoara, Président
M. Vitali TATARTCHENKO
Professeur à l'Université des aciers et des alliages de Moscou, Rapporteur
M. Horia ENE
Professeur à l'Institut de Mathématiques de l'Académie Roumaine, Rapporteur
M. Stefan BALINT
Professeur à l'Universitatea de Vest din Timisoara, Membre
M. Thierry DUFFAR
Professeur è l'Université de Grenoble, Membre

Acknowledgements

Above all, I would like to express my gratitude to all of those who helped make this thesis possible. I gratefully acknowledge the enthusiastic supervision of Prof. Thierry Duffar and Prof. Stefan Balint throughout the development of this project. Their vast knowledge and logical way of thinking have been of great value and assistance for me. Their understanding, encouraging and personal guidance have provided the keystone for the present thesis.

I warmly thank Assoc. Prof. Liliana Braescu for introducing me to the field of crystal growth research, for her valuable advice and friendly help. The extensive discussions we have had and her investigations around my work have been very helpful in undertaking this study. I wish to express my gratitude to all my colleagues from SIMaP-EPM laboratory, Grenoble, for being my surrogate family during the years that I have spent among them, and for their continued moral support thereafter. My highest regards go out to Prof. Yves Fautrelle and Mrs. Pascale Esteoule, for their unfathomable care and attention.

I also wish to thank my friends (too many to be listed here) for providing me with the support and consideration that I so much yearned for.

Finally, I am forever indebted to my family for their understanding, unending patience and supporting, when I most required them.

Simona

CONTENTS

NOMENCLATURE

$\tilde{b}$ - non-dimensional radius of the curvature at the top of the sample $\left(\tilde{b} = b/r_a\right)$;

Bo - non-dimensional Bond number $\left(Bo = \left(\rho_l \cdot g \cdot r_a^2\right)/\gamma\right)$;

c_l, c_s - specific heat in the liquid respectively solid ($J \cdot kg^{-1} \cdot K^{-1}$);

$\tilde{d}'$ - non-dimensional bottom coordinate of the ampoule with respect to the laboratory frame $z'O'r'$ $\left(\tilde{d}' = d/r_a\right)$;

D_{th}^l - thermal diffusivity in the liquid $\left(D_{th}^l = \lambda_l / c_l \rho_l\right)$;

D_{th}^s - thermal diffusivity in the solid $\left(D_{th}^s = \lambda_s / c_s \rho_s\right)$;

$\tilde{D}_{th}$ - non-dimensional thermal diffusivity $\left(\tilde{D}_{th} = D_{th}^s / D_{th}^l\right)$;

$\tilde{e}$ - non-dimensional thickness of the crystal-crucible gap $\left(\tilde{e} = e/r_a\right)$;

f - interface deflection (Chapter 3), also input oscillation frequency (Chapter 4);

g - gravitational acceleration ($m \cdot s^{-2}$);

$\tilde{G}_l$ - non-dimensional thermal gradient in the liquid;

$\tilde{G}_s$ - non-dimensional thermal gradient in the solid;

$\tilde{h}$ - non-dimensional meniscus height $\left(\tilde{h} = h/r_a\right)$;

$\tilde{H}_a$ - non-dimensional total length of the solid and melt $\left(\tilde{H}_a = H_a/r_a\right)$;

$\tilde{H}_f$ - non-dimensional furnace height $\left(\tilde{H}_f = H_f/r_a\right)$;

$\mathcal{K}$ - mean normal curvature;

i - input function (forcing term);

I - family of inputs;

$\tilde{k}$ - non-dimensional temperature gradient in the furnace $\left(\tilde{k} = k \cdot r_a / \left(\tilde{T}_m - \tilde{T}_c^f\right)\right)$;

$\tilde{l}$ - interface coordinate with respect to the body frame zOr $\left(\tilde{l} = l/r_a\right)$;;

$\tilde{L}_0$ - non-dimensional seed length $\left(\tilde{L}_0 = L_0 / r_a\right)$;

La - non-dimensional Laplace number $\left(La = \left[\left(P_c - P_h\right) \cdot r_a\right] / \gamma\right)$;

P_c - gas pressure at the cold side (Pa);

P_h - gas pressure at the hot side (Pa);

P_h^m - pressure due to the meniscus at the top (Pa);

$\Delta\tilde{P}$ - non-dimensional forcing term (total input);

Pe^l - Péclet number for the liquid $\left(Pe^l = v_a\, r_a / D_{th}^l\right)$;

r - radial coordinate (m);

$\tilde{r}_a$ - non-dimensional ampoule/ crucible radius $\left(\tilde{r}_a = r_a / r_a = 1\right)$;

$\tilde{r}_c$ - non-dimensional crystal radius $\left(\tilde{r}_c = r_c / r_a\right)$;

s - arc length (m);

St - non-dimensional Stefan number $\left(St = c_l \left(T_m - T_c^f\right) / \Lambda\right)$;

$\tilde{t}$ - non-dimensional time variable, $\left(\tilde{t} = t \cdot D_{th}^l / r_a^2\right)$;

T_h^a - temperature at the hot side of the ampoule (K);

T_c^a - temperature at the cold side of the ampoule (K);

T_c^f - cold temperature of the furnace;

T_h^f - hot temperature of the furnace (K);

$\tilde{T}_m$ - non-dimensional melting temperature $\left(\tilde{T}_m = \left(T_m - T_c^f\right) / \left(T_m - T_c^f\right) = 1\right)$;

v_a - pulling rate ($m \cdot s^{-1}$);

v_c - solid-liquid interface velocity ($m \cdot s^{-1}$);

z - coordinate with respect to the body frame zOr (m);

$\tilde{z}$ - non-dimensional coordinate with respect to the body frame zOr $\left(\tilde{z} = z / r_a\right)$;

α_e - growth angle;

Φ - heat flux;

γ - melt surface tension ($N \cdot m^{-1}$);

λ_l, λ_s - thermal conductivities of the melt and solid ($W \cdot m^{-1} \cdot K^{-1}$);

Λ - latent heat of fusion ($J \cdot kg^{-1}$);

θ_c - contact angle;

ρ_l, ρ_s - melt, respectively solid, density ($kg \cdot m^{-3}$);

ψ - angle between the tangent line to the meniscus free surface at the crystal-melt-gas triple point and the horizontal axis Or;

Subscripts

a - ampoule;

c - crystal;

g - gas;

l - liquid;

m - melting;

s - solid;

v - vapour.

CHAPTER 1: Introduction

Crystals, used as sensors, as laser radiation sources or detectors or as solar cells, are essential components of many high technology apparatuses produced in the opto and electronic industries. The quality of these apparatuses depends, in a large part, on the quality of the crystals (compositional uniformity, perfection of the shape of the crystal, smoothness of the surface, structural defects such as mechanical residual stresses, dislocations or twins).

Crystals can be obtained by different growth methods. When a crucible is used, the main problem is that during the solidification, the crystal usually sticks to the inner crucible wall because of the solid-solid interfacial energy. The crystal-crucible wall interaction leads to stresses in the crystal and to curvature of the solid-liquid interface: for a curved interface, the radial temperature gradient creates convection in the liquid which determines chemical segregation, and creates thermo-elastic stresses in the solid which determine defects, dislocations and grains. For these reasons those growth methods are preferred which does not use a crucible and allow obtaining the crystal with minimal defects. Techniques of crystal lateral surface shaping without contact with container wall are preferred: Czochralski, Floating-zone, Edge-defined film-fed growth, Dewetted Bridgman. The absence of contact between the crystallizing substance and crucible walls allows improving crystal structures and decreasing the mechanical stress level.

The II-VI compound semiconductors are technologically important as γ, X- ray and IR detectors. They are obtained typically by horizontal or vertical Bridgman crystal growth techniques. They cannot be obtained by the Czochralski or Floating-zone techniques because they cannot accept the relatively high thermal gradients involved in these processes. The classical Bridgman method involves heating a polycrystalline material above its melting point in a crucible and slowly cooling it from one colder end where an unmolten seed crystal is located (Figure 1.1(a)). Single crystal material is progressively formed along the length of the crucible. This method has the advantage of being simple on the technological point a view. The thermal gradients and the solid-liquid interface curvature can be easily adjusted by changing the temperatures at the ends of the sample. The disadvantage of this technique is that the crystal contacts the crucible wall, which generally results in increasing the mechanical stresses, impurity level, and defect density in the grown crystals. In order to manufacture high quality devices, the

semiconductors should have prescribed properties, which cannot be currently obtained with the classical Bridgman method. This disadvantage can, however, be overcome by the dewetting solidification technique.

1.1. Definition and experimental studies of Dewetting

The phenomenon of dewetting is characterized by the Bridgman growth of a crystal without contact with the crucible walls due to the existence of a liquid meniscus at the level of the solid-liquid interface which creates a gap between the grown crystal and the inner crucible walls (Figure 1.1(b)).

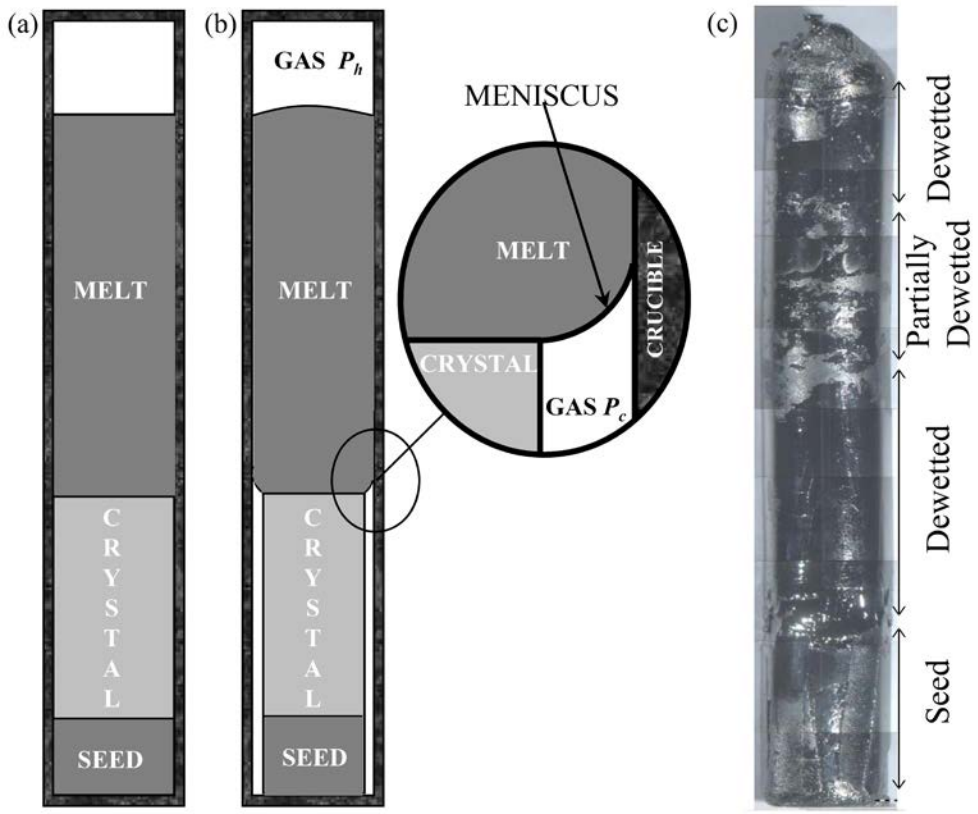

Figure 1.1 Schematic Bridgman (a), Dewetted Bridgman (b) crystal growth systems, and photograph of a *GaSb* ingot showing attached and detached regions [Sylla 2008-2] (c)

The dewetted Bridgman represents an exciting recent development for the growth of bulk single-crystals from the melt. One of the immediate consequences of this phenomenon is the

drastic improvement of the crystal quality. This improvement is essentially related to the absence of the interaction between the inner crucible wall and the grown crystal, so that no grain or twin spurious nucleation can occur (Fig. 1.2) and no differential dilatation stresses exist, which could generate dislocations (see Fig.1.3).

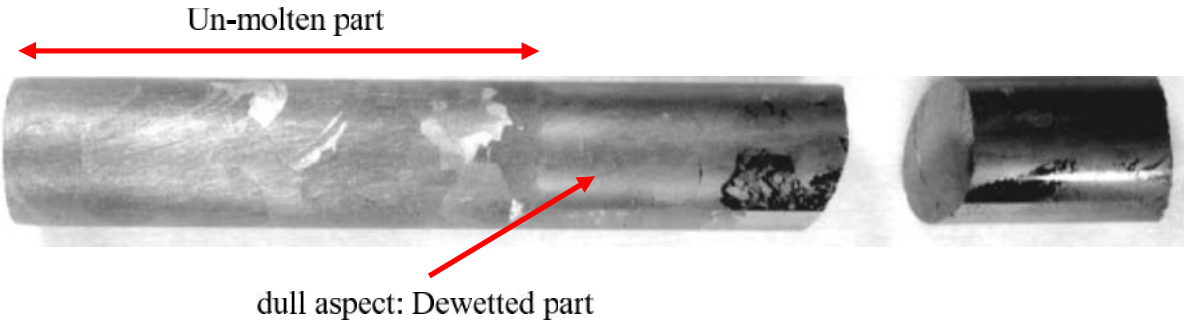

Figure 1.2 *CdTe* sample processed with improved thermal conditions [Chevalier 2004]. The cleavage plane shows that a single crystal has been grown.

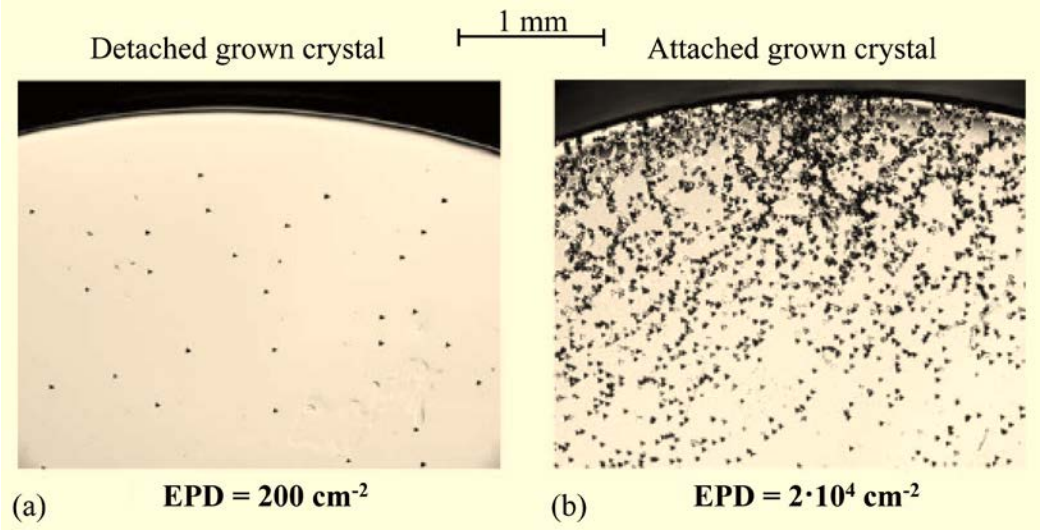

Figure 1.3 Micrograph from the (a) detached-grown Ge crystals grown in pBN crucible and (b) attached-grown Ge crystals [Schweizer 2002-1]. The Etch Pit Dislocation density (EPD) is decreased by two orders of magnitude.

This dewetting phenomenon was observed for the first time during space experiments of Bridgman solidification performed in Skylab-NASA mission-1973 [Witt 1975] and later in many experiments carried out in orbiting spacecraft on a wide variety of materials [Duffar 2004]. This

phenomenon was explained in the nineties by the Moving Meniscus Model (also called dewetting) in the case of rough crucibles [Duffar 1990] and later smooth crucibles [Duffar 1997]. This was confirmed through several experiments in Space [Duffar 1995, 1996, 1998]. Later it was proven that dewetting can be obtained on the Earth [Duffar 2000].

In the existent publications terms as “detached solidification”, “dewetted growth”, “detachment or dewetting” are used, but it must be emphasized that they refer to the same physical phenomenon that is defined and applied according to the criteria given in [Duffar 2010]:

- the material studied are pure, doped or compounds semiconductors;
- the growth procedure is based on the classical Bridgman technique;
- the existence of a narrow and constant gap (a few micrometers) along several millimeters or centimeters should be achieved;
- the crystal surface morphology is different from that of the crucible walls.

Owing to these criteria, other material (metals) or the occurence of voids, bubbles or other specific contactless morphologies, are not taken in consideration.

Dewetting in zero gravity condition

The first detailed review of the detached solidification process under microgravity condition was published in 1998, [Wilcox 1998]. The experimental results were exposed with respect to the observation of reduced contact between the grown crystal and the crucible wall, and the influence of the detachment on the crystallographic perfection and the compositional homogeneity. In 2004, Duffar also published a general review that includes the study of the crystal-crucible adhesion, the dewetting of III-V and II-VI materials, the transport and segregation phenomena under microgravity condition [Duffar 2004].

The existence of the crystal-crucible gap, when dewetting has occurred, was clearly proved after solidification process by the easy removal of the crystals from the crucible. Even a gap thickness of a few micrometers can provide this fact.

It was observed that most of the semiconductor crystals grown under microgravity conditions were characterized by the presence of microscopic irregularities, named ridges, when they grew

partially detached from rough or smooth crucibles [Witt, 1975]. After the analysis of crystals grown onboard Skylab IV [Witt, 1978] it was concluded that surface ridges appear when the crystal diameter increases and approaches the value of the internal diameter of the crucible. It is considered that the ridges result from a “partial” dewetting because in this case the detachment is local. In Figure 1.4 a typical ridge pattern on a crystal surface can be observed easily by the valleys formed on the surface that shows a local detachment. The shiny smooth surface shows places where the crystal was in contact with the crucible wall [Ostrogorsky 2009].

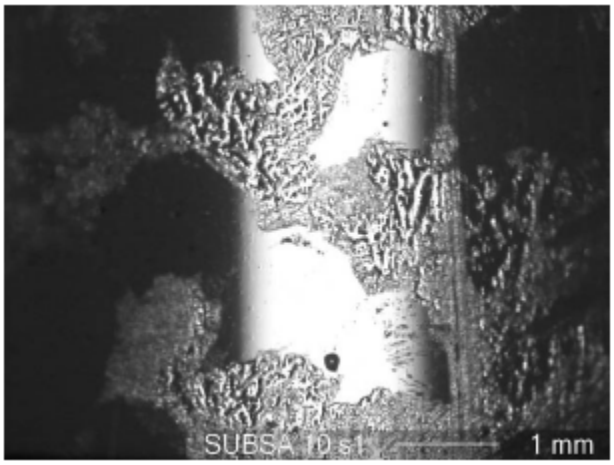

Figure 1.4 Picture of the surface of an *InSb*:*Te* ingot solidified on board the International Space Station during the SUBSA mission [Ostrogorsky 2009].

On the surface of space-grown crystals and, commonly, in non-confined growth conditions such as in the Czochralski technique, the formation of peripheral facets is also observed. Faceted free surfaces changed the crystal shape and result from anisotropy effects due to crystallography of these samples. The presence of ridges and facets is obviously an indication of contactless growth conditions.

In [Duhanian 1997] the effect of the crystal-crucible interactions leading to dewetting during the LMS-AGHF-ESA8 mission onboard Spacelab has been studied. A pseudo-binary *GaSb-InSb* semiconductor crystal was grown in a crucible made of two different parts, one from silica and the other one from boron nitride (*BN*). The crystal surface showed ridges and facets on the *BN* side. What must be emphasized here are the influence of the melt-crucible contact angle and the first quantification of a constant crystal-crucible gap value along several centimeters due

to the dewetting occurrence. The contact angle of *GaSb-InSb* melt on *BN* is higher than on silica, respectively 135° and 120° [Harter 1993]. Dewetting occurred obviously only within the *BN* crucible. Therefore, a higher value of the melt contact angle enhances the dewetting occurrence. A gap 70 µm thick was remarkably constant along 4 cm in the *BN* part. This shows that the dewetting phenomenon is self-stabilizing.

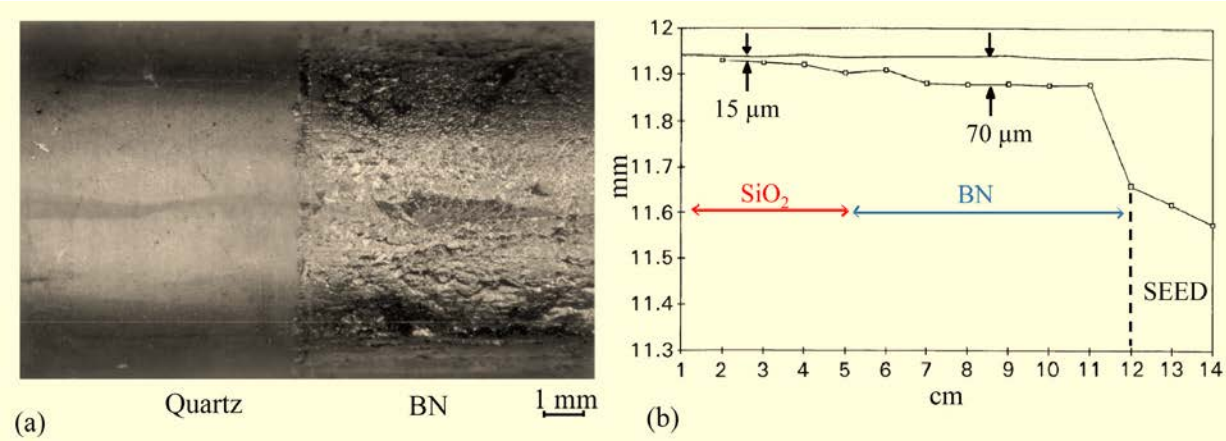

Figure 1.5 (a) Surface morphology of a *GaSb-InSb* polycrystal grown during the LMS-AGHF-ESA8 mission. (b) Corresponding measurement of the surface profile [Duhanian 1997].

In a large number of microgravity experiments, the crystal surfaces were characterized by a dark and dull layer that is assumed to be an oxide layer and therefore, the chemical pollution in the growth environment is suspected to participate to the dewetting phenomenon.

It must be emphasized that dewetting never occurred if the melt underwent an overpressure by a spring within a closed crucible. It was also shown that neither pressure difference nor the growth rate magnitudes have an effect on the dewetting phenomenon in microgravity [Duffar 2001-2].

It can be concluded that the main identified parameters that lead to the dewetting under microgravity conditions are the crucible roughness, the crucible material, the wetting properties of the melt and the chemical pollution. Apparently, the profile roughness (if any) should be sharp, the crucible material non adherent and the contact angle of the melt on the crucible high. In the case of semiconductor growth only, it is also expected that the growth angle, which is large for these materials, has an important role in the phenomenon. It is also important to underline that the dewetting is intrinsically stable, with the apparition of a constant crystal-crucible gap along several centimeters.

Dewetting in normal terrestrial gravity

The phenomenon of dewetting was later reproduced in normal terrestrial gravity [Duffar 2000, 2001] with also an improvement of the crystal quality. On the ground the dewetting has been obtained by introducing gas pressures at the hot (P_h) and cold (P_c) parts of the sample with the aim to counteract the hydrostatic pressure and detach the solid away from the crucible wall. This method reproduces artificially the effect of microgravity condition. Different methods were developed to obtain effectively the dewetting in normal gravity.

In the first method (Fig. 1.6 a) the pressure difference is applied using an accurate external controller that is connected to the two closed gas volumes at the ends of the sample. Fig. 1.6 b presents the second method that is similar to the first one; the external differential pressure system being more sophisticated and consists of differential and absolute pressure gauges with a vacuum/backfilling gas system, connected to both closed gas volumes separated by the melt. The third method (Fig. 1.6 c) aims to manipulate the thermal field inside the furnace or the closed crucible to decrease the hot pressure or increase the cold pressure. When the temperature is decreased in the hot part or increased in the cold part of the sample, the liquid is pushed away from the inner crucible wall. Controlling the pressure difference across the meniscus appeared to be a very effective way to produce the dewetting under normal gravity condition.

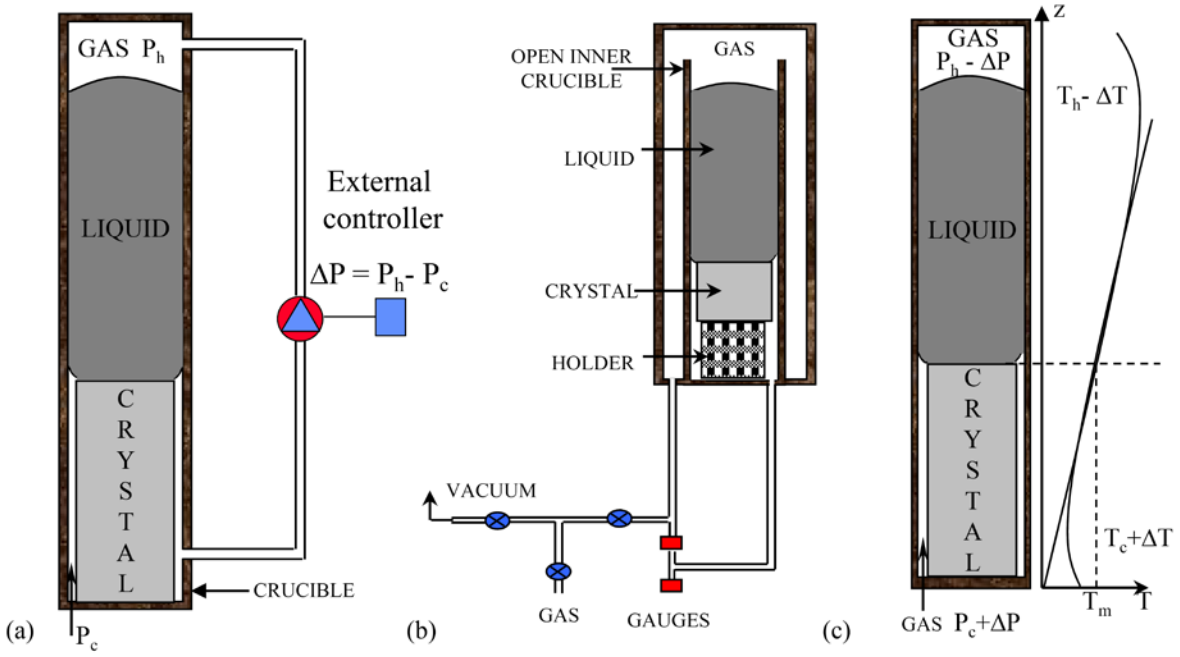

Figure 1.6 Vertical Bridgman configuration on the ground with different methods to control the pressure difference across the meniscus: (a) use of an external pressure controller [Duffar, 2000]; (b) pressure gauges with a vacuum/backfilling gas system [Palosz 2005]; (c) manipulating the thermal field inside the furnace or the closed crucible [Duffar, 2001-3].

Recent experiments performed by Sylla [Sylla 2008-2] permitted to validate a number of hypotheses, including the existence of the liquid meniscus (Fig. 1.7), at the level of the solid-liquid interface, and its control by manipulating the gas pressure in the crucible (Fig. 1.6 c) which generally leads to the apparition of a constant gap thickness between the solid crystal and the inner crucible walls.

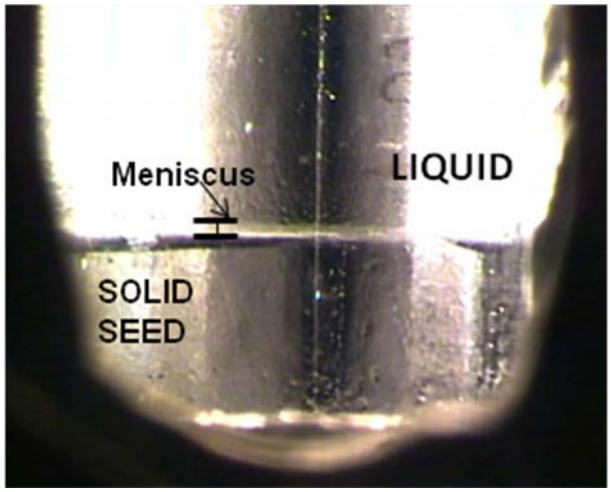

Figure 1.7 Picture of experimental meniscus taken during dewetting experiments of GaSb in silica tube [Sylla 2008-2].

One of the important characteristics of dewetting in normal gravity is the self-stabilizing gas pressure difference: it was observed that, once the process has begun, it is no more necessary to adjust the pressure difference. As the hydrostatic pressure decreases during the growth, the pressure at the bottom decreases, or the pressure at the top increases, such that the liquid meniscus remains unchanged all along the growth [Sylla 2008, Duffar 2010]. The mechanism is not totally understood yet, but some observations permitted to see gas passing upwards between the liquid and the crucible, looking like a small gas layer rather than a gas bubble [Sylla 2008, Duffar 2010]. Hence, in practice, dewetting in terrestrial condition can be controlled by

monitoring the gas pressure in the crucible, and the applied pressure difference should be of the order of the hydrostatic pressure.

Duffar and Sylla concluded in [Duffar 2010] that the main parameters identified to enhance the dewetting occurrence, under normal gravity conditions, are the following: the crucible material and the wetting properties of the melt, the value of the applied pressure difference across the meniscus, the sample and growth procedure, the growth atmosphere and polluting gases such as oxygen, growth velocity, surface morphology and the interface shape.
Sessile drop measurements [Harter 1993] have shown that the values of the contact angle of the III-V, II-VI and *Ge* materials increase respectively with the following crucible materials: SiO_2, *C*, *BN* and p-*BN*. Therefore, the experiments carried out on the ground using p-*BN* crucible material led to the dewetting. Values of the apparent contact angle, higher than 170° were measured by Kaiser [Kaiser 2001] for *Ge* on p-*BN*. Single crystals of *CdTe*, *Ge*, $Ge_{1-x}Si_x$, *GaSb* and *InSb* were grown thanks to a total dewetting.

Another critical wetting parameter is the growth angle that corresponds to the contact angle of a melt on its own solid under dynamic growth condition (see [Eustathopoulos 2010]). The growth angle, α_e, defines the point, on the meniscus line, where the meniscus joins the solid-liquid interface (see Fig. 1.8). The growth angle is a thermodynamic parameter of the material and values for semiconductors are between 7° and 30° (cf. [Eustathopoulos 2010]).

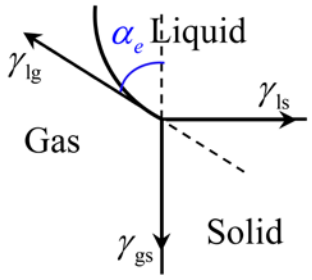

Figure 1.8 Schematic representation of the growth angle.

The growth atmosphere is a critical factor in the crystal growth process since its interaction with the solid and liquid phases influences the melt properties (wetting and growth angles) and the stoichiometry of the grown crystals. The purity of the growth atmosphere is another critical parameter. Some experiments performed under normal gravity conditions proved the involvement of oxygen activity in enhancing the dewetting process [Duffar 2000; Balikci

2004; Sylla 2008-1]. During the growth of *Ge* in graphite crucibles under various *Ar* atmosphere and gas flows ([Balikci 2004]) it was clearly reported non adhesion (or dewetting) under oxidizing conditions and attachment under high *Ar* flow rate, when oxidation was unlikely to occur.

The experiments performed by Sylla [Sylla 2008-2] showed that the presence of small or important amounts of oxygen promoted dewetting in the $GaSb$-SiO_2 system. The thermodynamic equilibrium analysis of the chemical compounds likely to exist in the quaternary *Ga-Sb-Si-O* system concluded that the gallium oxide acting as a layer on the meniscus increases the apparent contact angle and promotes dewetting.

1.2. Theoretical models of Dewetting

The different configurations leading to dewetting are presented in Figure 1.9 and their theoretical explanation has been proposed by Duffar and Sylla [Duffar 2010].

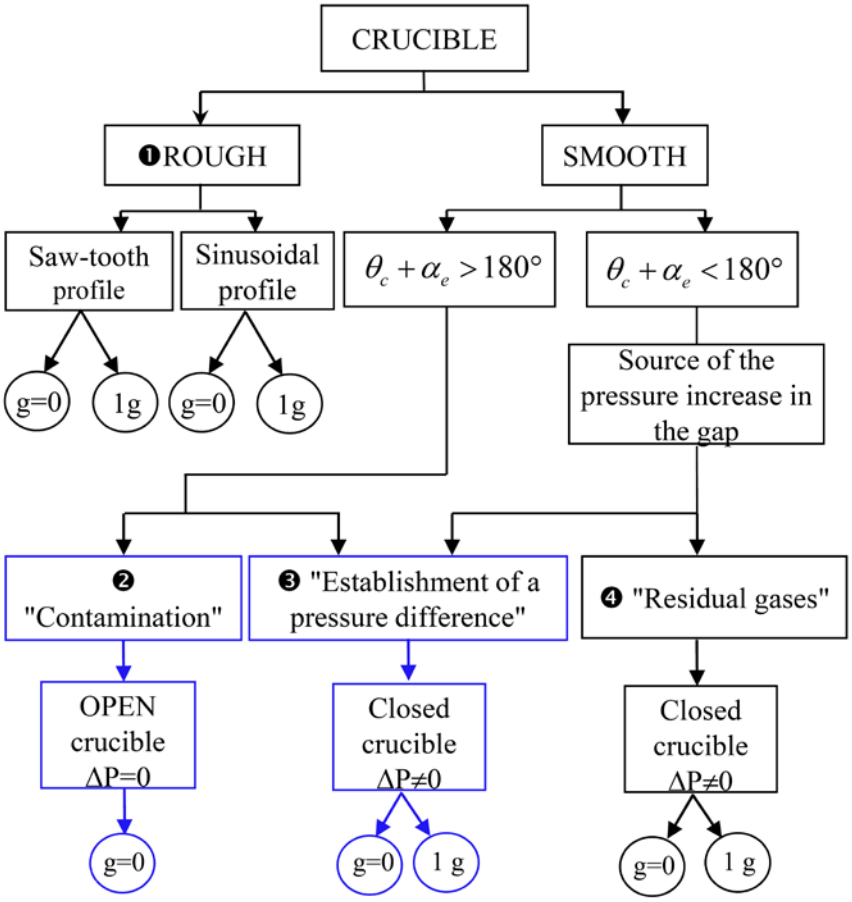

Figure 1.9 Classification of the different configurations leading to the dewetted Bridgman process.

Their classification is firstly based on the nature of the crucible that forms two groups: crucibles with a macroscopic roughness and smooth crucibles. This latter group is subdivided into two groups that are differentiated by the sum of the Young or apparent contact angle, θ_Y or θ_{app}, with the growth angle, α_e, of the semiconductor. The notations 1g and $g = 0$ refer to the presence or absence of the gravitational acceleration (i.e. experiments on the Earth or in Space). All models are based on the idea of Zemskov who postulated the existence of a liquid meniscus between the solid-liquid interface and the crucible in order to explain the decrease of crystal diameter that he observed after a space experiment [Zemskov 1983].

Model 1: Rough crucibles

In this model the explanation of dewetting involves the concepts of roughness, wetting angle and growth angle and was developed in [Duffar 1990].

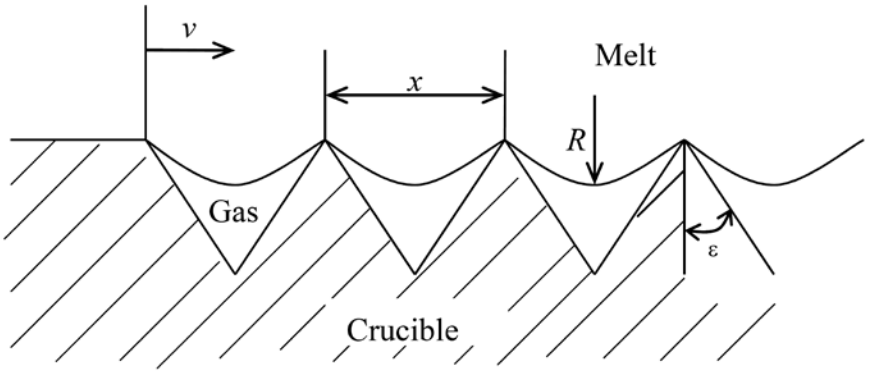

Figure 1.10 Composite wetting in the case of sharp roughness [Duffar 1990].

Dewetting can occur when the necessary condition of composite wetting is satisfied between the melt and the crucible roughness, i.e. when the cavities of the rough crucible surface are not penetrated by the melt. Figure 1.10 shows this wetting behavior where the roughness is simulated by a saw-tooth curve (sharp peaks). The radius of the liquid surface curvature, *R*, is given by the Laplace equation:

$$R = \frac{\gamma}{\Delta P}$$

where ΔP represents the pressure difference and γ is the surface tension.

In normal gravity conditions, the hydrostatic pressure gives:

$$R = \frac{\gamma}{\rho_l g H_l}$$

where ρ_l and H_l are respectively the density and the height of the liquid. As in microgravity the hydrostatic pressure is negligible, a very large radius of curvature is assumed compared to the characteristic roughness dimensions ($R>>x$) and then the liquid surface is assumed to be flat. Referring to Figure 1.10, the condition of composite wetting is satisfied by:

$$\frac{x}{R} \le -2\cos\left(\theta_c - \varepsilon\right)$$

where x is the distance separating the liquid-crucible punctual contacts.

In microgravity, due to the relative large value of R the above relation becomes:

$$\varepsilon \le \theta_c - \frac{\pi}{2}.$$

In the hypothesis of a planar front solidification and a constant growth angle between the solid and the liquid, it was found that the solidification trajectory corresponds to the equation of an infinite spiral for sharp peaks in polar coordinates under microgravity as well in normal gravity conditions.

It was concluded that, once the composite wetting conditions are satisfied, detachment of the melt takes place regardless of the growth angle value.

The theoretical predictions of the model 1 are in good agreement with the results of the space experiments TEXUS 31 and 32, Spacelab D2 and EURECA [Duffar, 1995, 1996, 1998]. This configuration was not widely used on Earth because the hydrostatic pressure forces the melt into the crucible wall cavities. Therefore it is not considered in this work.

Model 2: Contamination in a smooth crucible under microgravity

Under microgravity conditions, the melt free surface has a convex shape, viewed from the crystal side, because the melt contact angle is higher than 90°. This curvature fixes the pressure inside the liquid and the same curvature of the liquid meniscus joining the crystal-melt-gas and the

crucible-melt-gas triple lines. Because of the negligible hydrostatic pressure, the meniscus is then convex, that imposes the geometrical condition $\theta_c + \alpha_e > 180°$. From sessile drop measurements [Harter 1993] it is known that no semiconductor has a Young contact angle higher than 150° at equilibrium. Moreover, the growth angle values of semiconductor melts are between 7° and 30°. Therefore, when the equilibrium wetting parameters are considered it is impossible to satisfy the geometrical configuration $\theta_c + \alpha_e > 180°$. The concept of this second model relies on this inconsistency.

Duffar and co-authors suggested a possible effect of the chemical contamination that modifies the contact angle by increasing it artificially [Duffar 1997]. Therefore, analysing the space experimental results under microgravity conditions, they have proposed a theoretical explanation about the dewetting occurrence in smooth crucibles [Duffar 1997]. The major assumptions about model 2 are the following: i) the dewetting phenomenon results from the common formation of a constant crystal-crucible gap thickness, *e*, and a liquid meniscus joining the two triple lines (crucible-liquid-gas and crystal-liquid-gas); ii) both triple lines move at the same velocity during the contactless growth.

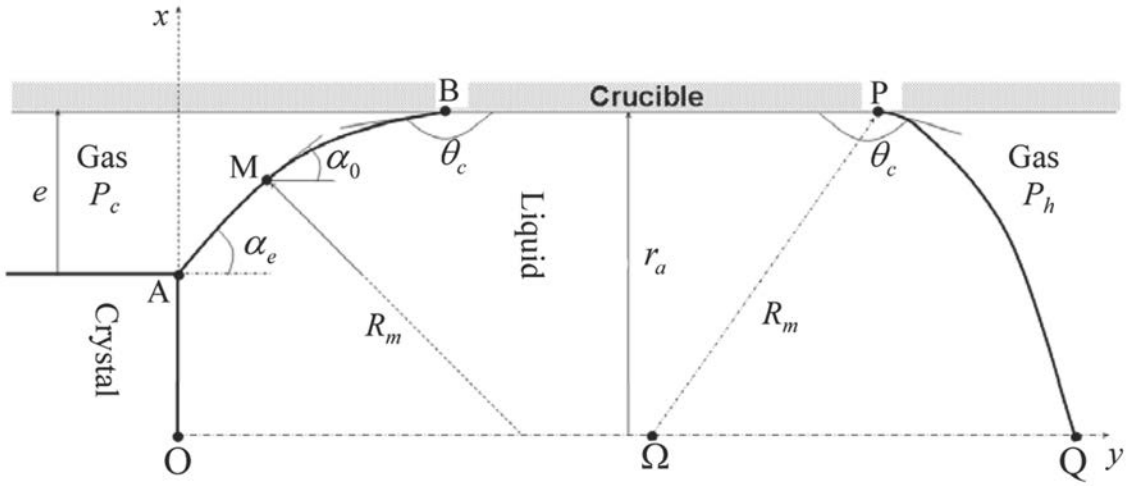

Figure 1.11 Growth configuration under microgravity condition.

This model aims to predict the crystal-crucible gap thickness *e* as a function of the different geometrical and physical parameters. In this model, both gas volumes are connected, for example the crucible is opened, such that the gas pressure at the hot side is equal to the gas

pressure at the cold side of the sample $P_h = P_c$. According to the Figure 1.11, the gap thickness is given by

$$e = r_a \left(\frac{\cos \alpha_e + \cos \theta_c}{\cos \theta_c} \right).$$

It appears that the gap thickness value is proportional to the crystal radius. Studying the variation of *e* as function of the wetting parameters θ_c and α_e for a *GaSb* crystal, the authors assumed that the dewetting of a crystal in an open crucible, in microgravity, is possible only when the contact angle is artificially increased. In order to explain the dewetting occurrence under these specific conditions, they suggested that the chemical pollution is the source of increased θ_c.

Model 3: Pressure difference in a smooth crucible

Case $g = 0$

Considering the configuration schematized in Fig. 1.11, where the gas free volumes are disconnected, i.e. $P_h \neq P_c$, where P_h is the gas pressure at the hot side and P_c the gas pressure at the cold (crystal) side, the following expression of the gap thickness [Duffar 1997] was obtained:

$$e_{1;2} = \frac{\left[r_a \left(\frac{P_h - P_c}{\gamma} \right) \right] - 2\cos\theta_c - \cos\alpha_e \pm \sqrt{2 r_a \frac{P_h - P_c}{\gamma} \left(r_a \frac{P_h - P_c}{2\gamma} - \cos\theta_c \right) + \cos^2 \alpha_e}}{\frac{P_h - P_c}{\gamma} - \frac{2\cos\theta_c}{r_a}}.$$

Studying the variation of the pressure difference $(P_h - P_c)$ for a given gap thickness in the case of an 11 mm diameter *GaSb* crystal under microgravity, the authors obtained a concave meniscus (viewed from the grown crystal side) when $\theta_c + \alpha_e < 180°$ and the gap thickness increases when the pressure P_c decreases. In the case $\theta_c + \alpha_e > 180°$ they found that the meniscus is convex (viewed from the grown crystal side) and the gap thickness increases with increasing $(P_h - P_c)$.

There was found a region of intermediate $(P_h - P_c)$ values that is characteristic of a convexo-concave meniscus. The meniscus adopts an "S" shape (Figure 1.12). The value of *e* decreases drastically with increasing $(P_h - P_c)$, for a given θ_c.

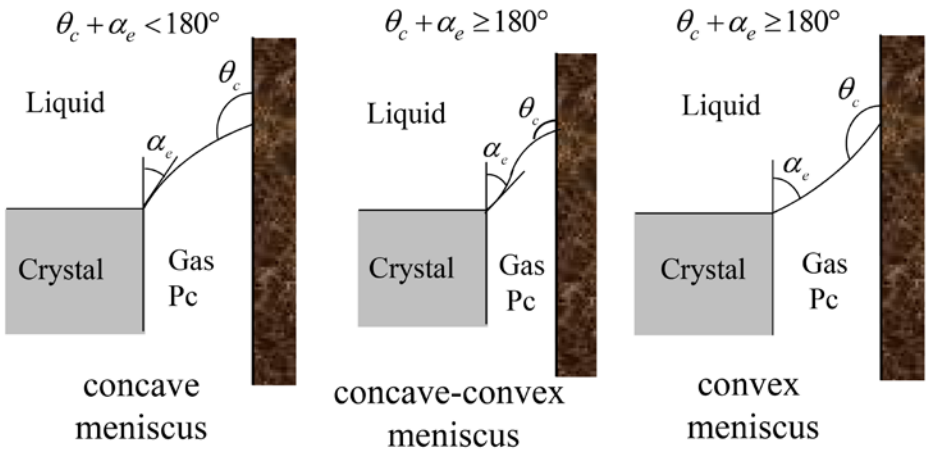

Figure 1.12 Meniscus shapes during dewetting in a smooth crucible with different values of $(P_h - P_c)$ and $\theta_c + \alpha_e$.

It was concluded that the dewetting in the case $\theta_c + \alpha_e < 180°$ imposes increasing the gas pressure at the cold side P_c (negative values of $(P_h - P_c)$) in order to obtain values of the gap thickness comparable to those measured experimentally (e<100 μm). When $\theta_c + \alpha_e > 180°$ (model 1), the pressure difference must be equal to the hydrostatic pressure or slightly larger. Therefore, when the pressure difference is not controlled, dewetting occurs more easily with a high contact angle.

Case $g \neq 0$

In normal gravity condition, different methods have been used experimentally in order to counterbalance the hydrostatic pressure and create a stable meniscus.

Duffar and co-authors [Duffar 2000] have calculated the meniscus shape by solving numerically the Laplace differential equation representative of the dewetting phenomenon on the ground. The calculations performed for *InSb* crystals showed that the absolute calculated pressure difference $(P_h - P_c)$ is very close to the value of the hydrostatic pressure.

Later, Palosz and co-authors have also used this model in order to explain the dewetting of *Ge* in SiO_2, *BN* and p-*BN* crucibles [Palosz 2005]. The experimental results are in good agreement with the model.

Model 4: Residual Gases: "Detached" Growth

Wilcox and co-workers [Wilcox 1995] have introduced another model that involves also the gas pressures as the previous model, but it further assumes that the excess pressure at the cold side is coming from the residual gases present in the crucible. Their explanation is based on the release of dissolved gas between the crucible and the sample at the level of the solid-liquid interface. This configuration has been named "detached solidification".

This model is based on physical parameters (segregation, diffusion and Henry coefficients of gases in semiconductors) that are unknown. When approximated values are used, this gives always too large crystal-crucible gap thicknesses and a dependence on the growth rate that is not in agreement with the experimental observations. This model can be applied only to closed crucibles and then cannot explain the results obtained in open crucibles, where the gas pressures are equal on both sides of the sample. Considering its specificity and weaknesses, it will not be considered in this work.

The main conclusion concerning the theoretical models is that all existing models involve a liquid meniscus joining the solid-liquid interface to a liquid-crucible triple line, with an equal velocity of both triple lines. As the liquid meniscus remained hypothetical until the experimental results obtained by Sylla [Sylla 2008-2], it is now accepted that dewetting is linked to the existence of the liquid meniscus.

On the basis of the theoretical physical models 2 and 3 it is possible to use mathematical tools in order to better understand and analyse the dewetted Bridgman process. In the literature there are two kinds of mathematical description of the dewetted Bridgman growth process:

(i). One is originated from Tatartchenko's work on shaped crystal growth process [Tatartchenko 1993], and consists in finding and analysing a simplified autonomous nonlinear system of differential equations describing the evolution of the crystal radius, crystallization-front level and possibly other process parameters (see [Duffar 1997, 2000; Bizet 2004; Fiederle 2004-1; Palosz 2005; Balint 2008-2; Braescu 2008]). The advantage of such modelling is that the number of the model variables is reduced (often two, the crystal radius and the crystallization front position) and the mathematical apparatus which treats the system of differential equations satisfied by these variables is well-developed (there are general theorems of existence, uniqueness, dependence on the

parameter and initial conditions, stability and schemes for the numerical approximation of the solutions). The drawback of this modelling is that it does not give information about the possible flows that occur in the melt, the shape of the crystallization front and the dopant repartition.

(ii). The other type of mathematical description is originated from the Bridgman growth analysis initiated by R.A. Brown [Chang 1983; Adornato 1987] and it consists in finding the numerical solution of the nonlinear system of partial differential equations including fluid-flow, heat and mass transport, and meniscus shape, in order to be able to simulate the dynamics of the dewetted Bridgman process for testing mechanical instabilities (see for example [Stelian 2009-1, 2009-2]). The advantage of this modelling is that it offers also information about the possible flows which appear in the melt, about the crystallization front shape and the dopant repartition. The major drawback of this modelling is linked to the fact that for the system of nonlinear partial differential equations and the free boundary conditions (which must be satisfied by the model variables) there are no general theorems concerning the existence, the uniqueness, the dependence on the parameter and the initial conditions, the stability of the solution. For this reason the legitimacy of the numerical results, obtained by different numerical schemes used for solving these problems, becomes questionable.

In this thesis both approaches and other mathematical tools will be used.

1.3. Stability analysis of Dewetted Bridgman: state of the art

As it was already explained in the previous section, the occurrence of the dewetting phenomenon is due to the existence of a liquid meniscus at the level of the solid-liquid interface. If there exists a meniscus such that its total free energy is minimum, then the meniscus is called statically stable (i.e., the meniscus is kept in equilibrium for any small perturbations occurring in the system [Braescu 2010-1]).

Dynamic stability is one of the most important parameters necessary for a successful and easy growth. Stability is necessary to achieve consistency, repeatability and uniformity - the keys to successful crystal growth in the laboratory and in industrial production.

It must be emphasized here that the dewetted growth process is stable only when both, static stability and dynamic stability are verified.

Recently, in [Braescu 2009-1, 2010-1] static stability of the menisci was investigated for crystals grown by dewetted Bridgman method in uncoated crucibles, and coated crucibles or pollution, via the conjugate point criterion of the calculus of variations. The main conclusion of this work consists in gap thickness limitations for which the menisci are statically stable. The mathematical and numerical investigations developed for *InSb* crystals grown in terrestrial conditions in uncoated crucible, showed that concave menisci (seen from the gas side) are statically stable and, for *Ge* crystals grown in pBN sleeve, globally convex and concave-convex menisci are statically stable.

The existing dynamic stability analysis of dewetting, as for all other capillary-based growth processes, is based on Tatartchenko's work [Tatartchenko 1993]. The objective of the analysis is to establish the necessary operating conditions in order to get a stable dewetting, i.e. a stable crystal diameter, or gap thickness when small perturbations occur during the solidification process.

A first study of the stability of dewetted Bridgman process under zero gravity conditions was based on simple geometrical assumptions and only the capillary effects were taken into account [Duffar 1997]. A very important hypothesis in this study was that the growth angle is a constant fixed by thermodynamic and then, the only point to take into account is the concavity or the convexity of the meniscus at the triple line with the solid-liquid interface.
In the same publication, the effect of pressure fluctuations on growth stability has also been studied under microgravity conditions. The authors have first considered the simple case where the pressure fluctuations are related to fluctuations of the gas volume by the ideal gas law. It follows that such fluctuations are not likely to destabilize a stable dewetting, however the analysis is simplified and further studies are necessary to ascertain this point.

A contribution to the stability analysis of the dewetting process [Bizet 2004] has been developed by taking into account both geometrical and thermal effects. This study was done also using the Lyapunov's method in the case of an open smooth crucible configuration under microgravity conditions, with the hypothesis that the liquid-crucible triple line of the meniscus is anchored by some hysteresis wetting. The study is restricted to the cases where an analytical

solution exists under various thermal boundary conditions. It has been shown that in the case of a sample without lateral thermal exchange the system is always stable on the geometrical and heat transfer point of view. In the approximation of a solid laterally insulated from its surrounding (for example by the gap caused by dewetting from the crucible) it was shown that thermal exchange through the liquid lateral surface does not change significantly the conclusion: if the liquid is long enough (semi-infinite) the system is always stable and if the liquid is of finite length with an imposed temperature at the top, stable solutions may exist.

Following this analysis, it appears that under microgravity conditions, there is only one variable parameter, the gap thickness, because the heat transfer cannot change the pressure in the meniscus (or only very marginally through modification of capillary parameters: melt surface tension, γ, and contact angle, θ_c) and then has no effect on the meniscus shape and then on the gap. Therefore only one equation is needed, which is Young-Laplace's equation.

Later, in [Duffar 2000] the capillary stability problem in normal gravity conditions was partly studied numerically, by solving Young-Laplace's equation when changing the parameters of the problem. The principle is identical to that used for microgravity conditions and based on Lyapunov's method giving the stability criterion on the sign of the meniscus curvature. The calculations obtained by the authors allowed plotting a diagram giving the pressure difference values as a function of the crucible radius, that furthermore fulfill the capillarity stability criteria of the meniscus (Fig.1.13). In the case of an *InSb* crystal, the absolute calculated pressure difference $\left(P_h - P_c\right)$ is very close to the value of the hydrostatic pressure.

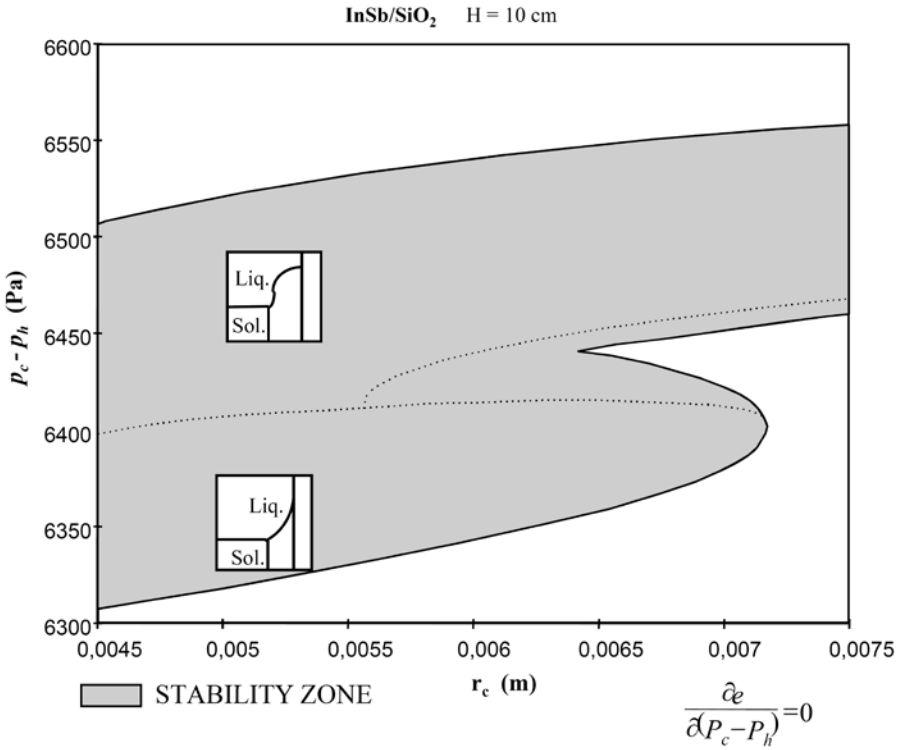

Figure 1.13 Stability diagram for the growth of InSb crystals in a silica crucible [Duffar 2000].

However the capillary stability presented here is only a particular case of the dynamic stability and further studies are needed in order to fully solve the stability problem in dewetting, especially on the Earth where it is of practical interest, and find, for all configurations, which are the stable conditions for dewetting phenomenon.

1.4. Objectives and organization of the thesis

The experimental observations under microgravity conditions have shown that the dewetting phenomenon is intrinsically stable with the formation of a constant crystal-crucible gap along several centimetres due to the existence of a moving liquid meniscus linking the crucible-melt-gas and crystal-melt-gas triple points. The main identified parameters that lead to this phenomenon are the crucible material, the crucible roughness, the wetting properties of the melt and the chemical pollution.

Also, the experiments performed under normal gravity conditions confirmed the existence of the liquid meniscus and its control by manipulating the gas pressure in the crucible

which generally leads to the apparition of a constant gap thickness between the grown crystal and the inner crucible walls.

As one of the immediate consequences of the dewetting phenomenon is the drastic improvement of the crystal quality, by this thesis work we want to give answers to the following questions:

- What is the crystal-crucible gap thickness, therefore the crystal radius?
- What is the shape of the liquid meniscus? This shape being related to the stability of the process.
- What is the influence of each process parameter on the stability of the growth process?
- What are the optimal process parameters able to control the crystal diameter?

Therefore, in order to bring crucial information concerning dewetted phenomenon, detailed theoretical results and numerical simulations are necessary, on the basis of the mathematical models able to reflect better the real phenomena which should include all essential processes appearing during the growth. The phenomenon complexity (which implies mathematical, computational, physical and chemical knowledge) emphases the needs of more theoretical explanations, careful comparisons between the theoretical and computational information with results extracted from experiments, and following feedback of the experimental data to identify the experimental set-up in terrestrial condition and the optimal process parameters. Moreover, the theoretical studies are essential into more exploitation of the experiments performed under microgravity conditions.

The main problem of the dewetting growth and the related improvements of the material quality is the stability of the growth process. Even if extensive work on the stability of the phenomenon was done by Duffar *et al*. and Wilcox *et al*., further work must be done in the important area of theoretical study of perturbation effect on the stability.

In this context, the main purpose of the present work is to perform analytical and numerical studies for capillarity, heat transfer and stability problems of the dewetted Bridgman process. For the calculation of the meniscus shape, its surface $z = z(x, y)$ will be given by the Young-Laplace equation describing the equilibrium under pressure. This equation will be transformed in a nonlinear system of differential equations. From qualitative and numerical

studies of the solution, the dependence of the meniscus shape (convex, concave, convex-concave) on the pressure difference and other parameters of the process will be determined. For studying the dynamic stability of the system, the crystal-crucible gap thickness and the solid-liquid interface position are variables of the problem and hence two equations will be needed, namely the Young-Laplace equation and the heat balance at the solid-liquid interface.
Therefore, the present work is organized as follows:

Recent contributions to the modelling of some capillarity problems are presented in the second chapter, starting with the mathematical formulation of the capillary problem governed by the Young-Laplace equation. Analytical and numerical studies for the meniscus equation are developed for the cases of zero and normal terrestrial gravity.

The third chapter deals with contributions to the modeling of heat transfer problems. Thus, analytical and numerical studies for the non-stationary one-dimensional heat transfer equation are performed in order to find analytical expressions of the temperature distribution and the temperature gradients in the melt and in the solid. The melt-solid interface displacement equation is also derived from the thermal energy balance at the level of the interface.

Further, the effect of the crystal-crucible gap on the curvature of the solid-liquid interface is studied for a set of non-dimensional parameters representative of classical semiconductor crystal growth. An analytical expression for the interface deflection, based on simple heat flux arguments is reported. In order to check the accuracy of the obtained analytical formula and to identify its limits of validity, the heat transfer equation is solved numerically in a 2D axial symmetry, stationary case, using the finite elements code COMSOL Multiphysics 3.3.

The last chapter is fully dedicated to the stability analysis. First, different concepts of Lyapunov stability which can occur in shaped crystal growth: classical, uniform, asymptotic, and exponential Lyapunov stabilities of a steady-state; partial Lyapunov stability of a steady-state; and the same types of Lyapunov stabilities for time-dependent regimes, are presented. In what follows, after the introduction of the concept of practical stability over a bounded time period, analytical and numerical investigations of the practical stability over a bounded time period of the nonlinear system of differential equations describing the melt-solid interface displacement and the gap thickness evolution for dewetted Bridgman crystals grown in terrestrial conditions are developed.

Finally, the general conclusions and perspectives of this work are exposed.

All the numerical computations will be made for the case of the semiconductors *InSb* or *GaSb* whose thermophysical properties are given in Table 1.1.

	Material	
Thermophysical properties	***InSb***	***GaSb***
Melting point T_m (K)	800	979
Latent heat of solidification Λ ($J \cdot kg^{-1}$)	$2.01 \cdot 10^5$	$3.14 \cdot 10^5$
Thermal conductivity in liquid λ_l ($W \cdot m^{-1} \cdot K^{-1}$)	9.23	10.24
Thermal conductivity in solid λ_s ($W \cdot m^{-1} \cdot K^{-1}$)	4.57	6.43
Specific heat in the liquid c_l ($J \cdot kg^{-1} \cdot K^{-1}$)	263	330
Specific heat in the solid c_s ($J \cdot kg^{-1} \cdot K^{-1}$)	260	304
Density of the liquid ρ_l ($kg \cdot m^{-3}$)	$6.47 \cdot 10^3$	$6.06 \cdot 10^3$
Density of the solid ρ_s ($kg \cdot m^{-3}$)	$5.76 \cdot 10^3$	$5.60 \cdot 10^3$
Surface tension γ ($N \cdot m^{-1}$)	0.42	0.45
Young contact angle θ_c on SiO_2 (degrees)	112	121
Young contact angle θ_c on BN (degrees)	134	132
Growth angle α_e (degrees)	25	31
Length of the liquid and solid H_a (m)	$8 \cdot 10^{-2}$	
Seed length L_0	$2 \cdot 10^{-2}$	
SiO_2 Ampoule radius r_a (m)	$5.5 \cdot 10^{-3}$	

Table 1.1 Thermophysical properties of *InSb* and *GaSb* and other input parameters used in all numerical simulations of this thesis

CHAPTER 2: Modeling of capillarity problems in dewetted Bridgman process

In the first chapter it has been explained that the dewetted Bridgman process is one of the crystal growth processes based on capillarity. Acting on the small liquid meniscus that joins the liquid surface in the crucible to the solid crystal side, capillarity has an important role in the problem of crystal diameter control.

Therefore, the first section of this chapter deals with a mathematical formulation of the capillarity problem governed by the Young-Laplace equation that relates the pressure inside and outside the liquid to the normal curvature of the liquid surface, called meniscus, and then allows computing the shape of liquid menisci involved in the crystal growth processes. Young-Laplace's equation is expressed using the principal normal curvatures of a surface in order to avoid the discussions concerning the sign that are required when the problem is expressed using the radius of curvature.

Once the mathematical formulation of the capillary problem is established, analytical and numerical studies for the meniscus surface equation are performed in the second section, for the case of dewetted Bridgman process in zero and normal gravity. In zero gravity, the analytical study leads to the formulas of the non-dimensional crystal-crucible gap thickness which are in agreement with those reported in dimensional form in [Duffar 1997]. The case of normal gravity involves qualitative studies for the meniscus shape using Taylor polynomial approximation, similar to those presented in [Balint 2008] and [Braescu 2008], and without approximation as in [Braescu 2009-2].

In the last section of this chapter a parametric study is presented in order to show the dependence of the crystal-crucible gap thickness on the relevant parameters of the dewetted Bridgman process (results published in [Epure 2010-2]).

2.1. Mathematical formulation of the capillarity problem: Young-Laplace's equation

Historically, the shape of a liquid meniscus was among the first phenomena studied in capillarity [Hauksbee 1709]. The first formal law concerning the free surface of the meniscus was given by Laplace [Laplace 1806], in terms of the *mean normal curvature* $\mathcal{H}$ defined as the average of the

principal normal curvatures [Young 1805]. In what follows, the mean normal curvature is presented with the notation of [Finn 1986] and the Young-Laplace equation is given in 3D and 2D axi-symmetric cases.

2.1.1. Mean normal curvature

In the case of a smooth surface *S*, it is known that through a point *M* of *S*, there exists a tangent plane, π_1, and a normal line, N_M (i.e. a perpendicular line to the plane π_1). On the normal line N_M there are two vectors, $\overline{n}_1$, $\overline{n}_2$, also known as versors, having their origin at the point *M* and opposite orientations (see Fig. 2.1), called unit normal vectors.

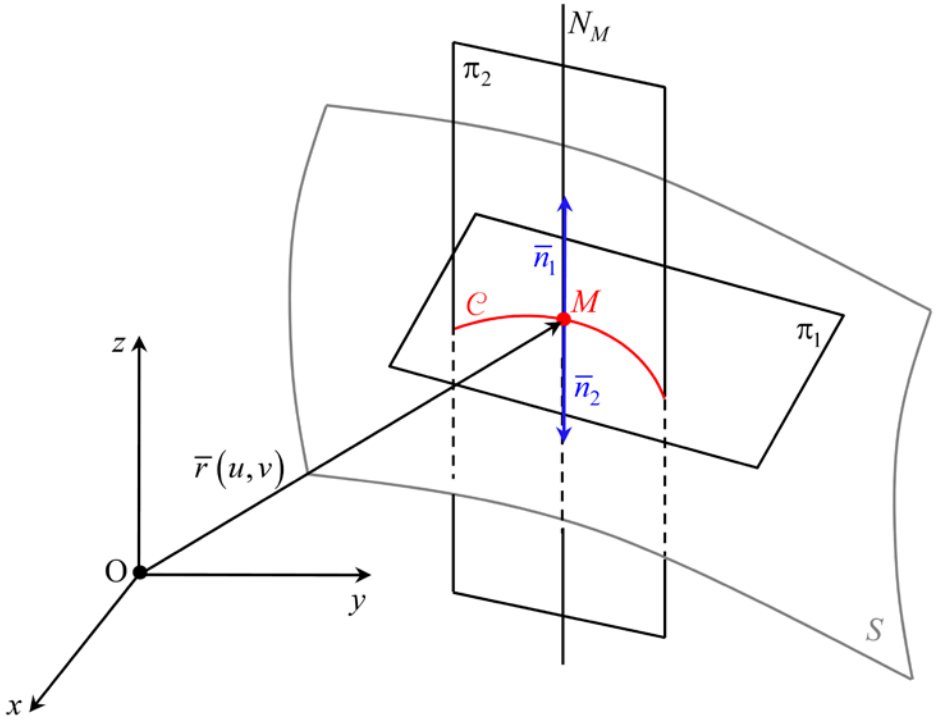

Figure 2.1 Normal section to *S* at the point *M* and the versors $\overline{n}_1$, $\overline{n}_2$.

If (u,v) are coordinates in a parametric space D and (*x*, *y*, *z*) represents the coordinates in $\mathbb{R}^3$, then a regular parametrization of the surface *S* is a C^3- class one-to-one function $\overline{r}: D \to S \subset \mathbb{R}^3$, $\overline{r} = \overline{r}(u,v)$ so that $\overline{r}_u \times \overline{r}_v \neq 0$ for some open set $D \subset \mathbb{R}^2$, where $\overline{r}_u = \dfrac{\partial \overline{r}}{\partial u}$ and

$\overline{r}_v = \dfrac{\partial \overline{r}}{\partial v}$. At the point $M = \overline{r}(u_0, v_0)$, the tangent plane of *S* is spanned by $\overline{r}_u$ and $\overline{r}_v$ (evaluated in (u_0, v_0)) i.e. $\overline{w} = \alpha \cdot \overline{r}_u + \beta \cdot \overline{r}_v$, $\alpha, \beta \in \mathbb{R}$.

For the given regular parametrization $\overline{r}$, it is known that the cross-product (called also vector product) $\overline{r}_u \times \overline{r}_v$ is a normal vector to the tangent plane. Dividing this vector by its length yields to one of the unit normal vector (versor) of the parametrized surface:

$$\overline{n} = \frac{\overline{r}_u \times \overline{r}_v}{\left\| \overline{r}_u \times \overline{r}_v \right\|} \tag{2.1}$$

The second normal vector orthogonal to the tangent plane of *S* at *M*, is $-\overline{n}$. Referring to Fig. 2.1, the versors $\overline{n}_1$, $\overline{n}_2$ are:

$$\overline{n}_1 = \frac{\overline{r}_u \times \overline{r}_v}{\left\| \overline{r}_u \times \overline{r}_v \right\|} \text{ and } \overline{n}_2 = -\frac{\overline{r}_u \times \overline{r}_v}{\left\| \overline{r}_u \times \overline{r}_v \right\|}. \tag{2.2}$$

If $\overline{r}(s) = \overline{r}(u(s), v(s))$ (*s* - the arc length) is a curve, $\mathcal{C}$, on the parametrized surface *S* with $\overline{r}(s_0) = \overline{r}(u_0, v_0) = M$, then the tangent vector to $\mathcal{C}$ at *M* is the corresponding linear combination $\overline{w}(s_0) = \dot{u}(s_0) \cdot \overline{r}_u(u(s_0), v(s_0)) + \dot{v}(s_0) \cdot \overline{r}_v(u(s_0), v(s_0))$.

Considering the curve $\mathcal{C}$ of the intersection of *S* with the plane π_2, containing the normal line N_M through the point *M* of *S*, the curvature of $\mathcal{C}$ with respect to $\overline{n}_1$ is defined by

$$k(\overline{n}_1, \mathcal{C}, M) = -\frac{d\overline{r}}{ds} \cdot \frac{d\overline{n}_1}{ds} \tag{2.3}$$

where $\overline{n}_1(s) = \overline{n}_1(u(s), v(s))$. Because $\overline{n}_2 = -\overline{n}_1$, the normal curvature with respect to $\overline{n}_2$ of the curve $\mathcal{C}$ at the point M verifies the relation $k(\overline{n}_2, \mathcal{C}, M) = -k(\overline{n}_1, \mathcal{C}, M)$ (see [Finn 1986]).

Introducing the following notations:

$$\dot{u} = \frac{du}{ds},\ \dot{v} = \frac{du}{ds},\ E_{\text{II}} = -\frac{\partial \overline{r}}{\partial u} \cdot \frac{\partial \overline{n}_1}{\partial u},\ 2F_{\text{II}} = -\left(\frac{\partial \overline{r}}{\partial u} \cdot \frac{\partial \overline{n}_1}{\partial v} + \frac{\partial \overline{r}}{\partial v} \cdot \frac{\partial \overline{n}_1}{\partial u} \right),\ G_{\text{II}} = -\frac{\partial \overline{r}}{\partial v} \cdot \frac{\partial \overline{n}_1}{\partial v} \tag{2.4}$$

the normal curvature $k(\overline{n}_1, \mathcal{C}, M)$ can be written as:

$$k(\overline{n}_1, \mathcal{C}, M) = E_{\text{II}} \cdot \dot{u}^2 + 2F_{\text{II}} \cdot \dot{u} \cdot \dot{v} + G_{\text{II}} \cdot \dot{v}^2. \tag{2.5}$$

The normal curvature $k(\bar{n}_1, \mathcal{C}, M)$ can be positive or negative (it is positive when the curve is convex when it is seen in the direction of $\bar{n}_1$) but its absolute value is positive and gives the curvature of the curve $\mathcal{C}$ at the point *M*.

Different planes π_2 containing the normal line N_M, called normal slices intersect the surface *S* giving different curves $\mathcal{C}$ which have different normal curvatures $k(\bar{n}_1, \mathcal{C}, M)$. Among these normal curvatures at the point *M*, there is one which is minimal and one which is maximal, known as the principal normal curvatures of *S* corresponding to the curves $\mathcal{C}_1$ and $\mathcal{C}_2$, and are denoted by: $k(\bar{n}_1, \mathcal{C}_1, M)$ and $k(\bar{n}_1, \mathcal{C}_2, M)$ respectively, i.e.

$$k(\bar{n}_1, \mathcal{C}_1, M) \le k(\bar{n}_1, \mathcal{C}, M) \le k(\bar{n}_1, \mathcal{C}_2, M)$$

The mean normal curvature of the surface *S* at the point *M* with respect to $\bar{n}_1$, $\mathcal{H}(\bar{n}_1, M)$, is defined as the average of the principal normal curvatures of *S*:

$$\mathcal{H}(\bar{n}_1, M) = \frac{1}{2}\left(k(\bar{n}_1, \mathcal{C}_1, M) + k(\bar{n}_1, \mathcal{C}_2, M)\right) \tag{2.6}$$

A formula of the mean normal curvature $\mathcal{H}(\bar{n}_1, M)$ with respect to $\bar{n}_1$ can be written, using the elements defining the surface, as follows:

$$\mathcal{H}(\bar{n}_1, M) = \frac{E_{\mathrm{I}} \cdot G_{\mathrm{II}} - 2F_{\mathrm{I}} \cdot F_{\mathrm{II}} + G_{\mathrm{I}} \cdot E_{\mathrm{II}}}{2\left(E_{\mathrm{I}} \cdot G_{\mathrm{I}} - F_{\mathrm{I}}^{\,2}\right)} \tag{2.7}$$

where $E_{\mathrm{I}} = |\bar{r}_u|^2$, $F_{\mathrm{I}} = \bar{r}_u \cdot \bar{r}_v$, $G_{\mathrm{I}} = |\bar{r}_v|^2$ are the coefficients of the first fundamental form of the surface *S* and E_{II}, F_{II}, G_{II} are given by (2.4) and represent the coefficients of the second fundamental form of the surface *S*. According to [Finn 1986], for a surface given in explicit form (the considered parametrization is $u = x, v = y$)

$$\begin{cases} x = x \\ y = y \\ z = z(x, y) \end{cases}, (x, y) \in D \subset \mathbb{R}^2$$

these coefficients are given by:

$$E_{\mathrm{I}} = 1 + \left(\frac{\partial z}{\partial x}\right)^2, \quad F_{\mathrm{I}} = \frac{\partial z}{\partial x} \cdot \frac{\partial z}{\partial y}, \quad G_{\mathrm{I}} = 1 + \left(\frac{\partial z}{\partial y}\right)^2,$$

$$E_{\mathrm{II}} = \frac{\dfrac{\partial^2 z}{\partial x^2}}{\sqrt{1+\left(\dfrac{\partial z}{\partial x}\right)^2+\left(\dfrac{\partial z}{\partial y}\right)^2}},\quad F_{\mathrm{II}} = \frac{\dfrac{\partial^2 z}{\partial x \partial y}}{\sqrt{1+\left(\dfrac{\partial z}{\partial x}\right)^2+\left(\dfrac{\partial z}{\partial y}\right)^2}},\quad G_{\mathrm{II}} = \frac{\dfrac{\partial^2 z}{\partial y^2}}{\sqrt{1+\left(\dfrac{\partial z}{\partial x}\right)^2+\left(\dfrac{\partial z}{\partial y}\right)^2}},$$

and hence, the mean normal curvature with respect to $\bar{n}_1$ becomes

$$\mathcal{H}\left(\bar{n}_1, M\right) = \frac{1}{2}\frac{\left[1+\left(\dfrac{\partial z}{\partial y}\right)^2\right]\dfrac{\partial^2 z}{\partial x^2} - 2\dfrac{\partial z}{\partial x}\dfrac{\partial z}{\partial y}\dfrac{\partial^2 z}{\partial x \partial y} + \left[1+\left(\dfrac{\partial z}{\partial x}\right)^2\right]\dfrac{\partial^2 z}{\partial y^2}}{\left[1+\left(\dfrac{\partial z}{\partial x}\right)^2+\left(\dfrac{\partial z}{\partial y}\right)^2\right]^{\frac{3}{2}}}. \tag{2.8}$$

The mean normal curvature with respect to $\bar{n}_2$ is $\mathcal{H}\left(\bar{n}_2, M\right) = -\mathcal{H}\left(\bar{n}_1, M\right)$.

2.1.2. Young-Laplace's equation

In the case of a capillary surface in equilibrium separating two regions containing fluids and whose shape is determined by the pressures in the two regions, Laplace [Laplace 1806] showed that the mean normal curvature with respect to $\bar{n}_1$ of the free surface is proportional to the pressure change across the surface:

$$2 \cdot \mathcal{H}\left(\bar{n}_1, M\right) = \frac{1}{\gamma}\left(P_i - P_o\right) \tag{2.9}$$

where P_i represents the pressure of the fluid in the region for which $\bar{n}_1$ is inner normal and P_o represents the pressure of the fluid in the region for which $\bar{n}_1$ is outer normal (see Figure 2.2).

The proportionality coefficient is $\frac{1}{\gamma}$ where γ represents the melt surface tension.

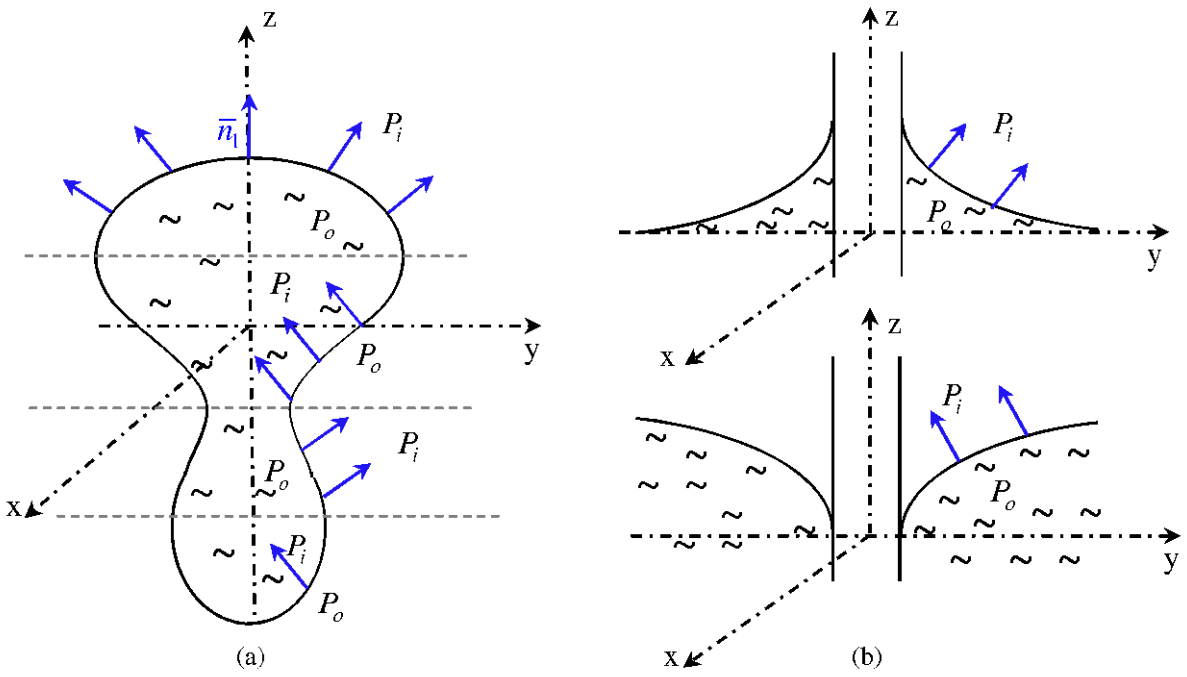

Figure 2.2 (a) Sessile or pendant drop; (b) External meniscus. P_i is chosen in the side of the curve where the normal points toward $z > 0$.

Let's consider the example of a gas bubble inside an incompressible ideal fluid [Frolov 2005]. The gas bubble can be represented as a liquid-free volume between two surfaces (see Fig. 2.3). The shape of the bubble is determined by the solution of (2.9). In the case of a slowly rising gas bubble in an incompressible ideal fluid, Eq. (2.9) can be written as:

- for the upper surface (Fig. 2.3 (a)): $2 \cdot \mathcal{H}_1(\bar{n}_1, M) = \frac{1}{\gamma}(P_1 - P_{gas})$,

- for the lower surface (Fig. 2.3 (b)): $2 \cdot \mathcal{H}_2(\bar{n}_1, M) = \frac{1}{\gamma}(P_{gas} - P_2)$

where P_1 and P_2 are the corresponding pressures on the upper and lower surfaces of the bubble, respectively. The pressure P_{gas} denotes the gas pressure inside the bubble. In these two equations, $\mathcal{H}_1$ and $\mathcal{H}_2$ are the mean curvature of the upper and lower surfaces, respectively.

If the bubble is small or $g = 0$ then $P_1 = P_2$. It follows, from the mathematical description of the mean normal curvature, that the curvature of the two hemispheres are equal but of opposite signs and the two equations are needed to describe the bubble. The physicists do not accept that two

equations are needed for a sole given phenomenon. They consider that the curvature of the bubble is constant everywhere and use only one equation. This is a matter of convention that very often led to misunderstandings.

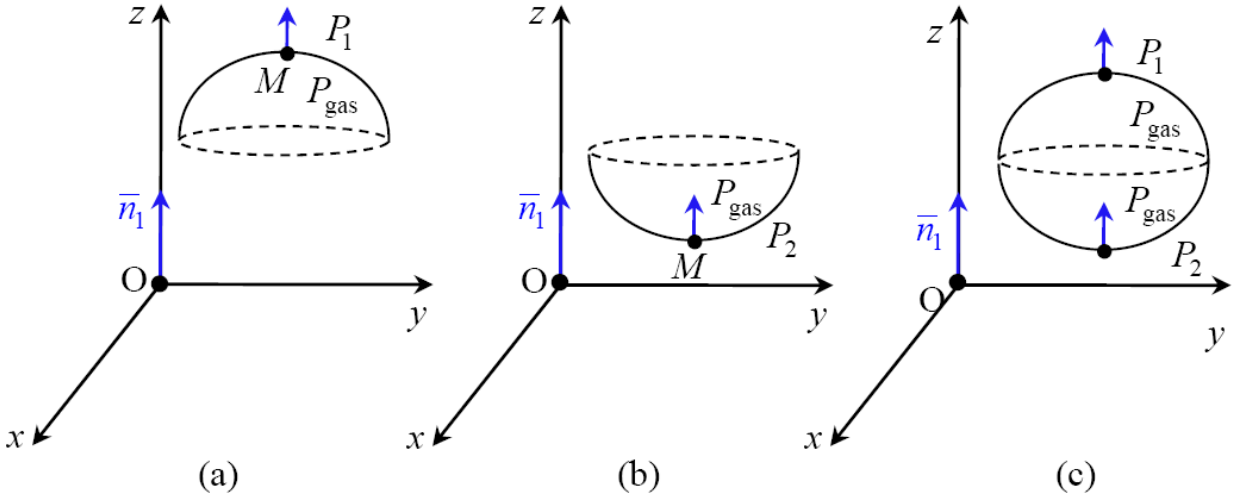

Figure 2.3 Geometrical representation of a gas bubble inside an incompressible fluid: (a) the upper surface of the bubble, (b) the lower surface of the bubble, and (c) the gas bubble.

It must be noted that there exist several expressions of the Young-Laplace equations. Turning to relations (2.8) and (2.9) the following equality known as Young-Laplace's equation must hold:

$$\frac{\left[1+\left(\frac{\partial z}{\partial y}\right)^2\right]\frac{\partial^2 z}{\partial x^2}-2\frac{\partial z}{\partial x}\frac{\partial z}{\partial y}\frac{\partial^2 z}{\partial x\partial y}+\left[1+\left(\frac{\partial z}{\partial x}\right)^2\right]\frac{\partial^2 z}{\partial y^2}}{\left[1+\left(\frac{\partial z}{\partial x}\right)^2+\left(\frac{\partial z}{\partial y}\right)^2\right]^{\frac{3}{2}}}=\frac{P_i-P_o}{\gamma}. \tag{2.10}$$

When axi-symmetric solution are searched for the Young-Laplace equation (2.10) then, using cylindrical polar coordinates

$$\begin{cases} x=r\cos\beta \\ y=r\sin\beta, \qquad r>0,\ \beta\in[0,\ 2\pi] \\ z=z(r) \end{cases}$$

it is obtained that these type of solutions verifies the equation

$$\frac{\frac{d^2z}{dr^2}+\frac{1}{r}\frac{dz}{dr}\left[1+\left(\frac{dz}{dr}\right)^2\right]}{\left[1+\left(\frac{dz}{dr}\right)^2\right]^{\frac{3}{2}}}=\frac{P_i-P_o}{\gamma}. \tag{2.11}$$

Here the solution $z=z(r)$ is sought depending on the radial coordinate. Another form of the Eq. (2.11) putting in evidence the principal normal curvatures is the following:

$$\frac{\frac{d^2z}{dr^2}}{\left[1+\left(\frac{dz}{dr}\right)^2\right]^{\frac{3}{2}}}+\frac{\frac{1}{r}\frac{dz}{dr}}{\left[1+\left(\frac{dz}{dr}\right)^2\right]^{\frac{1}{2}}}=\frac{P_i-P_o}{\gamma} \tag{2.12}$$

Here $\frac{\frac{d^2z}{dr^2}}{\left[1+\left(\frac{dz}{dr}\right)^2\right]^{\frac{3}{2}}}=k\left(\bar{n}_1,\mathcal{C}_1,M\right)$ and $\frac{\frac{1}{r}\cdot\frac{dz}{dr}}{\left[1+\left(\frac{dz}{dr}\right)^2\right]^{\frac{1}{2}}}=k\left(\bar{n}_1,\mathcal{C}_2,M\right)$.

The most used form of the axi-symmetric Young-Laplace equation is:

$$\frac{d^2z}{dr^2}=\frac{P_i-P_o}{\gamma}\left[1+\left(\frac{dz}{dr}\right)^2\right]^{\frac{3}{2}}-\frac{1}{r}\frac{dz}{dr}\left[1+\left(\frac{dz}{dr}\right)^2\right]. \tag{2.13}$$

This is a nonlinear second order differential equation and for obtaining a specified solution $z=z(r)$ two conditions are needed, which, associated to Eq. (2.13), gives an Initial Value Problem (IVP) when these conditions are given at the same point or a Boundary Value Problem (BVP) when these conditions are given at different points. In general, because of its nonlinearity, the problem does not have an explicit (analytical) solution. For solving the IVP (or BVP) it is necessary to perform its qualitative analysis and to develop specific numerical tools.

In order to make easier the analytical and numerical analysis, a dimensionless form of equation (2.13) is preferred. Considering a characteristic length *L* dimension of the problem and scaling:

$$\tilde{r}=\frac{r}{L};\ \tilde{z}=\frac{z}{L} \tag{2.14}$$

leads to:

$$\frac{dz}{dr}=\frac{d\left(\tilde{z}\cdot L\right)}{d\left(\tilde{r}\cdot L\right)}=\frac{d\tilde{z}}{d\tilde{r}},$$
$$\frac{d^2z}{dr^2}=\frac{d}{dr}\left(\frac{dz}{dr}\right)=\frac{1}{L}\frac{d}{d\tilde{r}}\left(\frac{d\tilde{z}}{d\tilde{r}}\right)=\frac{1}{L}\frac{d^2\tilde{z}}{d\tilde{r}^2}. \tag{2.15}$$

Replacing the dimensional variables in the equation (2.13) with their non-dimensional equivalents (2.14) and (2.15) gives:

$$\frac{d^2\tilde{z}}{d\tilde{r}^2}=-La\left[1+\left(\frac{d\tilde{z}}{d\tilde{r}}\right)^2\right]^{\frac{3}{2}}-\frac{1}{\tilde{r}}\frac{d\tilde{z}}{d\tilde{r}}\left[1+\left(\frac{d\tilde{z}}{d\tilde{r}}\right)^2\right] \tag{2.16}$$

where $La=\dfrac{\left(P_o-P_i\right)\cdot L}{\gamma}$ represents the Laplace number.

Introducing the new unknown function ψ defined by:

$$\frac{d\tilde{z}}{d\tilde{r}}=\pm\tan\psi \tag{2.17}$$

equation (2.16) is transformed into the system:

$$\begin{cases}\dfrac{d\tilde{z}}{d\tilde{r}}=\pm\tan\psi\\[2ex] \dfrac{d\psi}{d\tilde{r}}=\mp La\cdot\dfrac{1}{\cos\psi}-\dfrac{1}{\tilde{r}}\tan\psi\end{cases}. \tag{2.18}$$

The initial or/and boundary conditions required for solving the axi-symmetric Young-Laplace equation are determined by the structural features of each specific configuration. The features corresponding to typical boundary conditions of the capillary problem are: *the catching and wetting boundary conditions* and *the growth angle achievement* [Tatartchenko 2010].

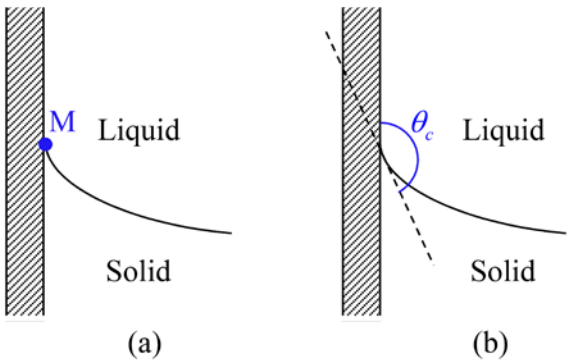

Figure 2.4 (a) Catching condition: the contact point M is fixed and the contact angle is unknown; (b) Wetting condition: the contact angle θ_c is fixed but the contact point coordinate is unknown.

The difference between the catching and wetting boundary conditions consists in: for the catching condition the contact point of the meniscus on the shaper is fixed (Fig. 2.4. (a)), but the contact angle (angle between the tangent to the meniscus and the tangent to the shaper surface) is free and is determined by the solution of the problem. On the contrary, for the wetting condition, the contact point can move along the shaper surface, but the contact angle (called wetting angle) is fixed by the shaper surface (Fig. 2.4. (b)).

The catching boundary condition (Fig. 2.5 (a)) is used for example in the case of E.F.G. technique where the counter line of the meniscus surface is fixed by the internal or external edge counter.

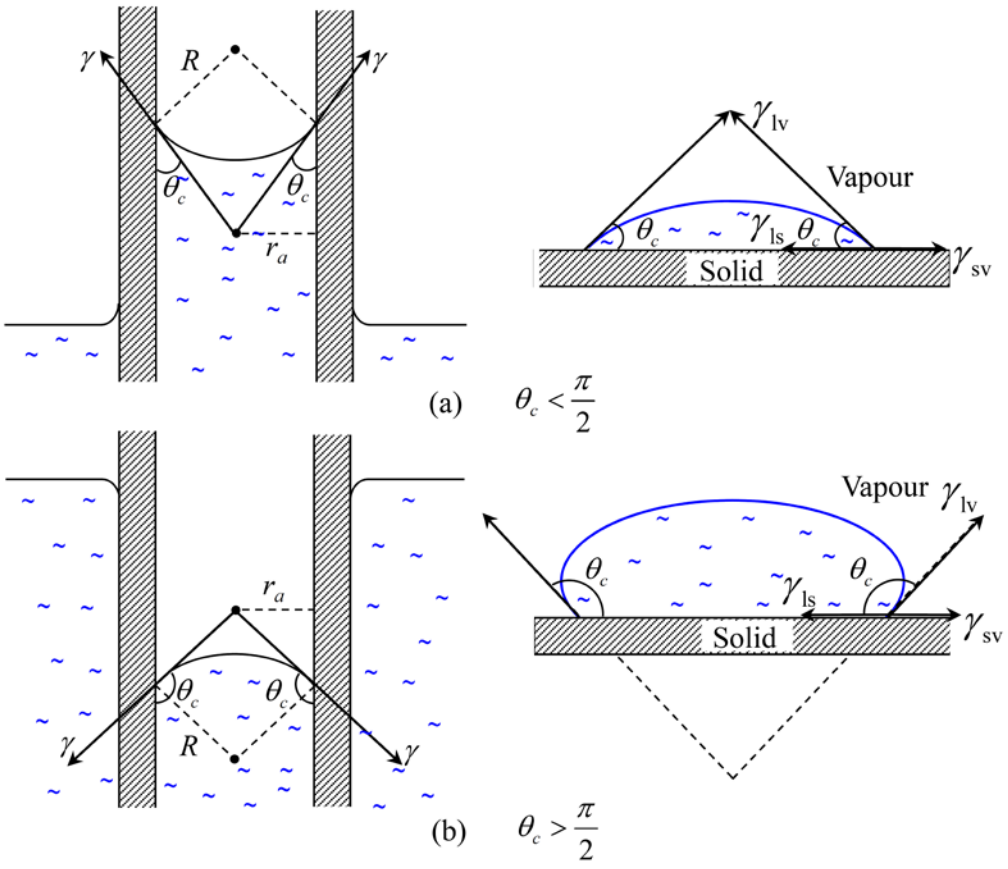

Figure 2.5 (a) Wettable shaper materials and (b) Non-wettable shaper materials.

The wetting boundary condition known also as the *angle of fixation boundary condition* (the contact angle θ_c is fixed but the contact point coordinate is unknown), is specific for non-wettable shaper materials ($\theta_c > \frac{\pi}{2}$ as in Fig. 2.5 (b)) as well as for wettable ones ($\theta_c < \frac{\pi}{2}$), and for pulling up as well as for lowering down shaped crystal growth (for more details see also [Tatartchenko 2010]).

In crystal growth, once the meniscus shape is obtained (global convex, global concave, convexo-concave or concave-convex, see [Braescu 2008]) *the growth angle criterion* must be imposed. This growth angle condition is expressed as follows:

$$\psi\big|_{\tilde{r}=\tilde{r}_c} = \frac{\pi}{2} - \alpha_e ,$$

where $\tilde{r}_c$ represents the non-dimensional crystal radius.

Even if the initial value problem of the Young-Laplace equation has a unique solution, however it is possible that this solution does not satisfy the condition of the growth angle achievement and a crystal cannot be grown. If this condition is satisfied then a crystal having a radius $\tilde{r}_c$ can be obtained (for more details see [Braescu 2010-2]).

2.2. Analytical and numerical studies for the meniscus surface equation in the case of dewetted Bridgman process

As it was shown in the first chapter, the pressure difference between the cold and hot sides of the sample determines the meniscus shape and size. Thus, for a better understanding of the dewetted Bridgman process, analytical and numerical studies of the axi-symmetric Young-Laplace equation describing the meniscus shape must be performed and the dependence of the meniscus shape and size on the pressure difference must be established. For this aim, we start from the Young-Laplace equation of a capillary surface (2.12) written in agreement with the configuration presented in Figure 2.6:

$$\frac{\frac{d^2z}{dr^2}}{\left[1+\left(\frac{dz}{dr}\right)^2\right]^{\frac{3}{2}}}+\frac{\frac{1}{r}\frac{dz}{dr}}{\left[1+\left(\frac{dz}{dr}\right)^2\right]^{\frac{1}{2}}}=\frac{P_i-P_o}{\gamma}.$$

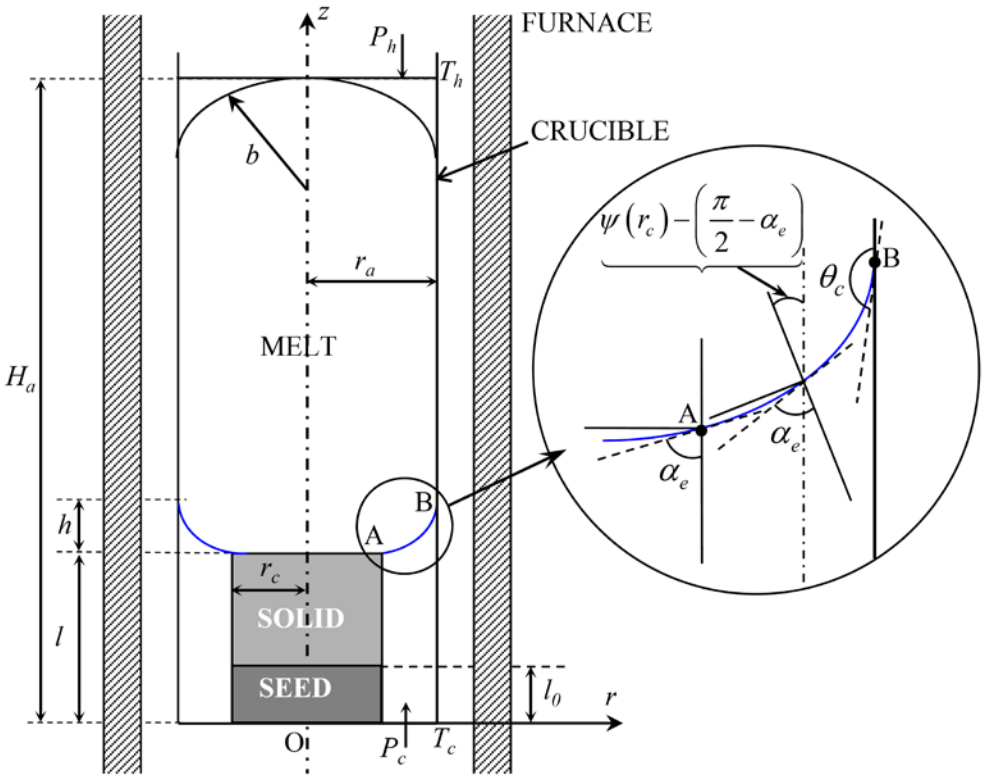

Figure 2.6 Schematic dewetted Bridgman technique.

In this case, the external pressure on the surface is $P_o = P_c$ and the internal pressure applied on the surface, P_i is defined as:

$$P_i = P_h + \rho_l g H_a - \rho_l g z + \frac{2\gamma}{b}$$

where P_h and P_c are the gas pressures at the hot and cold sides of the sample, and *b* is the radius of curvature at the apex of the liquid. Thus Young-Laplace's equation can be written as follows:

$$\frac{\frac{d^2z}{dr^2}}{\left[1+\left(\frac{dz}{dr}\right)^2\right]^{\frac{3}{2}}}+\frac{\frac{1}{r}\cdot\frac{dz}{dr}}{\left[1+\left(\frac{dz}{dr}\right)^2\right]^{\frac{1}{2}}}=\frac{\rho_l g\left(H_a-z\right)-\Delta P}{\gamma}+\frac{2}{b} \tag{2.19}$$

where $\Delta P = P_c - P_h$ represents the gas pressure difference between the cold and hot sides of the sample, H_a - the total length of the melt and solid, ρ_l - the density of the liquid, g - the gravitational acceleration, γ - the surface tension of the melt and the term $2/b$ is due to the curvature at the top, depending on the wetting angle θ_c and on the crucible radius r_a [Duffar 1997].

For writing the Young-Laplace equation in the non-dimensional form, the following non-dimensional numbers (obtained by using the ampoule radius r_a as length scale) are used:

$$\tilde{r}=\frac{r}{r_a},\ \tilde{H}_a=\frac{H_a}{r_a},\ \tilde{z}=\frac{z}{r_a},\ \tilde{b}=\frac{b}{r_a},\ \tilde{r}_a=\frac{r_a}{r_a}=1 \tag{2.20}$$

leading to

$$\frac{dz}{dr}=\frac{d\left(\tilde{z}\cdot r_a\right)}{d\left(\tilde{r}\cdot r_a\right)}=\frac{d\tilde{z}}{d\tilde{r}}$$

$$\frac{d^2z}{dr^2}=\frac{d}{dr}\left(\frac{dz}{dr}\right)=\frac{1}{r_a}\frac{d}{d\tilde{r}}\left(\frac{d\tilde{z}}{d\tilde{r}}\right)=\frac{1}{r_a}\frac{d^2\tilde{z}}{d\tilde{r}^2}.$$

Then, the non-dimensional form of Young Laplace's equation in the case of dewetted Bridgman process is:

$$\frac{\frac{d^2\tilde{z}}{d\tilde{r}^2}}{\left[1+\left(\frac{d\tilde{z}}{d\tilde{r}}\right)^2\right]^{\frac{3}{2}}}+\frac{\frac{1}{\tilde{r}}\frac{d\tilde{z}}{d\tilde{r}}}{\left[1+\left(\frac{d\tilde{z}}{d\tilde{r}}\right)^2\right]^{\frac{1}{2}}}=Bo\left(\tilde{H}_a-\tilde{z}\right)-La+\frac{2}{\tilde{b}}. \tag{2.21}$$

where $La=\frac{\left(P_c-P_h\right)r_a}{\gamma}$, $Bo=\frac{\rho_l g r_a^2}{\gamma}$.

2.2.1. Analytical and numerical solutions for the meniscus equation in zero gravity

Under zero gravity conditions $Bo = 0$ and then, the non-dimensional Young-Laplace equation (2.21) becomes:

$$\frac{\frac{d^2\tilde{z}}{d\tilde{r}^2}}{\left[1+\left(\frac{d\tilde{z}}{d\tilde{r}}\right)^2\right]^{\frac{3}{2}}} + \frac{\frac{1}{\tilde{r}}\frac{d\tilde{z}}{d\tilde{r}}}{\left[1+\left(\frac{d\tilde{z}}{d\tilde{r}}\right)^2\right]^{\frac{1}{2}}} = -La - 2\cos\theta_c \tag{2.22}$$

where the term $\left(-2\cdot\cos\theta_c\right)$ is due to the curvature at the top ($\frac{1}{\tilde{b}} = -\cos\theta_c$ [Duffar 1997]).

The solution $\tilde{z} = \tilde{z}\left(\tilde{r}\right)$ of (2.22) represents the meniscus surface if it satisfies the wetting boundary condition:

$$\tilde{z}\left(1\right) = \tilde{l} + \tilde{h};\ \frac{d\tilde{z}}{d\tilde{r}}\left(1\right) = \tan\left(\theta_c - \frac{\pi}{2}\right);\ \theta_c \in \left(\frac{\pi}{2}, \pi\right) \tag{2.23}$$

where $\tilde{h} = \frac{h}{r_a} > 0$, $\tilde{l} = \frac{l}{r_a} > 0$ are the non-dimensional meniscus height, crystallization front respectively ($\tilde{l} > \tilde{l}_0$, $\tilde{l}_0 = \frac{l_0}{r_a} > 0$ - the crystallization front at the beginning of the solidification process).

A crystal of radius $\tilde{r}_c$ is obtained by the dewetted Bridgman method, if the condition of the growth angle achievement is satisfied:

$$\tilde{z}\left(\tilde{r}_c\right) = \tilde{l};\frac{d\tilde{z}}{d\tilde{r}}\left(\tilde{r}_c\right) = \tan\left(\frac{\pi}{2} - \alpha_e\right). \tag{2.24}$$

For the determination of the meniscus equation we remark that Eq. (2.22) can be written as

$$\frac{\tilde{r}\frac{d^2\tilde{z}}{d\tilde{r}^2} + \frac{d\tilde{z}}{d\tilde{r}}\left[1+\left(\frac{d\tilde{z}}{d\tilde{r}}\right)^2\right]}{\left[1+\left(\frac{d\tilde{z}}{d\tilde{r}}\right)^2\right]^{\frac{3}{2}}} = -\left(La + 2\cos\theta_c\right)\tilde{r}$$

that is equivalent to

$$\frac{d}{d\tilde{r}}\left(\frac{\tilde{r}\dfrac{d\tilde{z}}{d\tilde{r}}}{\sqrt{1+\left(\dfrac{d\tilde{z}}{d\tilde{r}}\right)^2}}\right)=-\left(La+2\cos\theta_c\right)\tilde{r}$$

i.e., by integration

$$\frac{\tilde{r}\dfrac{d\tilde{z}}{d\tilde{r}}}{\sqrt{1+\left(\dfrac{d\tilde{z}}{d\tilde{r}}\right)^2}}=-\frac{\tilde{r}^2}{2}\left(La+2\cos\theta_c\right)+c_1\,.$$

The constant c_1 is determined from the boundary condition $\dfrac{d\tilde{z}}{d\tilde{r}}(1)=\tan\left(\theta_c-\dfrac{\pi}{2}\right)$ leading to:

$$\frac{\tilde{r}\dfrac{d\tilde{z}}{d\tilde{r}}}{\sqrt{1+\left(\dfrac{d\tilde{z}}{d\tilde{r}}\right)^2}}=-\frac{\tilde{r}^2}{2}\left(La+2\cos\theta_c\right)+\frac{La}{2}. \tag{2.25}$$

Because $\dfrac{\tilde{r}}{\sqrt{1+\left(\dfrac{d\tilde{z}}{d\tilde{r}}\right)^2}}>0$, the sign of the derivative $\dfrac{d\tilde{z}}{d\tilde{r}}$ depends on the sign of the right hand side of Eq. (2.25):

$$E(\tilde{r},La)=-\frac{\tilde{r}^2}{2}\left(La+2\cos\theta_c\right)+\frac{La}{2}. \tag{2.26}$$

Therefore, the following cases can exist:

a) $E(\tilde{r},La)>0$ and $\dfrac{d\tilde{z}}{d\tilde{r}}>0$ for: a$_1$) $La\in(-\infty;0)$ and $\tilde{r}\in\left(\sqrt{\dfrac{La}{La+2\cos\theta_c}};1\right)$

or a$_2$) $La\in[0,\infty)$ and $\tilde{r}\in(0;1)$;

b) $E(\tilde{r},La)<0$ and $\dfrac{d\tilde{z}}{d\tilde{r}}<0$ for $La\in(-\infty;0)$ and $\tilde{r}\in\left(0;\sqrt{\dfrac{La}{La+2\cos\theta_c}}\right)$.

Imposing to have the same sign for both sides of the relation (2.25), by squaring, gives:

$$\left(\frac{d\tilde{z}}{d\tilde{r}}\right)^2 = \frac{\left(-\tilde{r}^2\cos\theta_c - \tilde{r}^2\frac{La}{2} + \frac{La}{2}\right)^2}{\tilde{r}^2 - \left(-\tilde{r}^2\cos\theta_c - \tilde{r}^2\frac{La}{2} + \frac{La}{2}\right)^2}$$

from where is obtained

$$\frac{d\tilde{z}}{d\tilde{r}}(\tilde{r}) = \pm\frac{-\tilde{r}^2\cos\theta_c - \tilde{r}^2\frac{La}{2} + \frac{La}{2}}{\sqrt{\tilde{r}^2 - \left(-\tilde{r}^2\cos\theta_c - \tilde{r}^2\frac{La}{2} + \frac{La}{2}\right)^2}}$$

According to (a) and (b), $E(\tilde{r}, La)$ and $\frac{d\tilde{z}}{d\tilde{r}}$ have the same sign and hence only the equality

$$\frac{d\tilde{z}}{d\tilde{r}}(\tilde{r}) = \frac{-\tilde{r}^2\cos\theta_c - \tilde{r}^2\frac{La}{2} + \frac{La}{2}}{\sqrt{\tilde{r}^2 - \left(-\tilde{r}^2\cos\theta_c - \tilde{r}^2\frac{La}{2} + \frac{La}{2}\right)^2}}. \tag{2.27}$$

is valid.

The analytical expression of the meniscus can be obtained integrating relation (2.27) and imposing the boundary condition (2.23). As the integral can be expressed using elementary functions in some particular cases only, further two different cases will be treated separately: $La = 0$ and $La \neq 0$.

Case I: $La = 0$

On the physical point of view, this means that there is a connection between the cold and hot sides of the sample, so that the pressures P_c and P_h are equal.

In this case equality (2.25) becomes:

$$\frac{\tilde{r}\frac{d\tilde{z}}{d\tilde{r}}}{\sqrt{1+\left(\frac{d\tilde{z}}{d\tilde{r}}\right)^2}} = -\tilde{r}^2\cos\theta_c.$$

As $-\tilde{r}^2\cos\theta_c > 0$ we get

$$\frac{d\tilde{z}}{d\tilde{r}}(\tilde{r}) = \frac{-\tilde{r}^2\cos\theta_c}{\sqrt{\tilde{r}^2 - \left(\tilde{r}^2\cos\theta_c\right)^2}} \tag{2.28}$$

which by integration gives

$$\tilde{z}(\tilde{r}) = \frac{1}{\cos\theta_c}\sqrt{1-\tilde{r}^2\cos^2\theta_c} + c_2 . \tag{2.29}$$

Using the condition $\tilde{z}(1) = \tilde{l} + \tilde{h}$, the analytical expression of the meniscus surface in zero gravity when $La = 0$ is obtained:

$$\tilde{z}(\tilde{r}) = \frac{1}{\cos\theta_c}\left(\sqrt{1-\tilde{r}^2\cos^2\theta_c} - \sin\theta_c\right) + \tilde{l} + \tilde{h} \tag{2.30}$$

where $\tilde{r} \in [0,1]$.

Statement 2.1: *When* $Bo = 0$ *and* $La = 0$ *the function* $\tilde{z}(\tilde{r})$ *which describes the meniscus surface has the following properties [Epure 2010-1]:*

(i) $\tilde{z}(\tilde{r})$ *is strictly increasing for* $\tilde{r} \in [0,1]$ *and* $\theta_c > \frac{\pi}{2}$;

(ii) $\tilde{z}(\tilde{r})$ *is convex for* $\tilde{r} \in [0,1]$ *and* $\theta_c > \frac{\pi}{2}$.

From the above properties it results that in zero gravity condition and null gas pressure difference, the meniscus is always globally convex. This can be seen on the computed meniscus presented in Fig. 2.7.

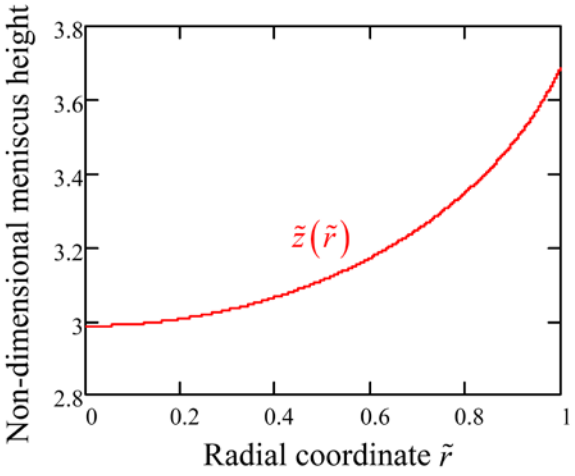

Figure 2.7 Meniscus shape $\tilde{z}(\tilde{r})$ for *InSb*, $\theta_c = 160^\circ$.

A meniscus is possible for the dewetted Bridgman growth configuration if the growth angle

$\alpha_e \in \left(0, \frac{\pi}{2}\right)$ (the angle between the tangent to the meniscus surface and the vertical) is achieved at least at one point on the meniscus surface, i.e. when the equation:

$$\psi(\tilde{r}) = \frac{\pi}{2} - \alpha_e \tag{2.31}$$

has at least one solution $\tilde{r}$ in the range $(0,1)$; ψ represents the angle between the plane $\tilde{z} = 0$ and the tangent plane to the meniscus. For this angle the equality $\tan\psi = \frac{d\tilde{z}}{d\tilde{r}}$ holds, and hence information concerning the achievement of the growth angle is given by the equation:

$$\tan\psi = \frac{-\tilde{r}\cos\theta_c}{\sqrt{1-\tilde{r}^2\cos^2\theta_c}}.$$

Rewriting the above relation as:

$$\frac{\sin\psi}{\sqrt{1-\sin^2\psi}} = \frac{-\tilde{r}\cos\theta_c}{\sqrt{1-\tilde{r}^2\cos^2\theta_c}}$$

gives

$$\sin\psi = -\tilde{r}\cos\theta_c \tag{2.32}$$

that is equivalent to

$$\psi = \arcsin(-\tilde{r}\cos\theta_c),\ \psi \in \left[-\frac{\pi}{2}, \frac{\pi}{2}\right], \theta_c \in \left(\frac{\pi}{2}, \pi\right) \text{ and } \tilde{r} \in [0,1]. \tag{2.33}$$

Relation (2.33) gives a necessary condition for dewetted growth which depends on the growth angle α_e and contact angle θ_c. From the positivity of the derivative

$$\frac{d\psi}{d\tilde{r}} = -\frac{\cos\theta_c}{\sqrt{1-\tilde{r}^2\cos^2\theta_c}} > 0,\ \theta_c \in \left(\frac{\pi}{2}, \pi\right) \tag{2.34}$$

it results that the function $\psi(\tilde{r})$ is strictly increasing for $\tilde{r} \in [0,1]$. Taking into account this monotony and the boundary condition (2.23) which is equivalent to $\psi(1) = \theta_c - \frac{\pi}{2}$, the growth angle can be achieved if $\psi(\tilde{r})$ increases from $\frac{\pi}{2} - \alpha_e$ to $\theta_c - \frac{\pi}{2}$, leading to $\frac{\pi}{2} - \alpha_e < \theta_c - \frac{\pi}{2}$ and

hence $\theta_c + \alpha_e > \pi$. In the opposite case, when $\theta_c + \alpha_e < \pi$, the growth angle cannot be achieved due to the monotony of $\psi(\tilde{r})$.

In the hypothesis that the growth angle criterion is satisfied, i.e. $\theta_c + \alpha_e > \pi$, equations (2.31) and (2.32) give:

$$\sin\left(\frac{\pi}{2} - \alpha_e\right) = -(1-\tilde{e})\cos\theta_c \tag{2.35}$$

where $\tilde{e} = \dfrac{e}{r_a}$ represents the non-dimensional gap thickness and $\tilde{r}_c = 1 - \tilde{e}$ the non-dimensional crystal radius. From (2.35), the following *non-dimensional gap thickness formula* [Duffar 1997] is obtained:

$$\tilde{e} = \frac{\cos\theta_c + \cos\alpha_e}{\cos\theta_c} \tag{2.36}$$

valid under *zero gravity* condition, $La = 0$, and $\theta_c + \alpha_e > \pi$.

On the basis of these results, the following proposition can be stated:

Statement 2.2: *For a given ampoule radius and* $La = 0$, *if* $\theta_c \in \left(\dfrac{\pi}{2}, \pi\right)$ *and* $\alpha_e \in \left(0, \dfrac{\pi}{2}\right)$ *satisfy the inequality* $\theta_c + \alpha_e > \pi$, *then, in the case of dewetted Bridgman process under zero gravity conditions, the meniscus height is constant and is given by the following relation:*

$$\tilde{h} = \frac{1}{\cos\theta_c}(\sin\theta_c - \sin\alpha_e). \tag{2.37}$$

Proof:

Imposing to the relation (2.30) the condition of the growth angle achievement $\tilde{z}(\tilde{r}_c) = \tilde{l}$, results:

$$\tilde{h} = \frac{-1}{\cos\theta_c}\left(\sqrt{1 - r_c^2\cos^2\theta_c} - \sin\theta_c\right).$$

Replacing in this relation $\tilde{r}_c = 1 - \tilde{e}$, where $\tilde{e}$ is given by (2.36) gives:

$$\tilde{h}=\frac{-1}{\cos\theta_c}\left(\sqrt{1-\left(1-\frac{\cos\theta_c+\cos\alpha_e}{\cos\theta_c}\right)^2\cos^2\theta_c}-\sin\theta_c\right)=\frac{-1}{\cos\theta_c}\left(\sqrt{1-\cos^2\alpha_e}-\sin\theta_c\right)$$

from where it results: $\tilde{h}=\frac{1}{\cos\theta_c}\left(\sin\theta_c-\sin\alpha_e\right)$. ■

Case II: $La\neq 0$

The physical meaning of $La\neq 0$ is that the gases between the cold and hot sides of the sample do not communicate, so that a pressure difference exists.

In order to obtain the meniscus equation, relation (2.27) should be integrated, but if $La\neq 0$ the integral cannot be expressed using elementary functions. Then, for obtaining information concerning the meniscus shape, achievement of the growth angle, and gap thickness, qualitative studies must be performed.

Introducing $\tan\psi=\frac{d\tilde{z}}{d\tilde{r}}$ in relation (2.27) gives:

$$\sin\psi=\frac{1}{\tilde{r}}\underbrace{\left[-\frac{\tilde{r}^2}{2}\left(La+2\cos\theta_c\right)+\frac{La}{2}\right]}_{E(\tilde{r},La)} \tag{2.38}$$

The conditions (a) and (b) concerning the sign of $E(\tilde{r},La)$ given by (2.26) leads to:

i) $\sin\psi>0$ for: $i_1)$ $La\in\left(-\infty;0\right)$ and $\tilde{r}\in\left(\sqrt{\frac{La}{La+2\cos\theta_c}};1\right)$

or $i_2)$ $La\in\left[0,\infty\right)$ and $\tilde{r}\in\left(0;1\right)$;

ii) $\sin\psi<0$ for $La\in\left(-\infty;0\right)$ and $\tilde{r}\in\left(0;\sqrt{\frac{La}{La+2\cos\theta_c}}\right)$.

Relation (2.38) is equivalent to

$$\psi=\arcsin\left\{\frac{1}{\tilde{r}}\left[-\frac{\tilde{r}^2}{2}\left(La+2\cos\theta_c\right)+\frac{La}{2}\right]\right\},\ \psi\in\left[-\frac{\pi}{2},\frac{\pi}{2}\right] \tag{2.39}$$

if

$$\frac{1}{\tilde{r}}\left[-\frac{\tilde{r}^2}{2}\left(La+2\cos\theta_c\right)+\frac{La}{2}\right]\in\left[-1,1\right]. \tag{2.40}$$

From (i), (ii) and (2.40) it is obtained that (2.39) is well defined in the following situations:

I) $\tilde{r} \in \left(\sqrt{\dfrac{La}{La + 2\cos\theta_c}}; 1 \right)$ and $La \in (-\infty; 0)$ i.e. $\sin\psi \in [0;1]$ and $\dfrac{d\tilde{z}}{d\tilde{r}} > 0$;

II) $\tilde{r} \in \left[\dfrac{-1 + \sqrt{1 + La\left(2\cos\theta_c + La\right)}}{2\cos\theta_c + La\sqrt{}}; 1 \right)$ ~~and $La \in [0, -2\cos\theta_c) \cup (-2\cos\theta_c; \infty)$~~ i.e.

$\sin\psi \in [0;1]$ and $\dfrac{d\tilde{z}}{d\tilde{r}} > 0$;

III) $\tilde{r} \in \left[\dfrac{1 - \sqrt{1 + La\left(2\cos\theta_c + La\right)}}{2\cos\theta_c + La\sqrt{}}; \sqrt{\dfrac{La}{La + 2\cos\theta_c}} \right)$ ~~and $La \in (-\infty; 0)$~~ i.e. $\sin\psi \in [-1; 0]$

and $\dfrac{d\tilde{z}}{d\tilde{r}} < 0$.

Similarly to the previous calculations developed in the case $La = 0$, the sign of the derivative $\dfrac{d\psi}{d\tilde{r}}$ will give information about the shape of the meniscus.

Deriving the relation (2.39) gives:

$$\frac{d\psi}{d\tilde{r}} = \frac{1}{\sqrt{1 - \left\{ \dfrac{1}{\tilde{r}} \left[-\dfrac{\tilde{r}^2}{2}\left(La + 2\cos\theta_c\right) + \dfrac{La}{2} \right] \right\}^2}} \left[-\frac{\tilde{r}^2}{2}\left(La + 2\cos\theta_c\right) - \frac{La}{2} \right] \frac{1}{\tilde{r}^2}. \qquad (2.41)$$

Taking into account that $\dfrac{d^2\tilde{z}}{d\tilde{r}^2} = \dfrac{1}{\cos^2\psi}\dfrac{d\psi}{d\tilde{r}}$, it can be easily seen that the concavity ($\dfrac{d^2\tilde{z}}{d\tilde{r}^2} < 0$), convexity ($\dfrac{d^2\tilde{z}}{d\tilde{r}^2} > 0$) and the inflexion ($\dfrac{d^2\tilde{z}}{d\tilde{r}^2} = 0$) are given by the sign of the expression depending on $\tilde{r}$ and La:

$$F\left(\tilde{r}, La\right) = -\frac{\tilde{r}^2}{2}\left(La + 2\cos\theta_c\right) - \frac{La}{2}. \qquad (2.42)$$

Imposing the growth angle criterion (2.31), Eq. (2.38) gives:

$$\sin\left(\frac{\pi}{2} - \alpha_e\right) = -\tilde{r}_c\cos\theta_c - \tilde{r}_c\frac{La}{2} + \frac{1}{\tilde{r}_c}\frac{La}{2} \qquad (2.43)$$

which is equivalent to

$$\tilde{r}_c^{\,2}\left(2\cos\theta_c + La\right) + 2\tilde{r}_c\cos\alpha_e - La = 0 \tag{2.44}$$

or written in terms of the crystal-crucible gap tickness ($\tilde{e} = 1 - \tilde{r}_c$):

$$\tilde{e}^2\left(2\cos\theta_c + La\right) - 2\tilde{e}\left(\cos\alpha_e + 2\cos\theta_c + La\right) + 2\left(\cos\alpha_e + \cos\theta_c\right) = 0\,.$$

The existence of the gap (i.e. dewetting occurrence) is determined by *La*, θ_c and α_e values for which inequality (2.40) is satisfied and equation (2.44) has at least one solution.

Further, Eq. (2.44) has solution if

$$\Delta = La^2 + 2La\cos\theta_c + \cos^2\alpha_e \geq 0\,. \tag{2.45}$$

Thus, for studying the existence of the crystal-crucible gap ($\tilde{e} = 1 - \tilde{r}_c$) and the menisci shape, the following cases must be considered:

I) If $La \in (-\infty; 0)$ and $\tilde{r} \in \left(\sqrt{\dfrac{La}{La + 2\cos\theta_c}}; 1\right)$ then $\dfrac{d\tilde{z}}{d\tilde{r}} > 0$ and $\dfrac{d\psi}{d\tilde{r}} > 0$ as $F\left(\tilde{r}, La\right) > 0$.

Hence, $\dfrac{d^2\tilde{z}}{d\tilde{r}^2} = \dfrac{1}{\cos^2\psi}\dfrac{d\psi}{d\tilde{r}} > 0$, i.e. the meniscus is globally convex, and the growth angle can be achieved only if $\theta_c + \alpha_e \geq \pi$. In this case Eq. (2.44) has two roots ($\Delta > 0$): $\tilde{r}_{c2} < 0$ and $\tilde{r}_{c1} \in \left(\sqrt{\dfrac{La}{La + 2\cos\theta_c}}; 1\right)$ leading to one achievement of the growth angle and then the following formula for the gap thickness (see also [Duffar 1997]) is obtained:

$$\tilde{e}_1 = \frac{2\cos\theta_c + La + \cos\alpha_e + \sqrt{La^2 + 2La\cos\theta_c + \cos^2\alpha_e}}{2\cos\theta_c + La}\,. \tag{2.46}$$

The numerical results, obtained by solving the problem (2.22)-(2.23), reveal this behaviour for $La = -1 \in (-\infty; 0]$ and $\theta_c + \alpha_e = 165^\circ + 25^\circ > \pi$, as it can be seen in Fig. 2.8.

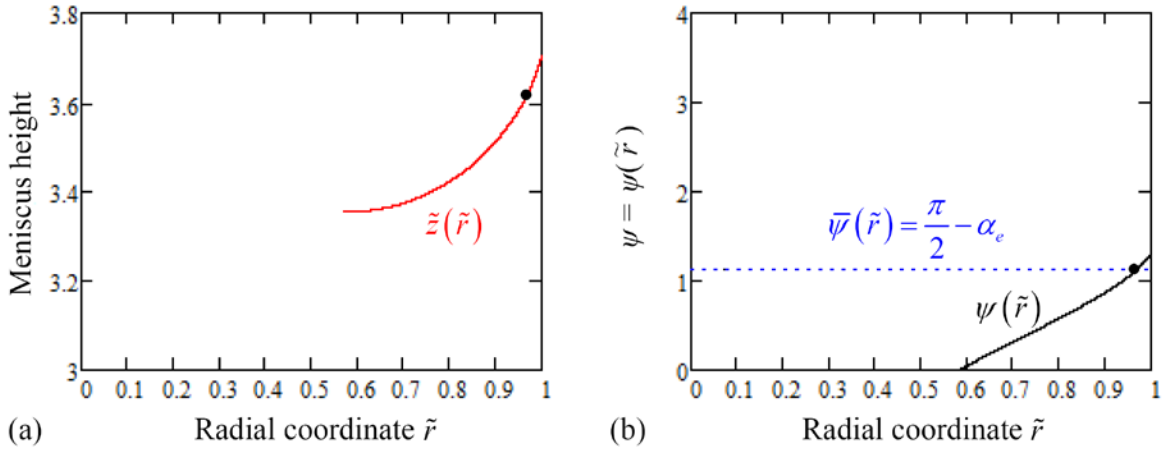

Figure 2.8 (a) Computed meniscus shape $\tilde{z}(\tilde{r})$ and (b) meniscus angle $\psi(\tilde{r})$ corresponding to $La = -1$ and $\theta_c + \alpha_e = 165^\circ + 25^\circ$ for *InSb*, g=0. The place where the growth angle ($\frac{\pi}{2} - \alpha_e = 1.13446$ rad) is achieved is shown by the black dot.

The figure shows that the meniscus is globally convex and that the growth angle is achieved. The computed gap thickness $\tilde{e} = 1 - \tilde{r}_{c1} = 1 - 0.969912 = 0.030088$ is equal to the one given by formula (2.46), i.e. $\tilde{e}_1 = 0.030088$.

In Figure 2.9 the same behaviour can be observed in the special case when $\theta_c + \alpha_e = \pi$. For $La = -1$ the computed gap thickness $\tilde{e} = 0$ is equal to the one given by formula (2.46), i.e. $\tilde{e}_1 = 0$.

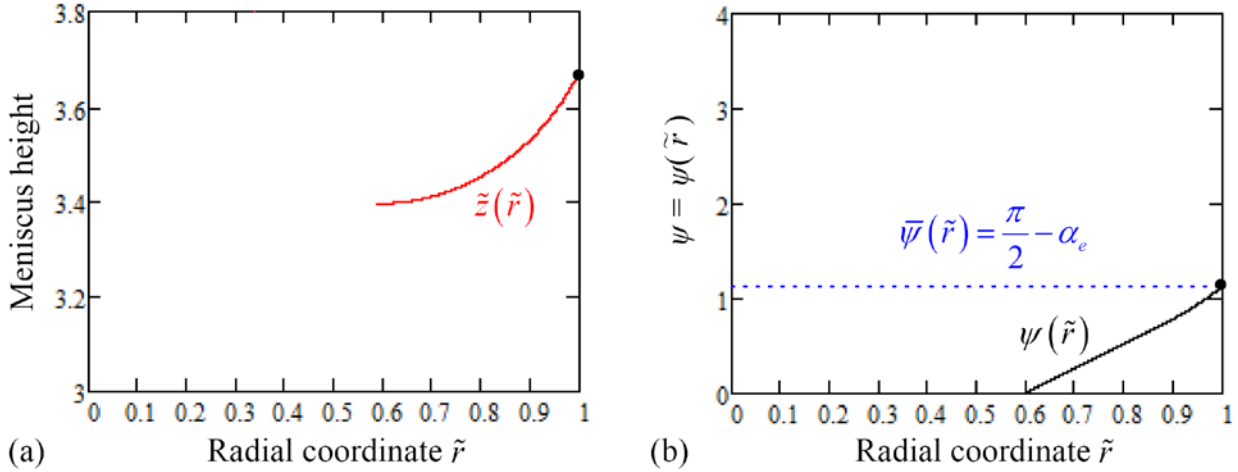

Figure 2.9 (a) Computed meniscus shape $\tilde{z}(\tilde{r})$ and (b) meniscus angle $\psi(\tilde{r})$ corresponding to $La=-1$ and $\theta_c+\alpha_e=155^\circ+25^\circ$ for *InSb*, g=0. The place where the growth angle ($\frac{\pi}{2}-\alpha_e=1.13446$ rad) is achieved is shown by the black dot.

II) If $La\in[0,-2\cos\theta_c)\cup(-2\cos\theta_c;\infty)$ and $\tilde{r}\in\left[\tilde{r}^*;1\right)=\left[\frac{-1+\sqrt{1+La\left(2\cos\theta_c+La\right)}}{2\cos\theta_c+La};1\right)$ then $\frac{d\tilde{z}}{d\tilde{r}}>0$, the meniscus can be globally concave or concave-convex, depending on the sign of $\frac{d\psi}{d\tilde{r}}$ which is determined by the sign of $F(\tilde{r},La)$. This splits the interval $[0;\infty)$ into:

II$_1$) $La\in(0;-\cos\theta_c]$ where the sign of $\frac{d\psi}{d\tilde{r}}$ changes from negative to positive at the point $\tilde{r}_I=\sqrt{\frac{La}{-2\cos\theta_c-La}}\in\left[\tilde{r}^*;1\right)$ and then the meniscus is concave-convex;

II$_2$) $La\in(-\cos\theta_c;-2\cos\theta_c)$ where the sign of $\frac{d\psi}{d\tilde{r}}$ is negative in the prescribed range of $\tilde{r}$ and the meniscus is globally concave.

II$_3$) $La\in(-2\cos\theta_c;\infty)$ where the sign of $\frac{d\psi}{d\tilde{r}}$ is negative because $F(\tilde{r},La)$ does not have real roots, and then the meniscus is globally concave.

Further, imposing the condition of the growth angle achievement and studying the validity of inequality (2.45) the above ranges of *La* are restricted by the sum of the wetting θ_c and growth angle α_e as follows:

Case $\theta_c+\alpha_e<\pi$: $\Delta=La^2+2La\cos\theta_c+\cos^2\alpha_e>0$ and hence Eq. (2.44) has too real roots $\tilde{r}_{c1,2}=\frac{-\cos\alpha_e\mp\sqrt{La^2+2La\cos\theta_c+\cos^2\alpha_e}}{2\cos\theta_c+La}$. The signs of $\tilde{r}_{c1},\tilde{r}_{c2}$ and their position with respect to the interval $\left[\tilde{r}^*;1\right)$ depends on the *La* values:

II$_1$) If $La \in (0; -\cos\theta_c]$, from the convexity of the meniscus in the neighbourhood of 1, is obtained that the growth angle can be achieved if $\theta_c + \alpha_e \geq \pi$ (case studied below).

II$_2$) If $La \in (-\cos\theta_c; -2\cos\theta_c)$ then $\tilde{r}_{c1} > 1$ and $\tilde{r}_{c2} \in [\tilde{r}^*; 1)$. In this case the meniscus is globally concave and the growth angle is achieved once as only the root $\tilde{r}_{c2}$ of Eq. (2.44) belongs to the prescribed range, leading to a crystal-crucible gap thickness expressed by

$$\tilde{e}_2 = \frac{2\cos\theta_c + La + \cos\alpha_e - \sqrt{La^2 + 2La\cos\theta_c + \cos^2\alpha_e}}{2\cos\theta_c + La}. \qquad (2.47)$$

The numerical results performed for $La = 0.5 \in (0.375; 0.749)$ shows that the growth angle is achieved once, as it can be seen on Fig. 2.10.

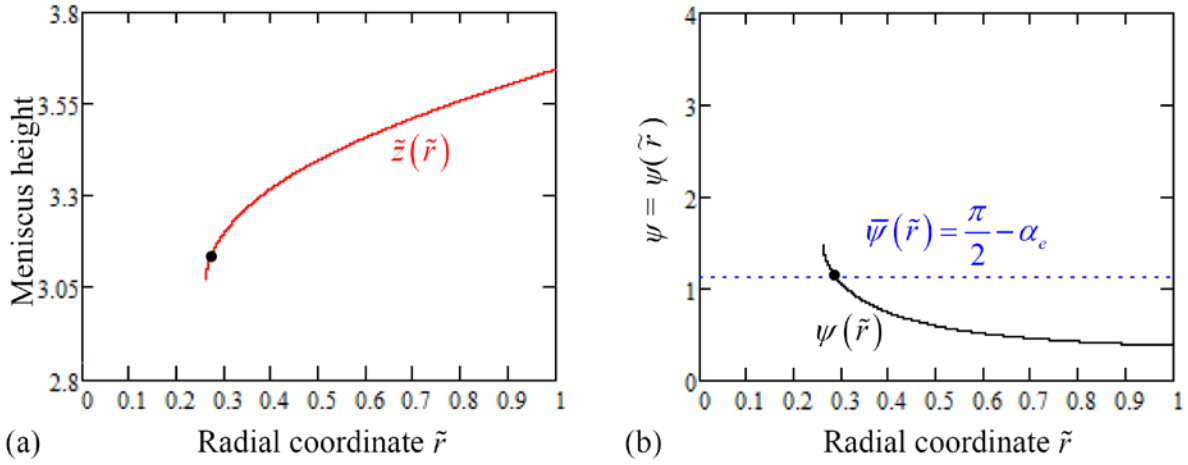

Figure 2.10 (a) Computed meniscus shape $\tilde{z}(\tilde{r})$ and (b) meniscus angle $\psi(\tilde{r})$ corresponding to $La = 0.5$ and $\theta_c + \alpha_e = 112^\circ + 25^\circ$ for *InSb*, g=0. The place where the growth angle ($\frac{\pi}{2} - \alpha_e = 1.13446$ rad) is achieved is shown by the black dot.

The Figure 2.10 shows a concave meniscus, the crystal radius $\tilde{r}_c = 0.2872 \in [0.258; 1]$ and the computed gap thickness $\tilde{e} = 1 - \tilde{r}_c = 1 - 0.2872 = 0.7128$ is equal to $\tilde{e}_2 = 0.7128$ given by formula (2.47).

II$_3$) If $La \in (-2\cos\theta_c;\infty)$ then $\tilde{r}_{c1} < 0$ and $\tilde{r}_{c2} \in [\tilde{r}^*;1)$ leading to a crystal-crucible gap thickness $\tilde{e}_2$ expressed by (2.47). In this case the meniscus is also globally concave.

The numerical results show that the meniscus is concave, and that for $\theta_c + \alpha_e = 112^\circ + 25^\circ < \pi$, $La = 0.8 \in (-2\cos\theta_c;\infty) = (0.749;\infty)$ the growth angle is achieved (Fig. 2.11).

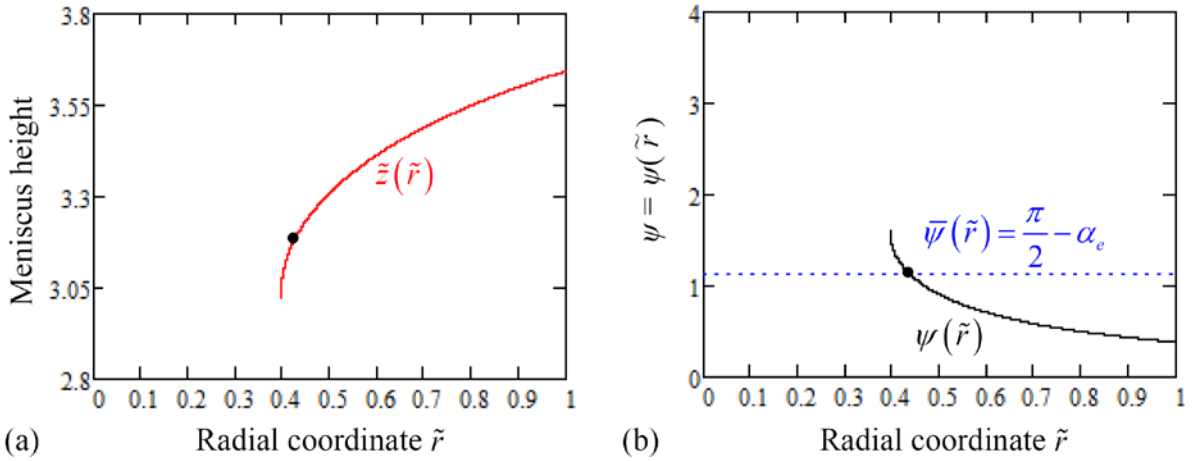

Figure 2.11 (a) Computed meniscus shape $\tilde{z}(\tilde{r})$ and (b) meniscus angle $\psi(\tilde{r})$ corresponding to the $La = 0.8$ and $\theta_c + \alpha_e = 112^\circ + 25^\circ$ for *InSb*, g=0. The place where the growth angle ($\frac{\pi}{2} - \alpha_e = 1.13446$ rad) is achieved is shown by the black dot.

The computed crystal radius is $\tilde{r}_{c2} = 0.436024 \in [0.396;1]$ and then the gap thickness $\tilde{e} = 1 - \tilde{r}_{c2} = 1 - 0.436024 = 0.563976$ is equal to $\tilde{e}_2 = 0.563976$.

Case $\theta_c + \alpha_e \geq \pi$: The sign of Δ depends on the roots of $\Delta = 0$, i.e.

$$La_{1,2} = -\cos\theta_c \mp \sqrt{-\sin(\theta_c + \alpha_e)\sin(\theta_c - \alpha_e)}.$$

La	0	La_1	$-\cos\theta_c$	La_2	$-2\cos\theta_c$
Δ	$+ \; + \; + \; 0$	$- \; - \; - \; - \; - \; - \; 0$	$+ \; + \; +$		
	$\text{II}_{1.1})$	$\text{II}_{1.2})$	$\text{II}_{2.1})$	$\text{II}_{2.2})$	

II$_{1.1}$) If $La \in (0; La_1]$ then $\tilde{r}_{c1} \in (\tilde{r}_I; 1)$ and $\tilde{r}_{c2} \in (\tilde{r}^*; \tilde{r}_I)$, and the meniscus is concave-convex. The growth angle is achieved once on the convex part of the meniscus at $\tilde{r}_{c1} \in (\tilde{r}_I; 1)$, the gap thickness being given by $\tilde{e}_1$ expressed by (2.46) and once on the concave part of the meniscus, at $\tilde{r}_{c2} \in (\tilde{r}^*; \tilde{r}_I)$ leading to a gap thickness $\tilde{e}_2$ expressed by (2.47).

The numerical results presented in Fig. 2.8 for $La = 0.35 \in (0; La_1) = (0; 0.632)$ show that the meniscus is concave-convex and the growth angle is achieved twice.

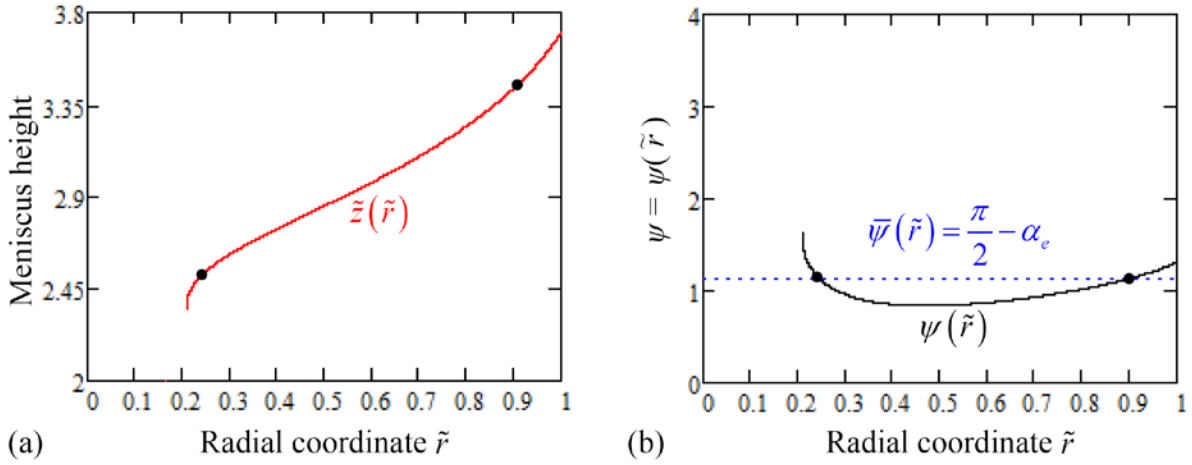

Figure 2.12 (a) Computed meniscus shape $\tilde{z}(\tilde{r})$ and (b) meniscus angle $\psi(\tilde{r})$ corresponding to $La = 0.35$ and $\theta_c + \alpha_e = 165^\circ + 25^\circ$ for *InSb*, g=0. The places where the growth angle ($\frac{\pi}{2} - \alpha_e = 1.13446$ rad) is achieved are shown by the black dots.

For the Fig. 2.12, the meniscus is concave-convex and the growth angle is achieved once on the convex part at $\tilde{r}_{c1} = 0.90005 \in (\tilde{r}_I; 1) = (0.47; 1)$ and once on the concave part at $\tilde{r}_{c2} = 0.24583 \in (\tilde{r}^*; \tilde{r}_I) = (0.21; 0.47)$. Therefore, when the growth angle is achieved on the convex part of the meniscus the computed gap thickness $\tilde{e} = 1 - \tilde{r}_{c1} = 0.09995$ is equal to $\tilde{e}_1 = 0.09995$ given by formula (2.46). When the growth angle is achieved on the

concave part of the meniscus, the computed gap thickness $\tilde{e} = 1 - \tilde{r}_{c2} = 0.75417$ is equal to $\tilde{e}_2 = 0.75417$ expressed by (2.47) .

II$_{1.2}$) If $La \in \left(La_1 ; -\cos\theta_c \right]$ then $\Delta = La^2 + 2La\cos\theta_c + \cos^2\alpha_e < 0$ and the growth angle is not achieved. This behavior can be observed on the Fig. 2.13, for $La = 0.8 \in \left(La_1 ; -\cos\theta_c \right] = \left(0.632 ; 0.966 \right]$.

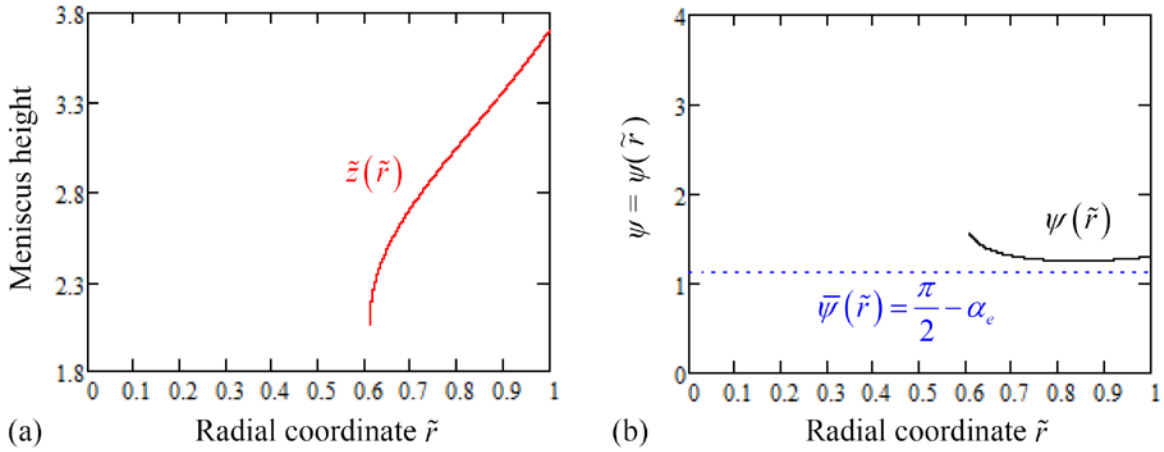

Figure 2.13 (a) Computed meniscus shape $\tilde{z}(\tilde{r})$ and (b) meniscus angle $\psi(\tilde{r})$ corresponding to $La = 0.8$ and $\theta_c + \alpha_e = 165^\circ + 25^\circ$ for *InSb*, g=0. The growth angle cannot be achieved.

II$_{2.1}$) If $La \in \left(-\cos\theta_c ; La_2 \right)$ then $\Delta = La^2 + 2La\cos\theta_c + \cos^2\alpha_e < 0$ and the growth angle is not achieved (similar behavior to the previous case II$_{1.2}$), the meniscus being also concave).

II$_{2.2}$) If $La \in \left[La_2 ; -2\cos\theta_c \right)$ then $\Delta = La^2 + 2La\cos\theta_c + \cos^2\alpha_e > 0$, there exist too roots $\tilde{r}_{c1}, \tilde{r}_{c2} > 1$ and hence the growth angle is not achieved on the prescribed range of $\tilde{r}$.

II$_{2.3}$) If $La \in \left(-2\cos\theta_c ; \infty \right)$ from the concavity of the meniscus in the neighbourhood of 1, is obtained that the growth angle can be achieved if $\theta_c + \alpha_e < \pi$ (see the case studied above).

III) If $La \in (-\infty;0)$ and $\tilde{r} \in \left[\frac{1-\sqrt{1+La\left(2\cos\theta_c+La\right)}}{2\cos\theta_c+La\sqrt{\ }};\sqrt{\frac{La}{La+2\cos\theta_c}}\right)$ then ~~$\frac{d\tilde{z}}{d\tilde{r}}<0$~~ and $\frac{d\psi}{d\tilde{r}}>0$ as $F\left(\tilde{r},La\right)>0$. Moreover, $\frac{d^2\tilde{z}}{d\tilde{r}^2}=\frac{1}{\cos^2\psi}\frac{d\psi}{d\tilde{r}}>0$, i.e. the meniscus is globally convex, but the growth angle cannot be achieved in the prescribed range because the roots of Eq. (2.44) satisfy $\tilde{r}_{c1}>\sqrt{\frac{La}{La+2\cos\theta_c}}$ and $\tilde{r}_{c2}<0$.

The numerical results performed for $La=-500\in(-\infty;0)$ (Fig. 2.14) show that the meniscus is convex, but the growth angle is achieved at $\tilde{r}_{c1}=0.9998$ which does not belong to $\left[\frac{1-\sqrt{1+La\left(2\cos\theta_c+La\right)}}{2\cos\theta_c+La};\sqrt{\frac{La}{La+2\cos\theta_c}}\right)=\left[0.996;0.998\right)$.

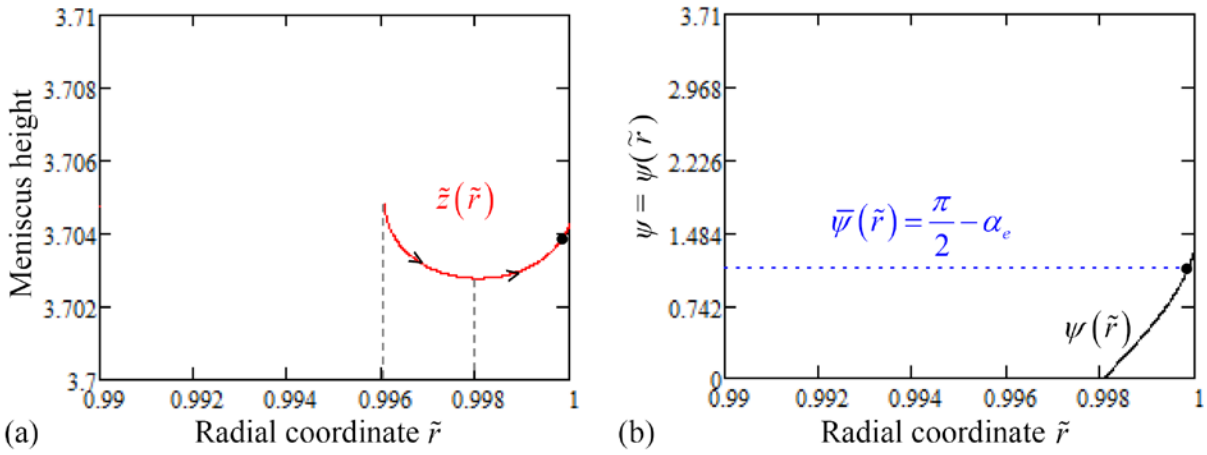

Figure 2.14 (a) Computed meniscus shape $\tilde{z}(\tilde{r})$ and (b) meniscus angle $\psi(\tilde{r})$ corresponding to the $La=-500$ and $\theta_c+\alpha_e=165^\circ+25^\circ$ for *InSb*, g=0. The place where the growth angle ($\frac{\pi}{2}-\alpha_e=1.13446$ rad) is achieved is shown by the black dot.

The above ranges for the Laplace number give information about the meniscus shape and the corresponding cases $\theta_c+\alpha_e\geq\pi$ or $\theta_c+\alpha_e<\pi$, in which the growth angle can be achieved, i.e. dewetting is feasible.

The gap formula (2.46) is valid when the growth angle is achieved on the convex part of the meniscus, and the second formula (2.47) is valid when the achievement of the growth angle occurs on the concave part of the meniscus.

More precisely, the numerical results, obtained by solving numerically the non-dimensional Young-Laplace equation by Runge-Kutta method for *InSb* crystals grown in zero gravity by the dewetted Bridgman technique (material parameters for *InSb* are those presented in Table 1.1, illustrate the behaviors obtained through the qualitative study. In Table 2.1 a summary of the obtained results from the analytical and numerical studies is presented.

La	$-\infty$	0		$-\cos\theta_c$		$-2\cos\theta_c$	$+\infty$
Meniscus shape	convex	](	concave-convex	](	concave	)(	concave
Gap thickness	the growth angle is not achieved			$\tilde{e}_2$		$\tilde{e}_2$	
(a)	$\theta_c + \alpha_e < 180°$						

La	$-\infty$	0	La_1	$-\cos\theta_c$	La_2	$-2\cos\theta_c$	$+\infty$
Meniscus shape	convex	](convex-concave	](concave	](concave	)[concave	)(concave	
Gap thickness	$\tilde{e}_1$	$\tilde{e}_1$	the growth angle is not achieved				
(b)	$\theta_c + \alpha_e > 180°$						

Table 2.1 Meniscus shape and gap thickness depending on the pressure difference for the two cases: (a) $\theta_c + \alpha_e < 180°$ and (b) $\theta_c + \alpha_e > 180°$, in microgravity conditions.

2.2.2. Analytical and numerical solutions for the meniscus equation in normal gravity

Under normal gravity conditions for a crucible radius larger than the capillary constant of the material, the curvature of the upper free liquid surface can be neglected (it is very small). For example for *InSb* the capillary constant is equal to 0.0036 m and the crucible radius is considered 0.0055 m. Hence the axi-symmetric Young-Laplace equation (2.21) becomes:

$$\frac{d^2\tilde{z}}{d\tilde{r}^2} = \left[Bo\left(\tilde{H}_a - \tilde{z}\right) - La \right] \left[1 + \left(\frac{d\tilde{z}}{d\tilde{r}} \right)^2 \right]^{\frac{3}{2}} - \frac{1}{\tilde{r}} \left[1 + \left(\frac{d\tilde{z}}{d\tilde{r}} \right)^2 \right] \frac{d\tilde{z}}{d\tilde{r}} \qquad (2.48)$$

where the axi-symmetric solution $\tilde{z} = \tilde{z}(\tilde{r})$ has to verify the following boundary condition:

$$\tilde{z}(1) = \tilde{l} + \tilde{h} \text{ and } \frac{d\tilde{z}}{d\tilde{r}}(1) = \tan\left(\theta_c - \frac{\pi}{2}\right),\ \theta_c \in \left(\frac{\pi}{2}, \pi\right). \tag{2.49}$$

The nonlinear equation (2.48) is transformed into the following nonlinear system of two differential equations:

$$\begin{cases} \dfrac{d\tilde{z}}{d\tilde{r}} = \tan\psi \\ \dfrac{d\psi}{d\tilde{r}} = \left[Bo\left(\tilde{H}_a - \tilde{z}\right) - La \right] \dfrac{1}{\cos\psi} - \dfrac{1}{\tilde{r}} \tan\psi \end{cases} \tag{2.50}$$

for which the boundary conditions (2.49) become [Balint 2008-2; Braescu 2008]:

$$\tilde{z}(1) = \tilde{l} + \tilde{h} \text{ and } \psi(1) = \theta_c - \frac{\pi}{2}\ ;\ \theta_c \in \left(\frac{\pi}{2}, \pi\right). \tag{2.51}$$

The functions from the right hand member of Eqs. (2.50) are real analytical, i.e. they can be expanded in Taylor series, and the conditions of existence and uniqueness of a solution are satisfied for the problem (2.50)-(2.51). The solution

$$\tilde{z} = \tilde{z}\left(\tilde{r};\ \theta_c,\ La, Bo, \tilde{H}_a, \tilde{l} + \tilde{h}\right), \quad \psi = \psi\left(\tilde{r};\ \theta_c,\ La, Bo, \tilde{H}_a, \tilde{l} + \tilde{h}\right)$$

which depends on $\tilde{r}$ and on the parameters θ_c, La, Bo, $\tilde{H}_a, \tilde{l} + \tilde{h}$ describes the meniscus if the growth angle is reached at a point $\tilde{r}_c \in [0,1]$, i.e.

$$\tilde{z}(\tilde{r}_c) = \tilde{l};\ \psi(\tilde{r}_c) = \frac{\pi}{2} - \alpha_e. \tag{2.52}$$

In the followings, this solution is denoted by $\tilde{z} = \tilde{z}(\tilde{r})$, $\psi = \psi(\tilde{r})$.

Because of the nonlinearity of the problem, *an analytical formula of the meniscus cannot be obtained*, hence analytical and numerical studies of the meniscus shapes are necessary. For this aim, the meniscus shape dependence on the pressure difference will be established, and inequalities of the pressure intervals which assure feasibility of dewetting will be determined.

Due to different behaviours of the meniscus shape in the cases (I) $\theta_c + \alpha_e < 180°$, and (II) $\theta_c + \alpha_e \geq 180°$, as it was already shown in the previous section for zero gravity, qualitative studies will be performed for each case separately. Generally for a clean, perfect liquid

semiconductor in a perfectly clean, smooth crucible surface, the wetting angles are less than 150° and the growth angles are less than 30° (see [Eustathopoulos 2010]) leading to $\theta_c + \alpha_e < 180°$.

However when the crucible surfaces are rough or polluted it has been shown by recent experimental developments [Sylla 2008-1] and by thermodynamical analysis [Sylla 2008-2] that these angles can be enlarged leading to the inequality $\theta_c + \alpha_e \geq 180°$.

which proved that contamination of the system during the growth process may greatly increase the wetting angle, leading to an unexpected inequality between the wetting angle θ_c and growth angle α_e, i.e., $\theta_c + \alpha_e \geq 180°$.

2.2.2.1. Qualitative studies on the meniscus shape using Taylor polynomial approximation

Case $\theta_c + \alpha_e < 180°$

In order to perform a qualitative study of the meniscus shape (convex, concave-convex, convex-concave, concave) as function of the Laplace number, the function $\tilde{z} = \tilde{z}(\tilde{r})$ is approximated by a Taylor polynomial of third degree $T_{\tilde{z}}^3(\tilde{r})$ in the neighbourhood of $\tilde{r}_a = 1$. Following [Braescu 2008], [Balint 2008-2], for establishing the inequalities of the pressure intervals (i.e. *La* numbers) which assure feasibility of dewetted Bridgman growth, the information obtained from Taylor approximation (approximate meniscus) are combined with properties deduced from the problem (2.50) - (2.51) which describes the shape of the real meniscus. The third order Taylor polynomial $T_{\tilde{z}}^3(\tilde{r})$ which approximates the meniscus surface $\tilde{z} = \tilde{z}(\tilde{r})$ is accurate only in a small neighbourhood of $\tilde{r} = \tilde{r}_a = 1$ and it is given by:

$$T_{\tilde{z}}^3(\tilde{r}) = \tilde{z}(1) + \tilde{z}'(1)\cdot(\tilde{r}-1) + \frac{\tilde{z}''(1)}{2}\cdot(\tilde{r}-1)^2 + \frac{\tilde{z}'''(1)}{6}\cdot(\tilde{r}-1)^3 \tag{2.53}$$

where: $\tilde{z}(1) = \tilde{l} + \tilde{h}$ and $\tilde{z}'(1)$, $\tilde{z}''(1)$, $\tilde{z}'''(1)$ represent the first, the second, and the third order derivatives of the function $\tilde{z} = \tilde{z}(\tilde{r})$ at $\tilde{r} = 1$, and are obtained from the system (2.50) and boundary conditions (2.51) as follows [Braescu 2008]:

$$\tilde{z}'(1) = -\frac{\cos\theta_c}{\sin\theta_c} = A_{\tilde{z}}^1 \tag{2.54}$$

$$\tilde{z}''(1) = -\frac{La}{\sin^3\theta_c} + \frac{\cos\theta_c}{\sin^3\theta_c} + \frac{Bo\left[\tilde{H}_a - \left(\tilde{l}+\tilde{h}\right)\right]}{\sin^3\theta_c} = -A_{\tilde{z}}^2 \cdot La + B_{\tilde{z}}^2 \tag{2.55}$$

$$\begin{aligned}\tilde{z}'''(1) = &-\frac{3\cos\theta_c}{\sin^5\theta_c} La^2 + \left(\frac{6\cos^2\theta_c}{\sin^5\theta_c} + \frac{1}{\sin^3\theta_c} + \frac{6Bo\left[\tilde{H}_a - \left(\tilde{l}+\tilde{h}\right)\right]\cos\theta_c}{\sin^5\theta_c}\right) La + \\ &+ \frac{1}{\sin^3\theta_c}\left[-\frac{3Bo^2\left[\tilde{H}_a - \left(\tilde{l}+\tilde{h}\right)\right]^2\cos\theta_c}{\sin^2\theta_c} - \frac{3\cos^3\theta_c}{\sin^2\theta_c} - 2\cos\theta_c + \frac{Bo\cdot\cos\theta_c}{\sin\theta_c} - \right. \\ &\left. - \frac{6Bo\left[\tilde{H}_a - \left(\tilde{l}+\tilde{h}\right)\right]\cos^2\theta_c}{\sin^2\theta_c} - Bo\left[\tilde{H}_a - \left(\tilde{l}+\tilde{h}\right)\right]\right] \\ &= A_{\tilde{z}}^3 \cdot La^2 - B_{\tilde{z}}^3 \cdot La + C_{\tilde{z}}^3\end{aligned} \tag{2.56}$$

Information about the concavity or convexity of the meniscus $\tilde{z} = \tilde{z}(\tilde{r})$ in a sufficiently small neighbourhood of $\tilde{r}_a = 1$, are given by the sign of the second derivative of the approximated meniscus $\tilde{z}_T(\tilde{r}) = T_{\tilde{z}}^3(\tilde{r})$:

$$\frac{d^2T_{\tilde{z}}^3}{d\tilde{r}^2} = -A_{\tilde{z}}^2 \cdot La + B_{\tilde{z}}^2 + \left[A_{\tilde{z}}^3 \cdot La^2 - B_{\tilde{z}}^3 \cdot La + C_{\tilde{z}}^3\right] \cdot (\tilde{r} - 1) = E_{\tilde{z}}^2 + E_{\tilde{z}}^3 \cdot (\tilde{r} - 1) \tag{2.57}$$

where is denoted: $E_{\tilde{z}}^2 = -A_{\tilde{z}}^2 \cdot La + B_{\tilde{z}}^2$ and $E_{\tilde{z}}^3 = A_{\tilde{z}}^3 \cdot La^2 - B_{\tilde{z}}^3 \cdot La + C_{\tilde{z}}^3$.

Thus, the following statement can be given:

Statement 2.3: The sets of *La* values that define convex, concave-convex, convex-concave and concave shapes of the approximate menisci, are determined by the following inequalities:

(i) if $E_{\tilde{z}}^2 > 0$ and $E_{\tilde{z}}^4 < 0$ (or $E_{\tilde{z}}^2 > 0$ and $E_{\tilde{z}}^4 > 1$), then the approximated meniscus is convex;

(ii) if $E_{\tilde{z}}^2 > 0$ and $0 < E_{\tilde{z}}^4 < 1$, then the approximated meniscus is concave-convex;

(iii) if $E_{\tilde{z}}^2 < 0$ and $0 < E_{\tilde{z}}^4 < 1$, then the approximated meniscus is convex-concave;

(iv) if $E_{\tilde{z}}^2 < 0$ and $E_{\tilde{z}}^4 < 0$ (or $E_{\tilde{z}}^2 < 0$ and $E_{\tilde{z}}^4 > 1$), then the approximated meniscus is concave;

where $E_{\tilde{z}}^4 = 1 - \frac{E_{\tilde{z}}^2}{E_{\tilde{z}}^3}$.

The achievement of the growth angle α_e of the approximated meniscus at some points in the interval $(0,1)$, (i.e. dewetting occurs) is given by the solution of the equation:

$$\frac{dT_{\tilde{z}}^3}{d\tilde{r}} = \tan\left(\frac{\pi}{2} - \alpha_e\right) \tag{2.58}$$

Because $\theta_c + \alpha_e < 180°$, the boundary condition for $\psi(\tilde{r}), \psi(\tilde{r}_c) = \frac{\pi}{2} - \alpha_e > \theta_c - \frac{\pi}{2} = \psi(1)$, shows that the growth angle can be achieved only if $\psi(\tilde{r})$ decreases, i.e. $\frac{d\psi}{d\tilde{r}} < 0$. On the other hand,

$$\frac{d\psi}{d\tilde{r}}(1) = E_{\tilde{z}}^2 \cdot \sin^2(\theta_c) \text{ and } \frac{d^2T_{\tilde{z}}^3}{d\tilde{r}^2}(1) = E_{\tilde{z}}^2.$$

Hence, if $\psi(\tilde{r})$ decreases then $\frac{d^2T_{\tilde{z}}^3}{d\tilde{r}^2}(1) = E_{\tilde{z}}^2 < 0$, and the approximate meniscus must be concave in the neighbourhood of $\tilde{r}_a = 1$. For this reason, special attention is paid on the convex-concave ("S" shape), and concave meniscus shapes. Moreover, the inequality $E_{\tilde{z}}^2 > 0$ which appears in both cases, gives the values of *La* that lead to a concave meniscus at 1:

$$La > \frac{B_{\tilde{z}}^2}{A_{\tilde{z}}^2} = \cos\theta_c + Bo\left[\tilde{H}_a - \left(\tilde{l} + \tilde{h}\right)\right]. \tag{2.59}$$

The inequality (2.59) states that the gas pressure difference must be larger than the hydrostatic pressure plus a term which depends on the capillary parameters.

For certain values of *La*, the growth angle can be achieved twice in the case of a convex-concave approximated meniscus (Eq. (2.58)) has two solutions), and once in the case of a concave approximated meniscus (Eq. (2.58)) has one solution). These values of *La* are given by the following statements (for details see [Braescu 2008]):

Statement 2.4: The set of *La* values for which the growth angle α_e can be achieved once on the approximated meniscus, is defined by the inequality:

$$F_{\tilde{z}}^{1}=\left(A_{\tilde{z}}^{1}-\frac{\cos\alpha_e}{\sin\alpha_e}\right)\left[\frac{1}{2}E_{\tilde{z}}^{3}-E_{\tilde{z}}^{2}+A_{\tilde{z}}^{1}-\frac{\cos\alpha_e}{\sin\alpha_e}\right]<0 \tag{2.60}$$

Statement 2.5: The set of La values for which, on the approximated meniscus, the growth angle α_e can be achieved twice in the interval $(0,1)$ is defined by the following inequalities:

$$\begin{aligned}
&F_{\tilde{z}}^{2}=\left(E_{\tilde{z}}^{2}\right)^{2}-2E_{\tilde{z}}^{3}\left(A_{\tilde{z}}^{1}-\frac{\cos\alpha_e}{\sin\alpha_e}\right)>0,\\
&F_{\tilde{z}}^{3}=\frac{A_{\tilde{z}}^{1}-\dfrac{\cos\alpha_e}{\sin\alpha_e}}{E_{\tilde{z}}^{3}}>0,\\
&F_{\tilde{z}}^{4}=\frac{F_{\tilde{z}}^{1}}{F_{\tilde{z}}^{3}}>0,\\
&F_{\tilde{z}}^{5}=\frac{E_{\tilde{z}}^{2}}{E_{\tilde{z}}^{3}}\in(0,1).
\end{aligned} \tag{2.61}$$

Statement 2.6: For $\theta_c+\alpha_e<180°$:

(i). If the real meniscus is concave at $\tilde{r}_a=1$, then $La>Bo\left[\tilde{H}_a-\left(\tilde{l}+\tilde{h}\right)\right]+\cos\theta_c$;

(ii). If the real meniscus is convex at the triple point $\tilde{r}_c$ where the growth angle is achieved, then $La<Bo\left(\tilde{H}_a-\tilde{l}\right)-\cos\alpha_e$.

Inequalities (i) and (ii) define the interval La_I for which dewetted Bridgman is feasible with a convex-concave meniscus ("S" shape). Moreover they show that the value $La_{(\text{concave})}$ for which the meniscus is concave can be deduced from the pressure difference values $La_{(\text{convex-concave})}$ for which the meniscus has the "S" shape.

The range La_I can be refined by using the approximation $\psi_T(\tilde{r})$ of the function $\psi(\tilde{r})$, and the growth angle achievement condition on the approximate meniscus $\tilde{z}_T(\tilde{r})$:

Statement 2.7: A refined range La^{Approx} of the interval La_I, for which dewetted Bridgman with convex-concave meniscus is feasible and the growth angle is achieved, is determined by the following inequalities:

i) $\quad Bo\left[\tilde{H}_a-\left(\tilde{l}+\tilde{h}\right)\right]+\cos\theta_c<La<Bo\left(\tilde{H}_a-\tilde{l}\right)-\cos\alpha_e,$

ii) $$F_{\tilde{z}}^{1}\left(La\right)=\left(A_{\tilde{z}}^{1}-\frac{\cos\alpha_e}{\sin\alpha_e}\right)\left[\frac{1}{2}E_{\tilde{z}}^{3}-E_{\tilde{z}}^{2}+A_{\tilde{z}}^{1}-\frac{\cos\alpha_e}{\sin\alpha_e}\right]<0,$$

iii) $$Bo\left(\tilde{H}_a-\tilde{l}\right)-\frac{\cos\alpha_e}{\tilde{r}_1\left(La\right)}>La,$$

where $\tilde{r}_1\left(La\right)$ represents the real root of the equation $\frac{1}{2}E_{\tilde{z}}^{3}\left(\tilde{r}-1\right)^2+E_{\tilde{z}}^{2}\left(\tilde{r}-1\right)+A_{\tilde{z}}^{1}-\frac{\cos\alpha_e}{\sin\alpha_e}=0$, and belongs to the interval $\left(0,\ 1\right)$ [Braescu 2008].

Inequalities (i) are related to the shape of the meniscus: concave at 1 and convex later. The second inequality (ii) expresses that the growth angle α_e is achieved once on the approximated meniscus. Inequality (iii) indicates that in $\tilde{r}_1\left(La\right)$ the approximated meniscus is convex.

Further, numerical results are presented by solving the problem (2.50) - (2.51) for *InSb* crystals grown under normal gravity conditions by the dewetted Bridgman process, similar to those reported in dimensional form in [Balint 2008-2], [Braescu 2008].

Inequalities (i)-(ii), from Statement 2.7, give the *La* range $\left[50.419;51.69\right]$. Through inequality (iii) it is refined to $La^{Approx}=\left[50.419;51.662\right]$ which represents the range of the Laplace number for which dewetted Bridgman with a convex-concave meniscus is possible and where the growth angle is achieved. Integrating numerically the system (2.50)-(2.51) for different values of the *La* from the refined range La^{Approx}, gives $La^{Real}=\left[50.792;51.531\right]$ which represents the real range of the pressure difference which gives a convex-concave real meniscus with two achievements of the growth angle (see Fig. 2.15).

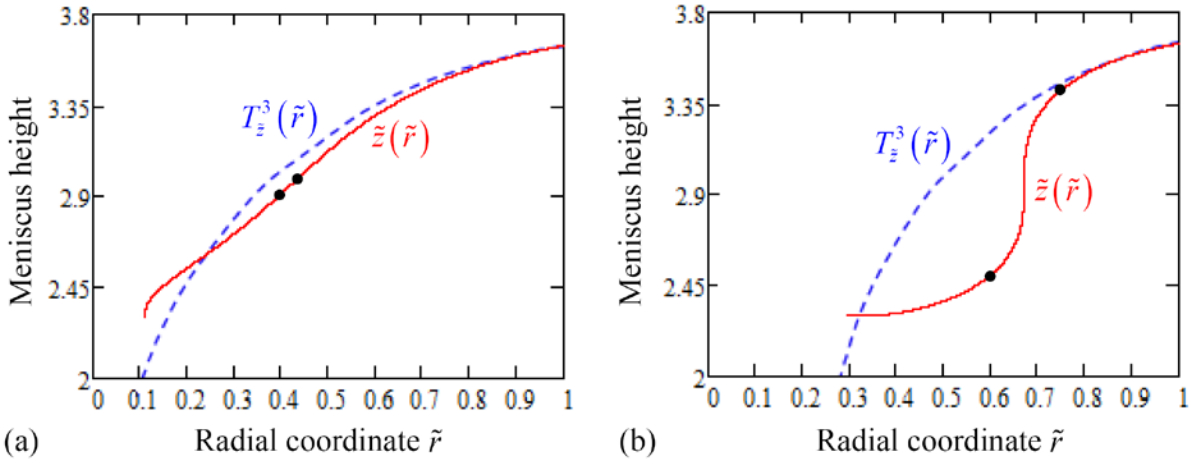

Figure 2.15 Approximated menisci $T_{\tilde{z}}^3(\tilde{r})$ (dashed line) and real (numerical) convex-concave menisci $\tilde{z}(\tilde{r})$ corresponding to $La = 50.792$ (a) and $La = 51.531$ (b) for *InSb*, $\tilde{H}_a = 14.545$. The places where the growth angle ($\frac{\pi}{2} - \alpha_e = 1.13446$ rad) is achieved are shown by the black dots.

If $La^{\text{Real}} \geq 51.532$ then the real meniscus is concave and the growth angle is achieved only once, as can be seen in the Fig. 2.16.

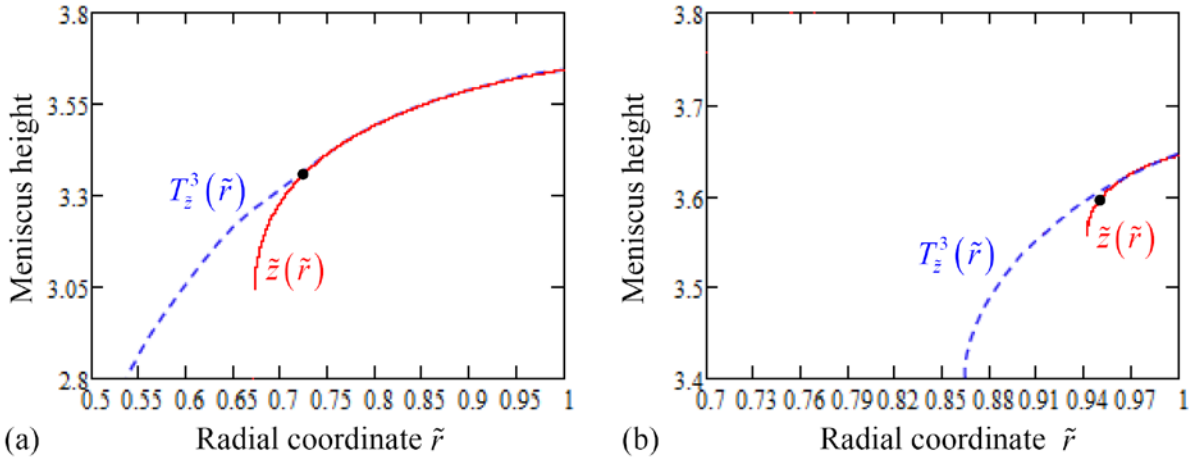

Figure 2.16 Approximated menisci $T_{\tilde{z}}^3(\tilde{r})$ (dashed line) and real (numerical) concave menisci $\tilde{z}(\tilde{r})$ corresponding to $La = 51.532$ (a) and $La = 60$ (b) for *InSb*, $\tilde{H}_a = 14.545$. The places where the growth angle ($\frac{\pi}{2} - \alpha_e = 1.13446$ rad) is achieved are shown by the black dots.

These figures show that the approximated meniscus given by the Taylor polynomial of third degree $T_{\tilde{z}}^3(\tilde{r})$ is accurate only in the neighborhood of $\tilde{r}_a = 1$.

Case $\theta_c + \alpha_e \geq 180°$

Similarly, using the Taylor polynomial of the third degree, $T_{\tilde{z}}^3(\tilde{r})$ which approximate the function $\tilde{z} = \tilde{z}(\tilde{r})$ in the neighborhood of 1, given by (2.53), qualitative results were obtained in the case $\theta_c + \alpha_e \geq 180°$.

The approximated meniscus shape is given by the sign of the second derivative $\frac{d^2T_{\tilde{z}}^3}{d\tilde{r}^2}$ and hence, the inequalities presented in Statement 2.3 are also valid for this case. The condition of the growth angle achievement led to different results from those obtained in the case $\theta_c + \alpha_e < 180°$. It was already shown that the achievement of the growth angle α_e at some points in the interval $(0;1)$ is given by the solution of the equation $\frac{dT_{\tilde{z}}^3}{d\tilde{r}} = \tan\left(\frac{\pi}{2} - \alpha_e\right)$.

As $\theta_c + \alpha_e \geq 180°$, the boundary condition for $\psi(\tilde{r})$ shows that the growth angle can be achieved only if $\psi(\tilde{r})$ decreases from $\theta_c - \frac{\pi}{2}$ to $\frac{\pi}{2} - \alpha_e$, i.e. $\frac{d\psi}{d\tilde{r}} > 0$. On the other hand, from Eqs. (2.50) :

$$\frac{d\psi}{d\tilde{r}}(1) = \left[Bo\left(\tilde{H}_a - \tilde{z}(1)\right) - La\right] \cdot \frac{1}{\cos\psi(1)} - \frac{1}{\tilde{r}} \cdot \tan\psi(1),$$

and using the boundary conditions $\tilde{z}(1) = \tilde{l} + \tilde{h}, \ \psi(1) = \theta_c - \frac{\pi}{2}$, gives:

$$\frac{d\psi}{d\tilde{r}}(1) = \frac{1}{\sin\theta_c}\left[Bo\left[\tilde{H}_a - \left(\tilde{l} + \tilde{h}\right)\right] - La + \cos\theta_c\right]. \tag{2.62}$$

As $\frac{d\psi}{d\tilde{r}}(1) > 0$, the following inequality for the pressure difference is obtained:

$$La < Bo\left[\tilde{H}_a - \left(\tilde{l} + \tilde{h}\right)\right] + \cos\theta_c \tag{2.63}$$

for which the growth angle can be achieved.

This inequality gives information about the meniscus shape at $\tilde{r}_a = 1$. Because $\frac{d^2\tilde{z}}{d\tilde{r}^2}(1) = \frac{1}{\cos^2\psi(1)}\frac{d\psi}{d\tilde{r}}(1)$ it is obtained that $\frac{d^2\tilde{z}}{d\tilde{r}^2} > 0$ in the neighbourhood of 1, which means that, the growth angle can be achieved if the meniscus is convex in the neighbourhood of 1. Then, for a pressure difference which satisfies the inequality (2.63) the meniscus is convex in the neighbourhood of 1 (this includes globally convex or concave-convex menisci), and the growth angle can be achieved. Thus, the following statements can be given:

Statement 2.8: If the values of *La* verifies the inequality $La < Bo\left[\tilde{H}_a - \left(\tilde{l} + \tilde{h}\right)\right] + \cos\theta_c$, then the real meniscus is convex at the point $\tilde{r} = \tilde{r}_a = 1$.

Statement 2.9: For $\theta_c + \alpha_e \geq \pi$:

(i) If the real meniscus is convex at 1, then $La < Bo\left[\tilde{H}_a - \left(\tilde{l} + \tilde{h}\right)\right] + \cos\theta_c$;

(ii) If the real meniscus is concave at the triple point $\tilde{r}_c$ where the growth angle is achieved, then $La > Bo\left(\tilde{H}_a - \tilde{l}\right) - \frac{1}{\tilde{r}_c}\cos\alpha_e$.

These analytical results prove that when *La* increases the meniscus height increases too and hence, the Taylor polynomial approximations can give accurate results only very close to the crucible wall. The problem (2.50) - (2.51) was solved numerically for *InSb* crystals, for different values of *La* which satisfies relation (2.63), i.e. $La < 48.594$ and the results are presented in Figure 2.17.

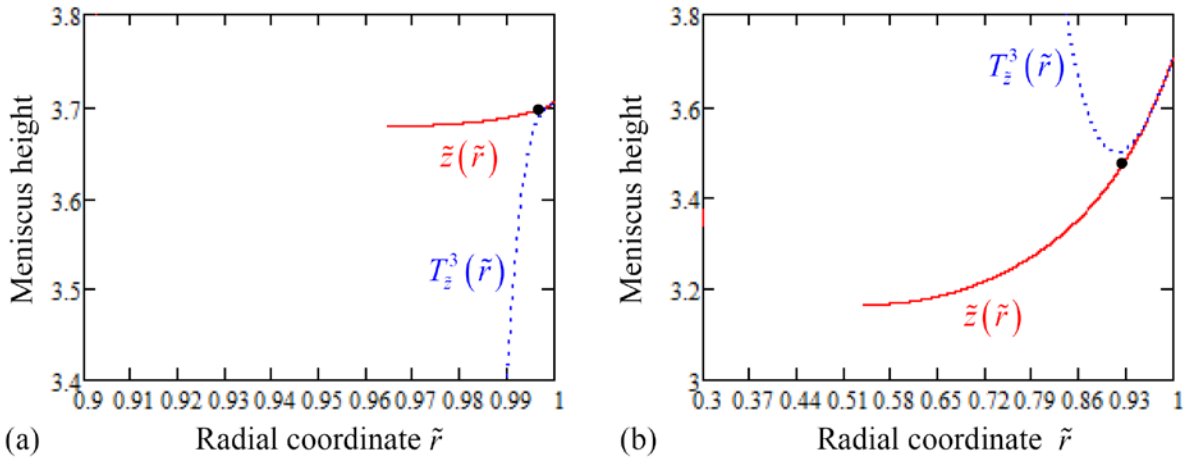

Figure 2.17: Approximated menisci $T_{\tilde{z}}^3(\tilde{r})$ (dotted line) and real (numerical) convex menisci $\tilde{z}(\tilde{r})$ corresponding to $La = 20$ (a) and $La = 48.5$ (b) for *InSb*, $\tilde{H}_a = 14.545$. The places where the growth angle ($\frac{\pi}{2} - \alpha_e = 1.13446$ rad) is achieved are shown by the black dots.

On the numerical illustrations presented in Figure 2.17 it can be seen that the Taylor polynomial approximation has a limited utility in the case $\theta_c + \alpha_e \geq \pi$.

Therefore, for finding *La* limits corresponding to a certain un-approximated meniscus shape, for which the growth angle is achieved, other mathematical tools must be used, especially in the case $\theta_c + \alpha_e \geq \pi$.

2.2.2.2. Qualitative studies on the meniscus shape without approximation

Case $\theta_c + \alpha_e \geq \pi$

As was shown in the previous section, when $\theta_c + \alpha_e \geq \pi$, the meniscus height increases if the *La* increases, hence the Taylor polynomial approximations cannot generally be used, this being an opposite behaviour to the previous case $\theta_c + \alpha_e < \pi$ where increasing *La* leads to a decrease of the meniscus. Then, to study qualitatively the meniscus shape as function of the Laplace number, only the properties obtained from the problem (2.50)-(2.51) and the growth angle criterion are used.

Therefore, the following theorem can be stated [Braescu 2009-2]:

Theorem 2.1: If the *meniscus is globally convex* and the function $\tilde{z}(\tilde{r})$ is strictly increasing on $[\tilde{r}_c, 1]$ and verifies the boundary value problem (2.50)-(2.51) and (2.52), then for a given non-dimensional gap thickness $\tilde{e} \in (0, 1)$, $\tilde{e} = 1 - \tilde{r}_c$, the Laplace number satisfies the inequalities:

$$\begin{aligned} -\frac{\theta_c + \alpha_e - \pi}{\tilde{e}} \sin\alpha_e + \frac{1}{1-\tilde{e}} \cos\theta_c + Bo\left[\tilde{H}_a - \left(\tilde{l} + \tilde{h}\right)\right] < La \\ < -\frac{\theta_c + \alpha_e - \pi}{\tilde{e}} \sin\theta_c - \cos\alpha_e + Bo\left[\tilde{H}_a - \tilde{l}\right] \end{aligned} \tag{2.64}$$

and the meniscus height $\tilde{h}$ satisfies:

$$\tilde{e} \tan\left(\frac{\pi}{2} - \alpha_e\right) < \tilde{h} < \tilde{e} \tan\left(\theta_c - \frac{\pi}{2}\right). \tag{2.65}$$

Proof: Applying the Lagrange mean value theorem for the function $\psi(\tilde{r})$, it is found that there exist $\tilde{r}_1 \in (\tilde{r}_c, 1) = (1 - \tilde{e}, 1)$ such that the following equality holds:

$$\left.\frac{d\psi}{d\tilde{r}}\right|_{\tilde{r}=\tilde{r}_1} = \frac{\psi(1) - \psi(\tilde{r}_c)}{1 - \tilde{r}_c}. \tag{2.66}$$

As $\psi(\tilde{r}_1)$ verifies $\left.\frac{d\psi}{d\tilde{r}}\right|_{\tilde{r}=\tilde{r}_1} = \frac{1}{\cos\psi(\tilde{r}_1)}\left\{Bo\left[\tilde{H}_a - \tilde{z}(\tilde{r}_1)\right] - La - \frac{1}{\tilde{r}_1}\sin\psi(\tilde{r}_1)\right\}$ and from the boundary conditions $\psi(1) = \theta_c - \frac{\pi}{2}$, $\psi(\tilde{r}_c) = \frac{\pi}{2} - \alpha_e$ and relation (2.66) results

$$La = Bo\left[\tilde{H}_a - \tilde{z}(\tilde{r}_1)\right] - \frac{1}{\tilde{r}_1}\sin\psi(\tilde{r}_1) - \frac{\theta_c + \alpha_e - \pi}{\tilde{e}}\cos\psi(\tilde{r}_1). \tag{2.67}$$

Because $\frac{d^2\tilde{z}}{d\tilde{r}^2} > 0$ for any $\tilde{r} \in [\tilde{r}_c, 1]$, the functions $\frac{d\tilde{z}}{d\tilde{r}}$ and $\psi(\tilde{r})$ are strictly increasing on $[\tilde{r}_c, 1]$ the following inequalities are satisfied:

i) $\psi(\tilde{r}_c) \le \psi(\tilde{r}_1) \le \psi(1)$ which is equivalent to $\frac{\pi}{2} - \alpha_e \le \psi(\tilde{r}_1) \le \theta_c - \frac{\pi}{2}$,

ii) $\sin\left(\frac{\pi}{2} - \alpha_e\right) \le \sin\psi(\tilde{r}_1) \le \sin\left(\theta_c - \frac{\pi}{2}\right)$,

iii) $\cos\left(\theta_c - \frac{\pi}{2}\right) \le \cos\psi(\tilde{r}_1) \le \cos\left(\frac{\pi}{2} - \alpha_e\right)$

leading to $\tilde{l} \le \left.\frac{d\tilde{z}}{d\tilde{r}}\right|_{\tilde{r}=\tilde{r}_1} \le \tilde{l} + \tilde{h}$.

Turning now to the relation (2.67) and taking into account these inequalities leads to the inequalities (2.64) for *La*.

In order to find the inequality for the meniscus height, the Lagrange mean value theorem for the function $\tilde{z}(\tilde{r})$ is applied and gives that there exist $\tilde{r}_2 \in (\tilde{r}_c, 1)$ such that

$$\left.\frac{d\tilde{z}}{d\tilde{r}}\right|_{\tilde{r}=\tilde{r}_2} = \frac{\tilde{z}(1) - \tilde{z}(\tilde{r}_c)}{1 - \tilde{r}_c}. \tag{2.68}$$

As $\tilde{z}(1) = \tilde{l} + \tilde{h}$ and $\tilde{z}(\tilde{r}_c) = \tilde{l}$ the relation (2.68) becomes

$$\left.\frac{d\tilde{z}}{d\tilde{r}}\right|_{\tilde{r}=\tilde{r}_2} = \frac{\tilde{h}}{\tilde{e}}. \tag{2.69}$$

Knowing that the functions $\frac{d\tilde{z}}{d\tilde{r}}$ and $\psi(\tilde{r})$ are strictly increasing on $[\tilde{r}_c, 1]$ the following inequalities are satisfied:

i) $\psi\left(\tilde{r}_c\right) \le \psi\left(\tilde{r}_2\right) \le \psi(1)$ which is equivalent to $\frac{\pi}{2} - \alpha_e \le \psi\left(\tilde{r}_2\right) \le \theta_c - \frac{\pi}{2}$

ii) $\tan\left(\frac{\pi}{2} - \alpha_e\right) \le \tan\psi\left(\tilde{r}_2\right) \le \tan\left(\theta_c - \frac{\pi}{2}\right)$

From the first equation of the system (2.50) results $\left.\frac{d\tilde{z}}{d\tilde{r}}\right|_{\tilde{r}=\tilde{r}_2} = \tan\psi\left(\tilde{r}_2\right)$ which replaced in (2.69) gives $\tan\psi\left(\tilde{r}_2\right) = \frac{\tilde{h}}{\tilde{e}}$. Then, inequality ii) becomes $\tan\left(\frac{\pi}{2} - \alpha_e\right) \le \frac{\tilde{h}}{\tilde{e}} \le \tan\left(\theta_c - \frac{\pi}{2}\right)$ which is equivalent to (2.65). ■

Similar studies to those presented in [Braescu 2009-2] and [Braescu 2010-1] were developed in order to obtain inequalities for concave-convex and convexo-concave menisci, and the results are presented here as statements.

Statement 2.10: If the *meniscus is concave-convex* and the function $\tilde{z}\left(\tilde{r}\right)$ is strictly increasing on $\left[\tilde{r}_c, 1\right]$ and verifies the boundary value problem (2.50)-(2.51), then for a given non-dimensional gap thickness $\tilde{e} \in (0, 1)$, $\tilde{e} = 1 - \tilde{r}_c$, the Laplace number satisfies the inequalities:

$$Bo\left[\tilde{H}_a - \left(\tilde{l} + \tilde{h}\right)\right] + \frac{1}{1-\tilde{e}}\cos\theta_c < La < Bo\left[\tilde{H}_a - \left(\tilde{l} + \tilde{h}\right)\right] + \cos\theta_c . \qquad (2.70)$$

Statement 2.11: If the *meniscus is convex-concave* and the function $\tilde{z}\left(\tilde{r}\right)$ is strictly increasing on $\left[\tilde{r}_c, 1\right]$ and verifies the boundary value problem (2.50)-(2.51), then for a given non-dimensional gap thickness $\tilde{e} \in (0, 1)$, $\tilde{e} = 1 - \tilde{r}_c$, the Laplace number satisfies the inequalities:

$$Bo\left[\tilde{H}_a - \left(\tilde{l} + \tilde{h}\right)\right] + \cos\theta_c < La < Bo\left(\tilde{H}_a - \tilde{l}\right) - \cos\alpha_e . \qquad (2.71)$$

Numerical results obtained by solving the problem (2.50) - (2.51) for *InSb* crystals grown on the ground by the dewetted Bridgman in the case of high apparent wetting angle (i.e. gas pollution case $\theta_c + \alpha_e = 165^\circ + 25^\circ > 180^\circ$) prove that, if the pressure difference satisfies the inequality (2.63), i.e. $La < 48.594$, then the meniscus is globally convex (see Fig. 2.18) or concave-convex (see Fig. 2.19; it is difficult to see this shape on the figure, but this can be seen in numerical results) and the growth angle is achieved once.

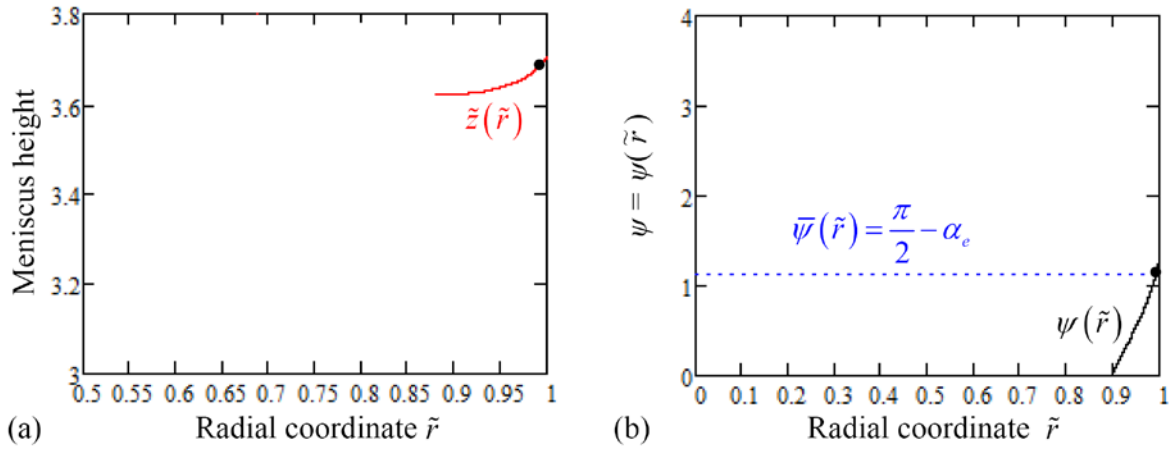

Figure 2.18 Meniscus shape $\tilde{z}(\tilde{r})$ and meniscus angle $\psi(\tilde{r})$ corresponding to $La = 40$ and $\theta_c + \alpha_e = 165^\circ + 25^\circ > \pi$ for *InSb*, $\tilde{H}_a = 14.545$. The place where the growth angle $(\frac{\pi}{2} - \alpha_e = 1.13446$ rad) is achieved is shown by the black dot.

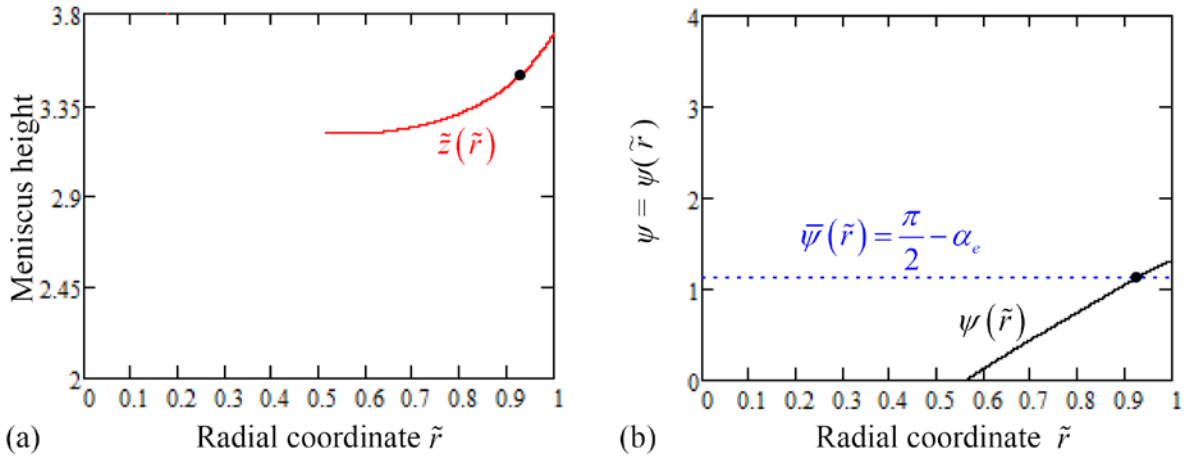

Figure 2.19 Meniscus shape $\tilde{z}(\tilde{r})$ and meniscus angle $\psi(\tilde{r})$ corresponding to $La = 48.3$ and $\theta_c + \alpha_e = 165^\circ + 25^\circ > \pi$ for *InSb*, $\tilde{H}_a = 14.545$. The place where the growth angle $(\frac{\pi}{2} - \alpha_e = 1.13446$ rad) is achieved is shown by the black dot.

In conclusion, for a convex-concave meniscus, the growth angle can be achieved (the crystal can be obtained) if inequalities (2.71) are satisfied. It is not sure if this achievement always takes place; this depends on the material and process parameters.

Numerical results obtained by solving the problem (2.50)-(2.51) for *InSb* crystals grown on the ground by the dewetted Bridgman in the case of $\theta_c + \alpha_e = 165^\circ + 25^\circ > \pi$, show that if $La = 49.5$ and $1 > \sqrt{\frac{1}{Bo} \cdot \sin\theta_c} = 0.238$, then the meniscus is convex-concave and the growth angle is achieved on the convex part of the meniscus (see Fig. 2.20).

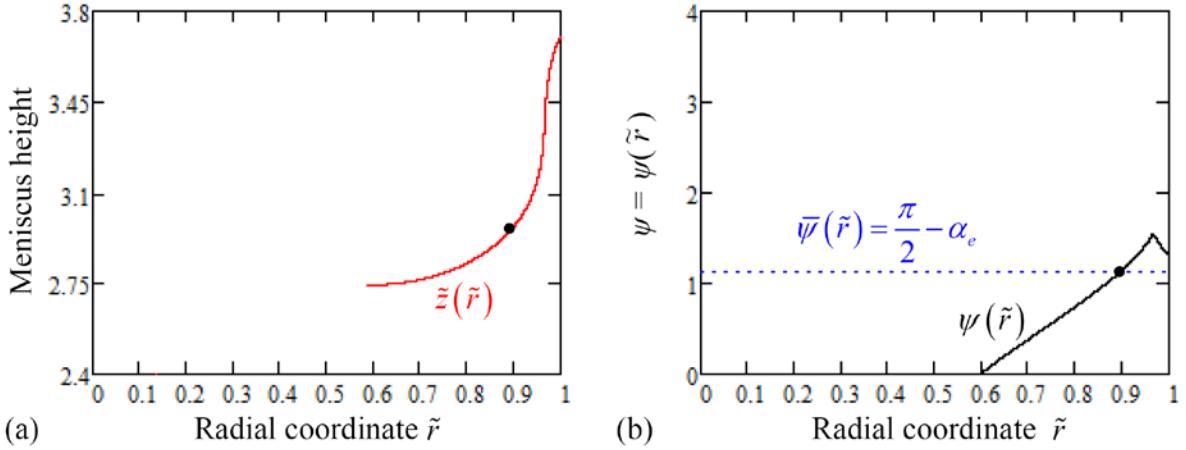

Figure 2.20 Convex-concave meniscus shape $\tilde{z}(\tilde{r})$ and meniscus angle $\psi(\tilde{r})$ corresponding to $La = 49.5$ and $\theta_c + \alpha_e = 165^\circ + 25^\circ > \pi$ for *InSb*, $\tilde{H}_a = 14.545$. The place where the growth angle ($\frac{\pi}{2} - \alpha_e = 1.13446$ rad) is achieved is shown by the black dot.

For the globally concave meniscus $\frac{d\psi}{d\tilde{r}} < 0$, and hence the function $\psi(\tilde{r})$ decreases on the interval $(0; 1)$; because $\frac{\pi}{2} - \alpha_e < \theta_c - \frac{\pi}{2}$ the growth angle cannot be achieved on the globally concave meniscus. Numerical results show that for $La = 60$ the meniscus is globally concave and the growth angle is not achieved (Fig. 2.21).

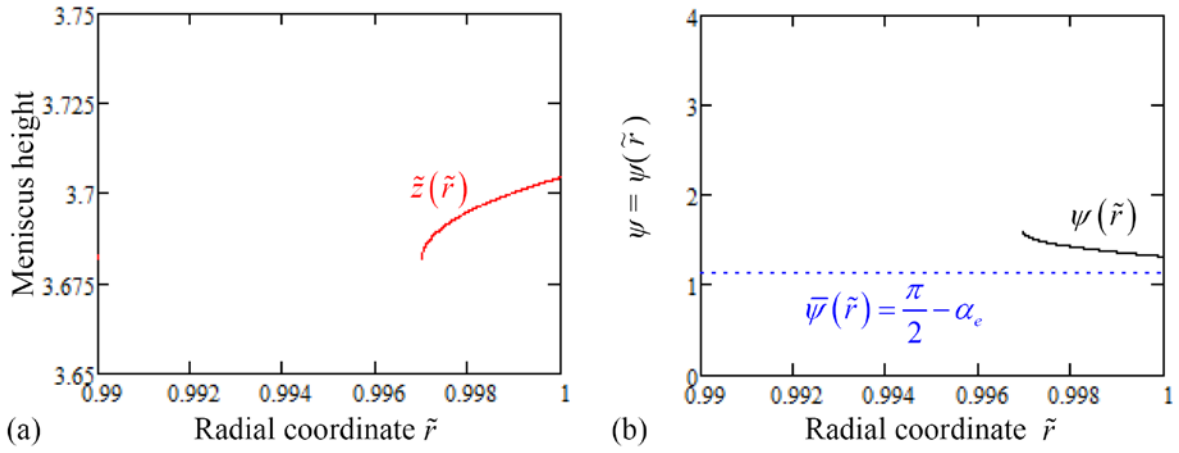

Figure 2.21 Globally concave meniscus shape $\tilde{z}(\tilde{r})$ and meniscus angle $\psi(\tilde{r})$ corresponding to $La = 60$ and $\theta_c + \alpha_e = 165^\circ + 25^\circ > \pi$ for *InSb*, $\tilde{H}_a = 14.545$. The growth angle ($\frac{\pi}{2} - \alpha_e = 1.13446$ rad) cannot be achieved.

Case $\theta_c + \alpha_e < \pi$

Similarly to the case $\theta_c + \alpha_e \geq \pi$, qualitative study of the meniscus shape as function of the Laplace number was performed using only the properties obtained from the problem (2.50)-(2.51) and the growth angle criterion, leading to the following theorem:

Theorem 2.2: If the *meniscus is globally concave* and the function $\tilde{z}(\tilde{r})$ is strictly increasing on $[\tilde{r}_c, 1]$ and verifies the boundary value problem (2.50)-(2.51) and (2.52), then for a given non-dimensional gap thickness $\tilde{e} \in (0, 1)$, $\tilde{e} = 1 - \tilde{r}_c$, the Laplace number, satisfies the inequalities:

$$-\frac{\theta_c + \alpha_e - \pi}{\tilde{e}} \sin\alpha_e - \frac{1}{1-\tilde{e}} \cos\alpha_e + Bo\left[\tilde{H}_a - \left(\tilde{l} + \tilde{h}\right)\right] < La < -\frac{\theta_c + \alpha_e - \pi}{\tilde{e}} \sin\theta_c + \cos\theta_c + Bo\left[\tilde{H}_a - \tilde{l}\right] \tag{2.72}$$

and the meniscus height $\tilde{h}$ satisfies:

$$\tilde{e} \tan\left(\theta_c - \frac{\pi}{2}\right) < \tilde{h} < \tilde{e} \tan\left(\frac{\pi}{2} - \alpha_e\right) \tag{2.73}$$

Proof: Applying the Lagrange mean value theorem for the function $\psi(\tilde{r})$, it is found that there exist $\tilde{r}_1 \in (\tilde{r}_c, 1) = (1-\tilde{e}, 1)$ such that the following equality holds:

$$\left.\frac{d\psi}{d\tilde{r}}\right|_{\tilde{r}=\tilde{r}_1} = \frac{\psi(1)-\psi(\tilde{r}_c)}{1-\tilde{r}_c} \tag{2.74}$$

As $\psi(\tilde{r}_1)$ verifies $\left.\frac{d\psi}{d\tilde{r}}\right|_{\tilde{r}=\tilde{r}_1} = \frac{1}{\cos\psi(\tilde{r}_1)}\left\{Bo\left[\tilde{H}_a - \tilde{z}(\tilde{r}_1)\right] - La - \frac{1}{\tilde{r}_1}\sin\psi(\tilde{r}_1)\right\}$ and from the boundary conditions $\psi(1) = \theta_c - \frac{\pi}{2}$, $\psi(\tilde{r}_c) = \frac{\pi}{2} - \alpha_e$ and relation (2.74) results

$$La = Bo\left[\tilde{H}_a - \tilde{z}(\tilde{r}_1)\right] - \frac{1}{\tilde{r}_1}\sin\psi(\tilde{r}_1) - \frac{\theta_c + \alpha_e - \pi}{\tilde{e}}\cos\psi(\tilde{r}_1) \tag{2.75}$$

As $\frac{d^2\tilde{z}}{d\tilde{r}^2} < 0$ for any $\tilde{r} \in [\tilde{r}_c, 1]$, the functions $\frac{d\tilde{z}}{d\tilde{r}}$ and $\psi(\tilde{r})$ are strictly decreasing on $[\tilde{r}_c, 1]$ the following inequalities are satisfied:

i) $\psi(\tilde{r}_c) \geq \psi(\tilde{r}_1) \geq \psi(1)$ which is equivalent to $\theta_c - \frac{\pi}{2} \leq \psi(\tilde{r}_1) \leq \frac{\pi}{2} - \alpha_e$,

ii) $\sin\left(\theta_c - \frac{\pi}{2}\right) \leq \sin\psi(\tilde{r}_1) \leq \sin\left(\frac{\pi}{2} - \alpha_e\right)$,

iii) $\cos\left(\frac{\pi}{2} - \alpha_e\right) \leq \cos\psi(\tilde{r}_1) \leq \cos\left(\theta_c - \frac{\pi}{2}\right)$,

leading to $\tilde{l} \leq \left.\frac{d\tilde{z}}{d\tilde{r}}\right|_{\tilde{r}=\tilde{r}_1} \leq \tilde{l} + \tilde{h}$.

Turning now to the relation (2.75) and taking into account these inequalities leads to the inequalities (2.72) for *La*.

In order to find the inequality for the meniscus height, the Lagrange mean value theorem for the function $\tilde{z}(\tilde{r})$ is applied and gives that there exist $\tilde{r}_2 \in (\tilde{r}_c, 1)$ such that

$$\left.\frac{d\tilde{z}}{d\tilde{r}}\right|_{\tilde{r}=\tilde{r}_2} = \frac{\tilde{z}(1)-\tilde{z}(\tilde{r}_c)}{1-\tilde{r}_c}. \tag{2.76}$$

Since $\tilde{z}(1) = \tilde{l} + \tilde{h}$ and $\tilde{z}(\tilde{r}_c) = \tilde{l}$ the relation (2.76) becomes

$$\left.\frac{d\tilde{z}}{d\tilde{r}}\right|_{\tilde{r}=\tilde{r}_2} = \frac{\tilde{h}}{\tilde{e}}. \tag{2.77}$$

As the functions $\frac{d\tilde{z}}{d\tilde{r}}$ and $\psi(\tilde{r})$ are strictly decreasing on $[\tilde{r}_c, 1]$ the following inequalities are satisfied:

i) $\psi(\tilde{r}_c) \geq \psi(\tilde{r}_1) \geq \psi(1)$ that is equivalent to $\theta_c - \frac{\pi}{2} \leq \psi(\tilde{r}_1) \leq \frac{\pi}{2} - \alpha_e$,

ii) $\tan\left(\theta_c - \frac{\pi}{2}\right) \leq \tan\psi(\tilde{r}_2) \leq \tan\left(\frac{\pi}{2} - \alpha_e\right)$

From the first equation of the system (2.50) results $\left.\frac{d\tilde{z}}{d\tilde{r}}\right|_{\tilde{r}=\tilde{r}_2} = \tan\psi(\tilde{r}_2)$ which introduced in (2.77) gives $\tan\psi(\tilde{r}_2) = \frac{\tilde{h}}{\tilde{e}}$. Then, inequality ii) becomes $\tan\left(\theta_c - \frac{\pi}{2}\right) \leq \frac{\tilde{h}}{\tilde{e}} \leq \tan\left(\frac{\pi}{2} - \alpha_e\right)$ that is equivalent to (2.73). ■

The above analytical and numerical studies of meniscus shapes were performed in order to derive the conditions which allow dewetting and lead to a crystal with a constant radius on the ground. The obtained results can be summarized as in Table 2.2. The results are useful for in situ control of the process and show the importance of a careful calculation of the meniscus shapes for the optimization of a stable dewetted Bridgman growth.

La	$-\infty$	0	$Bo\left[\tilde{H}_a - (\tilde{l} + \tilde{h})\right] + \cos\theta_c$	$La < Bo(\tilde{H}_a - \tilde{l}) - \cos\alpha_e$	$+\infty$
Meniscus shape	convex		convex-concave		concave
	the growth angle is not achieved		the growth angle is achieved twice		the growth angle is achieved once

(a) $\theta_c + \alpha_e < 180°$

La	$-\infty$	0	$Bo\left[\tilde{H}_a - (\tilde{l} + \tilde{h})\right] + \cos\theta_c$	$La < Bo(\tilde{H}_a - \tilde{l}) - \cos\alpha_e$	$+\infty$
Meniscus shape	convex or concave-convex		convex-concave		concave
	the growth angle is achieved once and just on the convex part				the growth angle is not achieved

(b) $\theta_c + \alpha_e > 180°$

Table 2.2 Meniscus shapes and the achievement of the growth angle depending on the pressure difference in normal gravity conditions.

2.3. Parametric study: crystal-crucible gap dependence on the main parameters to enhance the dewetting occurrence

The main purpose of this parametric study is to describe the dependency of the crystal-crucible gap thickness on the relevant parameters which enhance the dewetting occurrence under normal gravity conditions. The detailed parametric study was already published in [Epure 2010-2] and here only a summary will be given.

As already mentioned in the previous sections, on the physical point of view, the dewetting phenomenon is governed by the Young-Laplace equation through the Bond, *Bo*, (that for a given material depends only on the crucible radius) and Laplace, *La*, (that in a given configuration depends on the applied pressure difference) non-dimensional numbers. Other main parameters identified to enhance the dewetting occurrence are the crucible material through the wetting properties of the melt (Chapter 1).

In order to analyze the dependence of the crystal-crucible gap ($\tilde{e} = 1 - \tilde{r}_c$) on the *Bo* and *La* numbers, a parametric study has been performed for the two different cases: $\theta_c + \alpha_e < 180°$ and $\theta_c + \alpha_e > 180°$, as they lead to different behavior.

The limit regimes of the main parameters ($La \to -\infty$, $La \to +\infty$, $Bo \to +\infty$, $Bo \to 0$) which enhance the dewetting occurrence were first studied. Then the problem (2.50)-(2.51) has been solved numerically using the adaptive 4^{th} order Runge-Kutta method (details about this numerical method can be found in [Braescu 2010-2]) for various values of the parameters. Once all the solutions of the system are computed, the evolution of the crystal-crucible gap thickness can be presented as graphical plots.

The dependence of the non-dimensional gap thickness on the Laplace number is illustrated for different values of *Bo*, in the cases $\theta_c + \alpha_e < 180°$ (Figure 2.22) and $\theta_c + \alpha_e > 180°$ (Figure 2.23).

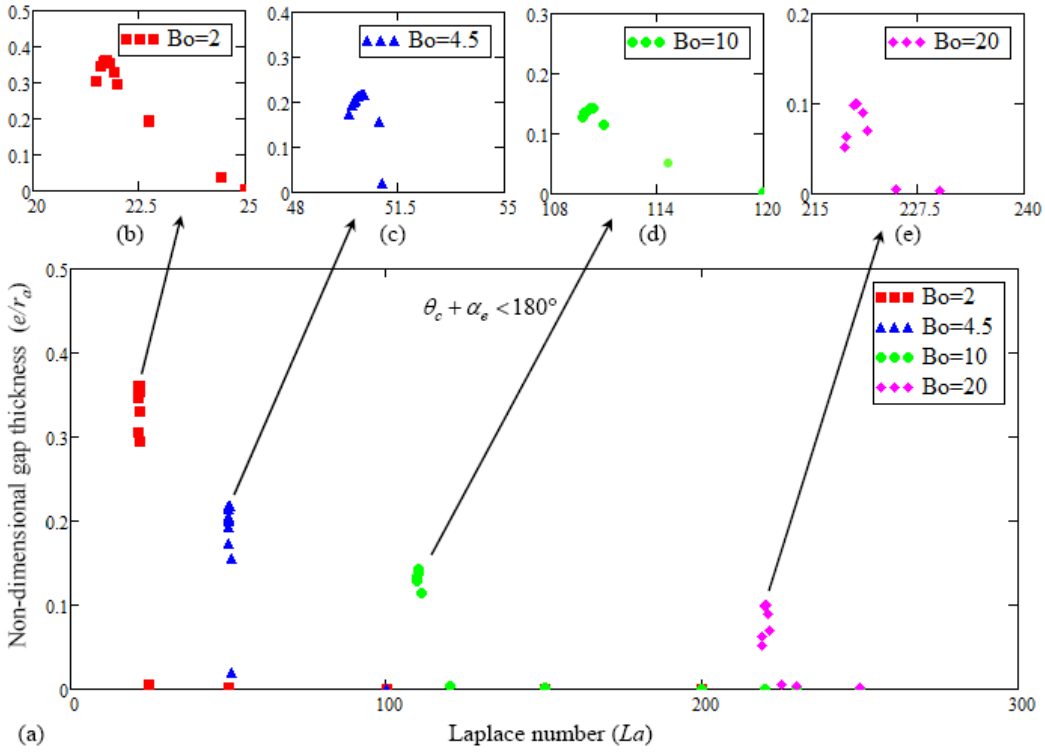

Figure 2.22 Non-dimensional gap thickness as function of Laplace number for the case $\theta_c + \alpha_e = 150° + 25° < 180°$.

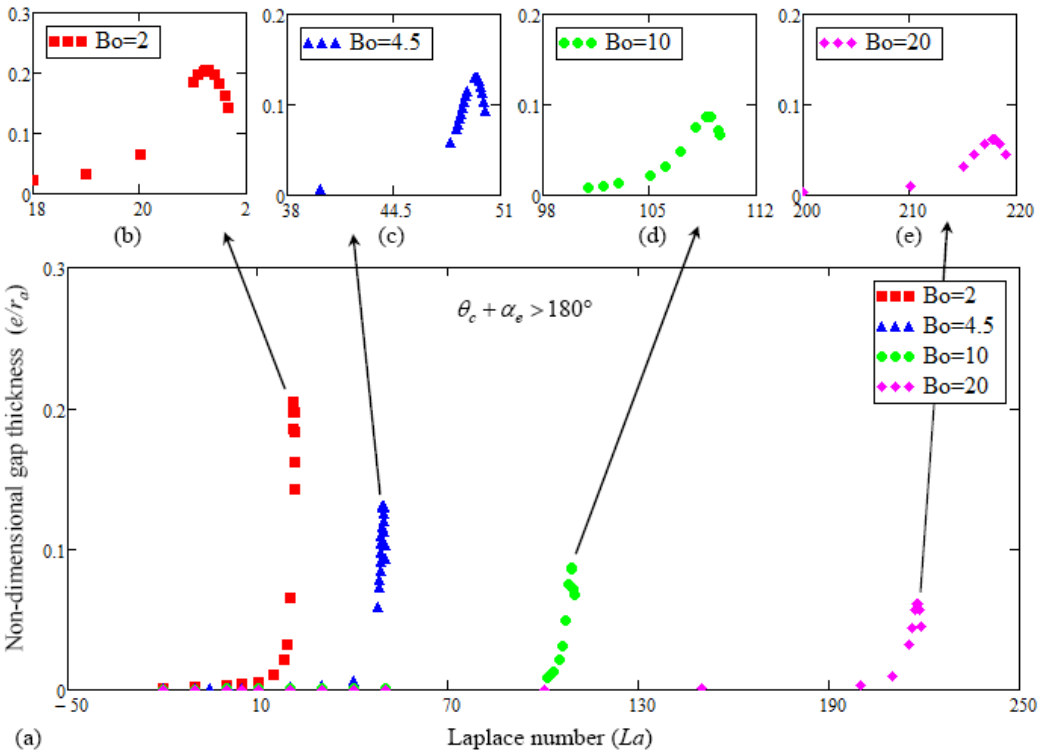

Figure 2.23 Non-dimensional gap thickness as function of Laplace number for the case $\theta_c + \alpha_e = 165° + 25° > 180°$.

The dependence of the dimensionless gap thickness on the Bond number, for different values of *La*, in the cases $\theta_c + \alpha_e < 180°$ and respectively $\theta_c + \alpha_e > 180°$ is shown in Figures 2.24 and 2.25.

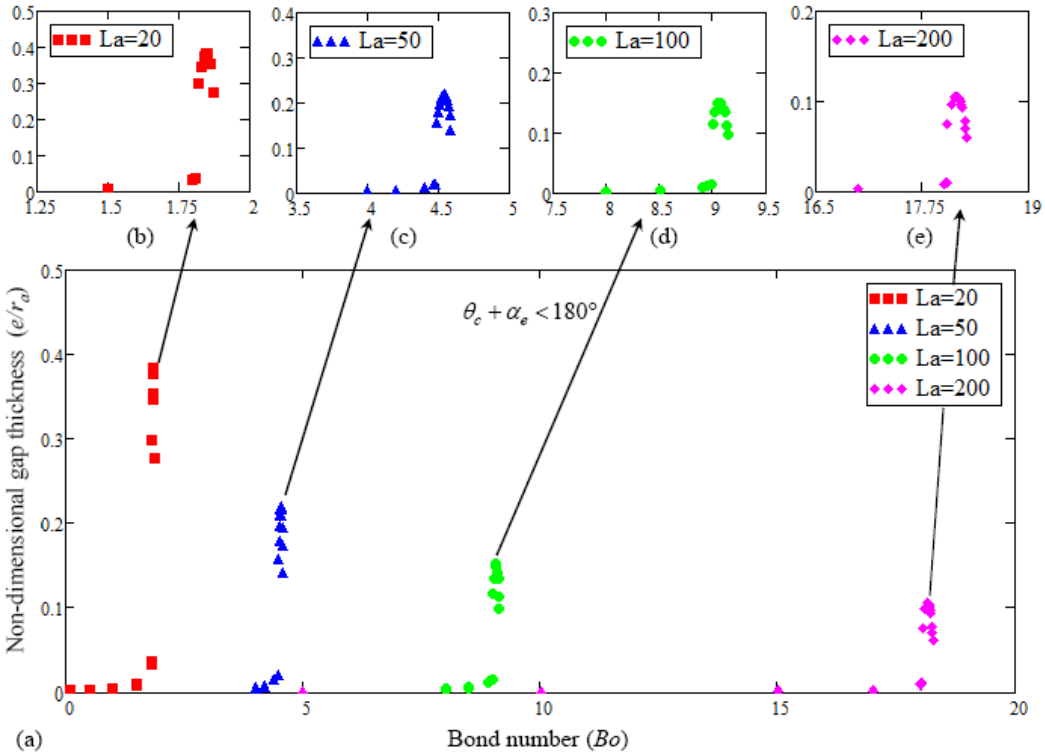

Figure 2.24 Non-dimensional gap thickness as function of Bond number for the case $\theta_c + \alpha_e = 150° + 25° < 180°$.

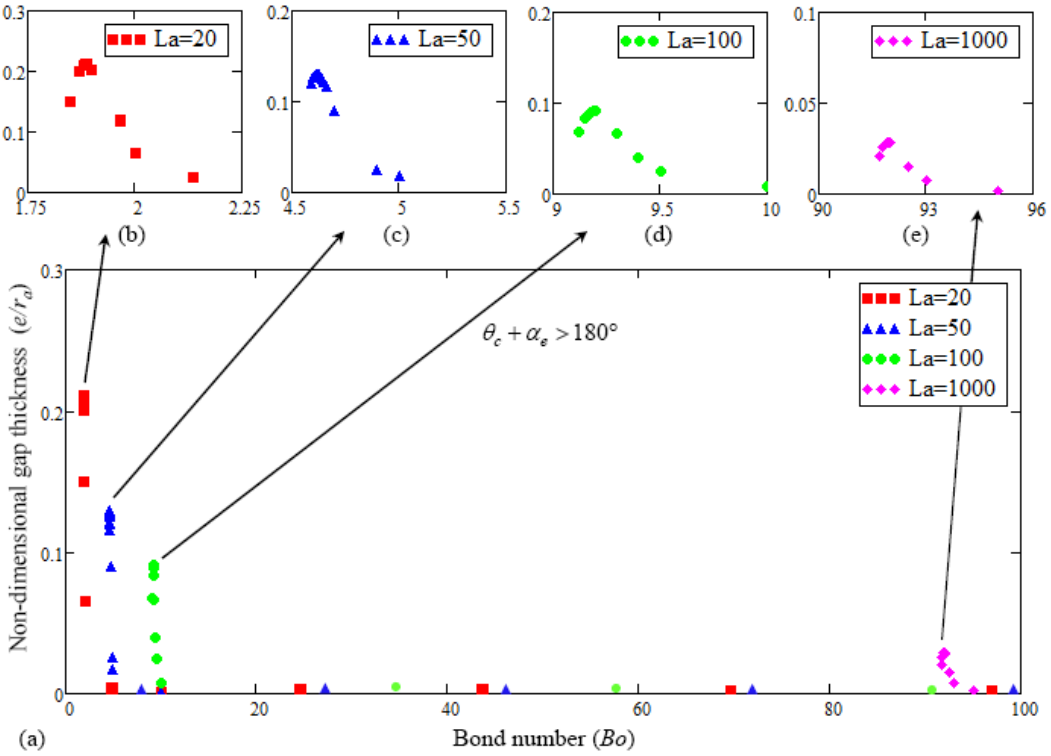

Figure 2.25 Non-dimensional gap thickness as function of Bond number for the case $\theta_c + \alpha_e = 165° + 25° > 180°$.

The illustrated dependences of the non-dimensional gap thickness on the Laplace and Bond numbers shows that the crystal-crucible gap thickness presents a maximum when the *Bo* and *La* numbers are varied. This maximum decreases when the *Bo* and *La* increase. For both cases $\theta_c + \alpha_e < 180°$ and $\theta_c + \alpha_e > 180°$, the maximum of the gap thickness appears in the cases where the growth angle is achieved on a convex part of the meniscus, which, for stability reasons, is the preferred practical case (see Chapter 4).

As for growing crystals with a uniform radius, it is important that small variations of the relevant parameters have a low effect on the crystal-crucible gap thickness, the maximal values are preferred for practical growth of crystals.

In Figure 2.26 the maximum crystal-crucible gap thickness is plotted versus the contact angle and respectively the growth angle.

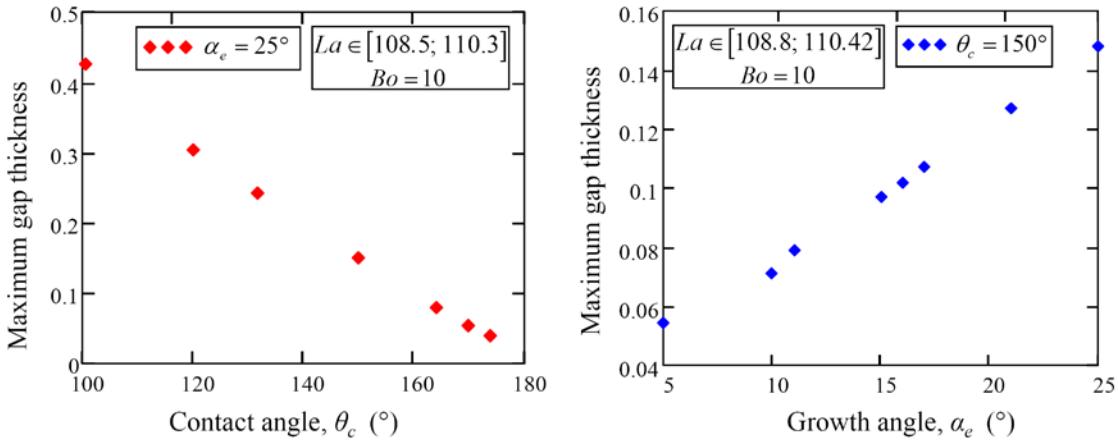

Figure 2.26 Non-dimensional maximum gap thickness as function of the contact angle and growth angle.

It can be easily seen, on the graphical plot, that an increase of the contact angle leads to a decrease of the maximum gap thickness and increasing the growth angle the maximum gap thickness will increase too.

After that, the Laplace number corresponding to the maximum value of the crystal-crucible gap thickness was plotted versus the Bond number for a fixed growth angle $\alpha_e = 25°$ and different values of the contact angle which leads to the cases $\theta_c + \alpha_e < 180°$, $\theta_c + \alpha_e = 180°$ and $\theta_c + \alpha_e > 180°$ (see Figure 2.27).

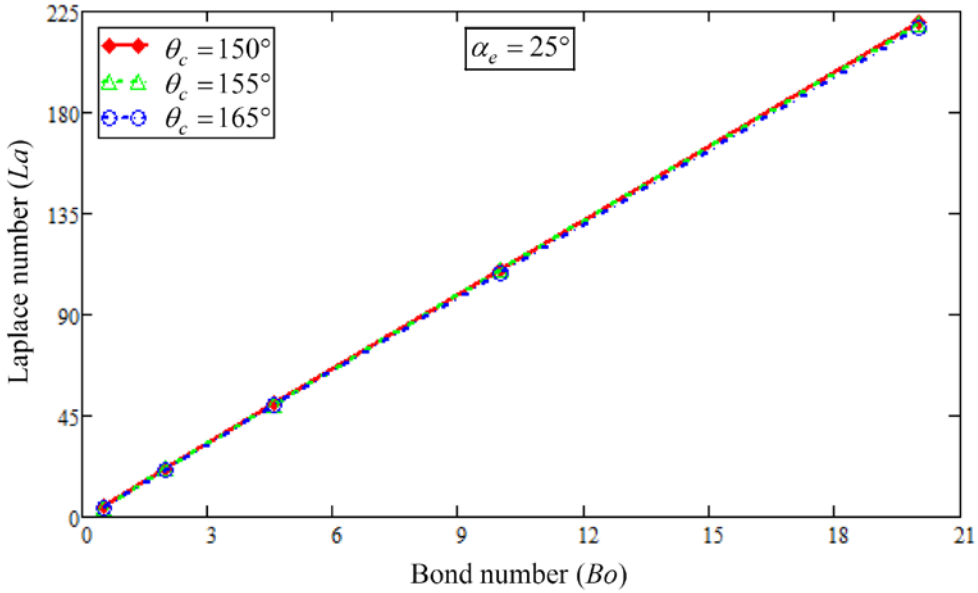

Figure 2.27 Optimal Laplace number corresponding to the maximum gap thickness, versus Bond number.

The variation of the optimal *La* number with *Bo* number is shown to be linear and practically independent of the value of the wetting and growth angles ([Epure 2010-2]). This means that *La* (the applied gas pressure) does not change practically for various crucible materials. In fact, the main effect of the gas pressure difference is to counteract the hydrostatic pressure which is almost independent of the contact angle.

These results give a good understanding of the physics of the dewetting process and are basic reference tools for the practical crystal growers working with a given equipment and given materials and also for the equipment designers.

Summary

In this chapter the capillarity problems involved in the dewetted Bridgman crystal growth process have been studied. Firstly, some concepts from differential geometry were presented, such as principal normal curvatures of a surface and mean normal curvature at a point on a surface. These "tools" were useful for the mathematical formulation of the capillarity problem governed by the Young-Laplace equation that further allows computing the shape of the liquid meniscus.

In order to understand better the dewetted Bridgman process, analytical and numerical studies of the axi-symmetric Young-Laplace equation describing the meniscus shape were performed and the dependence of the meniscus shape and size on the pressure difference was established in zero and normal gravity conditions. In zero gravity conditions, the analytical study led to the formulas of the non-dimensional crystal-crucible gap thickness that are in agreement with those already reported in a dimensional form. In the case of normal gravity conditions, the qualitative studies for the meniscus shape were performed using Taylor polynomial approximation and also, without approximation using the properties obtained from Young-Laplace equation and the growth angle criterion.

A parametric study has been performed in order to establish the dependence of the crystal-crucible gap thickness on the relevant parameters of the dewetted Bridgman process.

CHAPTER 3: Contributions to the modeling of heat transfer problems and melt – solid interface displacement

As the main objective of the present work is the stability analysis of the process, the necessary conditions in order to get a stable dewetting, i.e., a stable crystal diameter, or gap thickness must be found.

From the existent stability analysis of the dewetted Bridgman process and as will be shown in Chapter 4, it appears that under zero gravity conditions, the only one variable parameter is the crystal-crucible gap thickness, because the heat transfer cannot change the pressure in the meniscus and thus has no effect on the meniscus shape and then on the gap [Duffar 2010]. Then only one equation is needed, which is the Young-Laplace equation.

On the contrary, for experiments performed on the Earth, melting or solidification change the liquid height, then the hydrostatic pressure acting on the meniscus, and then the crystal-crucible gap thickness. In this case the gap thickness and the solid-liquid interface position are variables of the problem and hence two equations are needed, namely the Young-Laplace equation and the heat balance at the solid-liquid interface.

Therefore, this chapter deals with contributions to the modeling of heat transfer problems in the case of dewetted Bridgman crystal growth; these results being useful for the development of the dynamical stability analysis of the process. In order to establish analytical expressions of the temperature distribution and the temperature gradients in the melt and in the solid, the non-stationary one-dimensional heat transfer equation will be considered by neglecting the latent heat release (quasi steady-state approximation). The melt-solid interface displacement differential equation will be also derived from the thermal energy balance at the level of the interface and relevant properties concerning the solution $\tilde{l}(\tilde{t})$ of this equation will be established (Propositions 3.1 to 3.3). The novelty is that the solution $\tilde{l}(\tilde{t})$ will be found solving numerically by adaptive Runge-Kutta method its ordinary non-autonomous differential equation in which the analytical formulas of the temperature gradients will be used. Then, these results will be compared to those obtained by solving, by finite element method, the non-stationary one-dimensional heat transfer equation in which the latent heat release is considered. Here these

studies are presented in the non-dimensional form, the dimensional form being reported in [Balint 2011-2].

Further, for studying the effect of the crystal-crucible gap on the curvature of the solid-liquid interface for a set of non-dimensional parameters representative of classical semiconductor crystal growth, an analytical expression of the interface deflection, based on simple heat fluxes arguments will be found. In order to check the accuracy of the obtained analytical formula and to identify its limits of validity, the heat transfer equation will be solved numerically in 2D axial symmetry, stationary case, using the finite element code COMSOL Multiphysics 3.3. Parts of these results are published in [Epure 2008].

3.1. Analytical expression of the temperature distribution and temperature gradients in the melt and in the solid

In order to find analytical expressions of the temperature distribution and the temperature gradients in the melt and in the solid, the non-stationary one-dimensional heat transfer equation was considered in the following assumptions: the gap thickness does not influence the axial heat transfer; the temperature is constant in a cross-section of the melt-solid system; the lateral crucible wall is adiabatic; and the thermal flux is axial. The latent heat release is neglected which corresponds to cases where the latent heat flux due to solidification is low compared to the general heat flux in the sample (i.e., $\Lambda \cdot v_i << \lambda_l \cdot G_l$). This often happens in real Bridgman growth where the growth rate is generally small (of the order of 10^{-6} m/s or lower) for assuring a good crystal quality. For example, in the case of *InSb* crystals (see Table 1.1), $\Lambda \cdot v_i << \lambda_l \cdot G_l$ gives $1.3 \cdot 10^3 << 4.615 \cdot 10^5$.

The configuration under study is presented in Figure 3.1 in which z - coordinate with respect to the body frame zOr; d' - bottom coordinate of the ampoule with respect to the laboratory frame $z'O'r'$, at $t = 0$; H_a, H_f - the ampoule and furnace height; T_c^f, T_h^f - the cold respectively hot temperature of the furnace.

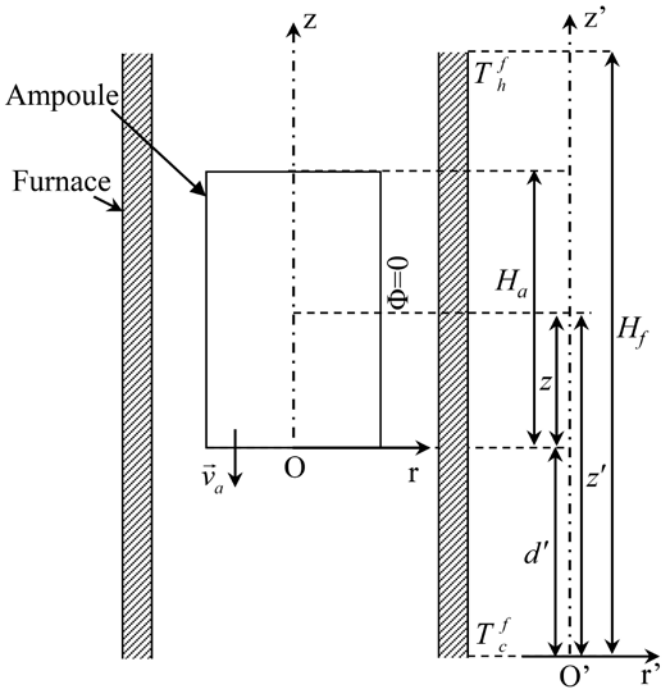

Figure 3.1 Configuration under study.

For the analytical study the following hypothesis are established:

- the ampoule moves with a constant rate v_a in a furnace having a constant vertical temperature gradient k (Figure 3.1).
- at every moment of time, the temperatures at the hot and at the cold sides of the ampoule are equal to the temperatures of the furnace at the corresponding levels.
- the temperature in the solid T_s, and in the liquid T_l are time dependent and at the initial moment of time, when the pulling starts, are linear functions of the axial coordinate *z*.
- the gap thickness does not influence the heat transfer because the radial heat fluxes are negligible.

Under the established hypothesis, during the solidification process, the temperature distribution $T_l = T_l(z,t)$ in the melt must satisfy the non-stationary one dimensional heat transfer equation ([Balint 2011-2])

$$\frac{\partial T_l}{\partial t} - D_{th}^l \frac{\partial^2 T_l}{\partial z^2} = 0, \text{ with } l \le z \le H_a \text{ and } D_{th}^l = \frac{\lambda_l}{c_l \rho_l} \tag{3.1}$$

with the corresponding boundary conditions:

$$T_l(H_a, t) = T_h^a(t) = T_c^f + k(d' + H_a - v_a t) \tag{3.2}$$

$$T_l(l, t) = T_m \tag{3.3}$$

and the initial condition in the melt:

$$\begin{aligned} T_l(z,0) &= \left[\frac{T_c^f - T_m}{H_a - l} + k\frac{d' + H_a}{H_a - l}\right] z + \frac{H_a T_m - l T_c^f}{H_a - l} - kl\frac{d' + H_a}{H_a - l} \\ &= \frac{T_h^a(0) - T_m}{H_a - l} z + \frac{H_a T_m - l T_h^a(0)}{H_a - l} \end{aligned} \tag{3.4}$$

The non-dimensional form of the heat transfer equation is done by setting:

$$\tilde{z} = \frac{z}{r_a}, \tilde{l} = \frac{l}{r_a}, \tilde{T}_l = \frac{T_l - T_c^f}{T_m - T_c^f}. \tag{3.5}$$

In order to non-dimensionalize *t*, it is necessary to multiply it by some combination of constants that has units of s^{-1}. Thus, for considering our set of equations $\tilde{t} = \frac{D_{th}^l}{r_a^2} t$ is chosen as the non-dimensional time variable [Fu 1981]. Physically speaking, this means that the time scale is given by the time needed for the diffusion of heat in a distance r_a. The order of magnitude is $\frac{r_a^2}{D_{th}^l}$ (which in the case of *InSb* is 5.6 s).

Replacing the dimensional variables in the initial equation (3.1) with their non-dimensional equivalents (3.5) the following non-dimensional heat transfer equation is obtained:

$$\frac{\partial \tilde{T}_l}{\partial \tilde{t}} - \frac{\partial^2 \tilde{T}_l}{\partial \tilde{z}^2} = 0, \text{ with } \tilde{l} \le \tilde{z} \le \tilde{H}_a \tag{3.6}$$

For the boundary conditions, using the same rules of non-dimensionalization gives:

$$\tilde{d}' = \frac{d'}{r_a},\ \tilde{H}_a = \frac{H_a}{r_a},\ \tilde{k} = \frac{r_a}{\left(\tilde{T}_m - \tilde{T}_c^f\right)}k,\ Pe^l = \frac{r_a}{D_{th}^l}v_a,$$
$$\tilde{T}_m = \frac{T_m - T_c^f}{T_m - T_c^f} = 1,\ \tilde{T}_c^f = \frac{T_c^f - T_c^f}{T_m - T_c^f} = 0. \tag{3.7}$$

Therefore, the non-dimensionalized boundary conditions can be written as:

$$\tilde{T}_l\left(\tilde{H}_a, \tilde{t}\right) = \tilde{T}_h^a\left(\tilde{t}\right) = \tilde{T}_c^f + \tilde{k}\left(\tilde{d}' + \tilde{H}_a - Pe^l \cdot \tilde{t}\right), \tag{3.8}$$

$$\tilde{T}_l\left(\tilde{l}, \tilde{t}\right) = \tilde{T}_m \tag{3.9}$$

and the initial condition

$$\begin{aligned}\tilde{T}_l\left(\tilde{z}, 0\right) &= \left[\frac{\tilde{T}_c^f - \tilde{T}_m}{\tilde{H}_a - \tilde{l}} + \tilde{k}\frac{\tilde{d}' + \tilde{H}_a}{\tilde{H}_a - \tilde{l}}\right]\tilde{z} + \frac{\tilde{H}_a\tilde{T}_m - \tilde{l}\tilde{T}_c^f}{\tilde{H}_a - \tilde{l}} - \tilde{k}\tilde{l}\,\frac{\tilde{d}' + \tilde{H}_a}{\tilde{H}_a - \tilde{l}} \\ &= \frac{\tilde{T}_h^a\left(0\right) - \tilde{T}_m}{\tilde{H}_a - \tilde{l}}\tilde{z} + \frac{\tilde{H}_a\tilde{T}_m - \tilde{l}\tilde{T}_h^a\left(0\right)}{\tilde{H}_a - \tilde{l}}.\end{aligned} \tag{3.10}$$

Similarly, the temperature distribution $T_s = T_s\left(z,t\right)$ in the solid must satisfy the non-stationary one dimensional heat transfer equation:

$$\frac{\partial T_s}{\partial t} - D_{th}^s\frac{\partial^2 T_s}{\partial z^2} = 0, \text{ with } 0 \le z \le l \text{ and } D_{th}^s = \frac{\lambda_s}{c_s\rho_s} \tag{3.11}$$

with the following boundary conditions:

$$T_s\left(l,t\right) = T_m, \tag{3.12}$$

$$T_s\left(0,t\right) = T_c^a\left(t\right) = T_c^f + k\left(d' - v_a t\right) \tag{3.13}$$

and the initial condition:

$$T_s\left(z,0\right) = \left[\frac{T_m - T_c^f}{l} - k\frac{d'}{l}\right]z + T_c^f + kd' = \frac{T_m - T_c^a\left(0\right)}{l}z + T_c^a\left(0\right) \tag{3.14}$$

Using the same rules of the non-dimensionalization as before, by setting:

$$\tilde{T}_s = \frac{T_s - T_c^f}{T_m - T_c^f} \text{ and } \tilde{t} = \frac{D_{th}^l}{r_a^2}t \tag{3.15}$$

the following non-dimensional heat transfer equation was obtained in the solid:

$$\frac{\partial \tilde{T}_s}{\partial \tilde{t}} - \tilde{D}_{th}\frac{\partial^2 \tilde{T}_s}{\partial \tilde{z}^2} = 0, \text{ with } 0 \le \tilde{z} \le \tilde{l} \text{ and } \tilde{D}_{th} = \frac{D_{th}^s}{D_{th}^l} \tag{3.16}$$

with the corresponding boundary conditions

$$\tilde{T}_s\left(\tilde{l},\tilde{t}\right)=\tilde{T}_m, \tag{3.17}$$

$$\tilde{T}_s\left(0,\tilde{t}\right)=\tilde{T}_c^a\left(\tilde{t}\right)=\tilde{T}_c^f+\tilde{k}\left(\tilde{d}'-Pe^l\cdot\tilde{t}\right) \tag{3.18}$$

and the initial condition

$$\tilde{T}_s\left(\tilde{z},0\right)=\left[\frac{\tilde{T}_m-\tilde{T}_c^f}{\tilde{l}}-\tilde{k}\frac{\tilde{d}'}{\tilde{l}}\right]\tilde{z}+\tilde{T}_c^f+\tilde{k}\tilde{d}'=\frac{\tilde{T}_m-\tilde{T}_c^a\left(0\right)}{\tilde{l}}\tilde{z}+\tilde{T}_c^a\left(0\right) \tag{3.19}$$

The significance of the non-dimensional parameters used in the previous formulas is $\tilde{t}$ - the non-dimensional moment of time; Pe^l - Péclet number for the liquid (compones velocity of heat carried by the sample by diffusion); $\tilde{l}$ - the non-dimensional interface coordinate with respect to the body frame *zOr*; $\tilde{H}_a$, $\tilde{H}_f$ - the non-dimensional ampoule and furnace height; $\tilde{T}_h^a\left(\tilde{t}\right),\tilde{T}_c^a\left(\tilde{t}\right)$ - the non-dimensional top and the bottom temperatures of the ampoule; $\tilde{T}_c^f$, $\tilde{T}_h^f$ - the non-dimensional cold respectively hot temperature of the furnace; $\tilde{T}_m$ - non-dimensional melting temperature; $\tilde{k}$ - non-dimensional temperature gradient in the furnace.

In a solidification process, the following inequalities necessarily hold:

$$0<\tilde{l}<\tilde{H}_a;\ \ \tilde{d}'+\tilde{H}_a\le\tilde{H}_f, \tag{3.20}$$

$$\tilde{T}_c^f+\tilde{k}\tilde{d}'\le\tilde{T}_m\le\tilde{T}_c^f+\tilde{k}\left(\tilde{d}'+\tilde{H}_a\right). \tag{3.21}$$

In order to obtain the analytical formula of the temperature distribution in the melt the Cauchy-Dirichlet problem

$$\begin{cases}\dfrac{\partial\tilde{T}_l}{\partial\tilde{t}}-\dfrac{\partial^2\tilde{T}_l}{\partial\tilde{z}^2}=0,\ \text{with}\ \tilde{l}\le\tilde{z}\le\tilde{H}_a\\ \tilde{T}_l\left(\tilde{H}_a,\tilde{t}\right)=\tilde{T}_h^a\left(\tilde{t}\right)=\tilde{T}_c^f+\tilde{k}\left(\tilde{d}'+\tilde{H}_a-Pe^l\cdot\tilde{t}\right)\\ \tilde{T}_l\left(\tilde{l},\tilde{t}\right)=\tilde{T}_m\end{cases} \tag{3.22}$$

in which the latent heat release was neglected (quasi steady state approximation [Tatartchenko 1993]), must be solved for $\tilde{t}$ in the range $\left[0,\tilde{t}_*\right]$ with

$$\tilde{t}_*=\frac{1}{Pe^l}\left(\tilde{d}'+\tilde{H}_a-\frac{\tilde{T}_m-\tilde{T}_c^f}{\tilde{k}}\right). \tag{3.23}$$

$\tilde{T}_l^o\left(\tilde{z},\tilde{t}\right)=A_1\left(\tilde{t}\right)\tilde{z}+B_1\left(\tilde{t}\right)$ is considered for the homogenization of the boundary conditions and then,

$$\tilde{T}_l^o\left(\tilde{H}_a,\tilde{t}\right)=\tilde{T}_h^a\left(\tilde{t}\right)=\tilde{T}_c^{\,f}+\tilde{k}\left(\tilde{d}'+\tilde{H}_a-Pe^l\cdot\tilde{t}\right)$$

$$\tilde{T}_l^o\left(\tilde{l},\tilde{t}\right)=\tilde{T}_m$$

wherefrom it results

$$\tilde{T}_l^o\left(\tilde{z},\tilde{t}\right)=\left[\frac{\tilde{T}_c^{\,f}-\tilde{T}_m}{\tilde{H}_a-\tilde{l}}+\tilde{k}\,\frac{\tilde{d}'+\tilde{H}_a-Pe^l\cdot\tilde{t}}{\tilde{H}_a-\tilde{l}}\right]\tilde{z}+\frac{\tilde{H}_a\tilde{T}_m-\tilde{l}}{\tilde{H}_a-\tilde{l}}-\tilde{k}\tilde{l}\,\frac{\tilde{d}'+\tilde{H}_a-Pe^l\cdot\tilde{t}}{\tilde{H}_a-\tilde{l}}. \tag{3.24}$$

Hence,

$$\tilde{T}_l\left(\tilde{z},\tilde{t}\right)=\overline{\tilde{T}}_l\left(\tilde{z},\tilde{t}\right)+\tilde{T}_l^o\left(\tilde{z},\tilde{t}\right) \tag{3.25}$$

and the Cauchy-Dirichlet problem becomes:

$$\begin{cases}\dfrac{\partial\overline{\tilde{T}}_l}{\partial\tilde{t}}=\dfrac{\partial^2\overline{\tilde{T}}_l}{\partial\tilde{z}^2}+\tilde{k}\cdot Pe^l\,\dfrac{\tilde{z}-\tilde{l}}{\tilde{H}_a-\tilde{l}},\ \left(\tilde{z},\tilde{t}\right)\in\left(\tilde{l},\tilde{H}_a\right)\times\left(0,\tilde{t}_*\right)\\ \overline{\tilde{T}}_l\left(\tilde{l},\tilde{t}\right)=\overline{\tilde{T}}_l\left(\tilde{H}_a,\tilde{t}\right)=0,\ \tilde{t}\in\left[0,\tilde{t}_*\right]\end{cases}. \tag{3.26}$$

In order to solve this non homogenous parabolic equation we shall look for the solution of the form:

$$\overline{\tilde{T}}_l\left(\tilde{z},\tilde{t}\right)=\sum_{n=1}^{\infty}M_n\left(\tilde{t}\right)\sin\left(\frac{n\pi}{\tilde{H}_a-\tilde{l}}\left(\tilde{z}-\tilde{l}\right)\right) \tag{3.27}$$

For $M_n\left(\tilde{t}\right)$ we arrive to the Cauchy problem:

$$M_n{}'+\left(\frac{n\pi}{\tilde{H}_a-\tilde{l}}\right)^2M_n=c_n^{(1)}\left(\tilde{t}\right), \tag{3.28}$$

$$M_n\left(0\right)=a_n^{(1)} \tag{3.29}$$

where $c_n^{(1)}$ and $a_n^{(1)}$ are the Fourier coefficients from the Fourier series of the data problem

$$\tilde{k}\cdot Pe^l\,\frac{\tilde{z}-\tilde{l}}{\tilde{H}_a-\tilde{l}}=\sum_{n=1}^{\infty}\left[c_n^{(1)}\left(\tilde{t}\right)\sin\left(\frac{n\pi}{\tilde{H}_a-\tilde{l}}\left(\tilde{z}-\tilde{l}\right)\right)\right],$$

$$\overline{\tilde{T}}_l\left(\tilde{z},0\right)=\sum_{n=1}^{\infty}\left[a_n^{(1)}\sin\left(\frac{n\pi}{\tilde{H}_a-\tilde{l}}\left(\tilde{z}-\tilde{l}\right)\right)\right],$$

hence,

$$c_n^{(1)}\left(\tilde{t}\right)=\frac{2}{\tilde{H}_a-\tilde{l}}\int_{\tilde{l}}^{\tilde{H}_a}\left[\tilde{k}\cdot Pe^{l}\,\frac{\tilde{z}-\tilde{l}}{\tilde{H}_a-\tilde{l}}\cdot\sin\left(\frac{n\pi}{\tilde{H}_a-\tilde{l}}\left(\tilde{z}-\tilde{l}\right)\right)\right]d\tilde{z} \tag{3.30}$$

$$a_n^{(1)}=\frac{2}{\tilde{H}_a-\tilde{l}}\int_{\tilde{l}}^{\tilde{H}_a}\left[\overline{\tilde{T}}_l\left(\tilde{z},0\right)\cdot\sin\left(\frac{n\pi}{\tilde{H}_a-\tilde{l}}\left(\tilde{z}-\tilde{l}\right)\right)\right]d\tilde{z} \tag{3.31}$$

Then, the solution of the Cauchy problem (3.28)-(3.29) is

$$M_n\left(\tilde{t}\right)=a_n^{(1)}e^{-\left(\frac{n\pi}{\tilde{H}_a-\tilde{l}}\right)^2\tilde{t}}+\int_0^{\tilde{t}}e^{-\left(\frac{n\pi}{\tilde{H}_a-\tilde{l}}\right)^2\left(\tilde{t}-\tau\right)}c_n^{(1)}\left(\tau\right)d\tau\,. \tag{3.32}$$

Introducing (3.32) into (3.27) the formal solution of the problem (3.26) is obtained:

$$\overline{\tilde{T}}_l\left(\tilde{z},\tilde{t}\right)=\sum_{n=1}^{\infty}\left[\left(a_n^{(1)}e^{-\left(\frac{n\pi}{\tilde{H}_a-\tilde{l}}\right)^2\tilde{t}}+\int_0^{\tilde{t}}e^{-\left(\frac{n\pi}{\tilde{H}_a-\tilde{l}}\right)^2\left(\tilde{t}-\tau\right)}c_n^{(1)}\left(\tau\right)d\tau\right)\sin\left(\frac{n\pi}{\tilde{H}_a-\tilde{l}}\left(\tilde{z}-\tilde{l}\right)\right)\right] \tag{3.33}$$

As $\tilde{T}_l\left(\tilde{z},\tilde{t}\right)$ was considered a linear function, $\overline{\tilde{T}}_l\left(\tilde{z},0\right)=0$ and then $a_n^{(1)}$ will be equal to zero and the coefficient $c_n^{(1)}\left(\tilde{t}\right)$ is computed from (3.30):

$$\begin{aligned}c_n^{(1)}\left(\tilde{t}\right)&=\frac{2}{\tilde{H}_a-\tilde{l}}\int_{\tilde{l}}^{\tilde{H}_a}\left[\tilde{k}\cdot Pe^{l}\,\frac{\tilde{z}-\tilde{l}}{\tilde{H}_a-\tilde{l}}\sin\left(\frac{n\pi}{\tilde{H}_a-\tilde{l}}\left(\tilde{z}-\tilde{l}\right)\right)\right]d\tilde{z}\\&=\frac{2\tilde{k}\cdot Pe^{l}}{\left(\tilde{H}_a-\tilde{l}\right)^2}\int_{\tilde{l}}^{\tilde{H}_a}\left[\left(\tilde{z}-\tilde{l}\right)\sin\left(\frac{n\pi}{\tilde{H}_a-\tilde{l}}\left(\tilde{z}-\tilde{l}\right)\right)\right]d\tilde{z}\\&=\frac{2\tilde{k}\cdot Pe^{l}}{\left(\tilde{H}_a-\tilde{l}\right)^2}\left[-\frac{\left(\tilde{H}_a-\tilde{l}\right)^2}{n\pi}\cdot\left(-1\right)^n\right]\\&=\frac{2\tilde{k}\cdot Pe^{l}}{n\pi}\left(-1\right)^{n+1}\end{aligned}$$

Replacing these coefficients in (3.33) gives

$$\begin{aligned}\overline{\tilde{T}}_l\left(\tilde{z},\tilde{t}\right)&=\sum_{n=1}^{\infty}\left[\left(\int_0^{\tilde{t}}\frac{2\tilde{k}\cdot Pe^l}{n\pi}(-1)^{n+1}e^{-\left(\frac{n\pi}{\tilde{H}_a-\tilde{l}}\right)^2(\tilde{t}-\tau)}d\tau\right)\sin\left(\frac{n\pi\left(\tilde{z}-\tilde{l}\right)}{\tilde{H}_a-\tilde{l}}\right)\right]\\&=\sum_{n=1}^{\infty}\left[\frac{2\tilde{k}\cdot Pe^l}{n\pi}(-1)^{n+1}\left(\left(\frac{\tilde{H}_a-\tilde{l}}{n\pi}\right)^2\left[1-e^{-\left(\frac{n\pi}{\tilde{H}_a-\tilde{l}}\right)^2\tilde{t}}\right]\right)\sin\left(\frac{n\pi\left(\tilde{z}-\tilde{l}\right)}{\tilde{H}_a-\tilde{l}}\right)\right].\\&=2\tilde{k}\cdot Pe^l\sum_{n=1}^{\infty}(-1)^{n+1}\frac{1}{n\pi}\left(\frac{\tilde{H}_a-\tilde{l}}{n\pi}\right)^2\left[1-e^{-\left(\frac{n\pi}{\tilde{H}_a-\tilde{l}}\right)^2\tilde{t}}\right]\sin\left(\frac{n\pi\left(\tilde{z}-\tilde{l}\right)}{\tilde{H}_a-\tilde{l}}\right)\end{aligned}\tag{3.34}$$

Introducing (3.34) into (3.25) the temperature distribution in the melt is obtained:

$$\begin{aligned}\tilde{T}_l\left(\tilde{z},\tilde{t}\right)&=\left[\frac{\tilde{T}_c^{\,f}-\tilde{T}_m}{\tilde{H}_a-\tilde{l}}+\tilde{k}\frac{\tilde{d}'+\tilde{H}_a-Pe^l\cdot\tilde{t}}{\tilde{H}_a-\tilde{l}}\right]\tilde{z}+\frac{\tilde{H}_a\tilde{T}_m-\tilde{l}}{\tilde{H}_a-\tilde{l}}-\tilde{k}\tilde{l}\frac{\tilde{d}'+\tilde{H}_a-Pe^l\cdot\tilde{t}}{\tilde{H}_a-\tilde{l}}\\&\quad+2\tilde{k}\cdot Pe^l\sum_{n=1}^{\infty}(-1)^{n+1}\frac{1}{n\pi}\left(\frac{\tilde{H}_a-\tilde{l}}{n\pi}\right)^2\left[1-e^{-\left(\frac{n\pi}{\tilde{H}_a-\tilde{l}}\right)^2\tilde{t}}\right]\sin\left(\frac{n\pi\left(\tilde{z}-\tilde{l}\right)}{\tilde{H}_a-\tilde{l}}\right)\\&=\frac{\tilde{T}_h^a\left(\tilde{t}\right)-\tilde{T}_m}{\tilde{H}_a-\tilde{l}}\tilde{z}+\frac{\tilde{H}_a\tilde{T}_m-\tilde{l}\tilde{T}_h^a\left(t\right)}{\tilde{H}_a-\tilde{l}}\\&\quad+2\tilde{k}\cdot Pe^l\sum_{n=1}^{\infty}(-1)^{n+1}\frac{1}{n\pi}\left(\frac{\tilde{H}_a-\tilde{l}}{n\pi}\right)^2\left[1-e^{-\left(\frac{n\pi}{\tilde{H}_a-\tilde{l}}\right)^2\tilde{t}}\right]\sin\left(\frac{n\pi\left(\tilde{z}-\tilde{l}\right)}{\tilde{H}_a-\tilde{l}}\right).\end{aligned}\tag{3.35}$$

Similarly, for finding the analytical formula for the temperature distribution in the solid, the following Cauchy-Dirichlet problem must be solved:

$$\begin{cases}\dfrac{\partial\tilde{T}_s}{\partial\tilde{t}}-\tilde{D}_{th}\dfrac{\partial^2\tilde{T}_s}{\partial\tilde{z}^2}=0,\ \text{with } 0\le\tilde{z}\le\tilde{l}\\ \tilde{T}_s\left(\tilde{l},\tilde{t}\right)=\tilde{T}_m\\ \tilde{T}_s\left(0,\tilde{t}\right)=\tilde{T}_c^a\left(\tilde{t}\right)=\tilde{T}_c^{\,f}+\tilde{k}\left(\tilde{d}'-Pe^l\cdot\tilde{t}\right)\end{cases}.\tag{3.36}$$

$\tilde{T}_s^o\left(\tilde{z},\tilde{t}\right)=A_2\left(\tilde{t}\right)\tilde{z}+B_2\left(\tilde{t}\right)$ is also considered for the homogenization of the boundary conditions and then,

$$\tilde{T}_s^o\left(\tilde{l},\tilde{t}\right)=\tilde{T}_m$$

$$\tilde{T}_s^o\left(0,\tilde{t}\right)=\tilde{T}_c^a\left(\tilde{t}\right)=\tilde{T}_c^{\,f}+\tilde{k}\left(\tilde{d}'-Pe^l\cdot\tilde{t}\right)$$

wherefrom

$$\tilde{T}_s^{\,o}\left(\tilde{z},\tilde{t}\right)=\frac{1}{\tilde{l}}\left[\tilde{T}_m-\tilde{T}_c^{\,f}-\tilde{k}\left(\tilde{d}'-Pe^l\cdot\tilde{t}\right)\right]\tilde{z}+\tilde{T}_c^{\,f}+\tilde{k}\left(\tilde{d}'-Pe^l\cdot\tilde{t}\right). \tag{3.37}$$

Hence,

$$\tilde{T}_s\left(\tilde{z},\tilde{t}\right)=\bar{\tilde{T}}_s\left(\tilde{z},\tilde{t}\right)+\tilde{T}_s^{\,o}\left(\tilde{z},\tilde{t}\right) \tag{3.38}$$

and the Cauchy-Dirichlet problem becomes:

$$\begin{cases}\dfrac{\partial\bar{\tilde{T}}_s}{\partial\tilde{t}}=\tilde{D}_{th}\dfrac{\partial^2\bar{\tilde{T}}_s}{\partial\tilde{z}^2}-\tilde{k}\cdot Pe^l\dfrac{\tilde{z}-\tilde{l}}{\tilde{l}},\ \left(\tilde{z},\tilde{t}\right)\in\left(0,\tilde{l}\right)\times\left(0,\tilde{t}_*\right)\\ \bar{\tilde{T}}_s\left(\tilde{l},\tilde{t}\right)=\bar{\tilde{T}}_s\left(0,\tilde{t}\right)=0,\ \tilde{t}\in\left[0,\tilde{t}_*\right].\end{cases} \tag{3.39}$$

Following the same procedure as before we look for a formal solution

$$\bar{\tilde{T}}_s\left(\tilde{z},\tilde{t}\right)=\sum_{n=1}^{\infty}\left[\left(a_n^{(2)}e^{-\tilde{D}_{th}\left(\frac{n\pi}{\tilde{l}}\right)^2\tilde{t}}+\int_0^{\tilde{t}}e^{-\tilde{D}_{th}\left(\frac{n\pi}{\tilde{l}}\right)^2(\tilde{t}-\tau)}c_n^{(2)}\left(\tau\right)d\tau\right)\sin\left(\frac{n\pi}{\tilde{l}}\tilde{z}\right)\right] \tag{3.40}$$

Computing the coefficients

$$\begin{aligned}c_n^{(2)}\left(\tilde{t}\right)&=\frac{2}{\tilde{l}}\int_0^{\tilde{l}}\left[-\tilde{k}\cdot Pe^l\frac{\tilde{z}-\tilde{l}}{\tilde{l}}\cdot\sin\left(\frac{n\pi}{\tilde{l}}\tilde{z}\right)\right]d\tilde{z}\\&=-\frac{2\tilde{k}\cdot Pe^l}{\tilde{l}^2}\left[-\frac{\tilde{l}^2}{n\pi}+\left(\frac{\tilde{l}}{n\pi}\right)^2\sin\left(\frac{n\pi}{\tilde{l}}\tilde{l}\right)\right]\\&=\frac{2}{n\pi}\tilde{k}\cdot Pe^l\end{aligned}$$

$a_n^{(2)}=\dfrac{2}{\tilde{l}}\displaystyle\int_0^{\tilde{l}}\left[\bar{\tilde{T}}_s\left(\tilde{z},0\right)\cdot\sin\left(\frac{n\pi}{\tilde{l}}\tilde{z}\right)\right]d\tilde{z}=0$ (as the function $\bar{\tilde{T}}_s\left(\tilde{z},0\right)=0$) lead to:

$$\begin{aligned}\bar{\tilde{T}}_s\left(\tilde{z},\tilde{t}\right)&=\sum_{n=1}^{\infty}\left[\left(\int_0^{\tilde{t}}\frac{2}{n\pi}\tilde{k}\cdot Pe^l e^{-\tilde{D}_{th}\left(\frac{n\pi}{\tilde{l}}\right)^2(\tilde{t}-\tau)}d\tau\right)\sin\left(\frac{n\pi}{\tilde{l}}\tilde{z}\right)\right]\\&=\sum_{n=1}^{\infty}\left[2\tilde{k}\cdot\frac{Pe^l}{\tilde{D}_{th}}\frac{1}{n\pi}\left(\frac{\tilde{l}}{n\pi}\right)^2\left[1-e^{-\tilde{D}_{th}\left(\frac{n\pi}{\tilde{l}}\right)^2\tilde{t}}\right]\sin\left(\frac{n\pi}{\tilde{l}}\tilde{z}\right)\right]\\&=2\tilde{k}\cdot\frac{Pe^l}{\tilde{D}_{th}}\sum_{n=1}^{\infty}\frac{1}{n\pi}\left(\frac{\tilde{l}}{n\pi}\right)^2\left[1-e^{-\tilde{D}_{th}\left(\frac{n\pi}{\tilde{l}}\right)^2\tilde{t}}\right]\sin\left(\frac{n\pi}{\tilde{l}}\tilde{z}\right).\end{aligned} \tag{3.41}$$

By introducing (3.41) into (3.38) the temperature distribution in the solid is obtained:

$$\tilde{T}_s\left(\tilde{z},\tilde{t}\right)=\frac{1}{\tilde{l}}\left[\tilde{T}_m-\tilde{T}_c^{\,f}-\tilde{k}\left(\tilde{d}'-Pe^l\cdot\tilde{t}\right)\right]\tilde{z}+\tilde{T}_c^{\,f}+\tilde{k}\left(\tilde{d}'-Pe^l\cdot\tilde{t}\right)$$
$$+2\tilde{k}\cdot\frac{Pe^l}{\tilde{D}_{th}}\sum_{n=1}^{\infty}\frac{1}{n\pi}\left(\frac{\tilde{l}}{n\pi}\right)^2\left[1-e^{-\tilde{D}_{th}\left(\frac{n\pi}{\tilde{l}}\right)^2\tilde{t}}\right]\sin\left(\frac{n\pi}{\tilde{l}}\tilde{z}\right) \tag{3.42}$$
$$=\frac{\tilde{T}_m-\tilde{T}_c^{\,a}\left(\tilde{t}\right)}{\tilde{l}}\tilde{z}+\tilde{T}_c^{\,a}\left(\tilde{t}\right)+2\tilde{k}\cdot\frac{Pe^l}{\tilde{D}_{th}}\sum_{n=1}^{\infty}\frac{1}{n\pi}\left(\frac{\tilde{l}}{n\pi}\right)^2\left[1-e^{-\tilde{D}_{th}\left(\frac{n\pi}{\tilde{l}}\right)^2\tilde{t}}\right]\sin\left(\frac{n\pi}{\tilde{l}}\tilde{z}\right).$$

Therefore, the temperature gradients in the melt and in the solid, at the level of the interface are given by:

$$\tilde{G}_l\left(\tilde{l},\tilde{t}\right)=\left.\frac{\partial\tilde{T}_l}{\partial\tilde{z}}\right|_{\tilde{z}=\tilde{l}}=\frac{\tilde{T}_h^{\,a}\left(\tilde{t}\right)-\tilde{T}_m}{\tilde{H}_a-\tilde{l}}+2\tilde{k}\left(\tilde{H}_a-\tilde{l}\right)\cdot Pe^l\sum_{n=1}^{\infty}(-1)^{n+1}\frac{1}{(n\pi)^2}\left[1-e^{-\left(\frac{n\pi}{\tilde{H}_a-\tilde{l}}\right)^2\tilde{t}}\right]$$
$$=\frac{\tilde{T}_c^{\,f}-\tilde{T}_m}{\tilde{H}_a-\tilde{l}}+\tilde{k}\frac{\tilde{d}'+\tilde{H}_a-Pe^l\cdot\tilde{t}}{\tilde{H}_a-\tilde{l}}+2\tilde{k}\left(\tilde{H}_a-\tilde{l}\right)\cdot Pe^l\sum_{n=1}^{\infty}(-1)^{n+1}\frac{1}{(n\pi)^2}\left[1-e^{-\left(\frac{n\pi}{\tilde{H}_a-\tilde{l}}\right)^2\tilde{t}}\right], \tag{3.43}$$

$$\tilde{G}_s\left(\tilde{l},\tilde{t}\right)=\left.\frac{\partial\tilde{T}_s}{\partial\tilde{z}}\right|_{\tilde{z}=\tilde{l}}=\frac{\tilde{T}_m-\tilde{T}_c^{\,a}\left(\tilde{t}\right)}{\tilde{l}}+2\tilde{k}\tilde{l}\cdot\frac{Pe^l}{\tilde{D}_{th}}\sum_{n=1}^{\infty}(-1)^{n}\frac{1}{(n\pi)^2}\left[1-e^{-\tilde{D}_{th}\left(\frac{n\pi}{\tilde{l}}\right)^2\tilde{t}}\right]$$
$$=\frac{1}{\tilde{l}}\left[\tilde{T}_m-1-\tilde{k}\left(\tilde{d}'-Pe^l\cdot\tilde{t}\right)\right]+2\tilde{k}\tilde{l}\cdot\frac{Pe^l}{\tilde{D}_{th}}\sum_{n=1}^{\infty}(-1)^{n}\frac{1}{(n\pi)^2}\left[1-e^{-\tilde{D}_{th}\left(\frac{n\pi}{\tilde{l}}\right)^2\tilde{t}}\right]. \tag{3.44}$$

3.2. Melt-solid interface displacement equation

In the previous section it has been considered, and shown that it is the case in crystal growth process, that the latent heat release is not considered because it is negligible compared to the general heat flux in the sample.

However there is a small difference between the heat flux in the solid and in the liquid, and then during the solidification process, the equation which describes the melt-solid interface displacement is obtained from the thermal energy balance at the level of the interface:

$$\frac{d\tilde{l}}{d\tilde{t}} = -St\left[\tilde{G}_l\left(\tilde{l},\tilde{t}\right) - \tilde{\lambda}\tilde{G}_s\left(\tilde{l},\tilde{t}\right)\right] \tag{3.45}$$

where: $St = \dfrac{c_l\left(T_m - T_c^f\right)}{\Lambda}$ - the Stefan number [Ayasoufi 2009], $\tilde{\lambda} = \dfrac{\lambda_s}{\lambda_l}$ - the non-dimensional thermal conductivity, $\tilde{G}_l\left(\tilde{l},\tilde{t}\right)$ and $\tilde{G}_s\left(\tilde{l},\tilde{t}\right)$ - the non-dimensional temperature gradients at the level of the interface in the liquid and solid respectively, given by (3.43) and (3.44).

The right-hand side of the equation (3.45) can be written as:

$$\begin{aligned} &-St\left[\tilde{G}_l\left(\tilde{l},\tilde{t}\right) - \tilde{\lambda}\tilde{G}_s\left(\tilde{l},\tilde{t}\right)\right] = -St\left[\frac{\tilde{T}_h^a\left(\tilde{t}\right) - \tilde{T}_m}{\tilde{H}_a - \tilde{l}} - \tilde{\lambda}\frac{\tilde{T}_m - \tilde{T}_c^a\left(\tilde{t}\right)}{\tilde{l}}\right] \\ &-2\tilde{k}\cdot Pe^l \cdot St\sum_{n=1}^{\infty}(-1)^{n+1}\left[\left(\tilde{H}_a - \tilde{l}\right)\left(1 - e^{-\left(\frac{n\pi}{\tilde{H}_a - \tilde{l}}\right)^2\tilde{t}}\right) + \frac{\tilde{\lambda}\tilde{l}}{\tilde{D}_{th}}\left(1 - e^{-\tilde{D}_{th}\left(\frac{n\pi}{\tilde{l}}\right)^2\tilde{t}}\right)\right]\frac{1}{n^2\pi^2}. \end{aligned} \tag{3.46}$$

Hence, the following inequalities hold:

$$\begin{aligned} &-St\left[\frac{\tilde{T}_h^a\left(\tilde{t}\right) - \tilde{T}_m}{\tilde{H}_a - \tilde{l}} - \tilde{\lambda}\frac{\tilde{T}_m - \tilde{T}_c^a\left(t\right)}{\tilde{l}}\right] - \frac{2\tilde{k}\cdot Pe^l}{\pi^2}St\left[\left(\tilde{H}_a - \tilde{l}\right)\left(1 - e^{-\left(\frac{n\pi}{\tilde{H}_a - \tilde{l}}\right)^2\tilde{t}}\right) + \frac{\tilde{\lambda}\tilde{l}}{\tilde{D}_{th}}\left(1 - e^{-\tilde{D}_{th}\left(\frac{n\pi}{\tilde{l}}\right)^2\tilde{t}}\right)\right] \\ &\le -St\left[\tilde{G}_l\left(\tilde{l},\tilde{t}\right) - \tilde{\lambda}\tilde{G}_s\left(\tilde{l},\tilde{t}\right)\right] < -St\left[\frac{\tilde{T}_h^a\left(\tilde{t}\right) - \tilde{T}_m}{\tilde{H}_a - \tilde{l}} - \tilde{\lambda}\frac{\tilde{T}_m - \tilde{T}_c^a\left(t\right)}{\tilde{l}}\right]. \end{aligned} \tag{3.47}$$

The above inequalities lead to the following proposition:

Proposition 3.1: *For every moment of time* $\tilde{t} \in \left[0, \tilde{t}_*\right]$ *the following equalities hold:*

$$\lim_{\substack{\tilde{l}\to 0 \\ \tilde{l}>0}}\left\{-St\left[\tilde{G}_l\left(\tilde{l},\tilde{t}\right) - \tilde{\lambda}\tilde{G}_s\left(\tilde{l},\tilde{t}\right)\right]\right\} = +\infty;\ \lim_{\substack{\tilde{l}\to \tilde{H}_a \\ l<\tilde{H}_a}}\left\{-St\left[\tilde{G}_l\left(\tilde{l},\tilde{t}\right) - \tilde{\lambda}\tilde{G}_s\left(\tilde{l},\tilde{t}\right)\right]\right\} = -\infty. \tag{3.48}$$

Equalities (3.48) with the inequality

$$\frac{\partial}{\partial\tilde{l}}\left\{-St\left[\tilde{G}_l\left(\tilde{l},\tilde{t}\right) - \tilde{\lambda}\tilde{G}_s\left(\tilde{l},\tilde{t}\right)\right]\right\} < 0 \tag{3.49}$$

(valid for Pe^l small compared to 1, which is the case for semiconductor growth) imply that for every moment of time $\tilde{t} \in \left[0, \tilde{t}_*\right]$, there exists a unique value $\tilde{l}_*\left(\tilde{t}\right) \in \left(0, \tilde{H}_a\right]$ such that:

$$-St\left[\tilde{G}_l\left(\tilde{l}_*(\tilde{t}),\tilde{t}\right)-\tilde{\lambda}\tilde{G}_s\left(\tilde{l}_*(\tilde{t}),\tilde{t}\right)\right]=0. \tag{3.50}$$

Therefore, the following proposition can be stated:

Proposition 3.2: *At a point* $\left(\tilde{l},\tilde{t}\right)$ *which belongs to the rectangle* $\left(0,\tilde{H}_a\right]\times\left[0,\tilde{t}_*\right]$ *one and only one of the following situations can occur:*

$$\begin{aligned}
&\tilde{l}>\tilde{l}_*(\tilde{t})\Leftrightarrow -St\left[\tilde{G}_l\left(\tilde{l},\tilde{t}\right)-\tilde{\lambda}\tilde{G}_s\left(\tilde{l},\tilde{t}\right)\right]<0,\\
&\tilde{l}=\tilde{l}_*(\tilde{t})\Leftrightarrow -St\left[\tilde{G}_l\left(\tilde{l},\tilde{t}\right)-\tilde{\lambda}\tilde{G}_s\left(\tilde{l},\tilde{t}\right)\right]=0,\\
&\tilde{l}<\tilde{l}_*(\tilde{t})\Leftrightarrow -St\left[\tilde{G}_l\left(\tilde{l},\tilde{t}\right)-\tilde{\lambda}\tilde{G}_s\left(\tilde{l},\tilde{t}\right)\right]>0.
\end{aligned} \tag{3.51}$$

where $\tilde{l}(\tilde{t})$ *represents the solution of Eq.* (3.45).

The value of $\tilde{l}_*(\tilde{t})$ at a moment of time $\tilde{t}\in\left[0,\tilde{t}_*\right]$ satisfies:

$$0<\tilde{l}_*(\tilde{t})\le\tilde{H}_a\left[1-\frac{\tilde{T}_h^a(\tilde{t})-\tilde{T}_m}{\tilde{T}_h^a(\tilde{t})-\tilde{T}_m+\tilde{\lambda}\left(\tilde{T}_m-\tilde{T}_c^a(t)\right)}\right] \tag{3.52}$$

Moreover, since $\frac{\partial}{\partial\tilde{t}}\left\{-St\left[\tilde{G}_l\left(\tilde{l},\tilde{t}\right)-\tilde{\lambda}\tilde{G}_s\left(\tilde{l},\tilde{t}\right)\right]\right\}>0$ (for Pe^l small), $\tilde{l}_*(\tilde{t})$ is an increasing function with:

$$\tilde{l}_*(0)=\tilde{H}_a\left[1-\frac{\tilde{T}_c^f+\tilde{k}\left(\tilde{d}'+\tilde{H}_a\right)-\tilde{T}_m}{1+\tilde{k}\left(\tilde{d}'+\tilde{H}_a\right)-\tilde{T}_m+\tilde{\lambda}\left(\tilde{T}_m-\tilde{T}_c^f-\tilde{k}\tilde{d}'\right)}\right] \text{ and } \tilde{l}_*(\tilde{t}_*)<\tilde{H}_a. \tag{3.53}$$

The value $\tilde{l}_*(\tilde{t})$ splits the interval $\left[0,\tilde{H}_a\right]$ in two ranges: $\left[0,\tilde{l}_*(\tilde{t})\right)$ and $\left(\tilde{l}_*(\tilde{t}),\tilde{H}_a\right]$ and is the boundary between the melting and solidification processes. If at the moment of time $\tilde{t}$ the crystallization front level $\tilde{l}(\tilde{t})$ is in the range $\left[0,\tilde{l}_*(\tilde{t})\right)$, then solidification takes place (Figure 3.2). If at the moment of time $\tilde{t}$, $\tilde{l}(\tilde{t})$ is in the range $\left(\tilde{l}_*(\tilde{t}),\tilde{H}_a\right]$ then melting takes place (see [Balint 2011-2]). In order to analyze the solidification process, the following proposition must be valid:

Proposition 3.3: *For an initial value* $\tilde{l}_0$ *which satisfies* $0<\tilde{l}_0\le\tilde{l}_*(0)$*, the solution of the initial value problem:*

$$\begin{cases} \dfrac{d\tilde{l}}{d\tilde{t}} = -St\left[\tilde{G}_l\left(\tilde{l},\tilde{t}\right) - \tilde{\lambda}\tilde{G}_s\left(\tilde{l},\tilde{t}\right)\right] \\ \tilde{l}\left(0\right) = \tilde{l}_0 \end{cases} \tag{3.54}$$

is defined for $t \in \left[0, t_*\right]$*, it is an increasing function and verifies* $l_0 < l\left(t;0,l_0\right) < l_*\left(t\right)$ ($\tilde{l}_*\left(\tilde{t}\right)$ *the solution of Eq.*(3.50)) *for every* $t \in \left[0, t_*\right]$.

Thus, for showing that the solution of IVP (3.54) is an increasing function, a solution $\tilde{l}_1\left(\tilde{t}\right)$ which starts below $\tilde{l}_*\left(\tilde{t}\right)$ (i.e., $\tilde{l}_1\left(0\right) < \tilde{l}_*\left(0\right)$) is considered and it will be proved by contradiction that $\tilde{l}_1\left(\tilde{t}\right)$ remains under $\tilde{l}_*\left(\tilde{t}\right)$ during the solidification process. Hence, supposing that the intersection of $\tilde{l}_1\left(\tilde{t}\right)$ and $\tilde{l}_*\left(\tilde{t}\right)$ occurs at time $\tilde{t}_0 \in \left[0, \tilde{t}_*\right]$, then $\tilde{l}_1\left(\tilde{t}_0\right) = \tilde{l}_*\left(\tilde{t}_0\right)$ and $\tilde{l}_1\left(\tilde{t}\right)$ can be expanded in Taylor series at the point $\tilde{t}_0$ as

$$\tilde{l}_1\left(\tilde{t}\right) = \tilde{l}_1\left(\tilde{t}_0\right) + \underbrace{\left.\frac{d\tilde{l}_1}{d\tilde{t}}\right|_{\tilde{t}=\tilde{t}_0}}_{0}\left(\tilde{t}-\tilde{t}_0\right) + \frac{1}{2!}\cdot\left.\frac{d^2\tilde{l}_1}{d\tilde{t}^2}\right|_{\tilde{t}=\tilde{t}_0}\left(\tilde{t}-\tilde{t}_0\right)^2 + \ldots \tag{3.55}$$

From (3.46) and (3.47) it gives: $\dfrac{d\tilde{l}_1}{d\tilde{t}} = -St\left[\dfrac{\tilde{T}_h^a\left(\tilde{t}\right) - \tilde{T}_m}{\tilde{H}_a - \tilde{l}_1\left(\tilde{t}\right)} - \tilde{\lambda}\dfrac{\tilde{T}_m - \tilde{T}_c^a\left(\tilde{t}\right)}{\tilde{l}_1\left(\tilde{t}\right)}\right]$.

Since the first derivative of $\tilde{l}_1\left(\tilde{t}\right)$ with respect to $\tilde{t}$, computed at $\tilde{t}_0$, is equal to zero, the sign of the second derivative must be studied:

$$\frac{d^2\tilde{l}_1}{d\tilde{t}^2} = -St\left\{\frac{\left[\tilde{H}_a - \tilde{l}_1\left(\tilde{t}\right)\right]\dfrac{d}{d\tilde{t}}\left(\tilde{T}_h^a\left(\tilde{t}\right)\right) + \left[\tilde{T}_h^a\left(\tilde{t}\right) - \tilde{T}_m\right]\dfrac{d\tilde{l}_1}{d\tilde{t}}}{\left[\tilde{H}_a - \tilde{l}_1\left(\tilde{t}\right)\right]^2} + \tilde{\lambda}\frac{\tilde{l}_1\left(\tilde{t}\right)\dfrac{d}{d\tilde{t}}\left(\tilde{T}_c^a\left(\tilde{t}\right)\right) + \left[\tilde{T}_m - \tilde{T}_c^a\left(\tilde{t}\right)\right]\dfrac{d\tilde{l}_1}{d\tilde{t}}}{\left[l_1\left(t\right)\right]^2}\right\}$$

$$= -St\left\{-\tilde{k}\cdot Pe^l\left[\frac{1}{\tilde{H}_a - \tilde{l}_1\left(\tilde{t}\right)} + \frac{1}{\tilde{l}_1\left(\tilde{t}\right)}\right] + \left[\frac{\tilde{T}_h^a\left(\tilde{t}\right) - \tilde{T}_m}{\left[\tilde{H}_a - \tilde{l}_1\left(\tilde{t}\right)\right]^2} + \tilde{\lambda}\frac{\tilde{T}_m - \tilde{T}_c^a\left(\tilde{t}\right)}{\left[\tilde{l}_1\left(\tilde{t}\right)\right]^2}\right]\frac{d\tilde{l}_1}{d\tilde{t}}\right\}.$$

Computing at $\tilde{t}_0$ gives:

$$\left.\frac{d^2\tilde{l}_1}{d\tilde{t}^2}\right|_{\tilde{t}=\tilde{t}_0} = -St\left\{-\tilde{k}\cdot Pe^l\left[\frac{1}{\tilde{H}_a-\tilde{l}_1(\tilde{t}_0)}+\frac{1}{\tilde{l}_1(\tilde{t}_0)}\right]+\left[\frac{\tilde{T}_h^a(\tilde{t}_0)-\tilde{T}_m}{\left[\tilde{H}_a-\tilde{l}_1(\tilde{t}_0)\right]^2}+\tilde{\lambda}\frac{\tilde{T}_m-\tilde{T}_c^a(\tilde{t}_0)}{\left[\tilde{l}_1(\tilde{t}_0)\right]^2}\right]\underbrace{\left.\frac{d\tilde{l}_1}{d\tilde{t}}\right|_{\tilde{t}=\tilde{t}_0}}_{0}\right\}$$

$$= \tilde{k}\cdot Pe^l\cdot St\left[\frac{1}{\tilde{H}_a-\tilde{l}_1(\tilde{t}_0)}+\frac{1}{\tilde{l}_1(\tilde{t}_0)}\right]>0.$$

From the positivity of this derivative and the relation (3.55) it results that $\tilde{l}_1(\tilde{t})>\tilde{l}_1(\tilde{t}_0)$ in a small neighbourhood of $\tilde{t}_0$, which is in contradiction with the implication of (3.51) that $\tilde{l}_1(\tilde{t})<\tilde{l}_1(\tilde{t}_0)$ for any $\tilde{t}<\tilde{t}_0$. Hence, the supposition is false, there is no intersection between $\tilde{l}_1(\tilde{t})$ and $\tilde{l}_*(\tilde{t})$. Thus, the solution of (3.54), defined for $\tilde{t}\in[0,\tilde{t}_*]$, is an increasing function and verifies $\tilde{l}_0<\tilde{l}(\tilde{t};0,\tilde{l}_0)<\tilde{l}_*(\tilde{t})$ for every $\tilde{t}\in[0,\tilde{t}_*]$.

Remark: When the filled ampoule is placed directly in the furnace such that the coordinate of the bottom of the ampoule is equal to $\tilde{d}'$ and the pulling up starts, a melting process followed by solidification takes place [Balint 2011-2]. This process is described by the equation (3.51) and the initial condition $\tilde{l}(0)=\tilde{H}_a$ (see Figure 3.5).

3.3. Numerical illustration of the melt-solid interface displacement

The theoretical studies presented in the previous sections will be illustrated numerically. The numerical computations are performed for two semiconductors *InSb* and *GaSb* (thermophysical properties are given in Table 1.1). Other common input parameters are: the temperature at the cold side of the furnace, $\tilde{T}_c^f=0$ and the pulling rate, $v_a=10^{-6}\,\mathrm{m}\cdot\mathrm{s}^{-1}$. Special attention must be paid in choosing the vertical temperature gradient in the furnace $\tilde{k}$ and the parameter $\tilde{d}'$ which gives the position of the ampoule in the furnace, in order to get solidification. A natural way to choose $\tilde{k}$ and $\tilde{d}'$, when $\tilde{T}_c^f$ is fixed, can be the following: $\tilde{k}=\left(\tilde{T}_m-\tilde{T}_c^f\right)\Big/\tilde{H}_a$ and $\tilde{d}'=\tilde{H}_a-\tilde{L}_0$ where $\tilde{L}_0$ is the seed length. Therefore, in the case of *InSb*, $k=5000\,\mathrm{K}\cdot\mathrm{m}^{-1}$ and in the case of *GaSb*, $k=7237.5\,\mathrm{K}\cdot\mathrm{m}^{-1}$.

For the numerical illustration of the melt-solid interface evolution, the following steps are required:

- Numerical determination of $\tilde{t}_*$ using relation (3.23), so that for *InSb* $\tilde{t}_* = 10758.89$ and for *GaSb* $\tilde{t}_* = 10156.39$ are obtained.
- Numerical determination of $\tilde{l}_*(\tilde{t})$ performed considering the first four terms for the thermal gradients $\tilde{G}_l(\tilde{l},\tilde{t})$, $\tilde{G}_s(\tilde{l},\tilde{t})$ in the equation (3.50) and $\tilde{t} \in [0,\tilde{t}_*]$. The values $\tilde{l}_*(0) = 2.061$, $\tilde{l}_*(\tilde{t}_*) = 14.545 \le \tilde{H}_a$ for *InSb* and $\tilde{l}_*(0) = 2.518$, $\tilde{l}_*(\tilde{t}_*) = 14.545 \le \tilde{H}_a$ for *GaSb* are obtained. Graphical representation of $\tilde{l}_*(\tilde{t})$ is shown in Figure 3.2 for both semiconductors.

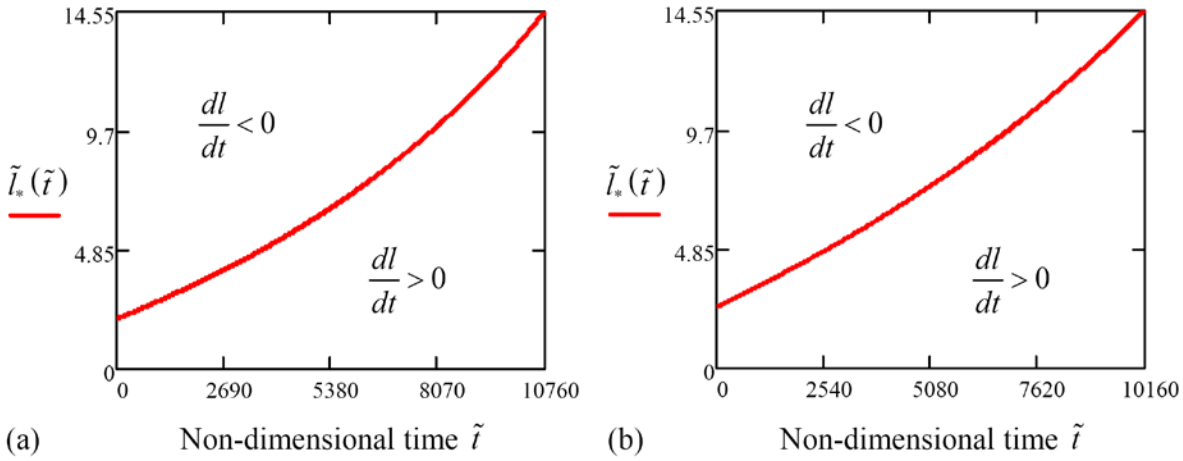

Figure 3.2 Solidification process boundaries of (a) *InSb* and (b) *GaSb*.

- Numerical determination of the solution $\tilde{l}(\tilde{t};0,\tilde{l}_0)$ of differential equation (3.45) using Mathcad 13. In Figure 3.3 the computed $\tilde{l}_*(\tilde{t})$ and $\tilde{l}(\tilde{t};0,\tilde{l}_0)$ corresponding to $\tilde{l}_0 = \tilde{l}_*(0) = 2.061$ are represented for *InSb*.

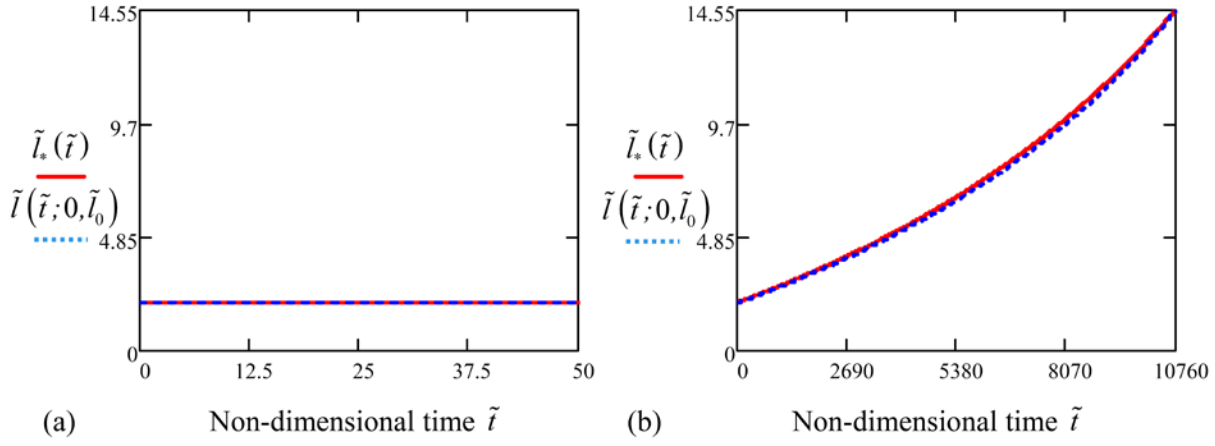

Figure 3.3 Evolution of the interface displacement for *InSb* (a) the beginning of the solidification and (b) the entire solidification process.

Similarly, in Figure 3.4 the computed $\tilde{l}_*(\tilde{t})$ and $\tilde{l}(\tilde{t};0,\tilde{l}_0)$ corresponding to $\tilde{l}_0 = \tilde{l}_*(0) = 2.518$ are represented for *GaSb*.

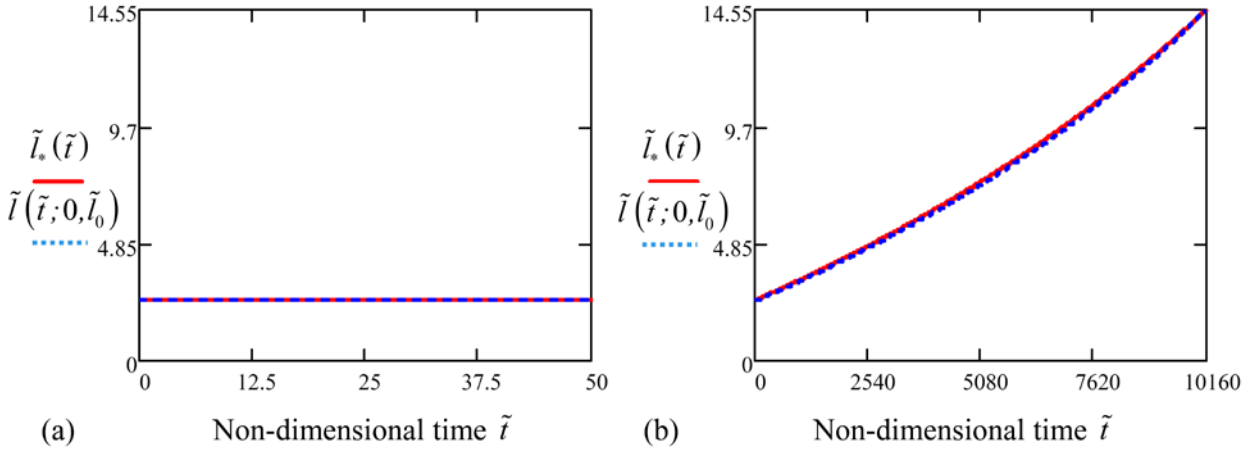

Figure 3.4 Evolution of the interface displacement for *GaSb* (a) the beginning of the solidification and (b) the entire solidification process.

Computations show that $\tilde{l}(\tilde{t};0,\tilde{l}_0)$ is an increasing function which satisfies $\tilde{l}_0 < \tilde{l}(\tilde{t};0,\tilde{l}_0) < \tilde{l}_*(\tilde{t})$ for every $\tilde{t} \in [0,\tilde{t}_*]$ (as it was mentioned in section 3.2). Moreover, it can be seen that

$\tilde{l}_*(\tilde{t}) - \tilde{l}(\tilde{t};0,\tilde{l}_0)$ becomes very small after a short period of time and $\tilde{l}(\tilde{t}_*;0,\tilde{l}_0) \cong \tilde{H}_a$ (i.e., the entire melt is solidified during the period $[0,\tilde{t}_*]$).

In Figure 3.5 the melting and solidification processes are illustrated for $\tilde{l}_0 = \tilde{H}_a = 14.545$.

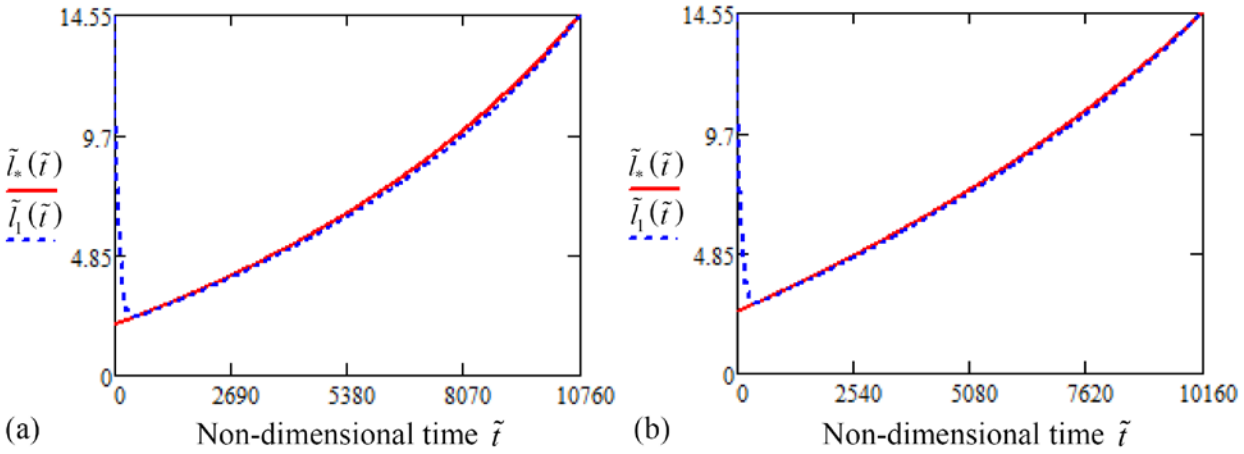

Figure 3.5 Melting-Solidification process of *InSb* (a) and *GaSb* (b).

The above numerical results were obtained on the basis of the analytical formulas of the temperature distribution presented in section 3.1. These formulas were found solving the heat transfer equation in the melt and in the solid by neglecting the latent heat release at the solid-liquid interface. Under these hypotheses the equation of the melt - solid interface displacement was determined from the thermal balance equation.

In order to check these hypothesis, the heat transfer problem taking into account an averaged value of the latent heat released all along the process, has been solved numerically with Comsol Multiphysics software. The results are presented on Figures 3.6 with dotted lines. The continuous line in this figure represents the computed crystallization front evolution using the analytical formulas of the temperature gradients.

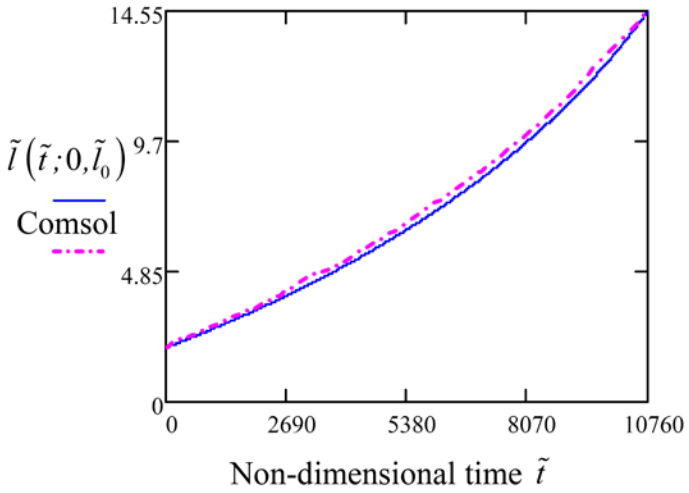

Figure 3.6 Evolution of the interface displacement during the solidification process of *InSb*- comparison between numerical results given by Comsol and Mathcad.

Both results compared in Figure 3.6 show the same behavior. It is important to underline that, generally, the heat transfer equation including the latent heat release at the level of the interface, does not have analytical solution.

3.4. Heat transfer in 2D axial symmetry (Stationary case)

Further improvements of the dewetted growth are related to the modification of the solid-liquid interface curvature when a gap exists between the crystal and the crucible: for a curved interface, the radial temperature gradient creates convection in the liquid which determines chemical segregation, and in solid creates thermo-elastic stresses which determine defects, dislocations and grains. In practice, slightly convex interfaces are preferred but are difficult to achieve in the case of semiconductors where the solid is a worse thermal conductor compared to the liquid. The experimental and theoretical analyses of the dewetted growth [Duffar 1997, 2000, 2001-1] have shown that it is possible to control the thickness of the crystal-crucible gap by controlling the gas pressure on the cold side of the growth ampoule. Then, in order to control the crystal quality, it is useful to know how the gap thickness influences the solid-liquid interface curvature.

3.4.1. Effect of the gap thickness on the solid-liquid interface

The main purpose of this study is to describe the effect of dewetting on the solid-liquid interface curvature defined as the maximum depletion against horizontal which passes through the solid-liquid-gas triple point. For this aim the procedure described in Refs. [Barat 1998, Stelian 2001] is applied: only the effects of the crucible and crystal parameters on the interface curvature are studied. It is well known that furnace related heat transfer (convection, radiation, etc.) influences the interface curvature, but this requires a case by case analysis totally depending on the furnace design. There is also generally little choice for the crucible material, especially if dewetting is requested. Then the dependence of the interface curvature on the gap thickness, crucible thickness, and on the liquid, solid and crucible thermal conductivities are studied from an analytical study and compared with those obtained from numerical simulations using finite element method. The equation of energy by conduction, in stationary case, is solved in order to find the isotherm of solidification which describes the shape of the solid-liquid interface. The melting temperature is assumed uniform all over the interface (the case of pure substance or diluted alloy) and the convective heat transport is neglected (convection has been shown to have virtually no effect on the interface shape because the Prandtl number for semiconductors is very low, around 0.01[Chang 1983, Crochet 1989]).

3.4.1.1. Dimensional analysis

The effect of the crystal-crucible gap on the curvature of the solid-liquid interface is studied in the following assumptions: the system is axially symmetric and the crucible wall is adiabatic (for example in Bridgman-Stockbarger furnace). The geometry of the dewetted Bridgman system is shown in Figure 3.8 (a), where the coordinate system is fixed at the bottom of the cylindrical ampoule.

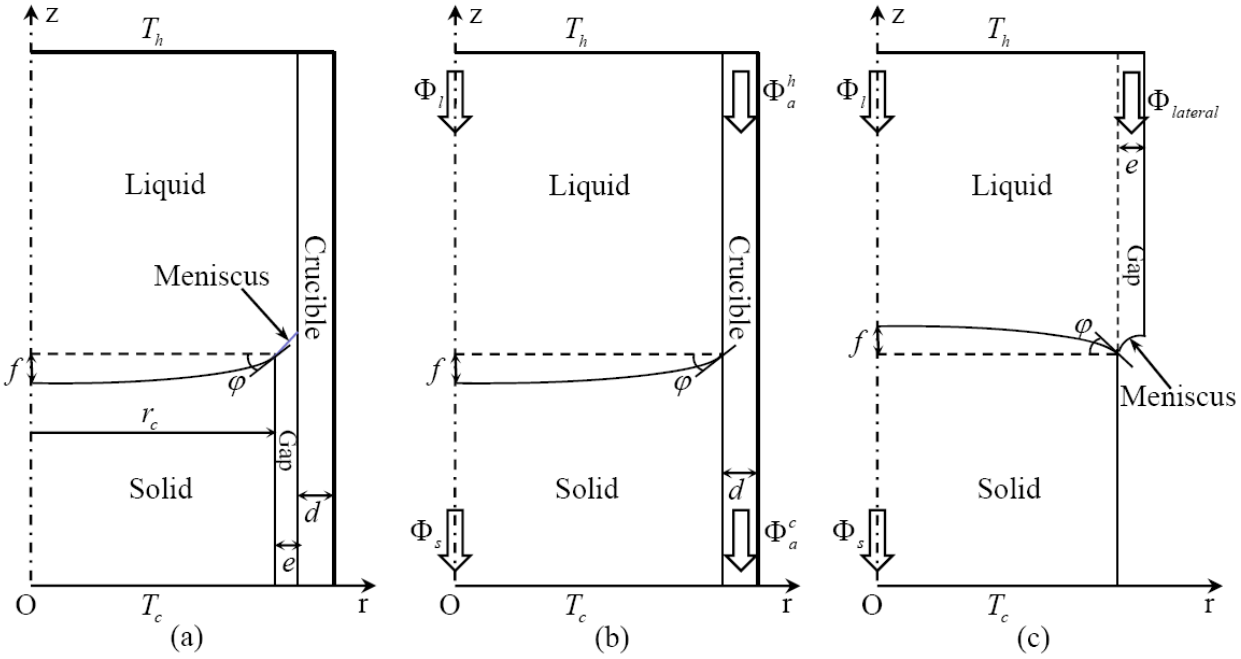

Figure 3.8 (a) Geometry and principal parameters of the problem; (b) Heat flux repartition - negligible gap; (c) Heat flux repartition - negligible crucible.

Generally, in order to develop equations and to design scale models that describe the physical phenomena, the dimensional analysis is used on the basis of the Vaschy-Buckingham theorem (so called Π-theorem) which states that a physically meaningful equation can be expressed as a function of $p = m - n$ non-dimensional quantities, where *m* represents the number of physical variables and *n* represents the number of basic dimensions used to describe the variables [Dobre 2007]. Thus, the equation can be written as

$$F\left(\Pi_1, \Pi_2, ..., \Pi_p\right) = 0 \text{ or equivalently } \Pi_1 = F_1\left(\Pi_2, ..., \Pi_p\right)$$

where $\Pi_1, \Pi_2, ..., \Pi_p$ are the non-dimensional quantities.

As the basic dimensions in the thermodynamic field are: the mass (*M*), the length (*L*), the time (*T*) and the temperature (θ), all physical variables can be expressed as a combination of these basic dimensions.

The matrix (developed by Remillard), which relates the set of physical variables involved in our problem and the fundamental set $MLT\theta$, is [Stelian 2001]:

	d	e	f	r_c	λ_a	λ_g	λ_s	λ_l	G_l	v_c	Λ
M	0	0	0	0	1	1	1	1	0	0	1
L	1	1	1	1	1	1	1	1	-1	1	-1
T	0	0	0	0	-3	-3	-3	-3	0	-1	-2
θ	0	0	0	0	-1	-1	-1	-1	1	0	0

(3.56)

where d is the thickness of the crucible, e is the thickness of the gap, f is the interface deflection, r_c represents the crystal radius, λ_a, λ_g, λ_s, λ_l are respectively the thermal conductivities of the ampoule, gap, solid and liquid, G_l is the thermal gradient in the liquid, v_c is the interface velocity and Λ is the latent heat of fusion.

In (3.56), the row elements represent the exponent of the dimensions corresponding to the physical quantities listed at the top of each column. For example, the dimensional representation of the interface velocity is [LT^{-1}].

The dimensional matrix has eleven variables (employed as in [Stelian 2001]) and four independent fundamental dimensions. Therefore, the Vaschy-Buckingham theorem gives the conclusion that seven non-dimensional quantities can be used, each of these quantities being a product of some physical variables at different powers. In order to calculate these powers, it is necessary to solve n simultaneous equations by choosing the appropriate columns of the matrix (3.56). For example, if we want to find the non-dimensional quantity $\Pi_7\left(\lambda_l, G_l, v_i, \Lambda\right)$ we can chose the last three columns as the coefficients of the matrix and the column headed by λ_l for the right-hand side [Stelian 2001]:

$$\begin{pmatrix} 0 & 0 & 1 \\ -1 & 1 & -1 \\ 0 & -1 & -2 \\ 1 & 0 & 0 \end{pmatrix} \begin{pmatrix} x \\ y \\ z \end{pmatrix} = \begin{pmatrix} 1 \\ 1 \\ -3 \\ -1 \end{pmatrix} \tag{3.57}$$

which is equivalent to $G_l^x v_i^y \Lambda^z = \Pi_7 \lambda_l$. Solving the simultaneous equation (3.57) gives: $x = -1$, $y = z = 1$. Therefore, the non-dimensional quantity Π_7, is given by:

$$\Pi_7 = \frac{v_i \Lambda}{G_l \lambda_l}. \tag{3.58}$$

Similarly, the other non-dimensional parameters can be obtained as:

$$\Pi_1 = \frac{f}{r_c},\ \Pi_2 = \frac{d}{r_c},\ \Pi_3 = \frac{e}{r_c}, \Pi_4 = \frac{\lambda_l}{\lambda_s},\ \Pi_5 = \frac{\lambda_l}{\lambda_a},\ \Pi_6 = \frac{\lambda_l}{\lambda_g} \tag{3.59}$$

So, the final result is

$$\Pi_1 = F\left(\Pi_2, ..., \Pi_7\right) \text{ or } \frac{f}{r_c} = F\left(\frac{d}{r_c}, \frac{e}{r_c}, \frac{\lambda_l}{\lambda_s}, \frac{\lambda_l}{\lambda_a}, \frac{\lambda_l}{\lambda_g}, \frac{v_i \Lambda}{G_l \lambda_l}\right). \tag{3.60}$$

Note that this set of non-dimensional parameters is not unique. They are however independent and form a complete set.

3.4.1.2. Analytical study

In order to find an approximate solution for the curvature of the solid-liquid interface the following hypothesis are established:

- quadratic interface;
- the thermal conductivity of the gas (in the gap) is negligible compared to the thermal conductivity of the solid, liquid and crucible;
- the angle between the local direction of the heat flux and the vertical is given by the ratio of the radial and axial heat fluxes;

We turn now to the thermal energy balance, that features the thermal fluxes in the liquid and out of the solid Φ_l and Φ_s as well as the thermal fluxes in the crucible at the hot and cold ends Φ_a^h and Φ_a^c. The external wall of the crucible is adiabatic, so that heat conservation requires:

$$\Phi_l + \Phi_a^h = \Phi_s + \Phi_a^c \tag{3.61}$$

The thermal fluxes can be locally expressed as

$$\Phi_i = \lambda_i G_i A_i \tag{3.62}$$

with G_i the thermal gradient and A_i the surface through which the flux is flowing and i=s, l, a or g. The thermal gradient in the sample and in the crucible equilibrate, yielding

$$G_s = G_l \frac{\lambda_l A_l + \lambda_a A_a}{\lambda_s A_s + \lambda_a A_a} \tag{3.63}$$

where G_s and G_l are the thermal gradients in the solid and liquid away from the interface and A_s and A_a the surfaces of the solid and crucible.

When the latent heat release at the melt-solid interface is accounted, then the corresponding heat flux can be expressed as:

$$\Phi_{\Lambda s} = \rho_s A_s v_i \Lambda \tag{3.64}$$

where ρ_s is the density of the solid, A_s is the surface of the solid, v_c represents the interface velocity and Λ is the latent heat. Because of the gap existing between the crucible and the solid crystal, the latent heat cannot be conducted to the crucible, hence, the amount of latent heat is conducted only to the solid.

As the thermal flux equation (3.62) is linear, in the case of interest ($\lambda_l > \lambda_s$ for semiconductors), the slope of the heat flux will be given by

$$\tan\varphi = \frac{\Phi_l - \Phi_s - \Phi_{lateral,l}}{\Phi_s + \Phi_{\Lambda s}} \tag{3.65}$$

which results from two different flux repartition at the level of the solid-liquid interface:

(i) case of the negligible gap (Fig. 3.8 (b)) studied in [Barat 1998, Stelian 2001] for which $\tan\varphi = \frac{\Phi_l - \Phi_s}{\Phi_s}$;

(ii) case of the negligible crucible (Fig. 3.8 (c)) for which the thermal flux in the lateral part of the liquid is deviated toward the crystal and hence $\tan\varphi = -\frac{\Phi_{lateral,l}}{\Phi_s}$.

Using Eqs. (3.62) and (3.63) we find that the slope of the heat flux (3.65) can be expressed as follows:

$$\tan\varphi = \frac{\lambda_l G_l A_l - \lambda_s G_s A_s - \lambda_l G_l A_g}{\lambda_s G_s A_s + \rho_s A_s v_i \Lambda} = \frac{\lambda_l\left(\lambda_s A_s + \lambda_a A_a\right) - \lambda_s\left(\lambda_l A_l + \lambda_a A_a\right)}{\lambda_s\left(\lambda_l A_l + \lambda_a A_a\right) + \frac{\rho_s v_i \Lambda}{G_l}\left(\lambda_s A_s + \lambda_a A_a\right)} \tag{3.66}$$

The interface is described as a parabola of equation $z = ar^2 + br + c$ where the coefficients *a*, *b*, *c* are given by the followings:

- the apex of the parabola is situated on the (Oz) axis: *b*=0 and $z(0) = c = L_s - f$ (see Fig. 3.8 (a), L_s represents the crystal length);
- the derivative in the triple point (r_c ; L_s): $2ar_c = \tan\varphi$;
- the triple point is situated on the parabola: $c = L_s - ar_c^{\,2} - br_c = L_s - \frac{r_c}{2}\tan\varphi$.

From these we obtain

$$f = \frac{r_c}{2}\tan\varphi,$$

and hence the interface curvature *f* is given by:

$$f = \frac{r_c}{2}\left[\frac{\lambda_l\left(\lambda_s A_s + \lambda_a A_a\right) - \lambda_s\left(\lambda_l A_l + \lambda_a A_a\right)}{\lambda_s\left(\lambda_l A_l + \lambda_a A_a\right) + \frac{\rho_s v_i \Lambda}{G_l}\left(\lambda_s A_s + \lambda_a A_a\right)}\right] \tag{3.67}$$

Comparison with numerical results shows that this formula overestimates the curvature of the interface by a factor 2.5, and then we propose the adjusted formula:

$$f = \frac{r_c}{5}\left[\frac{\lambda_l\left(\lambda_s A_s + \lambda_a A_a\right) - \lambda_s\left(\lambda_l A_l + \lambda_a A_a\right)}{\lambda_s\left(\lambda_l A_l + \lambda_a A_a\right) + \frac{\rho_s v_i \Lambda}{G_l}\left(\lambda_s A_s + \lambda_a A_a\right)}\right] \tag{3.68}$$

It should be noticed that a power 4 expression (instead of a parabola) for the interface curvature will give a factor ¼. In the case where $\Lambda \cdot v_i$ can be neglected it is easy to observe that this expression is independent of the magnitude of the temperature gradients in the liquid and solid, and then of the prescribed temperature difference between the hot and cold zones $\Delta T = T_h - T_C$ [Epure 2008]. In terms of non-dimensional parameters, equation (3.68) becomes:

$$\alpha = \frac{1}{5\sqrt{\pi}}\left[\frac{\delta - \beta\cdot\gamma\cdot\varepsilon - 1}{\beta\cdot\varepsilon\left(1+\gamma\right)+1+\xi\left(\beta\cdot\varepsilon+\delta\right)}\right] \tag{3.69}$$

where the non-dimensional parameters are similar to those given by (3.58) and (3.59):

- $\alpha = f/\left(A_s\right)^{1/2}$, the non-dimensional curvature of the interface, A_s being the surface of the solid crystal, $A_s = \pi\cdot r_c^2$;
- $\beta = A_s / A_a$, the ratio of the surfaces of the solid and crucible, where $A_a = \pi\cdot d\left(2\left(r_c + e\right) + d\right)$;
- $\gamma = A_g / A_s$, the ratio of the surfaces of the gap and solid crystal, where $A_g = \pi\cdot e\left(2\cdot r_c + e\right)$;
- $\delta = \lambda_l / \lambda_s$, the ratio of the thermal conductivities of the liquid and solid;
- $\varepsilon = \lambda_l / \lambda_a$, the ratio of the thermal conductivities of the liquid and crucible;
- $\eta = \lambda_l / \lambda_g$, the ratio of the thermal conductivities of the liquid and gas;
- $\xi = \frac{\rho_s v_i \Lambda}{\lambda_l G_l}$, the ratio representing the effect of latent heat on the interface deflection.

It should be mentioned that the parameter η does not appear in Eq. (3.69) because we made the assumption that the thermal conductivity of the gas is negligible compared to the other conductivities.

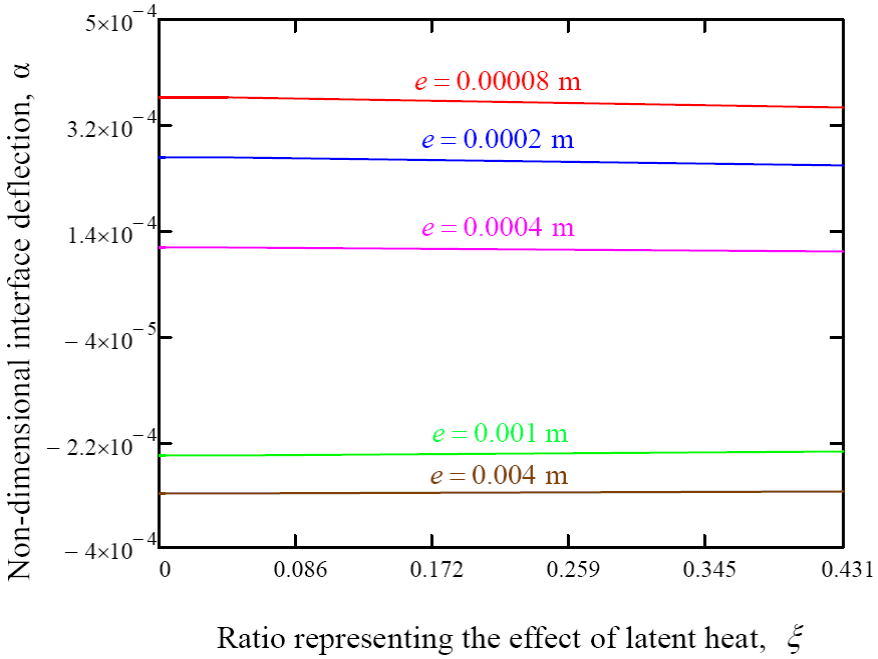

Figure 3.9 Dependence of the non-dimensional interface deflection on the ratio representing the effect of the latent heat.

The dependence of the non-dimensional curvature α on the ratio ξ presented in Fig. 3.9, shows that for interface velocities smaller than 10^{-6} m/s, the effect of the latent heat on the liquid-solid interface deflection can be neglected. This often happens in real Bridgman growth where the growth rate is generally small (of the order of 10^{-6} m/s or lower) for assuring a good crystal quality.

It can be observed that, in the case where the latent heat release is not taken into account, Eq. (3.69) becomes [Epure 2008]:

$$\alpha = \frac{1}{5\sqrt{\pi}}\left[\frac{\beta\cdot\varepsilon+\delta}{\beta\cdot\varepsilon+\beta\cdot\gamma\cdot\varepsilon+1}-1\right]. \tag{3.70}$$

The obtained formulas are similar to those reported in [Barat 1998, Stelian 2001], the only one difference is that now the surface of the liquid and gap appears because the surface of the liquid is different from the surface of the solid, due to the existence of the crystal-crucible gap.

3.4.2. Comparative study

In order to check the accuracy of the obtained analytical formula (3.70) and to identify its limits of validity, numerical modelling of the thermal problem has been carried out, using the finite elements code COMSOL Multiphysics 3.3.

We have considered the axisymmetrical geometry shown in Fig. 3.8 (a) with a thermal flux resulting from fixed temperatures T_h and T_c at the hot and cold ends. In agreement with the theoretical approach, we supposed latent heat and convective heat transport to be negligible and we have used an adiabatic boundary condition at the outer crucible wall.

Heaviside functions were used to define the thermal conductivities as functions of temperature, which makes the problem nonlinear. In order to solve this problem a mapped mesh with 1050 quadrilateral elements, very fine in the *r* direction and somewhat coarser in the *z* direction, was used. According to the considering geometry 4400 degrees of freedom were obtained.

The convergence of this model is difficult and it was necessary to use a nonlinear stationary solver with relative tolerance 10^{-6} and 25 iterations.

First, numerical studies were performed with a fixed meniscus in the geometry and it was observed that the shape of the solidification isotherm is following the shape of the meniscus and then, in order to get better and easier convergence, the next studies were performed without a fixed meniscus in the geometry.

For the length of the crucible not to influence the results, it was taken as at least 10 times its radius. It was also verified that the solution is independent of the applied temperature difference, $\Delta T = T_h - T_C$ in agreement with the results of the dimensional analysis of the problem [Epure 2008].

The non-dimensional interface curvatures, α, obtained in the numerical simulations are compared to the predictions of the analytical formula (3.70) as can be seen in Figure 3.10 (a) versus the ratio of the surfaces of the solid crystal and crucible, β; (b) versus the ratio of the surfaces of the gap and solid crystal, γ; (c) versus the ratio of the thermal conductivities of the liquid and solid, δ and (d) versus the ratio of the thermal conductivities of the liquid end crucible, ε.

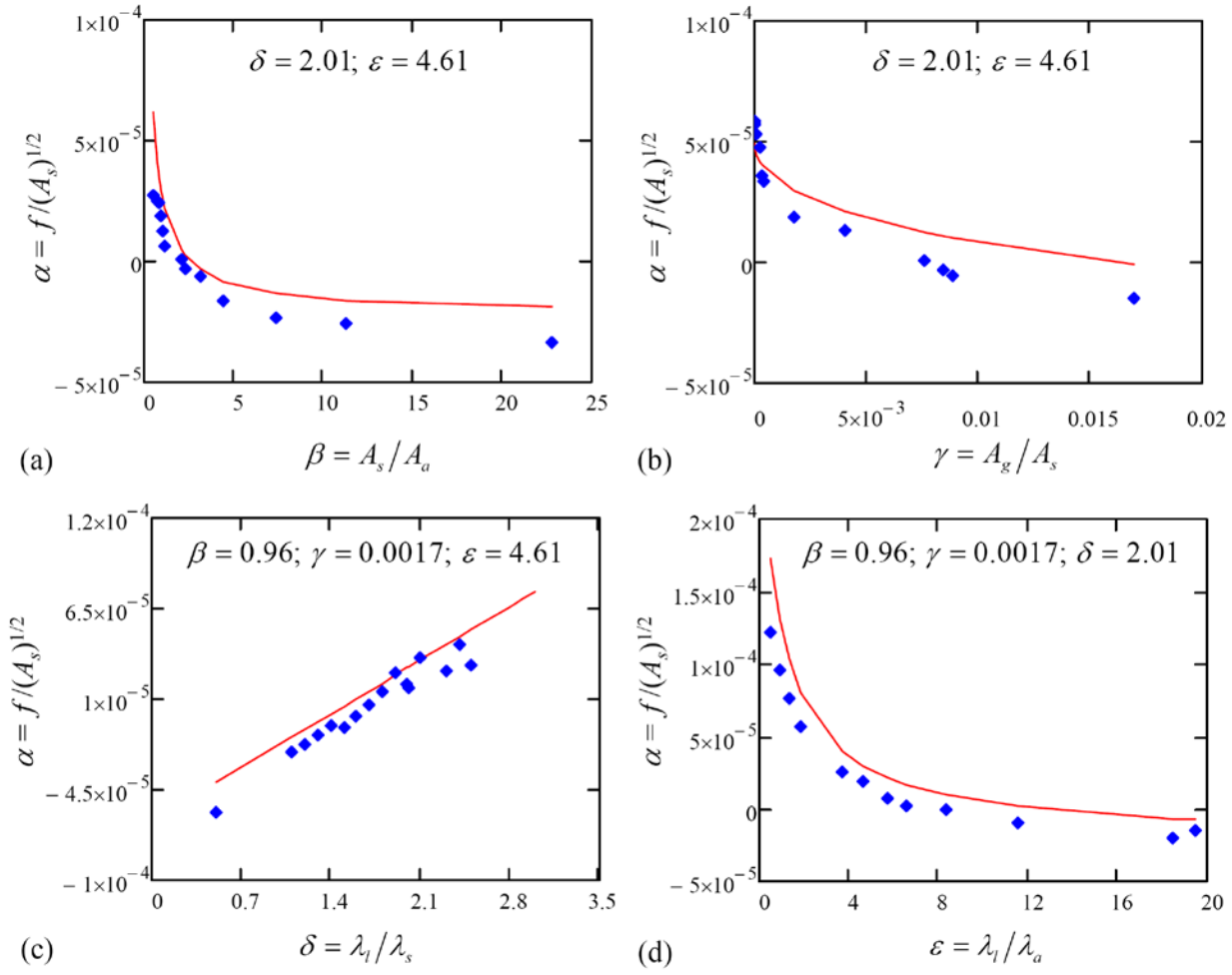

Figure 3.10 Non-dimensional liquid-solid interface deflection α, as a function of the non-dimensional parameters of the process.

The numerical results presented in Fig. 3.10 show that both solutions are of the same order of magnitude and the variation of the curvature with the various parameters follows the same trend which proves the usefulness of the analytical formula. Concerning its limits of validity, COMSOL code proved that solution converges for gap of maximum 430 micrometers. Moreover, computations show that some cases (gap between 400 and 430 micrometers) the curvature can be reversed from convex to concave.

As it was found in the dimensional analysis, numerical studies show that the curvature of the solid-liquid interface is influenced also, but not very much, by the ratio of the thermal conductivities of the liquid and gas (Fig. 3.11).

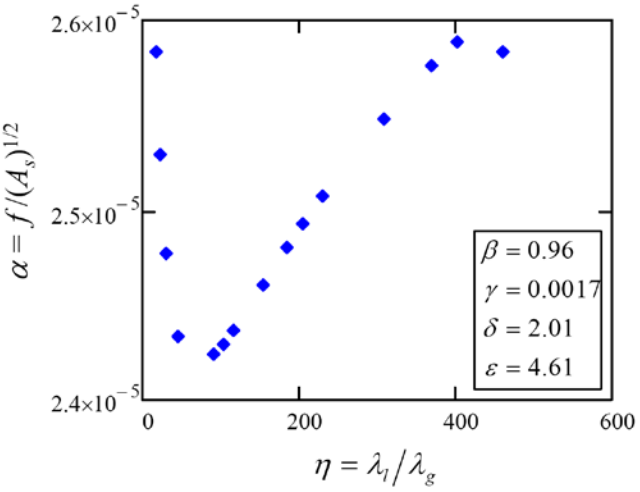

Figure 3.11 Non-dimensional curvature of the solid-liquid interface α, as a function of the ratio of thermal conductivities of the liquid and gas, η.

Summary

In this chapter a simplified problem of the dewetted Bridgman process with adiabatic walls was treated for modelling heat transfer problems. Analytical expressions of the temperature distribution and the temperature gradients in the melt and in the solid were established by solving analytically the non-stationary one-dimensional heat transfer equation by neglecting the latent heat release (quasi steady-state approximation). The melt-solid interface displacement differential equation was also derived from the thermal energy balance at the level of the interface and relevant properties concerning the solution $\tilde{l}(\tilde{t})$ *of this equation were established (Propositions 3.1 to 3.3). The solution* $\tilde{l}(\tilde{t})$ *was obtained by numerical integration (using adaptive Runge-Kutta method) of its ordinary non-autonomous differential equation in which the analytical formulas of the temperature gradients were used. Further, the results were compared to those obtained by solving, by finite element method, the non-stationary one-dimensional heat transfer equation in which the latent heat release was considered.*

The effect of the crystal-crucible gap on the curvature of the solid-liquid interface has been studied for a set of non-dimensional parameters representative of classical semiconductor crystal growth. An analytical expression for the interface curvature, based on simple heat fluxes arguments was found.

The analysis shows that the shape of the interface depends on the thickness of the gap, the thickness of the crucible, and on the thermal conductivities of the liquid, solid, gas and crucible. As expected, the curvature of the interface decreases when the crystal-crucible gap increases. An interesting result is that, for a large enough gap, the curvature of the interface may be reversed.

Therefore, the Bridgman crystal grower has now a new degree of freedom for the improvement of crystal quality. By adjusting the gap thickness in the dewetted mode, it is possible to modify the interface curvature. The proposed analytical expression can be used for a rough initial design of the growth process. In order to get more precise values of interface curvature it is anyhow necessary to use numerical simulation and to take into account more realistic parameters, including the furnace design.

CHAPTER 4: Contributions to the dynamical stability of the dewetted Bridgman crystal growth

As it was explained in the first chapter, stability is necessary to achieve consistency, repeatability and uniformity - the keys to successful crystal growth in the laboratory and in industrial production. In crystal growth the concept of stability is used as a generic concept but is generally not precisely defined from the mathematical point of view. Therefore, in this chapter, different concepts of stability occurring in shaped crystal growth will be defined and applied in the case of crystals grown by the dewetted Bridgman technique. Some of these concepts were applied for others crystal growth processes by Tatartchenko [Tatartchenko 1993, 2010].

Further, after the concept of practical stability over a bounded time period will be introduced ([Balint 2011-2]), analytical and numerical investigations of the practical stability over a bounded time period of the nonlinear system of differential equations describing the melt-solid interface displacement and the gap thickness evolution for dewetted Bridgman crystals grown in terrestrial conditions will be developed.

4.1. Lyapunov dynamic stability in crystal growth involving free liquid surfaces

The aim of this section is to present different concepts of Lyapunov stability which can occur in shaped crystal growth: classical, uniform, asymptotic, and exponential Lyapunov stabilities of a steady-state; partial Lyapunov stability of a steady-state; and the same types of Lyapunov stabilities for time-dependent regimes ([Balint 2011-1]). It will be emphasized that Lyapunov stability in the more general case in crystal growth does not assure the recovery of the non-perturbed regime. For recovery of the non-perturbed regime it is necessary to have at least asymptotic stability; while exponential stability implies recovery of the non-perturbed regime. Also, it will be proved that Hurwitz criterion can not be applied in the case of time-dependent regime, and that classical Lyapunov stability implies partial stability.

4.1.1. Lyapunov stability of a steady-state solution and a time-dependent solution respectively

The mathematical description of the shaped crystal growth process consists in a set of ordinary differential equations [Tatartchenko 1993] of the form:

$$\frac{dX_i}{dt} = f_i\left(X_1,...,X_n,t,C\right),\quad i=\overline{1,n} \tag{4.1}$$

where t denotes the time, n is the number of unknowns depending on the crystallization technique and the crystal cross-section, C denotes a set of controllable crystallization parameters, the thermophysical and other constants of the substance being crystallized. The stationary values X_i^* of the variables X_i present special interest when crystals having constant cross-section with stationary crystallization-front positions must be grown.

The Lyapunov stability of a *steady-state solution* $X_i(t)\equiv X_i^*, i=\overline{1,n}, t\geq 0, \left(X_i^*=\text{constant}\right)$ of the system (4.1) is defined as follows [Coddington 1955, Halanay 1966, Rouche 1977, Gruyitch 2004, Balint 2008-1]:

Definition 4.1.1: The steady-state solution $X_i(t)\equiv X_i^*$ of the system (4.1) is *Lyapunov stable* if for any $\varepsilon>0$ and $t_0\geq 0$ there exists $\delta=\delta(\varepsilon,t_0)>0$ such that for any X_i^0, $i=\overline{1,n}$ which satisfies $\left|X_i^0-X_i^*\right|<\delta(\varepsilon,t_0), i=\overline{1,n}$, the solution $X_i\left(t;X_1^0,...,X_n^0\right), i=\overline{1,n}$ of the system (4.1) is defined for any $t\geq t_0$ and satisfies:

$$\left|X_i\left(t;X_1^0,...,X_n^0\right)-X_i^*\right|<\varepsilon,\ i=\overline{1,n}. \tag{4.2}$$

Comments:

i) In the above definition $X_i\left(t;X_1^0,...,X_n^0\right), i=\overline{1,n}$ is called perturbed solution and represents that solution of (4.1) which at the moment $t=t_0$ starts from $\left(X_1^0,...,X_n^0\right)$, i.e., $X_i\left(t_0;X_1^0,...,X_n^0\right)=X_i^0, i=\overline{1,n}$. This makes sense when there exist a unique solution $X_i\left(t;X_1^0,...,X_n^0\right), i=\overline{1,n}$ of the equation (4.1) satisfying $X_i\left(t_0;X_1^0,...,X_n^0\right)=X_i^0, i=\overline{1,n}$, which is assured when functions $f_i\left(X_1,...,X_n;t,C\right), i=\overline{1,n}$ have continuous partial derivatives.

ii) Definition 4.1.1 expresses the fact that, if a small perturbation $\left(X_1^0,...,X_n^0\right)$ of the steady-state $\left(X_1^*,...,X_n^*\right)$ occurs at a certain moment $t_0 \geq 0$ ($\left|X_i^0 - X_i^*\right| < \delta\left(\varepsilon,t_0\right), i=\overline{1,n}$, $\delta\left(\varepsilon,t_0\right)>0$ and sufficiently small), then the time dependent perturbed solution $X_i\left(t;X_1^0,...,X_n^0\right), i=\overline{1,n}$ rests close to the steady-state solution $X_i\left(t\right)\equiv X_i^*, i=\overline{1,n}$ (i.e. $\left|X_i\left(t;X_1^0,...,X_n^0\right)-X_i^*\right|<\varepsilon$ for $t\geq t_0$, $i=\overline{1,n}$ and $\varepsilon>0$ small).

iii) When $\delta=\delta\left(\varepsilon,t_0\right)$ is independent of t_0 then the steady-state $X_i\left(t\right)\equiv X_i^*, i=\overline{1,n}$ is called *uniformly Lyapunov stable*.

iv) It should be mentioned that there are systems for which every steady-state is stable (e.g., for n=1 and the Eqs. $\dot{X}=0$ or $\dot{X}=-X$), or all steady-states are unstable (e.g., for n=1 and the Eq. $\dot{X}=X^2$), or some steady-states are stable and others are unstable (e.g., for n=1 and the Eq. $\dot{X}=-X+X^2$, the steady-state $X^*=0$ is stable and the steady-state $X^{**}=1$ is unstable) ([Balint 2011-1]).

Definition 4.1.2: If the steady-state $X_i^*, i=\overline{1,n}$ is Lyapunov stable, and for every $t_0\geq 0$ there exists $\eta\left(t_0\right)>0$ such that for any $X_i^0, i=\overline{1,n}$ which satisfies $\left|X_i^0-X_i^*\right|<\eta\left(t_0\right), i=\overline{1,n}$, the perturbed solution $X_i\left(t;X_1^0,...,X_n^0\right), i=\overline{1,n}$ of the system (4.1) satisfies $\lim\limits_{t\to+\infty}\left|X_i\left(t;X_1^0,...,X_n^0\right)-X_i^*\right|=0,\ i=\overline{1,n}$, then the steady-state $X_i^*, i=\overline{1,n}$ is *Lyapunov asymptotically stable.*

Definition 4.1.3: If there exist two positive constants, $\nu>0$ and $B>0$ such that for any $X_i^0, i=\overline{1,n}$ and $t\geq t_0$ the inequality $\left|X_i\left(t;t_0,X_1^0,...,X_n^0\right)-X_i^*\right|<B\cdot e^{-\nu\left(t-t_0\right)}\left|X_i^0-X_i^*\right|$ holds, then the steady-state $X_i^*, i=\overline{1,n}$ is called *exponentially stable*.

Concerning the stability analysis of a steady-state $X_i\left(t\right)\equiv X_i^*, i=\overline{1,n}$ of the system (4.1), Lyapunov showed that this can be reduced to the analysis of the stability for zero steady-state, $\left(Y_1^*,...,Y_n^*\right)=\left(0,...,0\right)$, of the perturbed system defined as follows [Coddington 1955, Halanay 1966, Rouche 1977, Gruyitch 2004, Balint 2008-1]:

$$\dot{Y}_i = f_i\left(Y_1 + X_1^*, ..., Y_n + X_n^*, t, C\right), i = \overline{1,n} \tag{4.3}$$

The perturbed system (4.3) is obtained making the change of variables $Y_i = X_i - X_i^*, i = \overline{1,n}$ in (4.1). In fact, Lyapunov showed that the steady-state solution $\left(X_1^*, ..., X_n^*\right)$ of the system (4.1) is Lyapunov stable if and only if the steady-state solution $\left(Y_1^*, ..., Y_n^*\right) = \left(0, ..., 0\right)$ of the system (4.3) is stable.

For analyzing the stability of the steady-state $\left(Y_1^*, ..., Y_n^*\right) = \left(0, ..., 0\right)$ of the perturbed system (4.3), Lyapunov developed the right- hand side of (4.3) in the form:

$$\dot{Y}_i = \sum_{k=1}^{n} \frac{\partial f_i}{\partial X_k}\left(X_1^*, ..., X_n^*, t, C\right)Y_k + \sum_{k=1}^{n}\sum_{l=1}^{n} \frac{\partial^2 f_i}{\partial X_k \partial X_l}\left(X_1^*, ..., X_n^*, t, C\right)Y_k Y_l + ..., i = \overline{1,n}\,. \tag{4.4}$$

Retaining only the first term of the development, Lyapunov associated to the perturbed system (4.4), the following linear system:

$$\dot{Z}_i = \sum_{k=1}^{n} \frac{\partial f_i}{\partial X_k}\left(X_1^*, ..., X_n^*, t, C\right) \cdot Z_k \tag{4.5}$$

so-called the linearized set of equations around the steady-state $\left(X_1^*, ..., X_n^*\right)$.

Remarks 4.1:

i) If the system (4.1) is autonomous then the system (4.5) is a linear system of differential equations with constant coefficients and can be solved explicitly. Taking into account the analytical expression of the solutions (see [Halanay 1966]) it follows that, if all roots *S* of the characteristic equation

$$\det\left(\frac{\partial f}{\partial X_k} - S \cdot \delta_{ik}\right) = 0, \ \delta_{ik} \text{ the Kronecker delta,} \tag{4.6}$$

have negative real components, then the steady-state $\left(Z_1^*, ..., Z_n^*\right) = \left(0, ..., 0\right)$ of the linearized system is stable. Moreover, this solution is exponentially stable.

ii) In the case of an autonomous system, if the Hurwitz conditions [Halanay 1966] are satisfied, then the roots *S* of the characteristic equation (4.6) have negative real components and the steady-state $\left(Z_1^*, ..., Z_n^*\right) = \left(0, ..., 0\right)$ of the linearized system is

exponentially stable. Lyapunov showed ([Halanay 1966]) that in these conditions the steady-state $\left(Y_1^*,...,Y_n^*\right)=\left(0,...,0\right)$ of the perturbed system (4.4) is exponentially stable.

iii) It must be mentioned that the above statement is not valid if the system (4.1) is non-autonomous. For example, for the non-autonomous system

$$\begin{cases}\dot{X}_1=-\dfrac{1}{t+1}\cdot X_1+X_2\\ \dot{X}_2=-\dfrac{1}{2}\cdot\dfrac{1}{t+1}\cdot X_2\end{cases}$$

and the steady-state $\left(X_1^*,X_2^*\right)=\left(0,0\right)$, the rots of the characteristic equation corresponding to the linearized system $\begin{cases}\dot{Z}_1=-\dfrac{1}{t+1}\cdot Z_1+Z_2\\ \dot{Z}_2=-\dfrac{1}{2}\cdot\dfrac{1}{t+1}\cdot Z_2\end{cases}$, have negative real components but the solution $\left(Z_1^*,Z_2^*\right)=\left(0,0\right)$ is not stable because $Z_1\left(t;Z_1^0,Z_2^0\right)=\dfrac{Z_1^0}{t+1}+\dfrac{Z_2^0}{t+1}\cdot\dfrac{2}{3}\cdot\left[\left(t+1\right)^{\frac{3}{2}}-1\right]$ tends to $+\infty$ as t tends to $+\infty$.

Further, the stability concept for a time dependent solution of a system (4.1) will be presented as was reported in [Balint 2011-1].

Let $\bar{X}_i\left(t\right),i=\overline{1,n}$, $t\geq 0$ be a *time dependent solution* of the system (4.1).

Definition 4.1.4: The solution $\bar{X}_i\left(t\right),i=\overline{1,n}$, $t\geq 0$ is called *Lyapunov stable* if for any $\varepsilon>0$ and $t_0\geq 0$ there exists $\delta=\delta\left(\varepsilon,t_0\right)>0$ such that for any $X_i^0,i=\overline{1,n}$ which satisfies $\left|X_i^0-\bar{X}_i\left(t_0\right)\right|<\delta\left(\varepsilon,t_0\right)$, the solution $X_i\left(t;X_1^0,...,X_n^0\right)$, $i=\overline{1,n}$ of the system (4.1) is defined for any $t\geq t_0$ and verifies:

$$\left|X_i\left(t;X_1^0,...,X_n^0\right)-\bar{X}_i\left(t_0\right)\right|<\varepsilon,\ t\geq t_0 \text{ and } i=\overline{1,n}. \tag{4.7}$$

Here $X_i\left(t;X_1^0,...,X_n^0\right)$, $i=\overline{1,n}$ is the perturbed solution and $X_i\left(t_0;X_1^0,...,X_n^0\right)=X_i^0$, $i=\overline{1,n}$.

In this case, the perturbed system is defined as:

$$\dot{Y}_i=f_i\left(Y_1+\bar{X}_1\left(t\right),...,Y_n+\bar{X}_n\left(t\right),t,C\right)-\dot{\bar{X}}_i\left(t\right),i=\overline{1,n} \tag{4.8}$$

and depends on *t*, even if the system (4.1) is autonomous.

It can be seen that the solution $\bar{X}_i(t), i=\overline{1,n}$ of (4.1) is stable if and only if the steady-state $Y_i(t)\equiv 0, i=\overline{1,n}$ of the perturbed system (4.8) is stable.

Starting from the perturbed system (4.8) the linearized set of equations is defined as:

$$\dot{Z}_i = \sum_{k=1}^{n} \frac{\partial f_i}{\partial X_k}\left(\bar{X}_1(t),...,\bar{X}_n(t),t,C\right)\cdot Z_k \tag{4.9}$$

The linearized set of equations (4.9) is a linear system of differential equations with time dependent coefficients, even for autonomous systems. Generally, the system (4.9) cannot be solved explicitly.

There are no Hurwitz type criteria concerning the stability of the steady-state $\left(Z_1(t),...,Z_n(t)\right)\equiv(0,...,0)$ of this kind of system (see [Coddington 1955, Halanay 1966, Rouche 1977, Gruyitch 2004, Balint 2008-1]).

Therefore, if the steady-state $\left(Z_1^*,...,Z_n^*\right)=(0,...,0)$ of the system (4.9) is exponentially stable and some supplementary conditions which concern the nonlinear part of the perturbed system (4.8) are satisfied, then the steady-state $\left(Y_1^*,...,Y_n^*\right)=(0,...,0)$ of the perturbed system (4.8) is still exponentially stable [Halanay 1966]. Hence the solution $\bar{X}_i(t), i=\overline{1,n}$ of the system (4.1) is exponentially stable.

Remarks 4.2:

i) In the case of a small perturbation, the Lyapunov stability of the steady-state of an autonomous system, alone, cannot assure the recovery of the steady-state. What can be said is that, after a small perturbation, the evolution is near the steady-state.

ii) Exponential stability is more than Lyapunov stability. When the steady-state of an autonomous system is exponentially stable then, in the case of a small perturbation, the steady-state is recovered after a transition period.

iii) In the case of an autonomous system, if Hurwitz inequalities are satisfied for the linearized set of equations, then the steady-state is exponentially stable.

iv) If the linearized set of equations is time dependent, then the Hurwitz inequalities are not sufficient to assure the exponential stability.

4.1.2. Partial Lyapunov stability and capillary stability

According to [Tatartchenko 1993] (page 59) it is refered to capillary stability when the stability of a system can be provided only by the capillary effects i.e., in the case when it is considered that "a change in crystal dimensions and crystallization front position does not lead to any change in liquid- and solid-phase temperature gradients at the crystallization front".

Analyzing the system of differential equations considered in [Tatartchenko 1993] that governs the process in Czochralski technique:

$$\begin{cases} \dfrac{d\tilde{r}_c}{d\tilde{t}} = -Pe^l \cdot \tan\left[\psi\left(\tilde{r}_c,\tilde{l}\right) - \left(\dfrac{\pi}{2} - \alpha_e\right)\right] \\ \dfrac{d\tilde{l}}{d\tilde{t}} = Pe^l - St\left[\tilde{G}_l\left(\tilde{r}_c,\tilde{l}\right) - \tilde{\lambda}\tilde{G}_s\left(\tilde{r}_c,\tilde{l}\right)\right] \end{cases} \tag{4.10}$$

the requirement that: the non-dimensional crystal radius $\tilde{r}_c$ and crystallization front position $\tilde{l}$ do not lead to change in liquid- and solid- phase temperature gradients at the crystallization front, means that $\tilde{G}_l\left(\tilde{r}_c,\tilde{l}\right)$ and $\tilde{G}_s\left(\tilde{r}_c,\tilde{l}\right)$ are constant ([Balint 2011-1]). Hence the right-hand side of the second equation in system (4.10) is a constant. In order to have at least one steady-state the right-hand side terms must be equal to zero, thus $\dfrac{d\tilde{l}}{d\tilde{t}} = 0$ and $Pe^l = St\left[\tilde{G}_l\left(\tilde{r}_c,\tilde{l}\right) - \tilde{\lambda}\tilde{G}_s\left(\tilde{r}_c,\tilde{l}\right)\right]$. In (4.10) Pe^l and St represent the non-dimensional Péclet (in the liquid) and Stefan numbers.

Now for an arbitrary $\tilde{l}^* > 0$, $\tilde{r}_c^*$ should be found such that:

$$\psi\left(\tilde{r}_c^*,\tilde{l}^*\right) = \frac{\pi}{2} - \alpha_e. \tag{4.11}$$

Assuming that this was found as it was shown in [Tatartchenko 1993], the linearized set of equations at $\left(\tilde{r}_c^*,\tilde{l}^*\right)$ can be written:

$$\begin{cases} \dfrac{d}{d\tilde{t}}\left(\delta\tilde{r}_c\right) = -Pe^l \cdot \dfrac{\partial\psi}{\partial\tilde{r}_c}\left(\tilde{r}_c^*,\tilde{l}^*\right)\cdot\delta\tilde{r}_c - Pe^l \cdot \dfrac{\partial\psi}{\partial\tilde{l}}\left(\tilde{r}_c^*,\tilde{l}^*\right)\cdot\delta\tilde{l} \\ \dfrac{d}{d\tilde{t}}\left(\delta\tilde{l}\right) = 0 \end{cases} \tag{4.12}$$

and the roots S of the corresponding characteristic equation (4.6) are: $S_1 = -Pe^l \cdot \frac{\partial \psi}{\partial \tilde{r}_c}\left(\tilde{r}_c^*, \tilde{l}^*\right)$ and $S_2 = 0$. If $S_1 = -Pe^l \cdot \frac{\partial \psi}{\partial \tilde{r}_c}\left(\tilde{r}_c^*, \tilde{l}^*\right) = A_{\tilde{r}_c \tilde{r}_c} < 0$ then the steady-state $\left(\delta\tilde{r}_c, \delta\tilde{l}\right) \equiv (0,0)$ of the linearized set of equations (4.12) is stable. It must be mentioned that the steady-state $\left(\delta\tilde{r}_c, \delta\tilde{l}\right) \equiv (0,0)$ is not exponentially stable; the perturbation of crystal dimension will attenuate, but that of the crystallization front position will not attenuate.

The transfer of the stability from the linearized system (4.12) to the nonlinear system:

$$\begin{cases} \dfrac{d\tilde{r}_c}{d\tilde{t}} = -Pe^l \cdot \tan\left[\psi\left(\tilde{r}_c, \tilde{l}\right) - \left(\dfrac{\pi}{2} - \alpha_e\right)\right] \\ \dfrac{d\tilde{l}}{d\tilde{t}} = 0 \end{cases} \tag{4.13}$$

when $S_1 = -\nu \cdot \frac{\partial \psi}{\partial r_c}\left(r_c^*, l^*\right)$ is working in this particular case, but not according to the general Lyapunov stability theorem concerning stability after the first approximation. More precisely, when a root S of the characteristic Eq. (4.6) has zero real component, then the zero steady-state of the nonlinear perturbed system (4.4) can be stable or unstable. Therefore, the stability of a steady-state of system (4.10) in the hypothesis assumed by Tatartchenko, should not be analyzed via Lyapunov theorem concerning stability after the first approximation [Balint 2011-1].

The graphical explanation presented in [Tatartchenko 1993] suggests that capillary stability is, in fact, the so-called partial stability. This type of stability is of interest when only the behavior of a pre-specified component (e.g., component $\tilde{r}_c\left(\tilde{t}; \tilde{r}_0, \tilde{l}_0\right)$) of an evolution (e.g., $E\left(\tilde{t}; \tilde{r}_0, \tilde{l}_0\right) = \left(\tilde{r}_c\left(\tilde{t}; \tilde{r}_0, \tilde{l}_0\right), \tilde{l}\left(\tilde{t}; \tilde{r}_0, \tilde{l}_0\right)\right)$) is of interest, or when stability with respect to only one component (component $\tilde{r}_c\left(\tilde{t}; \tilde{r}_0, \tilde{l}_0\right)$) is in fact possible.

The initial work in this area concerns partial stability with respect to disturbances in the entire initial value ($\left(\tilde{r}_0, \tilde{l}_0\right)$ is perturbed) [Rumyantsev 1957], while in subsequent work, partial stability with respect to disturbances in only part of the initial value, $\tilde{r}_0$ is of interest [Fergola

1970, Rouche 1967]. A complex but general description of this subject can be found in [Vorotnikov 1998].

In what follows, just some elements concerning the partial stability with respect to $\tilde{r}_c$ of the system (4.10) are presented, in order to illustrate that this concept covers the concept of capillary stability.

Let $\left(\tilde{r}_c^*, \tilde{l}^*\right)$ be a steady-state of system (4.10).

Definition 4.1.5: The steady-state solution $\left(\tilde{r}_c(\tilde{t}), \tilde{l}(\tilde{t})\right) \equiv \left(\tilde{r}_c^*, \tilde{l}^*\right)$, $\tilde{t} \geq 0$ of (4.10) is *Lyapunov partially stable* with respect to $\tilde{r}_c$ if for any $\varepsilon > 0$ and $\tilde{t} \geq \tilde{t}_0$ there exists $\delta = \delta\left(\varepsilon, \tilde{t}_0\right) > 0$ such that for any $\tilde{r}_0$ satisfying $\left|\tilde{r}_0 - \tilde{r}_c^*\right| < \delta$, the solution $\left(\tilde{r}_c\left(\tilde{t}; \tilde{r}_0, \tilde{l}^*\right), \tilde{l}\left(\tilde{t}; \tilde{r}_0, \tilde{l}^*\right)\right)$ of the system (4.10) is defined for every $\tilde{t} \geq \tilde{t}_0$ and verifies: $\left|\tilde{r}_c\left(\tilde{t}; \tilde{r}_0, \tilde{l}^*\right) - \tilde{r}_c^*\right| < \varepsilon, \ \forall \tilde{t} \geq \tilde{t}_0$.

Remarks 4.3:

i) Here $\left(\tilde{r}_c\left(\tilde{t}; \tilde{r}_0, \tilde{l}^*\right), \tilde{l}\left(\tilde{t}; \tilde{r}_0, \tilde{l}^*\right)\right)$ represents the solution of (4.10) which at the moment $\tilde{t} = \tilde{t}_0$ starts from $\left(\tilde{r}_0, \tilde{l}^*\right)$, i.e. $\tilde{r}_c\left(\tilde{t}_0; \tilde{r}_0, \tilde{l}^*\right) = \tilde{r}_0; \ \tilde{l}\left(\tilde{t}_0; \tilde{r}_0, \tilde{l}^*\right) = \tilde{l}^*$. In this case, only the crystal dimension $\tilde{r}_c^*$ is perturbed.

ii) Definition 4.1.5 expresses the fact that, if at a certain moment $\tilde{t}_0 \geq 0$, a small perturbation $\tilde{r}_0$ of the steady-state $\tilde{r}_c^*$ occurs ($\left|\tilde{r}_0 - \tilde{r}_c^*\right| < \delta\left(\varepsilon, \tilde{t}_0\right)$, $\delta\left(\varepsilon, \tilde{t}_0\right) > 0$ and sufficiently small), then the time dependent solution $\left(\tilde{r}_c\left(\tilde{t}; \tilde{r}_0, \tilde{l}^*\right), \tilde{l}\left(\tilde{t}; \tilde{r}_0, \tilde{l}^*\right)\right)$ which appears after the perturbation remains close to the steady-state $\tilde{r}_c^*$ (i.e. $\left|\tilde{r}_c\left(\tilde{t}; \tilde{r}_0, \tilde{l}^*\right) - \tilde{r}_c^*\right| < \varepsilon$ for $\tilde{t} \geq \tilde{t}_0$ and ε small).

iii) If in Definition 4.1.5 $\delta = \delta\left(\varepsilon, \tilde{t}_0\right)$ is independent of $\tilde{t}_0$, then the steady-state $\left(\tilde{r}_c^*, \tilde{l}^*\right)$ is *Lyapunov uniformly partially stable* with respect to $\tilde{r}_c$.

The system of the perturbed equations with respect to $\tilde{r}_c$ in this case is defined as

$$\begin{cases} \dfrac{d}{d\tilde{t}}\left(\delta\tilde{r}_c\right) = -Pe^l \cdot \tan\left[\psi\left(\delta\tilde{r}_c + \tilde{r}_c^*, \tilde{l}^*\right) - \left(\dfrac{\pi}{2} - \alpha_e\right)\right] \\ \dfrac{d}{d\tilde{t}}\left(\delta\tilde{l}\right) = Pe^l - St\left[\tilde{G}_l\left(\delta\tilde{r}_c + \tilde{r}_c^*, \tilde{l}^*\right) - \tilde{\lambda}G_s\left(\delta\tilde{r}_c + \tilde{r}_c^*, \tilde{l}^*\right)\right] \end{cases} \tag{4.14}$$

If it is considered that the melt and crystal temperature gradients at the melt/solid interface are independent of the crystal dimension, the second equation of (4.14) becomes: $\dfrac{d}{d\tilde{t}}\left(\delta\tilde{l}\right) = 0$ and the system of the perturbed equations is reduced to the equation:

$$\frac{d}{d\tilde{t}}\left(\delta\tilde{r}_c\right) = -Pe^l \cdot \tan\left[\psi\left(\delta\tilde{r}_c + \tilde{r}_c^*, \tilde{l}^*\right) - \left(\frac{\pi}{2} - \alpha_e\right)\right]. \tag{4.15}$$

It can be seen that the function $\delta\tilde{r}_c \equiv 0$ is a solution of the perturbed equation (4.15) and is Lyapunov stable (Def. 4.1) if and only if the steady-state $\left(\tilde{r}_c^*,\ \tilde{l}^*\right)$ of (4.10) is partially Lyapunov stable with respect to $\tilde{r}_c$ [Balint 2011-1].

In order to investigate the stability of the steady-state $\delta\tilde{r}_c \equiv 0$ of the perturbed equation (4.15), the right-hand side of the eq. (4.10) is developed in the form:

$$\frac{d}{d\tilde{t}}\left(\delta\tilde{r}_c\right) = -Pe^l \cdot \frac{\partial\psi}{\partial\tilde{r}_c}\left(\tilde{r}_c^*, \tilde{l}^*\right) \cdot \delta\tilde{r}_c + \ldots \tag{4.16}$$

Considering only the first term of the above development, the linearized system is:

$$\dot{Z} = -Pe^l \cdot \frac{\partial\psi}{\partial\tilde{r}_c}\left(\tilde{r}_c^*, \tilde{l}^*\right) \cdot Z. \tag{4.17}$$

If $-Pe^l \cdot \dfrac{\partial\psi}{\partial\tilde{r}_c}\left(\tilde{r}_c^*, \tilde{l}^*\right)$ is negative, then the steady-state $Z\left(\tilde{t}\right) \equiv 0$ of (4.17) is exponentially stable, i.e.,

$$\left|Z\left(\tilde{t}; Z_0\right)\right| < \left|Z_0\right| \cdot e^{-Pe^l \cdot \frac{\partial\psi}{\partial\tilde{r}_c}\left(\tilde{r}_c^*, \tilde{l}^*\right) \cdot \tilde{t}} \tag{4.18}$$

and it can be shown that the steady-state $\delta\tilde{r}_c \equiv 0$ of the perturbed system (4.15) is also exponentially stable, i.e., there exists $Pe^l{}_1 > 0$ such that for every $\varepsilon > 0$ there exists $\delta\left(\varepsilon\right) > 0$ such that if $\left|\delta\tilde{r}_0\right| < \delta\left(\varepsilon\right)$ then

$$\left|\delta\tilde{r}_c\left(\tilde{t}; \delta\tilde{r}_0\right)\right| < \varepsilon \cdot e^{-Pe^l{}_1 \cdot \tilde{t}},\ \forall\tilde{t} \geq 0 \tag{4.19}$$

Hence the steady-state $\left(\tilde{r}_c^*, \tilde{l}^*\right)$ of the system (4.10) is partially exponentially stable with respect to $\tilde{r}_c$.

4.1.3. Analytical studies of the Lyapunov stability occurring in a mathematical model of the dewetted Bridgman crystal growth under zero gravity conditions

In 2004, Bizet and co-workers developed a study concerning the stability of the dewetting phenomenon under zero gravity conditions, in the frame of the Lyapunov stability theory, [Bizet 2004]. A more thorough investigation of this problem reveals that the presented study is valid only in the case where the liquid meniscus (the liquid free surface at the level of the solid-liquid interface) is fixed at a point on the crucible wall, for example because of sharp roughness or chemical heterogeneities on the crucible wall. In more classical situations the liquid meniscus advances along the crucible wall with a constant wetting angle, which, in case of hysteresis, is a receding angle. For such more usual situations, the analysis of the stability of the radius of the crystal should be studied in a more general way as follows [Balint 2011-1].

In the mathematical description of dewetted Bridgman crystal growth under zero gravity conditions, described in [Bizet 2004] two variables were considered: the crystal radius $\tilde{r}_c$ (or gap thickness $\tilde{e} = \tilde{r}_a - \tilde{r}_c$) and the crystallization front position $\tilde{l}$ (see Fig. 2.6). It was assumed that: (i) the solid and the melt are insulated (adiabatic lateral crucible wall) and the thermal flux is axial; (ii) in a cross-section of the melt/solid system, the temperature is constant; (iii) the gap does not influence the heat transfer because there is no radial heat flux; (iv) the non-dimensional temperature in the solid, $\tilde{T}_s$, and in the liquid, $\tilde{T}_l$, are linear functions of the non-dimensional axial coordinate $\tilde{z}$ and do not depend on the non-dimensional moment of time $\tilde{t}$; (v) the thermal problem is considered as a quasi-steady state, i.e., the thermal fluxes in the solid and in the liquid are constant at each moment.

The melt-solid interface displacement equation is obtained from the thermal balance at the interface:

$$\frac{d\tilde{l}}{d\tilde{t}} = -St\left[\frac{\tilde{T}_h - \tilde{T}_m}{\tilde{H}_a - \tilde{l}} - \tilde{\lambda}\frac{\tilde{T}_m - \tilde{T}_c}{\tilde{l}}\right] \tag{4.20}$$

where: St - Stefan number, $\tilde{\lambda}$ - the non-dimensional thermal conductivity, $\tilde{T}_h$ = constant represents hot temperature at the top of the melt, $\tilde{T}_m$ – the non-dimensional melting temperature, $\tilde{T}_c$ = constant represents cold temperature at the bottom of the seed ($\tilde{T}_c < \tilde{T}_m < \tilde{T}_h$), $\tilde{H}_a$ – the non-dimensional total length of the melt and solid, $\tilde{l}$ is the non-dimensional *z*-coordinate of the melt-solid interface (see Fig. 2.6).

Eq. (4.20) has a unique steady-state solution $\tilde{l}^*$ given by:

$$\tilde{l}^* = \tilde{H}_a \left[1 - \frac{\tilde{T}_h - \tilde{T}_m}{\tilde{T}_h - \tilde{T}_m + \tilde{\lambda}\left(\tilde{T}_m - \tilde{T}_c\right)} \right]. \tag{4.21}$$

It is easy to see that: $0 < \tilde{l}^* < \tilde{H}_a$; $\tilde{l}^* = 0$ if and only if $\tilde{T}_c = \tilde{T}_m$, and $\tilde{l}^* = \tilde{H}_a$ if and only if $\tilde{T}_h = \tilde{T}_m$ ([Balint 2011-1]).

As the derivative of the right-hand side of the Eq. (4.20) at $\tilde{l}^*$ is strictly negative:

$$\frac{d}{d\tilde{l}} \left\{ -St \left[\frac{\tilde{T}_h - \tilde{T}_m}{\tilde{H}_a - \tilde{l}} - \tilde{\lambda} \frac{\tilde{T}_m - \tilde{T}_c}{\tilde{l}} \right] \right\}_{l=l^*} = -St \left[\frac{\tilde{T}_h - \tilde{T}_m}{\left(\tilde{H}_a - \tilde{l}^*\right)^2} + \tilde{\lambda} \frac{\tilde{T}_m - \tilde{T}_c}{\left(\tilde{l}^*\right)^2} \right] < 0, \tag{4.22}$$

it follows that the steady-state solution $\tilde{l}\left(\tilde{t}\right) \equiv \tilde{l}^*$ of the Eq. (4.20) is exponentially stable.

Moreover, since the right-hand side of (4.20) is negative for $\tilde{l}$ in the range $\left(\tilde{l}^*, \tilde{H}_a\right)$, and it is positive for $\tilde{l}$ in the range $\left(0, \tilde{l}^*\right)$, a solution $\tilde{l}\left(\tilde{t}; \tilde{l}'\right)$ of the Eq. (4.20) which starts from $\tilde{l}' \in \left(0, \tilde{l}^*\right)$ increases and tends to $\tilde{l}^*$ as *t* tends to $+\infty$; while a solution $\tilde{l}\left(\tilde{t}; \tilde{l}'\right)$ which starts from $\tilde{l}' \in \left(\tilde{l}^*, \tilde{H}_a\right)$ decreases and tends to $\tilde{l}^*$ as *t* tends to $+\infty$. This means that the region of attraction [Balint 2008-1] of the steady-state solution $\tilde{l}\left(\tilde{t}\right) \equiv \tilde{l}^*$ is equal to the interval $\left(0, \tilde{H}_a\right)$.

From the crystal growth point of view, the time-dependent solution $\tilde{l}\left(\tilde{t}; \tilde{l}_0\right)$ with $\tilde{l}_0$ =seed length ($0 < \tilde{l}_0 < \tilde{l}^*$) presents interest. This solution will be denoted by $\overline{\tilde{l}}\left(\tilde{t}\right)$ and can be found by solving the equation [Balint 2011-1]:

$$\frac{1}{St}\cdot\int_{\tilde{l}_0}^{\bar{\tilde{l}}(\tilde{t})}\frac{\left(u^2-\tilde{H}_a\cdot u\right)du}{\left[\tilde{T}_h-\tilde{T}_m+\tilde{\lambda}\left(\tilde{T}_m-\tilde{T}_c\right)\right]\cdot u-\tilde{H}_a\cdot\tilde{\lambda}\left(\tilde{T}_m-\tilde{T}_c\right)}=\tilde{t} \tag{4.23}$$

The gap size evolution in [Bizet 2004] was treated via crystal radius evolution for which the equation used in E.F.G technique was employed [Tatartchenko 1993]. More precisely, it was assumed that between the hot and cold volumes a communication exists (open crucible). Hence, the gas pressure on both sides is the same, the menisci are spherical and the radii are equal. It was stated that menisci are concave seen from the melt. This last statement implies that the wetting angle θ_c satisfies $\theta_c>\frac{\pi}{2}$ (the crucible is not wetted by the melt). It was also assumed that the growth angle α_e can be reached. These implies that the inequality $\frac{\pi}{2}-\alpha_e<\theta_c-\frac{\pi}{2}$ holds (i.e. $\alpha_e+\theta_c>\pi$).

Under the above hypothesis the deviation (with respect to the crucible wall) of the tangent to the crystal at the crystal-melt-gas triple point, for which the $\tilde{r}$ coordinate is equal to $\tilde{r}_c$, is given by [Balint 2011-1]:

$$\psi\left(\tilde{r}_c\right)-\left(\frac{\pi}{2}-\alpha_e\right)=-\arctan\left(\frac{\tilde{r}_c\cdot\cos\theta_c}{\sqrt{1-\tilde{r}_c^2\cos^2\theta_c}}\right)-\left(\frac{\pi}{2}-\alpha_e\right) \tag{4.24}$$

The deviation $\psi\left(\tilde{r}_c\right)-\left(\frac{\pi}{2}-\alpha_e\right)$ is equal to zero (i.e. the tangent to the crystal wall at the triple point is parallel to the ampoule wall) if and only if $\tilde{r}_c$ is given by:

$$\tilde{r}_c=\tilde{r}_c^*=-\frac{\cos\alpha_e}{\cos\theta_c} \tag{4.25}$$

Therefore, the equation which governs the crystal radius evolution is:

$$\frac{d\tilde{r}_c}{d\tilde{t}}=St\left[\frac{\tilde{T}_h-\tilde{T}_m}{\tilde{H}_a-\tilde{l}\left(\tilde{t}\right)}-\tilde{\lambda}\frac{\tilde{T}_m-\tilde{T}_c}{\tilde{l}\left(\tilde{t}\right)}\right]\cdot\tan\left(\arctan\frac{\tilde{r}_c\cdot\sin\left(\theta_c-\frac{\pi}{2}\right)}{\sqrt{1-\tilde{r}_c^2\cdot\cos^2\theta_c}}-\left(\frac{\pi}{2}-\alpha_e\right)\right). \tag{4.26}$$

In terms of the gap size ($\tilde{e}=\tilde{r}_a-\tilde{r}_c=1-\tilde{r}_c$) and the crystallization front position $\tilde{l}$, the system describing the process, according to [Bizet 2004], is:

$$\begin{cases} \dfrac{d\tilde{l}}{d\tilde{t}} = -St\left[\dfrac{\tilde{T}_h - \tilde{T}_m}{\tilde{H}_a - \tilde{l}(\tilde{t})} - \tilde{\lambda}\dfrac{\tilde{T}_m - \tilde{T}_c}{\tilde{l}(\tilde{t})}\right] \\ \dfrac{d\tilde{e}}{d\tilde{t}} = -St\left[\dfrac{\tilde{T}_h - \tilde{T}_m}{\tilde{H}_a - \tilde{l}(\tilde{t})} - \tilde{\lambda}\dfrac{\tilde{T}_m - \tilde{T}_c}{\tilde{l}(\tilde{t})}\right]\cdot\tan\left(\arctan\dfrac{(1-\tilde{e})\cdot\sin\left(\theta_c - \dfrac{\pi}{2}\right)}{\sqrt{1-(1-\tilde{e})^2\cdot\cos^2\theta_c}} - \left(\dfrac{\pi}{2} - \alpha_e\right)\right) \end{cases} \quad (4.27)$$

Equation (4.26) and the system (4.27) are built up on geometrical considerations rather than modeling the physics of the changes due to the presence of the seed (crystal) [Tatartchenko 1993].

The system (4.27) has the family of steady-states $\left(\tilde{l}^*, \tilde{e}\right)$ with:

$$\begin{cases} \tilde{l}^* = \tilde{H}_a\left[1 - \dfrac{\tilde{T}_h - \tilde{T}_m}{\tilde{T}_h - \tilde{T}_m + \tilde{\lambda}\left(\tilde{T}_m - \tilde{T}_c\right)}\right]. \\ \tilde{e} \in (0,1) \end{cases} \quad (4.28)$$

In this family of the steady-states, $\left(\tilde{l}^*, \tilde{e}_1\right)$ with $\tilde{e}_1 = 1 + \dfrac{\cos\alpha_e}{\cos\theta_c}$ presents special interest since the gap size $\tilde{e}_1$ corresponds to the situation where the tangent to the crystal wall is parallel to the crucible wall.

In order to investigate the Lyapunov stability of the steady-state $\left(\tilde{l}^*, \tilde{e}_1\right)$ using Hurwitz criterion, the right-hand sides of the equations of system (4.20) were denoted by $f\left(\tilde{l}, \tilde{e}\right)$ and $g\left(\tilde{l}, \tilde{e}\right)$:

$$\begin{cases} f\left(\tilde{l}, \tilde{e}\right) = -St\left[\dfrac{\tilde{T}_h - \tilde{T}_m}{\tilde{H}_a - \tilde{l}(\tilde{t})} - \tilde{\lambda}\dfrac{\tilde{T}_m - \tilde{T}_c}{\tilde{l}(\tilde{t})}\right] \\ g\left(\tilde{l}, \tilde{e}\right) = -St\left[\dfrac{\tilde{T}_h - \tilde{T}_m}{\tilde{H}_a - \tilde{l}(\tilde{t})} - \tilde{\lambda}\dfrac{\tilde{T}_m - \tilde{T}_c}{\tilde{l}(\tilde{t})}\right]\tan\left(\arctan\dfrac{(1-\tilde{e})\sin\left(\theta_c - \dfrac{\pi}{2}\right)}{\sqrt{1-(1-\tilde{e})^2\cdot\cos^2\theta_c}} - \left(\dfrac{\pi}{2} - \alpha_e\right)\right). \end{cases} \quad (4.29)$$

According to Hurwitz criterion if the following inequalities hold:

$$\begin{cases} \dfrac{\partial f}{\partial \tilde{l}}\left(\tilde{l}^*,\tilde{e}_1\right)+\dfrac{\partial g}{\partial \tilde{e}}\left(\tilde{l}^*,\tilde{e}_1\right)<0 \\ \dfrac{\partial f}{\partial \tilde{l}}\left(\tilde{l}^*,\tilde{e}_1\right)\cdot\dfrac{\partial g}{\partial \tilde{e}}\left(\tilde{l}^*,\tilde{e}_1\right)-\dfrac{\partial f}{\partial \tilde{e}}\left(\tilde{l}^*,\tilde{e}_1\right)\cdot\dfrac{\partial g}{\partial \tilde{l}}\left(\tilde{l}^*,\tilde{e}_1\right)>0 \end{cases} \tag{4.30}$$

then the steady-state solution $\left(\tilde{l}\left(\tilde{t}\right),\tilde{e}\left(\tilde{t}\right)\right)\equiv\left(\tilde{l}^*,\tilde{e}_1\right)$ is exponentially stable. Then, if at a certain moment $\tilde{t}_0\geq 0$ there is a small perturbation of the steady-state $\left(\tilde{l}^*,\tilde{e}_1\right)$, the steady-state will be recovered.

Concerning the conditions (4.30) it gives:

$$\frac{\partial f}{\partial \tilde{l}}\left(\tilde{l}^*,\tilde{e}_1\right)=-St\left[\frac{\tilde{T}_h-\tilde{T}_m}{\left(\tilde{H}_a-\tilde{l}^*\right)^2}+\tilde{\lambda}\frac{\tilde{T}_m-\tilde{T}_c}{\tilde{l}^{*2}}\right]<0$$

$$\frac{\partial f}{\partial \tilde{e}}\left(\tilde{l}^*,\tilde{e}_1\right)=0$$

$$\frac{\partial g}{\partial \tilde{e}}\left(\tilde{l}^*,\tilde{e}_1\right)=-St\left[\frac{\tilde{T}_h-\tilde{T}_m}{\tilde{H}_a-\tilde{l}^*}-\tilde{\lambda}\frac{\tilde{T}_m-\tilde{T}_c}{\tilde{l}^*}\right]\cdot\frac{\partial}{\partial \tilde{e}}\left[\arctan\frac{\left(1-\tilde{e}\right)\sin\left(\theta_c-\dfrac{\pi}{2}\right)}{\sqrt{1-\left(1-\tilde{e}\right)^2\cos^2\theta_c}}-\left(\frac{\pi}{2}-\alpha_e\right)\right]\left(\tilde{l}^*,\tilde{e}_1\right)=0$$

and hence the first condition of (4.30) is satisfied but the second condition is not satisfied.

Therefore, Hurwitz criterion cannot be applied in order to establish the Lyapunov stability (exponential stability) of the steady-state $\left(\tilde{l}^*,\tilde{e}_1\right)$ (see also [Balint 2011-1]).

In fact, even if the steady-state $\left(\tilde{l}^*,\tilde{e}_1\right)$ is Lyapunov stable, it can be said that if there is a small perturbation of the steady-state $\left(\tilde{l}^*,\tilde{e}_1\right)$, then the time dependent perturbed solution remains close to the steady-state. Such information is not interesting for crystal growth since when the growth process starts, $\tilde{l}$ is equal to $\tilde{l}_0$ - the non-dimensional seed length, which is in general, close to $\tilde{l}^*$ but in some cases can be significantly different (only at the end of the process $\tilde{l}$ approaches $\tilde{l}^*$) [Balint 2011-1].

What is more important is to know if the time-dependent solution $\overline{\tilde{l}}=\overline{\tilde{l}}\left(\tilde{t}\right)$, $\overline{\tilde{e}}=\overline{\tilde{e}}\left(\tilde{t}\right)\equiv\tilde{e}_1$ of the system (4.27) is Lyapunov stable, with $\overline{\tilde{l}}\left(0\right)=\tilde{l}_0$ - seed length. In other words, as was

emphasized in [Balint 2011-1], it is interesting to check if the recovery of the evolution $\left(\overline{\tilde{l}} = \overline{\tilde{l}}\left(\tilde{t}\right),\ \overline{\tilde{e}} = \overline{\tilde{e}}\left(\tilde{t}\right)\right)$ is assured in the case where during the growth, at a moment $\tilde{t}_0 \geq 0$ there are perturbations in the crystal length and gap size.

In this case, the linearized set of equations is written as:

$$\begin{cases} \dot{Z}_1 = a_{11}\left(\tilde{t}\right)\cdot Z_1 + a_{12}\left(\tilde{t}\right)\cdot Z_2 \\ \dot{Z}_2 = a_{21}\left(\tilde{t}\right)\cdot Z_1 + a_{22}\left(\tilde{t}\right)\cdot Z_2 \end{cases} \tag{4.31}$$

where the coefficients $a_{ij}\left(\tilde{t}\right)$ are given by:

$$\left.\begin{aligned}
a_{11}\left(\tilde{t}\right) &= \frac{\partial f}{\partial \tilde{l}}\left(\overline{\tilde{l}}\left(\tilde{t}\right), \tilde{e}_1\right) = -St\left[\frac{\tilde{T}_h - \tilde{T}_m}{\left(\tilde{H}_a - \overline{\tilde{l}}\left(\tilde{t}\right)\right)^2} + \tilde{\lambda}\frac{\tilde{T}_m - \tilde{T}_c}{\left(\overline{\tilde{l}}\left(\tilde{t}\right)\right)^2}\right] < 0 \\
a_{12}\left(\tilde{t}\right) &= \frac{\partial f}{\partial \tilde{e}}\left(\overline{\tilde{l}}\left(\tilde{t}\right), \tilde{e}_1\right) = 0 \\
a_{21}\left(\tilde{t}\right) &= \frac{\partial g}{\partial \tilde{l}}\left(\overline{\tilde{l}}\left(\tilde{t}\right), \tilde{e}_1\right) = -St\left[\frac{\tilde{T}_h - \tilde{T}_m}{\left(\tilde{H}_a - \overline{\tilde{l}}\left(\tilde{t}\right)\right)^2} + \tilde{\lambda}\frac{\tilde{T}_m - \tilde{T}_c}{\left(\overline{\tilde{l}}\left(\tilde{t}\right)\right)^2}\right]\times \\
&\quad \tan\left(\arctan\frac{\left(1-\tilde{e}_1\right)\cdot\sin\left(\theta_c - \frac{\pi}{2}\right)}{\sqrt{1-\left(1-\tilde{e}_1\right)^2\cdot\cos^2\theta_c}} - \left(\frac{\pi}{2} - \alpha_e\right)\right) = 0 \\
a_{22}\left(\tilde{t}\right) &= \frac{\partial g}{\partial \tilde{e}}\left(\overline{\tilde{l}}\left(\tilde{t}\right), \tilde{e}_1\right) = -St\left[\frac{\tilde{T}_h - \tilde{T}_m}{\tilde{H}_a - \overline{\tilde{l}}\left(\tilde{t}\right)} - \tilde{\lambda}\frac{\tilde{T}_m - \tilde{T}_c}{\overline{\tilde{l}}\left(\tilde{t}\right)}\right]\times \\
&\quad \frac{\partial}{\partial \tilde{e}}\tan\left(\arctan\frac{\left(1-\tilde{e}\right)\cdot\sin\left(\theta_c - \frac{\pi}{2}\right)}{\sqrt{1-\left(1-\tilde{e}\right)^2\cdot\cos^2\theta_c}} - \left(\frac{\pi}{2} - \alpha_e\right)\right)\Bigg|_{\tilde{e}=\tilde{e}_1} < 0
\end{aligned}\right\} \tag{4.32}$$

and $\overline{\tilde{l}}\left(\tilde{t}\right)$ is the solution of the initial value problem:

$$\begin{cases} \dfrac{d\tilde{l}}{d\tilde{t}} = -St\left[\dfrac{\tilde{T}_h - \tilde{T}_m}{\tilde{H}_a - \tilde{l}} - \tilde{\lambda}\dfrac{\tilde{T}_m - \tilde{T}_c}{\tilde{l}}\right] \\ \tilde{l}\left(0\right) = \tilde{l}_0 \end{cases} \tag{4.33}$$

Since $\tilde{l}_0 < \tilde{l}^*$ and $\tilde{T}_c < \tilde{T}_m < \tilde{T}_h$, the solution $\overline{\tilde{l}}(\tilde{t})$ of (4.33) (defined for $\tilde{t} \geq 0$) is increasing, concave, bounded above by $\tilde{l}^*$ and tends to $\tilde{l}^*$ as $\tilde{t}$ tends to $+\infty$. Moreover, it is asymptotically Lyapunov stable.

Hence, the coefficients $a_{11}(\tilde{t})$, $a_{22}(\tilde{t})$ are bounded above by some negative constants i.e., there exist $c_1 > 0$ and $c_2 > 0$ such that

$$a_{11}(\tilde{t}) \leq -c_1 \text{ and } a_{22}(\tilde{t}) \leq -c_2 \text{ for } \tilde{t} \geq 0. \tag{4.34}$$

Since the system of the linearized equations (4.31) in this case, according to (4.32), has the form:

$$\begin{cases} \dot{Z}_1 = a_{11}(\tilde{t}) \cdot Z_1 \\ \dot{Z}_2 = a_{22}(\tilde{t}) \cdot Z_2 \end{cases} \tag{4.35}$$

applying the Levinson-Flato theorem (see [Coddington 1955]) it follows that the steady-state solution $\left(Z_1(\tilde{t}), Z_2(\tilde{t})\right) \equiv (0,\ 0)$ of (4.35) is exponentially stable.

Therefore the time dependent solution $\overline{\tilde{l}} = \overline{\tilde{l}}(\tilde{t}), \overline{\tilde{e}}(\tilde{t}) \equiv \tilde{e}_1$ of system (4.27) is exponentially stable.

In more physical terms this stability can be explained in the following way.

Under zero gravity conditions the pressure inside the liquid is imposed by the hot free surface of the liquid and depends only on the ampoule radius and on the wetting angle, θ_c. Then the curvature of the meniscus at the level of the melt-solid interface is totally fixed. Analytical expressions of the gap thickness $\tilde{e}$ have been established [Duffar 1997] for two different cases. As the crystal-crucible gap thickness $\tilde{e}$ is controlled by the growth angle, it follows that $\tilde{e}$ is totally independent of the evolution of the solidification and then of the heat transfer.

1) If there is a connection between the hot and cold sides of the sample, so that the *La*=0, then the following expression is obtained:

$$\tilde{e} = \frac{\cos\alpha_e + \cos\theta_c}{\cos\theta_c} \text{ (see section 2.2.1).}$$

2) If the gases between the hot and cold sides of the sample do not communicate, so that a pressure difference exists ($La \neq 0$), the following expressions are obtained:

$$\tilde{e}_{1,2} = \frac{2\cos\theta_c + La + \cos\alpha_e \pm \sqrt{La^2 + 2La\cos\theta_c + \cos^2\alpha_e}}{2\cos\theta_c + La}$$

which are valid in certain conditions satisfied by *La*, θ_c and α_e values (see section 2.2.1).

It can be observed from the above formulas that the gap thickness does not depend on the meniscus height $\tilde{h}$ and hence the crystal radius ($\tilde{r}_c = 1 - \tilde{e}$) is independent of the solid-liquid interface position.

During solidification, the growth rate is positive and the stability of the radius depends only on the curvature of the meniscus at the melt-solid-gas triple line. It should be pointed out that the crystal radius stability is totally controlled by capillarity.

As explained in chapter 1, the experimental observations under zero gravity conditions have shown, that the crystal-crucible gap is remarkably stable which is in agreement with the above analysis: in zero gravity, the meniscus is convex (i.e. the second derivative of the function which describes the evolution of the meniscus height is positive) as its curvature is imposed by the melt free surface at the hot side (see Figure 4.1.2). Only in case of large Laplace number, *La* the shape of the meniscus at the liquid- solid -gas triple line can be concave (the gap thickness given by $\tilde{e}_2$), so that the crystal radius is not stable.

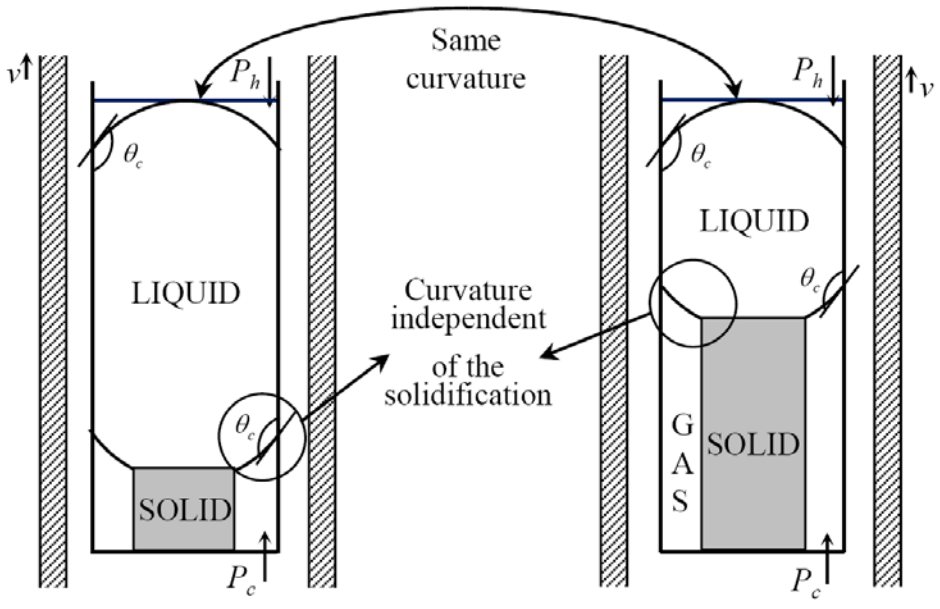

Figure 4.1.1 Dewetting configuration in zero gravity conditions.

4.1.4. Capillary stability in normal gravity: Young-Laplace's equation

In this study, the stability of the growth process is analysed from the capillary point of view only, being assumed that the thermal and pressure effects can be neglected. Therefore, only one equation is needed for stability analysis, which is the Young-Laplace equation. This capillary stability is a particular case of the dynamic stability, taking into account only variations of the crystal-crucible gap thickness such that the crystal side is no longer parallel to the crucible wall [Duffar 1997]. This study of the capillary stability was performed using the Lyapunov approach and was published in [Epure 2010-3].

In the dewetted Bridgman process, the equation which describes the evolution of the crystal radius with time in normal gravity is given by:

$$\frac{d\tilde{r}_c}{d\tilde{t}} = -\frac{d\tilde{l}}{d\tilde{t}} tan\left[\psi\left(\tilde{r}_c,\tilde{l}\right) - \left(\frac{\pi}{2} - \alpha_e\right)\right] \tag{4.36}$$

where $\frac{d\tilde{l}}{d\tilde{t}}$ represents the non-dimensioanl growth rate (i.e. the solid-liquid interface velocity, considered here constant >0).

Denoting by $\tilde{r}_c^*$ the steady-state of (4.36) the perturbed equation with respect to $\tilde{r}_c$ is:

$$\frac{d\left(\delta\tilde{r}_c\right)}{d\tilde{t}} = -\frac{d\tilde{l}}{d\tilde{t}} tan\left[\psi\left(\delta\tilde{r}_c + \tilde{r}_c^*;\tilde{l}\right) - \left(\frac{\pi}{2} - \alpha_e\right)\right] \tag{4.37}$$

where $\delta\tilde{r}_c = \tilde{r}_c - \tilde{r}_c^*$ and $\tilde{l}$ is a parameter ($\tilde{r}_c^*$ is a unique steady-state for any $\tilde{l} \in \left[\tilde{l}_0, \tilde{H}_a - \tilde{l}_0\right]$, [Balint 2008-1]). It can be easily seen that $\delta\tilde{r}_c = 0$ is a solution of the perturbed equation (4.37) and it is stable in Lyapunov sense if and only if the steady-state solution $\tilde{r}_c^*$ of (4.36) is stable.

In order to investigate the stability of the steady-state $\delta\tilde{r}_c = 0$ of the perturbed equation (4.37) the linearized equation with respect to $\tilde{r}_c$ is considered:

$$\frac{d\left(\delta\tilde{r}_c\right)}{d\tilde{t}} = -\tilde{v}_c \cdot \frac{d\psi}{d\tilde{r}_c}\left(\tilde{r}_c^*,\tilde{l}\right) \cdot \delta\tilde{r}_c \tag{4.38}$$

Equation (4.38) is a linear differential equation of the first order and its solution satisfies the inequality:

$$\left|\delta\tilde{r}_c\right| < c \cdot e^{-\tilde{v}_c \cdot \frac{d\psi}{d\tilde{r}_c}\left(\tilde{r}_c^*;\tilde{l}\right)\cdot\tilde{t}} \tag{4.39}$$

The steady-state $\delta\tilde{r}_c = 0$ is stable if and only if the right hand side of the inequality (4.39) tends to zero. This condition is accomplished only if:

$$\frac{d\psi}{d\tilde{r}_c}\left(\tilde{r}_c^*;\tilde{l}\right) > 0 \tag{4.40}$$

which leads to $\frac{d^2\tilde{z}}{d\tilde{r}_c^{\,2}}\left(\tilde{r}_c^*\right) = \frac{1}{cos^2\psi\left(\tilde{r}_c^*\right)} \cdot \frac{d\psi}{d\tilde{r}_c}\left(\tilde{r}_c^*\right) > 0$.

It can be concluded that if $\frac{d^2\tilde{z}}{d\tilde{r}_c^{\,2}}\left(\tilde{r}_c^*\right) > 0$ then the steady-state $\delta\tilde{r}_c = 0$ is a stable solution of the perturbed eq. (4.37) and the steady-state $\tilde{r}_c^*$ of (4.36) is stable.

Therefore, under these hypotheses, it is proved that the capillary stability is linked to the shape of the meniscus at the triple line: with a global concave meniscus (i.e. the second derivative is negative) it is unstable (Fig. 4.1.2 (a)), and with a convex meniscus (i.e. the second derivative, at the triple point, of the function which describes the meniscus surface is positive) the growth is stable (Fig. 4.1.2 (b)). The physical description of this is shown on Figure 4.1.2: as the growth angle α_e should be kept at the triple line, on figure (a) any perturbation of $\tilde{r}_c$ increases. On the contrary, with a convex meniscus (b) the perturbation disappears (i.e. crystal radius variation tends to zero).

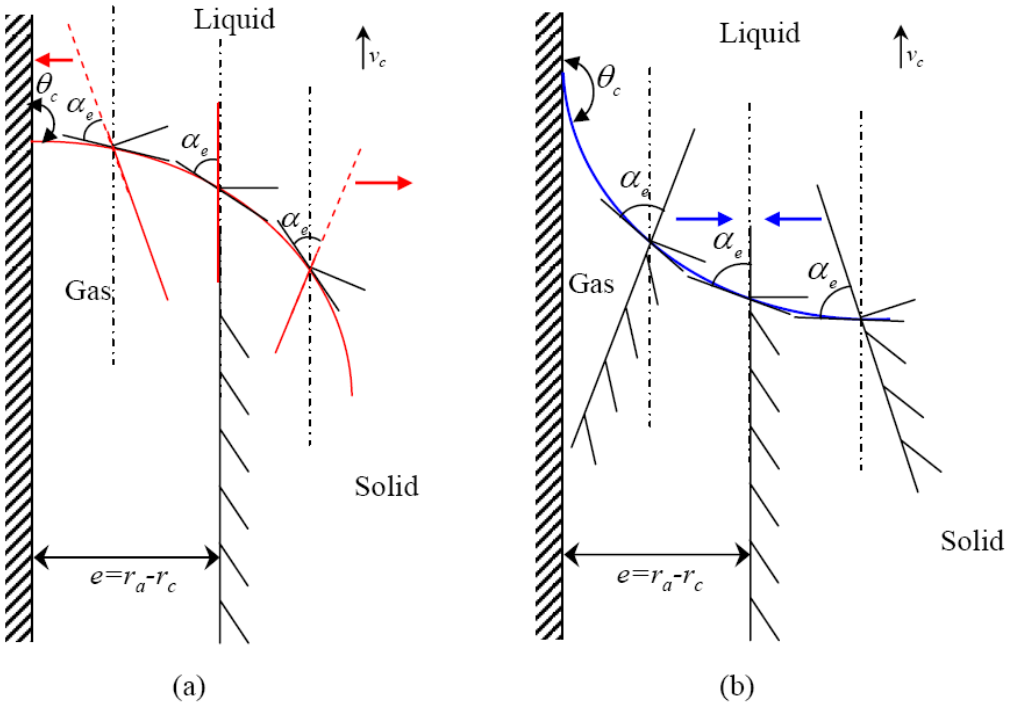

Figure 4.1.2 Physical description of the capillary stability ([Epure 2010-3]).

The dependence of the crystal-crucible gap thickness on the relevant parameters which determine the dewetting occurrence on the ground have been studied, leading to the plot of a diagram (Figure 4.13) with Laplace's number as a function of the Bond number, that furthermore fulfill the capillary stability criteria of the crystal diameter (Figure 4.1.2).

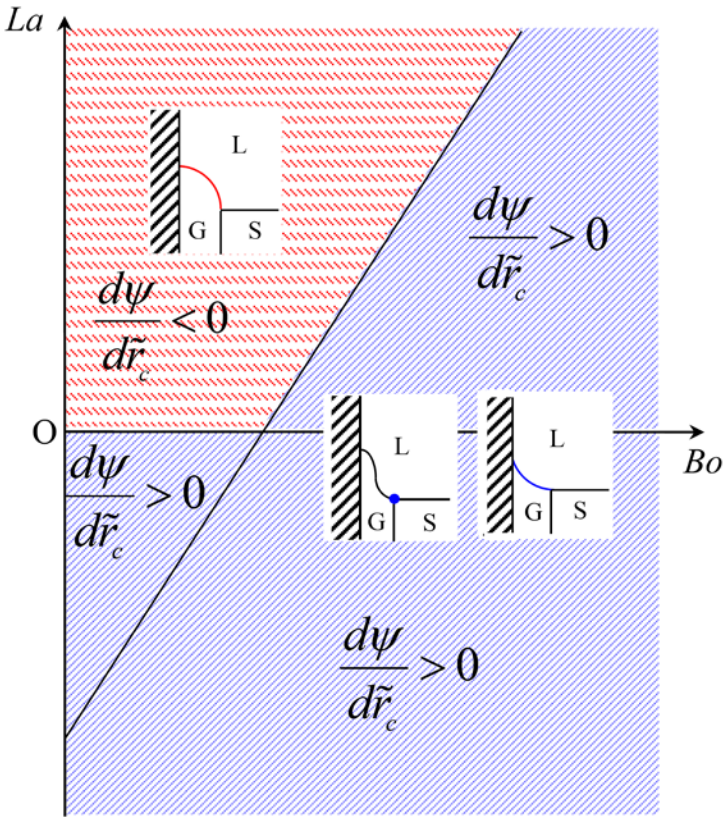

Figure 4.1.3 Stability and meniscus shape zones, in the *La-Bo* plane.

However the capillary stability presented here is only a particular case of the dynamic stability and further studies are needed in order to fully solve the stability problem in dewetting Bridgman process. For experiments performed in terrestrial conditions, melting or solidification change the height of liquid, then the hydrostatic pressure acting on the meniscus, and then the gap thickness. In this case the gap thickness and the solid-liquid interface position are two variables of the problem and two equations are needed, the Young-Laplace equation and the heat balance at the interface, as it will be presented in the next sections of this chapter.

4.2. Practical dynamic stability in terrestrial conditions

In the study of Lyapunov stability, an interesting set of problems deal with bringing the system close to a certain state, rather than the state $x = 0$. In some cases, the desired state of a system may be unstable in the sense of Lyapunov and yet the system may oscillate sufficiently near this

state whose performance is considered acceptable in practice. Many problems fall into this category, for example an aircraft or a missile may oscillate around a mathematically unstable path yet its performance may be acceptable, the problem in a chemical process of keeping the temperature within certain bounds, etc. According to [Gruyitch 2004], Chetaev was the first who described the need of a non-Lyapunov dynamic stability concept ([Chetaev 1961]) for studying the stability of some kinds of airplane movements: he was interested in finding the necessary limits in which can vary the input determined by unknown factors (e.g. time-dependent impervious external conditions) in order to get a stable movement. In western literature, the new concept of stability, so-called practical stability, which is neither weaker nor stronger, but different, than Lyapunov stability was introduced by [La Salle 1961] and further treated in [Bernfeld 1980], [Lakshmikantham 1990], [Gruyitch 2004] and others.

Compared to the Lyapunov stability (which concerns the stability of a specified solution over an unbounded time interval) used frequently in crystal growth, the practical stability of the system over a bounded time interval reflects better the reality because in practice, the dewetted Bridgman solidification process takes place in a bounded time interval, and the interest is the behaviour of the whole process, when unexpected perturbations occur.

4.2.1. Practical stability over a bounded time interval in a forced regime

In order to define this concept the following system of differential equations is considered:

$$\frac{dX_j}{dt} = f_j\left(X_1,...,X_n;t,C,i_1,...,i_m\right),\ \ j=\overline{1,n} \tag{4.41}$$

where t denotes the time, n is the number of unknown functions (which depends on the crystallization technique), C denotes a set of crystallization parameters (thermophysical and other constants of the substance being crystallized, see for example [Tatartchenko 1993]), $\left(i_1,...,i_m\right)$ is an input function (forcing terms) which belongs to a family I of inputs of our interest (as for example the gas pressure diference or the furnace power).

Let $\left[0,\tau\right]$ be a bounded interval of time and $X_A^0,\ X_A^\tau$ two subsets of $\mathbb{R}^n$.

Definition 4.2.1: The system (4.41) is practically stable with respect to X_A^0, X_A^τ, I over the bounded time period $[0,\tau]$ if its solutions obey $\left(X_1\left(t;X_1^0,...,X_n^0,i_1(t),...,i_m(t)\right),...,X_n\left(t;X_1^0,...,X_n^0,i_1(t),...,i_m(t)\right)\right)\in X_A^\tau$ for every $t\in[0,\tau]$, $\left(X_1^0,...,X_n^0\right)\in X_A^0$ and $\left(i_1(t),...,i_m(t)\right)\in I$ (see [La Salle 1961], [Michel 1970-1], [Michel 1970-2]).

Comments:

i) In the previous definition $X_j\left(t;X_1^0,...,X_n^0,i_1(t),...,i_m(t)\right)$, $j=\overline{1,n}$ represents that solution of (4.41) which corresponds to the input $\left(i_1(t),...,i_m(t)\right)$ and at the moment of time $t=0$ starts from $\left(X_1^0,...,X_n^0\right)$, i.e., $X_j\left(0;X_1^0,...,X_n^0,i_1(t),...,i_m(t)\right)=X_j^0$, $j=\overline{1,n}$. This is possible only when there is a unique solution of the equation (4.41) with these properties. For example, when the functions $f_j\left(X_1,...,X_n;t,C,i_1,...,i_m\right)$, $j=\overline{1,n}$ have continuous partial derivatives it can be demonstrated that this is always true [Balint 2011-2].

ii) Definition 4.2.1 expresses the fact that for every input function $\left(i_1(t),...,i_m(t)\right)\in I$, the solution of (4.41) which starts from a point $\left(X_1^0,...,X_n^0\right)\in X_A^0$, during the period of time $[0,\tau]$, has the value included in the set X_A^τ [Balint 2011-2].

Here just some elements concerning the practical stability over a bounded time interval were presented, in order to illustrate that this concept covers a certain stability having practical significance. A complex and general treatment of the subject can be found in [Grujic 1973] and [Gruyitch 2004]. It must be underlined that the mathematical tools used for proving practical stability over a bounded time interval are different from those used for proving the Lyapunov stability, i.e., they are similar to those used for proving continuous dependence on the initial values.

4.2.2. Practical stability of the melt-solid interface displacement equation of the dewetted Bridgman process

In the following, the practical stability over a bounded time period of the equation which describes the melt-solid interface displacement during the solidification process, presented in Section 3.1.2, will be illustrated analytically and numerically as in [Balint 2011-2].

As the solidification process will be analyzed, for solving Eq. (3.51) the initial condition $\tilde{l}_0$ satisfying the inequality $0 < \tilde{l}_0 \le \tilde{l}_*(0)$ must be considered.

In order to show that the melt-solid interface displacement equation is practically stable with respect to $X_A^0 = \left(0, \tilde{l}_*(0)\right)$, $X_A^{t_*} = \left(0, \tilde{H}_a\right)$, $I = \varnothing$ over the bounded time period $\left[0, \tilde{t}_*\right]$ it is necessary to show that the solution of the initial value problem:

$$\begin{cases} \dfrac{d\tilde{l}}{d\tilde{t}} = -St\left[\tilde{G}_l\left(\tilde{l},\tilde{t}\right) - \tilde{\lambda}\tilde{G}_s\left(\tilde{l},\tilde{t}\right)\right] \\ \tilde{l}(0) = \tilde{l}_0 \end{cases} \tag{4.42}$$

is defined for $\tilde{t} \in \left[0, \tilde{t}_*\right]$, is an increasing function and verifies $\tilde{l}_0 < \tilde{l}\left(\tilde{t}; 0, \tilde{l}_0\right) < \tilde{l}_*\left(\tilde{t}\right)$ for every $\tilde{t} \in \left[0, \tilde{t}_*\right]$, where $\tilde{l}_*\left(\tilde{t}\right)$ is the solution of Eq. (3.50) (what was already proved in section 3.1.2.). This means that the melt-solid interface displacement equation is practically stable with respect to $X_A^0 = \left(0, \tilde{l}_*(0)\right)$, $X_A^{t_*} = \left(0, \tilde{H}_a\right)$, $I = \varnothing$ over the bounded time period $\left[0, \tilde{t}_*\right]$.

Remark: In this case there is no forcing term, i.e. $I = \varnothing$.

Below, the practical stability of the melt-solid interface displacement equation was illustrated numerically. In Figure 4.2.1 are represented $\tilde{l}_*\left(\tilde{t}\right)$ and the computed solutions of equation (3.45) $\tilde{l}_1\left(\tilde{t}\right)$, $\tilde{l}_2\left(\tilde{t}\right)$, $\tilde{l}_3\left(\tilde{t}\right)$ representing $\tilde{l}\left(\tilde{t}; 0, \tilde{l}_0\right)$ for $\tilde{l}_0$ equal to 0.36, 1.03, respectively 1.63, for *InSb*. In Figure 4.2.2 are represented $\tilde{l}_*\left(\tilde{t}\right)$ and $\tilde{l}_1\left(\tilde{t}\right)$, $\tilde{l}_2\left(\tilde{t}\right)$, $\tilde{l}_3\left(\tilde{t}\right)$ representing $\tilde{l}\left(\tilde{t}; 0, \tilde{l}_0\right)$ for $\tilde{l}_0$ equal to 0.36, 1.26, respectively 2, for *GaSb*.

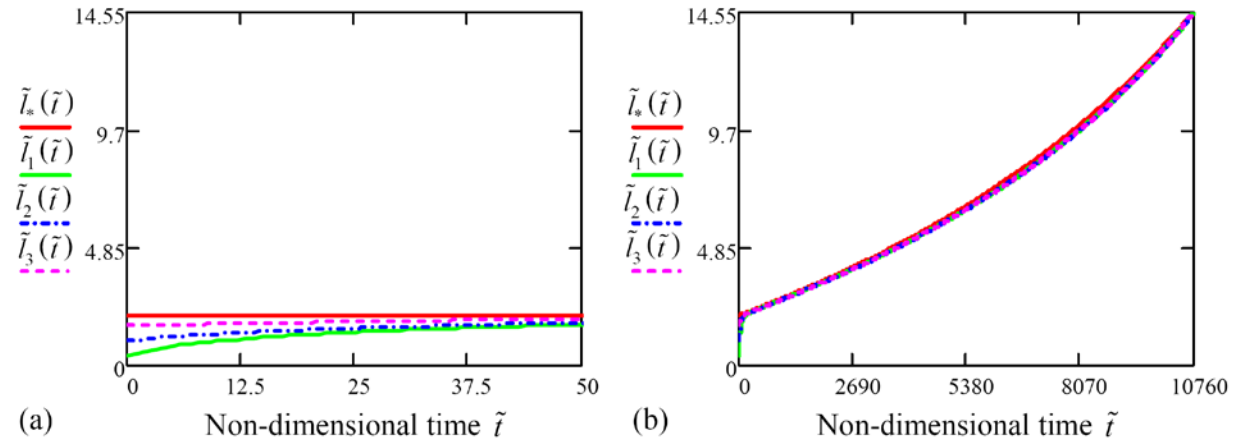

Figure 4.2.1 Practical stability of the melt-solid interface displacement for *InSb* (a) the beginning of the solidification process and (b) the entire solidification process.

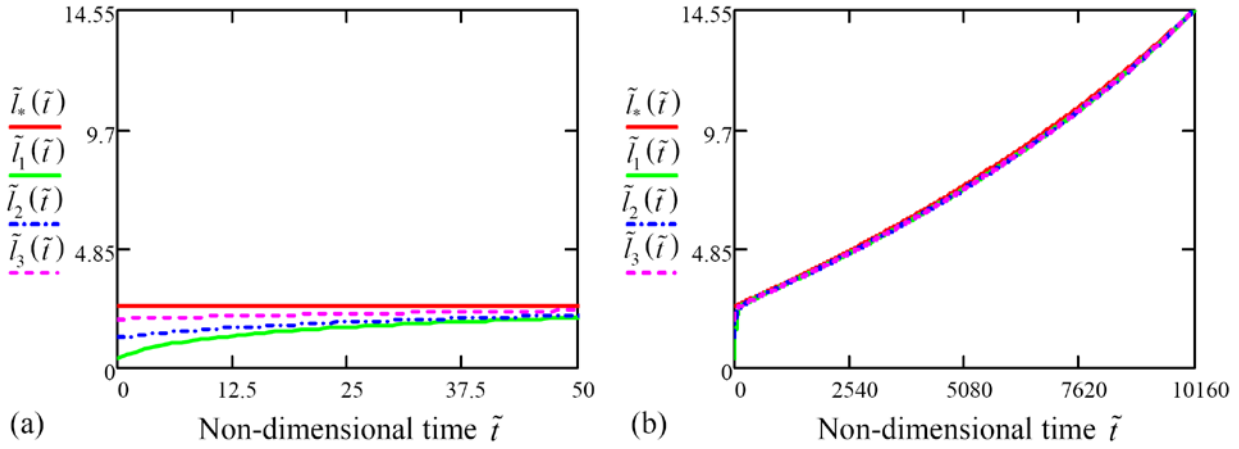

Figure 4.2.2 Practical stability of the melt-solid interface displacement for *GaSb* (a) the beginning of the solidification process and (b) the entire solidification process.

On the Figures 4.2.1 and 4.2.2 it can be seen that $\tilde{l}_*(\tilde{t}) - \tilde{l}\left(\tilde{t};0,\tilde{l}_0\right)$ becomes very small after about 10 minutes, which is a typical relaxation time for antimonide samples of this size [33] and that $l\left(t_*;0,l_0\right) \cong H_a$ (i.e., the entire melt is solidified during the period $[0,t_*]$).

4.2.3. Equations governing the crystal-crucible gap thickness evolution

According to [Tatartchenko 1993], the equation which governs the crystal radius evolution is

$$\frac{d\tilde{r}_c}{d\tilde{t}} = St\left[\tilde{G}_l\left(\tilde{l},\tilde{t}\right) - \tilde{\lambda}\tilde{G}_s\left(\tilde{l},\tilde{t}\right)\right]\tan\left[\psi - \left(\frac{\pi}{2} - \alpha_e\right)\right] \tag{4.43}$$

where ψ represents the angle between the tangent line to the meniscus free surface at the crystal-melt-gas triple point A and the horizontal axis Or.

The angle ψ can be found solving the Young-Laplace equation which describes the free surface of the meniscus:

$$\left(\frac{1}{\tilde{R}_1} + \frac{1}{\tilde{R}_2}\right) = -La + Bo\left(\tilde{H}_a - \tilde{z}\right) + La_{hyd} + La_h^m \tag{4.44}$$

where $1/\tilde{R}_1$, $1/\tilde{R}_2$ – the non-dimensional principal normal curvatures at an arbitrary point M of the free surface, $\tilde{H}_a$ - the non-dimensional coordinate of the top of the melt column with respect to the Oz axis, $\tilde{z}$ - the non-dimensional coordinate of M with respect to the Oz axis, $La = \frac{\left(P_c - P_h\right)\cdot r_a}{\gamma}$ is the non-dimensional Laplace number, $Bo = \frac{\rho_l \cdot g \cdot r_a^2}{\gamma}$ is the non-dimensional Bond number, $Bo\left(\tilde{H}_a - \tilde{z}\right)$ represents the non-dimensional hydrostatic pressure of the melt column, La_{hyd} - the hydrodynamic *La* number due to the convection (see Fig. 4.2.3).

It is assumed that the ampoule is closed and the gas pressures in the hot and cold volumes are controlled independently [Balint 2011-2].

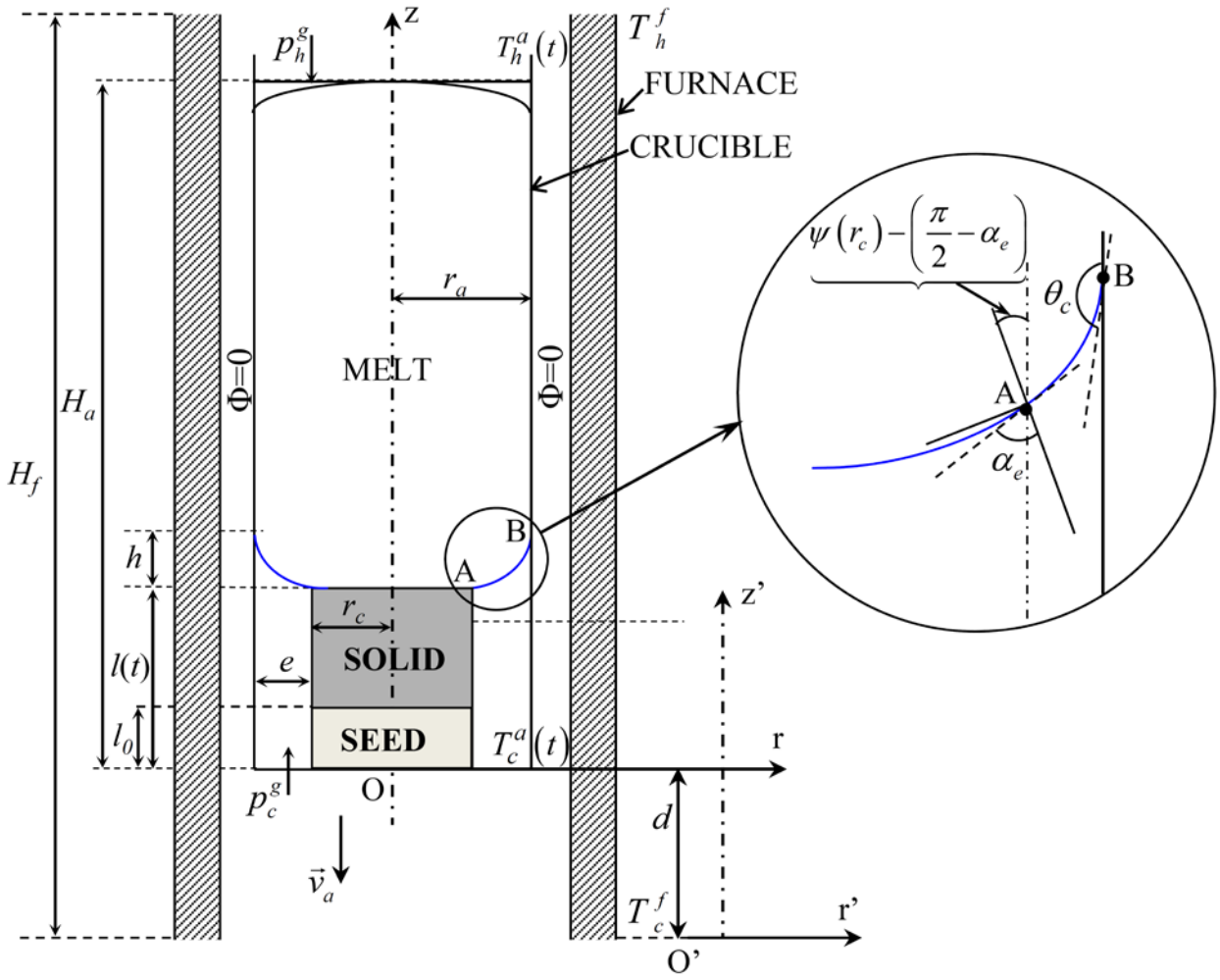

Figure 4.2.3 Schematic dewetted Bridgman technique in normal gravity conditions.

The pressure difference across the free surface appearing in the right-hand side of the equation (4.43) can be written as [Balint 2011-2]:

$$\begin{aligned} -La + Bo\left(\tilde{H}_a - \tilde{z}\right) + La_{hyd} + La_h^m &= -Bo\cdot\tilde{z} - \left(La - Bo\cdot\tilde{H}_a - La_{hyd} - La_h^m\right) \\ &= -Bo\cdot\tilde{z} - \tilde{P} \end{aligned} \tag{4.45}$$

where

$$\tilde{P} = La - Bo\cdot\tilde{H}_a - La_{hyd} - La_h^m = \Delta\tilde{P} - Bo\cdot\tilde{H}_a \quad \text{and} \quad \Delta\tilde{P} = La - La_{hyd} - La_h^m \tag{4.46}$$

The pressure $\tilde{P}$ does not depend on the axial coordinate *z* but it depends on the moment of time during the growth process. In the following, $\Delta\tilde{P}$ will be called forcing term (or total input) and it will be written as

$$\Delta\tilde{P} = Bo\left[\tilde{H}_a - \tilde{l}\left(\tilde{t}\right)\right] + i\left(\tilde{t}\right) \tag{4.47}$$

The part $Bo\left[\tilde{H}_a - \tilde{l}\left(\tilde{t}\right)\right]$ of $\Delta\tilde{P}$ represents that part of the cold gas pressure which compensates the hydrostatic pressure of the melt column at the moment of time $\tilde{t}$ and it is determined by the coordinate of the melt-solid interface $\tilde{l}\left(\tilde{t}\right)$. The part $i\left(\tilde{t}\right)$ is unknown and cumulates $i\left(\tilde{t}\right) = La - Bo\left(\tilde{H}_a - \tilde{l}\left(\tilde{t}\right)\right) - La_{hyd} - La_h^m$.

The main objective is to find the range where the values of $i\left(\tilde{t}\right)$ must be included, in order to have an appropriate meniscus for the crystal growth (i.e. strictly positive gap thickness).

In the case of an axisymmetric meniscus the equation (4.44) becomes:

$$\frac{d^2\tilde{z}}{d\tilde{r}^2} = -\left(Bo\cdot\tilde{z} + \tilde{P}\right)\left[1+\left(\frac{d\tilde{z}}{d\tilde{r}}\right)^2\right]^{\frac{3}{2}} - \frac{1}{\tilde{r}}\left[1+\left(\frac{d\tilde{z}}{d\tilde{r}}\right)^2\right]\frac{d\tilde{z}}{d\tilde{r}}. \tag{4.48}$$

The solutions of this equation should verify the following conditions: the wetting angle θ_c on the crucible and the growth angle α_e at the triple phase line which is at the height *l*.

In order to grow a crystal with constant radius $\tilde{r}_c$, the solution of equation (4.48) must verify the following conditions:

$$\begin{aligned}
&\tilde{z}\left(\tilde{r}_c\right) = \tilde{l};\ \frac{d\tilde{z}}{d\tilde{r}}\left(\tilde{r}_c\right) = \tan\left(\frac{\pi}{2} - \alpha_e\right);\\
&\tilde{z}\left(1\right) = \tilde{l} + \tilde{h};\ \frac{d\tilde{z}}{d\tilde{r}}\left(1\right) = \tan\left(\theta_c - \frac{\pi}{2}\right);\\
&\tilde{z}\left(\tilde{r}\right)\text{is strictly increasing on } \left[\tilde{r}_c, 1\right].
\end{aligned} \tag{4.49}$$

It should be noticed that the nonlinear boundary value problem given by (4.48)-(4.49) represents the formal mathematical transcription of the equilibrium state presented on the Figure 4.2.3 (see [Balint 2011-2]). This is an overspecified boundary value problem and has no solution for arbitrary values of $\tilde{P}$ and $\tilde{h}$. Therefore, we are interested in finding those ranges of $\tilde{P}$ and $\tilde{h}$ for which the above problem has approximate solution, i.e. a solution that verifies the equation

(4.48) and conditions (4.49) for for r_c' and l' closed to r_c and l respectively. This means that small variations of the crystal radius r_c and the crystallization front position l are allowed. The crystal radius variations must be sufficiently small for avoiding the crystal reattchment to the inner crucible wall. Then, in order to reach the proposed objective, the nonlinear boundary value problem (4.48)-(4.49) is transformed into the problem:

$$\begin{cases} \dfrac{d\tilde{z}}{d\tilde{r}} = \tan\psi \\ \dfrac{d\psi}{d\tilde{r}} = -\left(Bo\cdot\tilde{z}+\tilde{P}\right)\dfrac{1}{\cos\psi} - \dfrac{1}{\tilde{r}}\tan\psi \end{cases} \tag{4.50}$$

$$\begin{aligned} &\tilde{z}\left(\tilde{r}_c\right) = \tilde{l};\ \psi\left(\tilde{r}_c\right) = \frac{\pi}{2} - \alpha_e; \\ &\tilde{z}\left(1\right) = \tilde{l} + \tilde{h};\ \psi\left(1\right) = \theta_c - \frac{\pi}{2}; \\ &\tilde{z}\left(\tilde{r}\right) \text{ is strictly increasing on } \left[\tilde{r}_c, 1\right]. \end{aligned} \tag{4.51}$$

Because of different behaviours of the meniscus shape in the cases (I) $\theta_c + \alpha_e > 180°$, and (II) $\theta_c + \alpha_e < \pi$, as already explained in Chapter 2, qualitative studies must be performed in each case separately.

Case I: $\theta_c + \alpha_e > 180°$

In order to get information about the pressure difference, the meniscus height and the function $\tilde{z}\left(\tilde{r}\right)$ that describes the meniscus surface, mathematical tools were used leading to some theorems presented below in non-dimensional terms. These theorems were reported in dimensional terms in [Balint 2011-2].

Considering the nonlinear boundary value problem (NLBVP) given by (4.48) and (4.49) it can be stated:

Theorem 4.1 *If* $\tilde{z}\left(\tilde{r}\right)$ *is a convex solution of the NLBVP* (4.48) - (4.49)*, then for the gap thicknesss* $\tilde{e} = 1 - \tilde{r}_c$*, the pressure difference* $\Delta\tilde{P} = \tilde{P} + Bo\cdot\tilde{H}_a$*, the meniscus height* $\tilde{h}$ *and* $\tilde{z}\left(\tilde{r}\right)$ *the following inequalities hold:*

$$\left.\begin{aligned}
&Bo\left[\tilde{H}_a-\left(\tilde{l}+\tilde{h}\right)\right]-\frac{\theta_c+\alpha_e-\pi}{\tilde{e}}\sin\alpha_e+\frac{1}{1-\tilde{e}}\cos\theta_c\le\Delta\tilde{P}\\
&\quad\le Bo\left[\tilde{H}_a-\tilde{l}\right]-\frac{\theta_c+\alpha_e-\pi}{\tilde{e}}\sin\theta_c-\cos\alpha_e,\\
&\tilde{e}\cdot\tan\left(\frac{\pi}{2}-\alpha_e\right)\le\tilde{h}\le\tilde{e}\cdot\tan\left(\theta_c-\frac{\pi}{2}\right),\\
&\tilde{l}+\tilde{h}-\left(1-\tilde{r}\right)\tan\left(\theta_c-\frac{\pi}{2}\right)\le\tilde{z}\left(\tilde{r}\right)\le\tilde{l}+\tilde{h}-\left(1-\tilde{r}\right)\tan\left(\frac{\pi}{2}-\alpha_e\right).
\end{aligned}\right\}\tag{4.52}$$

Proof: Let $\tilde{z}\left(\tilde{r}\right)$ be a convex ($\frac{d^2\tilde{z}}{d\tilde{r}^2}>0$) solution of the NLBVP (4.48) - (4.49) and $\psi\left(\tilde{r}\right)=\arctan\frac{d\tilde{z}}{d\tilde{r}}$. Since $\psi\left(\tilde{r}\right)$ verifies:

$$\left.\begin{aligned}
&\frac{d\psi}{d\tilde{r}}=-\frac{1}{\cos\psi\left(\tilde{r}\right)}\left[Bo\cdot\tilde{z}\left(\tilde{r}\right)+\tilde{P}+\frac{1}{\tilde{r}}\sin\psi\left(\tilde{r}\right)\right],\\
&\psi\left(\tilde{r}_c\right)=\frac{\pi}{2}-\alpha_e\ \text{and}\ \psi\left(1\right)=\theta_c-\frac{\pi}{2}.
\end{aligned}\right\}\tag{4.53}$$

according to the Lagrange mean value theorem, there exist $\tilde{r}_1\in\left(\tilde{r}_c,1\right)=\left(1-\tilde{e},1\right)$ such that the following equality holds

$$\tilde{P}=-\frac{\theta_c+\alpha_e-\pi}{\tilde{e}}\cos\psi\left(\tilde{r}_1\right)-Bo\cdot\tilde{z}\left(\tilde{r}_1\right)-\frac{1}{\tilde{r}_1}\sin\psi\left(\tilde{r}_1\right)\tag{4.54}$$

Since $\frac{d^2\tilde{z}}{d\tilde{r}^2}\left(\tilde{r}\right)>0$ for any $\tilde{r}\in\left[\tilde{r}_c,1\right]$, the function $\frac{d\tilde{z}}{d\tilde{r}}\left(\tilde{r}\right)$ is strictly increasing on $\left[\tilde{r}_c,1\right]$, and hence the following inequalities are satisfied:

$$\left.\begin{aligned}
&\frac{\pi}{2}-\alpha_e\le\psi\left(\tilde{r}_1\right)\le\theta_c-\frac{\pi}{2},\\
&\cos\left(\theta_c-\frac{\pi}{2}\right)\le\cos\psi\left(\tilde{r}_1\right)\le\cos\left(\frac{\pi}{2}-\alpha_e\right),\\
&\sin\left(\frac{\pi}{2}-\alpha_e\right)\le\sin\psi\left(\tilde{r}_1\right)\le\sin\left(\theta_c-\frac{\pi}{2}\right),\\
&\tan\left(\frac{\pi}{2}-\alpha_e\right)\le\tan\psi\left(\tilde{r}_1\right)\le\tan\left(\theta_c-\frac{\pi}{2}\right).
\end{aligned}\right\}\tag{4.55}$$

Because $\tilde{z}\left(1\right)-\tilde{z}\left(\tilde{r}_c\right)=\tilde{h}=\left(1-\tilde{r}_c\right)\tan\psi\left(\tilde{r}_2\right)$ it follows that $\tilde{h}$ verifies

$$\tilde{e}\cdot\tan\left(\frac{\pi}{2}-\alpha_e\right)\le\tilde{h}\le\tilde{e}\cdot\tan\left(\theta_c-\frac{\pi}{2}\right). \tag{4.56}$$

Taking into account inequalities (4.55) and substituting $\tilde{P}=\Delta\tilde{P}-Bo\cdot\tilde{H}_a$, the inequalities $(4.52)_1$ are obtained. Inequalities $(4.52)_3$ can be obtained integrating $(4.55)_4$ on $\left[\tilde{r}_c,1\right]$. ■

Remark: If in $(4.52)_1$, $\Delta\tilde{P}$ is replaced by $Bo\left(\tilde{H}_a-\tilde{l}\right)+i\left(\tilde{t}\right)$, then the following inequality is obtained:

$$-Bo\cdot\tilde{h}-\frac{\theta_c+\alpha_e-\pi}{\tilde{e}}\sin\alpha_e+\frac{1}{1-\tilde{e}}\cos\theta_c\le i\left(\tilde{t}\right)\le-\frac{\theta_c+\alpha_e-\pi}{\tilde{e}}\sin\theta_c-\cos\alpha_e. \tag{4.57}$$

Theorem 4.2 *If* $\tilde{e}\in(0,1)$, $\tilde{l}>0$, $\tilde{h}\in\left(\tilde{e}\cdot\tan\left(\frac{\pi}{2}-\alpha_e\right),\tilde{e}\cdot\tan\left(\theta_c-\frac{\pi}{2}\right)\right)$ *and* $\Delta\tilde{P}=\tilde{P}+Bo\cdot\tilde{H}_a$ *satisfies :*

$$\Delta\tilde{P}<Bo\left[\tilde{H}_a-\left(\tilde{l}+\tilde{h}\right)\right]-\frac{\theta_c+\alpha_e-\pi}{\tilde{e}}\sin\alpha_e+\frac{1}{1-\tilde{e}}\cos\theta_c \tag{4.58}$$

then there exist $\tilde{r}_c\in(1-\tilde{e},1)$, $l'\in\left(l+h-e\cdot\tan\left(\theta_c-\frac{\pi}{2}\right),\ l+h-\left(r_a-r_c\right)\tan\left(\frac{\pi}{2}-\alpha_e\right)\right)$ *and a convex solution of the initial value problem (IVP):*

$$\frac{d^2\tilde{z}}{d\tilde{r}^2}=-\left(Bo\cdot\tilde{z}+\tilde{P}\right)\cdot\left[1+\left(\frac{d\tilde{z}}{d\tilde{r}}\right)^2\right]^{\frac{3}{2}}-\frac{1}{\tilde{r}}\left[1+\left(\frac{d\tilde{z}}{d\tilde{r}}\right)^2\right]\cdot\frac{d\tilde{z}}{d\tilde{r}} \tag{4.59}$$

$$\tilde{z}(1)=\tilde{l}+\tilde{h};\ \frac{d\tilde{z}}{d\tilde{r}}(1)=\tan\left(\theta_c-\frac{\pi}{2}\right), \tag{4.60}$$

which verifies $\tilde{z}\left(\tilde{r}_c\right)=\tilde{l}';\ \frac{d\tilde{z}}{d\tilde{r}}\left(\tilde{r}_c\right)=\tan\left(\frac{\pi}{2}-\alpha_e\right)$.

Proof: Because (4.58) implies:

$$\tilde{P}<-Bo\left(\tilde{l}+\tilde{h}\right)-\frac{\theta_c+\alpha_e-\pi}{\tilde{e}}\sin\alpha_e+\frac{1}{1-\tilde{e}}\cos\theta_c \tag{4.61}$$

the inequality

$$\tilde{P}+Bo\left(\tilde{l}+\tilde{h}\right)-\frac{1}{1-\tilde{e}}\cos\theta_c<-\frac{\theta_c+\alpha_e-\pi}{\tilde{e}}\sin\alpha_e<0$$

is obtained. Then, the solution $\tilde{z}=\tilde{z}\left(\tilde{r}\right)$ of the IVP (4.59) - (4.60) at $\tilde{r}_a=1$ satisfies:

$$\frac{d\psi}{d\tilde{r}} = -\frac{1}{\cos\left(\theta_c - \frac{\pi}{2}\right)}\left[\tilde{P} + Bo\left(\tilde{l} + \tilde{h}\right) - \cos\theta_c\right], \text{ where } \psi\left(\tilde{r}\right) = \arctan\frac{d\tilde{z}}{d\tilde{r}}.$$

Thus, it follows that $\frac{d\psi}{d\tilde{r}}(1) > 0$ and hence there is $\tilde{r}' \in I \cap (0,1)$ such that the following inequalities hold:

$$\frac{d^2\tilde{z}}{d\tilde{r}^2}\left(\tilde{r}\right) > 0;\ \frac{d\tilde{z}}{d\tilde{r}}\left(\tilde{r}\right) > \tan\left(\frac{\pi}{2} - \alpha_e\right);\ \frac{d\tilde{z}}{d\tilde{r}}\left(\tilde{r}\right) \le \tan\left(\theta_c - \frac{\pi}{2}\right), \tag{4.62}$$

for any $\tilde{r} \in \left[\tilde{r}', 1\right]$. Here I represents the maximal interval of existence for the considered solution $\tilde{z}\left(\tilde{r}\right)$ of the IVP (4.59) - (4.60).

Let consider that $\tilde{r}_*$ is defined as:

$$\tilde{r}_* = \inf\left\{\tilde{r}' \in I \cap (0,1) \,\middle|\, \text{inequalities (4.58) hold}, \forall\, \tilde{r} \in \left[\tilde{r}', 1\right]\right\} \tag{4.63}$$

It is obvious that $\tilde{r}_* \ge 0$, and for any $\tilde{r} \in \left(\tilde{r}_*, 1\right]$ inequalities (4.62) hold. Also, the limits $\frac{d\tilde{z}}{d\tilde{r}}\left(\tilde{r}_* + 0\right) = \lim_{\tilde{r} \searrow \tilde{r}_*} \frac{d\tilde{z}}{d\tilde{r}}\left(\tilde{r}\right)$; $\tilde{z}\left(\tilde{r}_* + 0\right) = \lim_{\tilde{r} \searrow \tilde{r}_*} \tilde{z}\left(\tilde{r}\right)$ exist and satisfy:

$$\left.\begin{aligned} &\tan\left(\frac{\pi}{2} - \alpha_e\right) \le \frac{d\tilde{z}}{d\tilde{r}}\left(\tilde{r}_* + 0\right) \le \tan\left(\theta_c - \frac{\pi}{2}\right), \\ &\tilde{l} + \tilde{h} - \left(1 - \tilde{r}_*\right)\tan\left(\theta_c - \frac{\pi}{2}\right) \le \tilde{z}\left(\tilde{r}_* + 0\right) \le \tilde{l} + \tilde{h} - \left(1 - \tilde{r}_*\right)\tan\left(\frac{\pi}{2} - \alpha_e\right). \end{aligned}\right\} \tag{4.64}$$

Similarly, the limit $\frac{d^2\tilde{z}}{d\tilde{r}^2}\left(\tilde{r}_* + 0\right) = \lim_{\tilde{r} \searrow \tilde{r}_*} \frac{d^2\tilde{z}}{d\tilde{r}^2}\left(\tilde{r}\right)$ exists and satisfies $\frac{d^2\tilde{z}}{d\tilde{r}^2}\left(\tilde{r}_* + 0\right) \ge 0$.

Due to the fact that $\tilde{r}_*$ is the infimum defined by (4.63), and

$$\frac{d^2\tilde{z}}{d\tilde{r}^2}\left(\tilde{r}_* + 0\right) \ge 0\ ;\ \frac{d\tilde{z}}{d\tilde{r}}\left(\tilde{r}_* + 0\right) \ge \tan\left(\frac{\pi}{2} - \alpha_e\right)\ ;\ \frac{d\tilde{z}}{d\tilde{r}}\left(\tilde{r}_* + 0\right) \le \tan\left(\theta_c - \frac{\pi}{2}\right),$$

one of these inequalities must become equality.

Since $\frac{d\tilde{z}}{d\tilde{r}}\left(\tilde{r}_* + 0\right) < \frac{d\tilde{z}}{d\tilde{r}}\left(\tilde{r}\right) \le \tan\left(\theta_c - \frac{\pi}{2}\right)$ for any $\tilde{r} \in \left(\tilde{r}_*, 1\right]$ it is impossible to obtain $\frac{d\tilde{z}}{d\tilde{r}}\left(\tilde{r}_* + 0\right) = \tan\left(\theta_c - \frac{\pi}{2}\right)$. Therefore, it must be found which one of the other two inequalities: $\frac{d^2\tilde{z}}{d\tilde{r}^2}\left(\tilde{r}_* + 0\right) \ge 0$; $\frac{d\tilde{z}}{d\tilde{r}}\left(\tilde{r}_* + 0\right) \ge \tan\left(\frac{\pi}{2} - \alpha_e\right)$ has to become equality.

Firstly, we will show that the inequality $\tilde{r}_* > 1 - \tilde{e}$ holds. For this purpose the contrary is assumed, i.e., $\tilde{r}_* \le 1 - \tilde{e}$. According to the Lagrange mean value theorem there is $\xi \in \left(1 - \tilde{e}, 1\right)$ such that the following equality holds:

$$\psi\left(1\right) - \psi\left(1 - \tilde{e}\right) = \tilde{e} \cdot \frac{d\psi}{d\tilde{r}}\left(\xi\right) = -\frac{\tilde{e}}{\cos\psi\left(\xi\right)}\left[Bo \cdot \tilde{z}\left(\xi\right) + \tilde{P} + \frac{1}{\xi}\sin\psi\left(\xi\right)\right].$$

Using (4.61) the following estimations can be obtained:

$$\psi\left(1\right) - \psi\left(1 - \tilde{e}\right) >$$

$$-\frac{\tilde{e}}{\cos\psi\left(\xi\right)}\left[-Bo\left(\tilde{l} + \tilde{h}\right) - \frac{\theta_c + \alpha_e - \pi}{\tilde{e}}\sin\alpha_e + \frac{1}{1 - \tilde{e}}\cos\theta_c + Bo \cdot \tilde{z}\left(\xi\right) + \frac{\sin\psi\left(\xi\right)}{\xi}\right]$$

$$= \frac{\tilde{e}}{\cos\psi\left(\xi\right)}\left[Bo\left(\tilde{l} + \tilde{h} - \tilde{z}\left(\xi\right)\right) + \frac{\theta_c + \alpha_e - \pi}{\tilde{e}}\sin\alpha_e + \frac{\sin\left(\theta_c - \frac{\pi}{2}\right)}{1 - \tilde{e}} - \frac{\sin\psi\left(\xi\right)}{\xi}\right] >$$

$$> \frac{1}{\cos\psi\left(\xi\right)}\left(\theta_c + \alpha_e - \pi\right)\sin\alpha_e = \left(\theta_c + \alpha_e - \pi\right)\frac{\cos\left(\frac{\pi}{2} - \alpha_e\right)}{\cos\psi\left(\xi\right)}$$

$$> \left(\theta_c + \alpha_e - \pi\right)\frac{\cos\left(\frac{\pi}{2} - \alpha_e\right)}{\cos\left(\theta_c - \frac{\pi}{2}\right)} > \theta_c + \alpha_e - \pi.$$

Hence $\psi\left(1 - \tilde{e}\right) < \frac{\pi}{2} - \alpha_e$, which is impossible. In this way it is shown that $\tilde{r}_* > 1 - \tilde{e}$.

Further, we will show that from $\tilde{r}_* > 1-\tilde{e}$ it follows that $\frac{d^2\tilde{z}}{d\tilde{r}^2}\left(\tilde{r}_* + 0\right) \neq 0$. For this purpose we assume the contrary i.e. $\frac{d^2\tilde{z}}{d\tilde{r}^2}\left(\tilde{r}_* + 0\right) = 0$. Hence, according to the eq. (4.59) we obtain:

$$\tilde{z}\left(\tilde{r}_* + 0\right) = -\frac{\tilde{P}}{Bo} - \frac{1}{Bo \cdot \tilde{r}_*}\sin\psi\left(\tilde{r}_* + 0\right)$$

$$> \frac{1}{Bo}\frac{\theta_c + \alpha_e - \pi}{\tilde{e}}\sin\alpha_e - \frac{1}{Bo}\frac{1}{1-\tilde{e}}\cos\theta_c + \tilde{l} + \tilde{h} - \frac{1}{Bo \cdot \tilde{r}_*}\sin\psi\left(\tilde{r}_* + 0\right)$$

$$= \frac{1}{Bo}\frac{\theta_c + \alpha_e - \pi}{\tilde{e}}\sin\alpha_e + \tilde{l} + \tilde{h} + \frac{1}{Bo}\left[\frac{\sin\left(\theta_c - \frac{\pi}{2}\right)}{1-\tilde{e}} - \frac{\sin\psi\left(\tilde{r}_* + 0\right)}{\tilde{r}_*}\right] > \tilde{l} + \tilde{h}$$

that is not possible. In this way it is proven that $\frac{d^2\tilde{z}}{d\tilde{r}^2}\left(\tilde{r}_* + 0\right) \neq 0$.

Taking into account that $\frac{d\tilde{z}}{d\tilde{r}}\left(\tilde{r}_* + 0\right) \neq \tan\left(\theta_c - \frac{\pi}{2}\right)$ and $\frac{d^2\tilde{z}}{d\tilde{r}^2}\left(\tilde{r}_* + 0\right) \neq 0$, it is deduced that $\frac{d\tilde{z}}{d\tilde{r}}\left(\tilde{r}_* + 0\right) = \tan\left(\frac{\pi}{2} - \alpha_e\right)$. Concerning the value $\tilde{z}\left(\tilde{r}_* + 0\right)$, the inequality $\tilde{r}_* > 1-\tilde{e}$ implies:

$$\tilde{l} + \tilde{h} - \tilde{e}\tan\left(\theta_c - \frac{\pi}{2}\right) \leq \tilde{z}\left(\tilde{r}_* + 0\right) \leq \tilde{l} + \tilde{h} - \left(1-\tilde{r}_*\right)\tan\left(\frac{\pi}{2} - \alpha_e\right).$$

Considering $\tilde{r}_c = \tilde{r}_*$ and $\tilde{l}' = \tilde{z}\left(\tilde{r}_* + 0\right)$, it is obtained that the Theorem 4.2 is valid.■

Remark: Replacing in (4.58) $\Delta\tilde{P}$ by $Bo\left(\tilde{H}_a - \tilde{l}\right) + i\left(\tilde{t}\right)$, the following inequality holds:

$$i\left(\tilde{t}\right) < -\frac{\theta_c + \alpha_e - \pi}{\tilde{e}}\sin\alpha_e + \frac{1}{1-\tilde{e}}\cos\theta_c - Bo \cdot \tilde{h}\,.$$

Theorem 4.3 *If* $\tilde{e}_1, \tilde{e}_2 \in (0,1)$, $\tilde{e}_1 < \tilde{e}_2$, $\tilde{l} > 0$, $\tilde{h} \in \left(\tilde{e}_2 \cdot \tan\left(\frac{\pi}{2} - \alpha_e\right), \tilde{e}_2 \cdot \tan\left(\theta_c - \frac{\pi}{2}\right)\right)$ *and* $\Delta\tilde{P} = \tilde{P} + Bo \cdot \tilde{H}_a$ *verifies:*

$$Bo\left[\tilde{H}_a-\tilde{l}\right]-\frac{\theta_c+\alpha_e-\pi}{\tilde{e}_1}\sin\theta_c-\cos\alpha_e<\Delta\tilde{P}$$
$$<Bo\left[\tilde{H}_a-\left(\tilde{l}+\tilde{h}\right)\right]-\frac{\theta_c+\alpha_e-\pi}{\tilde{e}_2}\sin\alpha_e+\frac{1}{1-\tilde{e}_2}\cos\theta_c \tag{4.65}$$

then there exist $\tilde{r}_c\in\left(1-\tilde{e}_2,1-\tilde{e}_1\right)$, $\tilde{l}'\in\left[\tilde{l}+\tilde{h}-\tilde{e}_2\tan\left(\theta_c-\frac{\pi}{2}\right),\ \tilde{l}+\tilde{h}-\tilde{e}_1\tan\left(\frac{\pi}{2}-\alpha_e\right)\right]$ *and a convex solution* $\tilde{z}(\tilde{r})$ *of the IVP* (4.59)-(4.60) *which verifies* $\tilde{z}\left(\tilde{r}_c\right)=\tilde{l}'$ *and* $\tilde{z}\left(\tilde{r}_c\right)=\tan\left(\frac{\pi}{2}-\alpha_e\right)$.

Proof: The existence of $\tilde{r}_c$ and the inequality $\tilde{r}_c\geq 1-\tilde{e}_2$ follows from Theorem 4.2 and the inequality $\tilde{r}_c<1-\tilde{e}_1$ results from Theorem 4.1. The fact that $\tilde{l}'$ is in the interval $\left[\tilde{l}+\tilde{h}-\tilde{e}_2\tan\left(\theta_c-\frac{\pi}{2}\right),\ \tilde{l}+\tilde{h}-\tilde{e}_1\tan\left(\frac{\pi}{2}-\alpha_e\right)\right]$ is also a consequence of Theorems 4.1 and 4.2. ■

Remark: Replacing in (4.65) $\Delta\tilde{P}$ by $\Delta\tilde{P}=Bo\left(\tilde{H}_a-\tilde{l}\right)+i\left(\tilde{t}\right)$ gives:

$$-\frac{\theta_c+\alpha_e-\pi}{\tilde{e}_1}\sin\theta_c-\cos\alpha_e<i\left(\tilde{t}\right)<-Bo\cdot\tilde{h}-\frac{\theta_c+\alpha_e-\pi}{\tilde{e}_2}\sin\alpha_e+\frac{1}{1-\tilde{e}_2}\cos\theta_c.$$

Theorem 4.4 *If for* $\tilde{l}_0>0,\ \tilde{h}>0$ *and* $P_0=-Bo\cdot\tilde{l}_0+i\left(\tilde{t}\right)$ *the function* $\tilde{z}_{\tilde{l}_0}(\tilde{r})$ *is a solution of the NLBVP* (4.48)-(4.49) *then for every* $\tilde{l}$ *the function* $\tilde{z}_{\tilde{l}}(\tilde{r})=\tilde{z}_{\tilde{l}_0}(\tilde{r})+\tilde{l}-\tilde{l}_0$ *is a solution of the NLBVP* (4.48)-(4.49) *for* $\tilde{P}_l=-Bo\cdot\tilde{l}+i(\tilde{t})$.

Proof: By hypothesis we have:

$$\begin{cases}\dfrac{d^2\tilde{z}_{\tilde{l}_0}}{d\tilde{r}^2}=-\left[Bo\cdot\tilde{z}_{\tilde{l}_0}+\tilde{P}_0\right]\left[1+\left(\dfrac{d\tilde{z}_{\tilde{l}_0}}{d\tilde{r}}\right)^2\right]^{3/2}-\dfrac{1}{\tilde{r}}\left[1+\left(\dfrac{d\tilde{z}_{\tilde{l}_0}}{d\tilde{r}}\right)^2\right]\dfrac{d\tilde{z}_{\tilde{l}_0}}{d\tilde{r}}\\ \dfrac{d\tilde{z}_{\tilde{l}_0}}{d\tilde{r}}\left(\tilde{r}_c\right)=\tan\left(\dfrac{\pi}{2}-\alpha_e\right);\ \tilde{z}_{\tilde{l}_0}\left(\tilde{r}_c\right)=\tilde{l}_0\\ \dfrac{d\tilde{z}_{\tilde{l}_0}}{d\tilde{r}}(1)=\tan\left(\theta_c-\dfrac{\pi}{2}\right);\ \tilde{z}_{\tilde{l}_0}(1)=\tilde{l}_0+\tilde{h}.\end{cases}$$

It is easy to verify that the function $\tilde{z}_{\tilde{l}}(\tilde{r})=\tilde{z}_{\tilde{l}_0}(\tilde{r})+\tilde{l}-\tilde{l}_0$ satisfies

$$\begin{cases} \dfrac{d^2\tilde{z}_{\tilde{l}}}{d\tilde{r}^2} = -\left[Bo\cdot\tilde{z}_{\tilde{l}} + \tilde{P}_0 \right]\left[1+\left(\dfrac{d\tilde{z}_{\tilde{l}}}{d\tilde{r}} \right)^2 \right]^{3/2} - \dfrac{1}{\tilde{r}}\left[1+\left(\dfrac{d\tilde{z}_{\tilde{l}}}{d\tilde{r}} \right)^2 \right]\dfrac{d\tilde{z}_{\tilde{l}}}{d\tilde{r}} \\ \dfrac{d\tilde{z}_{\tilde{l}}}{d\tilde{r}}\left(\tilde{r}_c \right) = \tan\left(\dfrac{\pi}{2} - \alpha_e \right);\ \tilde{z}_{\tilde{l}}\left(\tilde{r}_c \right) = \tilde{l} \\ \dfrac{d\tilde{z}_{\tilde{l}}}{d\tilde{r}}(1) = \tan\left(\theta_c - \dfrac{\pi}{2} \right);\ \tilde{z}_{\tilde{l}}(1) = \tilde{l} + \tilde{h}. \end{cases}$$

Hence $\tilde{z}_{\tilde{l}}$ is a solution of the NLBVP (4.48)-(4.49) for $\tilde{P}_l = -Bo\cdot\tilde{l} + i(\tilde{t})$. ■

Remark: Similar studies were reported by Balint and co-workers in the case of cylindrical tubes ([Balint 2008-3]), ribbons ([Balint 2008-4]) and rods grown by Edge-defined Film-fed Growth (EFG) technique ([Balint 2010], [Balint 2010-1]).

On the basis of Theorems 4.1-4.3 the following statement holds ([Balint 2011-2]):

Statement 4.1. For $0 < \tilde{e}_1 < \tilde{e}_2 < 1$, $\tilde{h} \in \left[\tilde{e}_2 \tan\left(\dfrac{\pi}{2} - \alpha_e \right), \tilde{e}_2 \tan\left(\theta_c - \dfrac{\pi}{2} \right) \right]$ and $i(\tilde{t})$ satisfying :

$$-\frac{\theta_c + \alpha_e - \pi}{\tilde{e}_1}\sin\theta_c - \cos\alpha_e < i(\tilde{t}) < -\frac{\theta_c + \alpha_e - \pi}{\tilde{e}_2}\sin\alpha_e + \frac{1}{1-e_2}\cos\theta_c - Bo\cdot\tilde{h} \qquad (4.66)$$

there exists $\tilde{r}_c \in \left[1-\tilde{e}_2, 1-\tilde{e}_1 \right]$, $\tilde{l}'(\tilde{t}) \in \left[\tilde{l}(\tilde{t}) + \tilde{h} - \tilde{e}_2 \tan\left(\theta_c - \dfrac{\pi}{2} \right), \tilde{l}(\tilde{t}) + \tilde{h} - \tilde{e}_1 \tan\left(\dfrac{\pi}{2} - \alpha_e \right) \right]$ and a convex solution $\tilde{z}(\tilde{r})$ (i.e., $\dfrac{d^2\tilde{z}}{d\tilde{r}^2} > 0$) of the initial value problem:

$$\begin{cases} \dfrac{d^2\tilde{z}}{d\tilde{r}^2} = -\left(Bo\cdot\tilde{z} + \tilde{P} \right)\cdot\left[1+\left(\dfrac{d\tilde{z}}{d\tilde{r}} \right)^2 \right]^{\frac{3}{2}} - \dfrac{1}{\tilde{r}}\left[1+\left(\dfrac{d\tilde{z}}{d\tilde{r}} \right)^2 \right]\dfrac{d\tilde{z}}{d\tilde{r}} \\ \tilde{z}(1) = \tilde{l}'(\tilde{t}) + \tilde{h};\ \dfrac{d\tilde{z}}{d\tilde{r}}(1) = \tan\left(\theta_c - \dfrac{\pi}{2} \right) \end{cases} \qquad (4.67)$$

which verifies $\tilde{z}(\tilde{r}_c) = \tilde{l}'(\tilde{t});\ \dfrac{d\tilde{z}}{d\tilde{r}}(\tilde{r}_c) = \tan\left(\dfrac{\pi}{2} - \alpha_e \right)$.

Comment: The above statement gives an answer to the main problem. It states that if the value of the unknown part $i(\tilde{t})$ of the forcing term $\Delta\tilde{P}$ is in the range defined by (4.66) then an appropriate meniscus with convex free surface appears.

The upper limitation of the crystal radius $\tilde{r}_c$ given by the constant $1-\tilde{e}_1$ shows that the gap $\tilde{e}=1-\tilde{r}_c$ during the growth process must be larger than $\tilde{e}_1$. The lower limitation of the crystal radius $\tilde{r}_c$ given by the constant $1-\tilde{e}_2$ shows that the gap $\tilde{e}=1-\tilde{r}_c$ must be smaller than $\tilde{e}_2$. By choosing $\tilde{e}_2$ such that the following inequality

$$\frac{\tilde{e}_2}{\sqrt{1-\tilde{e}_2}} < \pi\sqrt{\frac{\sin^3\theta_c}{Bo}} \tag{4.68}$$

holds, the static stability [Braescu 2010-1] of the menisci for which the gap thickness is less than $\tilde{e}_2$ is assured.

On the basis of Statement 4.1, the function ψ (which depends on the crystal radius $\tilde{r}_c$ and on the value of *i*, $\psi=\psi\left(\tilde{r}_c,i\right)$) can be built ([Balint 2010-2]). Its construction is based on the numerical integration of the system (4.50) ([Balint 2011-2]). More precisely, the following steps have to be followed:

(i) A value of $\tilde{e}_2$ in the range $(0,1)$ has to be chosen such that the inequality (4.68) is satisfied, and the value $\tilde{h}_0$ in the range $\left[\tilde{e}_2\tan\left(\frac{\pi}{2}-\alpha_e\right),\tilde{e}_2\tan\left(\theta_c-\frac{\pi}{2}\right)\right]$ has to be considered (for example $\tilde{h}_0=\tilde{e}_2\tan\left(\theta_c-\frac{\pi}{2}\right)$).

(ii) A value $0<\tilde{e}_1<\tilde{e}_2$ has to be chosen such that the inequality

$$E_1=-\frac{\theta_c+\alpha_e-\pi}{\tilde{e}_1}\sin\theta_c-\cos\alpha_e<-\frac{\theta_c+\alpha_e-\pi}{\tilde{e}_2}\sin\alpha_e+\frac{1}{1-\tilde{e}_2}\cos\theta_c-Bo\cdot\tilde{h}_0=E_2 \tag{4.69}$$

holds.

(iii) For the input *i* a set of *m* values $i_1=E_1<i_2<...<i_m=E_2$ is chosen.

(iv) In a given range $\left[\underline{\psi},\overline{\psi}\right]$ having the property $\underline{\psi}<\frac{\pi}{2}-\alpha_e<\overline{\psi}<\frac{\pi}{2}$, a set of *n* values is chosen: $\underline{\psi}=\psi^1<\psi^2<...<\psi^n=\overline{\psi}$.

(v) For an arbitrary $\tilde{l}_0$ (let say $\tilde{l}_0$ = the seed length or $\tilde{H}_a/2$) and $\tilde{P}_0 = -Bo\cdot\tilde{l}_0 + i_p$ the solution of the system (4.50) which satisfies $\tilde{z}(1) = \tilde{l}_0 + \tilde{h}_0$; $\psi(\tilde{r}_c) = \frac{\pi}{2} - \alpha_e$ is determined numerically, obtaining the functions $\tilde{z} = \tilde{z}(\tilde{r}; i_p)$ and $\psi = \psi(\tilde{r}; i_p)$, $p = \overline{1,m}$.

(vi) The values $\tilde{r}_{p,q}$ defined by $\psi(\tilde{r}_{pq}; i_p) = \psi^q$, $p = \overline{1,m}$, $q = \overline{1,n}$ are found. Fitting the data $\tilde{r}_{p,q}$, i_p and ψ^q the function $\psi(\tilde{r}_c, i)$ is found.

Remark 1: The function $\psi(\tilde{r}_c, i)$ obtained for an arbitrary $\tilde{l}_0$ coincides with that obtained applying the same steps for any $\tilde{l} \neq \tilde{l}_0$, $\tilde{l} \in (0, \tilde{H}_a)$ (see Theorem 4.4).

Remark 2: In the case of zero gravity, for an open ampoule ($La = 0$), if the Marangoni convection is neglected, then according to (4.46) and (4.47) we have $\Delta\tilde{P} = -La_h^m = i(\tilde{t}) = const.$, and hence $\tilde{P} = -La_h^m$. Solving $(4.50)_2$ in this case the function $\psi(\tilde{r}_c) = -\arctan\left(\frac{\tilde{r}_c\cos\theta_c}{\sqrt{1-\tilde{r}_c^2\cos^2\theta_c}}\right)$ is obtained.

Case II: $\theta_c + \alpha_e < 180°$

Similarly to the previous case, in the case of $\theta_c + \alpha_e < 180°$ the following statement can be given:

Statement 4.2. For $0 < \tilde{e}_1 < \tilde{e}_2 < 1$, $\tilde{h} \in \left[\tilde{e}_2\tan\left(\theta_c - \frac{\pi}{2}\right), \tilde{e}_2\tan\left(\frac{\pi}{2} - \alpha_e\right)\right]$ and $i(\tilde{t})$ satisfying:

$$Bo\left[-\tilde{h} + \tilde{e}_2\tan\left(\frac{\pi}{2} - \alpha_e\right)\right] - \frac{\theta_c + \alpha_e - \pi}{\tilde{e}_2}\sin\theta_c + \cos\theta_c < i(\tilde{t}) < -Bo\cdot\tilde{h} - \frac{\theta_c + \alpha_e - \pi}{\tilde{e}_1}\sin\alpha_e - \frac{1}{1-\tilde{e}_1}\cos\alpha_e \tag{4.70}$$

there exists $\tilde{r}_c \in [1-\tilde{e}_2, 1-\tilde{e}_1]$, $\tilde{l}'(\tilde{t}) \in \left[\tilde{l}(\tilde{t}) + \tilde{h} - \tilde{e}_2\tan\left(\frac{\pi}{2} - \alpha_e\right), \tilde{l}(\tilde{t}) + \tilde{h} - \tilde{e}_1\tan\left(\theta_c - \frac{\pi}{2}\right)\right]$ and a concave solution $\tilde{z}(\tilde{r})$ (i.e., $\frac{d^2\tilde{z}}{d\tilde{r}^2} < 0$) of the initial value problem:

$$\begin{cases} \dfrac{d^2\tilde{z}}{d\tilde{r}^2} = -\left(Bo\cdot\tilde{z}+\tilde{P}\right)\cdot\left[1+\left(\dfrac{d\tilde{z}}{d\tilde{r}}\right)^2\right]^{\frac{3}{2}} - \dfrac{1}{\tilde{r}}\left[1+\left(\dfrac{d\tilde{z}}{d\tilde{r}}\right)^2\right]\dfrac{d\tilde{z}}{d\tilde{r}} \\ \tilde{z}(1) = \tilde{l}'(\tilde{t})+\tilde{h};\ \dfrac{d\tilde{z}}{d\tilde{r}}(1) = \tan\left(\theta_c - \dfrac{\pi}{2}\right) \end{cases}$$

which verifies $\tilde{z}(\tilde{r}_c) = \tilde{l}'(\tilde{t});\ \dfrac{d\tilde{z}}{d\tilde{r}}(\tilde{r}_c) = \tan\left(\dfrac{\pi}{2} - \alpha_e\right)$.

Comment: Statement 4.2 ensures the fact that if the value of the unknown part $i(\tilde{t})$ of the forcing term $\Delta\tilde{P}$ is in the range defined by (4.70) then an appropriate meniscus with concave free surface appears.

The upper limitation of the crystal radius $\tilde{r}_c$ given by the constant $1-\tilde{e}_1$ shows that the gap $\tilde{e} = 1-\tilde{r}_c$ during the growth process must be larger than $\tilde{e}_1$. The lower limitation of the crystal radius $\tilde{r}_c$ given by the constant $1-\tilde{e}_2$ shows that the gap $\tilde{e} = 1-\tilde{r}_c$ must be smaller than $\tilde{e}_2$. By choosing $\tilde{e}_2$ such that the following inequality

$$\frac{\tilde{e}_2}{\sqrt{1-\tilde{e}_2}} < \pi\sqrt{\frac{\sin^3\alpha_e}{Bo}} \tag{4.71}$$

holds, the static stability [Braescu 2010-1] of the menisci for which the gap thickness is less than $\tilde{e}_2$ is assured.

On the basis of Statement 4.2, the function ψ (which depends on the crystal radius $\tilde{r}_c$ and on the value of *i*, $\psi = \psi(\tilde{r}_c, i)$) can be built, as it was already explained in the case $\theta_c + \alpha_e > 180°$.

It should be mentioned that in this case also, the function $\psi(\tilde{r}_c, i)$ obtained for an arbitrary $\tilde{l}_0$ coincides with that obtained applying the same steps for any $\tilde{l} \neq \tilde{l}_0$, $\tilde{l} \in (0, \tilde{H}_a)$.

4.2.4. Practical stability of the nonlinear system of differential equations describing the melt-solid interface displacement and gap thickness evolution

The system of differential equations governing the solidification process is:

$$\begin{cases} \dfrac{d\tilde{l}}{d\tilde{t}} = -St\left[\tilde{G}_l\left(\tilde{l},\tilde{t}\right) - \tilde{\lambda}\tilde{G}_s\left(\tilde{l},\tilde{t}\right)\right] \\ \dfrac{d\tilde{r}_c}{d\tilde{t}} = St\left[\tilde{G}_l\left(\tilde{l},\tilde{t}\right) - \tilde{\lambda}\tilde{G}_s\left(\tilde{l},\tilde{t}\right)\right]\tan\left[\psi\left(\tilde{r}_c,i\right) - \left(\dfrac{\pi}{2} - \alpha_e\right)\right] \end{cases} \tag{4.72}$$

Eq. $(4.72)_2$ is built up on geometrical considerations rather than modeling the physics of the changes due to the presence of the crystal [Tatartchenko 1993].

The information which presents interest for crystal growth is the practical stability of the system (4.72) on the bounded time period $\left[0,\tilde{t}_*\right]$ (period of growth) with respect to: the set of initial conditions $X_A^0 = \left(0,\tilde{l}_*\left(0\right)\right)\times\left(1-\tilde{e}_2,1-\tilde{e}_1\right)$, the set of inputs I and the set of final values $X_A^{\tilde{t}_*} = \left(0,\tilde{H}_a\right)\times\left(1-\tilde{e}_2,1-\tilde{e}_1\right)$ (that are not the same for both cases). This stability is presented in what follows.

From the growth angle criterion we get:

$$\psi\left(\tilde{r}_c^0,i\right) = \frac{\pi}{2} - \alpha_e$$

Expanding in Taylor series $\psi\left(\tilde{r}_c,i\right)$ at the point $\left(\tilde{r}_c^0,i\right)$ where the growth angle is achieved, and retaining only the first two terms:

$$\psi\left(\tilde{r}_c,i\right) = \psi\left(\tilde{r}_c^0,i\right) + \left(\frac{\partial\psi}{\partial\tilde{r}_c}\left(\tilde{r}_c^0,i\right)\right)\left(\tilde{r}_c - \tilde{r}_c^0\right) + \ldots$$

the argument of the tangent function from $(4.72)_2$ becomes:

$$\tan\left[\frac{\pi}{2} - \alpha_e + \left(\frac{\partial\psi}{\partial\tilde{r}_c}\left(\tilde{r}_c^0,i\right)\right)\left(\tilde{r}_c - \tilde{r}_c^0\right) - \left(\frac{\pi}{2} - \alpha_e\right)\right] = \tan\left[\left(\frac{\partial\psi}{\partial\tilde{r}_c}\left(\tilde{r}_c^0,i\right)\right)\left(\tilde{r}_c - \tilde{r}_c^0\right)\right]$$

It can be observed that in the second equation of the system (4.72) there is a function F depending on $\tilde{l}$, $\tilde{t}$, $\tilde{r}_c$ and i, whose Taylor series expansion at the point $\tilde{r}_c^0$ is:

$$F\left(\tilde{l},\tilde{t},\tilde{r}_c,i\right) = F\left(\tilde{l},\tilde{t},\tilde{r}_c^0,i\right) + \left(\frac{\partial F}{\partial\tilde{r}_c}\left(\tilde{l},\tilde{t},\tilde{r}_c^0,i\right)\right)\left(\tilde{r}_c - \tilde{r}_c^0\right) + \ldots$$

where

$$F\left(\tilde{l},\tilde{t},\tilde{r}_c^0,i\right) = St\left[\tilde{G}_l\left(\tilde{l},\tilde{t}\right) - \tilde{\lambda}\tilde{G}_s\left(\tilde{l},\tilde{t}\right)\right]\tan\left[\left(\frac{\partial\psi}{\partial\tilde{r}_c}\left(\tilde{r}_c^0,i\right)\right)\left(\tilde{r}_c^0 - \tilde{r}_c^0\right)\right] = 0$$

$$\frac{\partial F}{\partial \tilde{r}_c}\left(\tilde{l},\tilde{t},\tilde{r}_c^0,i\right)=St\left[\tilde{G}_l\left(\tilde{l},\tilde{t}\right)-\tilde{\lambda}\tilde{G}_s\left(\tilde{l},\tilde{t}\right)\right]\left(\frac{\partial}{\partial \tilde{r}_c}\tan\left[\left(\frac{\partial \psi}{\partial \tilde{r}_c}\left(\tilde{r}_c^0,i\right)\right)\left(\tilde{r}_c-\tilde{r}_c^0\right)\right]\right)\Bigg|_{\tilde{r}_c=\tilde{r}_c^0}$$

$$=St\left[\tilde{G}_l\left(\tilde{l},\tilde{t}\right)-\tilde{\lambda}\tilde{G}_s\left(\tilde{l},\tilde{t}\right)\right]\frac{1}{\cos^2\left[\left(\frac{\partial \psi}{\partial \tilde{r}_c}\left(\tilde{r}_c^0,i\right)\right)\left(\tilde{r}_c^0-\tilde{r}_c^0\right)\right]}\left(\frac{\partial \psi}{\partial \tilde{r}_c}\left(\tilde{r}_c^0,i\right)\right)\left(\tilde{r}_c-\tilde{r}_c^0\right)$$

$$=St\left[\tilde{G}_l\left(\tilde{l},\tilde{t}\right)-\tilde{\lambda}\tilde{G}_s\left(\tilde{l},\tilde{t}\right)\right]\left(\frac{\partial \psi}{\partial \tilde{r}_c}\left(\tilde{r}_c^0,i\right)\right)\left(\tilde{r}_c-\tilde{r}_c^0\right)$$

Therefore, the second equation of the system, can be written as

$$\frac{dr_c}{dt}=St\left[\tilde{G}_l\left(\tilde{l},\tilde{t}\right)-\tilde{\lambda}\tilde{G}_s\left(\tilde{l},\tilde{t}\right)\right]\left(\frac{\partial \psi}{\partial \tilde{r}_c}\left(\tilde{r}_c^0,i\right)\right)\left(\tilde{r}_c-\tilde{r}_c^0\right)$$

$$\frac{dr_c}{dt}=\underbrace{St\left[\tilde{G}_l\left(\tilde{l},\tilde{t}\right)-\tilde{\lambda}\tilde{G}_s\left(\tilde{l},\tilde{t}\right)\right]}_{E_1<0}\underbrace{\left(\frac{\partial \psi}{\partial \tilde{r}_c}\left(\tilde{r}_c,i\right)\right)}_{E_2}\underbrace{\left(\tilde{r}_c-\tilde{r}_c^0\right)}_{E_3}$$

For a *convex meniscus,* $\frac{\partial^2 \tilde{z}}{\partial \tilde{r}_c^2}>0$ i.e. $\frac{1}{\cos^2\psi}\frac{\partial \psi}{\partial \tilde{r}_c}>0\Rightarrow\frac{\partial \psi}{\partial \tilde{r}_c}>0$ and

i) If $\tilde{r}_c<\tilde{r}_c^0\Rightarrow\frac{d\tilde{r}_c}{d\tilde{t}}>0$ i.e. $r_c\nearrow r_c^0$;

ii) If $r_c>r_c^0\Rightarrow\frac{dr_c}{dt}<0$ i.e. $r_c\searrow r_c^0$.

It results that the crystal radius $\tilde{r}_c$ converges to $\tilde{r}_c^0$ and rests in the interval $\left[1-\tilde{e}_2,1-\tilde{e}_1\right]$(Figure 4.2.4 (a)). Thus the system (4.72) is practically stable.

For a *concave meniscus,* $\frac{\partial^2 z}{\partial r_c^2}<0$ i.e. $\frac{1}{\cos^2\psi}\frac{\partial \psi}{\partial r_c}<0\Rightarrow\frac{\partial \psi}{\partial r_c}<0$ and

i) If $\tilde{r}_c<\tilde{r}_c^0\Rightarrow\frac{d\tilde{r}_c}{d\tilde{t}}<0$;

ii) If $\tilde{r}_c>\tilde{r}_c^0\Rightarrow\frac{d\tilde{r}_c}{d\tilde{t}}>0$

It results that the crystal radius $\tilde{r}_c$ diverges and cross over the interval $\left[1-\tilde{e}_2,1-\tilde{e}_1\right]$ (Figure 4.2.4 (b)). Thus the system (4.72) is practically unstable.

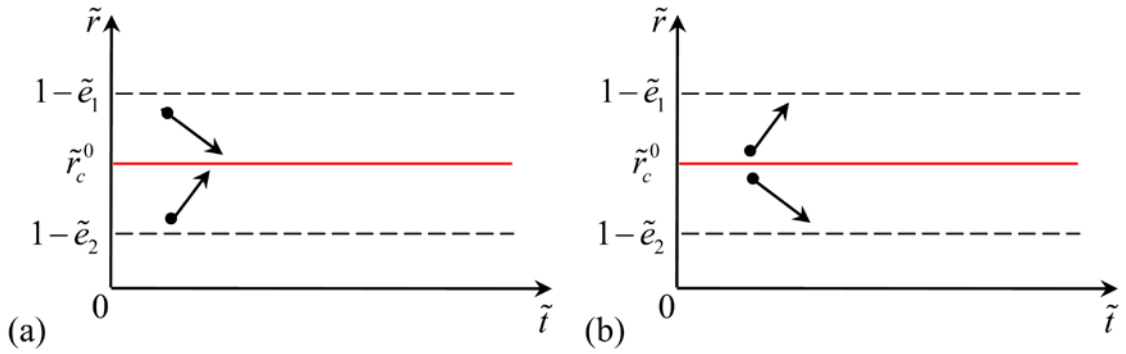

Figure 4.2.4 Convergence of the crystal radius: (a) case of a convex meniscus and (b) case of a concave meniscus.

Case I: $\theta_c + \alpha_e > 180°$

In this case, for the set of initial conditions $X_A^0 = \left(0, \tilde{l}_*(0)\right) \times \left(1-\tilde{e}_2, 1-\tilde{e}_1\right)$, the set of the inputs is:

$$I = \left\{ i(\tilde{t}) \middle| -Bo \cdot \tilde{h} - \frac{\theta_c + \alpha_e - \pi}{\tilde{e}} \sin\alpha_e + \frac{1}{1-\tilde{e}} \cos\theta_c \le i(\tilde{t}) \le -\frac{\theta_c + \alpha_e - \pi}{\tilde{e}} \sin\theta_c - \cos\alpha_e \right\}$$ and the

set of final values $X_A^{t_*} = \left(0, \tilde{H}_a\right) \times \left(1-\tilde{e}_2, 1-\tilde{e}_1\right)$.

According to the considerations presented in section 4.2.2, $\tilde{l}(\tilde{t}) \in \left(0, \tilde{H}_a\right)$ for any $\tilde{l}_0 \in \left(0, \tilde{l}_*(0)\right)$.

In order to show that $\tilde{r}_c(\tilde{t}) \in \left[1-\tilde{e}_2, 1-\tilde{e}_1\right]$ it can be remarked that, according to statement 4.1 (section 4.2.3) $i(\tilde{t}) \in I$ assures the existence of a convex meniscus. This implies $\frac{\partial \psi}{\partial \tilde{r}_c}(\tilde{r}_c, i) > 0$ which proves that $\tilde{r}_c(\tilde{t}) \in \left[1-\tilde{e}_2, 1-\tilde{e}_1\right]$. Therefore, the system (4.72) is practically stable with respect to X_A^0, $X_A^{t_*}$, I defined above.

Remark: If $\left(-La_h^m - La_{hyd}\right)$ is negligible with respect to La then $\Delta\tilde{P} = La$ and $La = Bo\left[\tilde{H}_a - \tilde{l}\right] + i(\tilde{t})$. Therefore the pressure difference La has to satisfy:

$$\begin{aligned} Bo\left[\tilde{H}_a - \tilde{l}\right] - \frac{\theta_c + \alpha_e - \pi}{\tilde{e}_1} \sin\theta_c - \cos\alpha_e < La \\ < Bo\left[\tilde{H}_a - \left(\tilde{l} + \tilde{h}\right)\right] - \frac{\theta_c + \alpha_e - \pi}{\tilde{e}_2} \sin\alpha_e + \frac{1}{1-\tilde{e}_2} \cos\theta_c. \end{aligned} \tag{4.73}$$

This means that if during the growth, the pressure difference between the cold and hot sides of the sample is maintained between the limits given by the above inequalities then the dewetted Bridgman process is successfull.

Case II: $\theta_c + \alpha_e < 180°$

In this case, for the set of initial conditions $X_A^0 = \left(0, \tilde{l}_*(0)\right) \times \left(1-\tilde{e}_2, 1-\tilde{e}_1\right)$, the set of the inputs is:

$$I = \left\{ i(\tilde{t}) \middle| -Bo \cdot \tilde{h} - \frac{\theta_c + \alpha_e - \pi}{\tilde{e}} \sin\alpha_e - \frac{1}{1-\tilde{e}} \cos\alpha_e \le i(\tilde{t}) \right.$$
$$\left. \le Bo\left[-\tilde{h} + \tilde{e} \tan\left(\frac{\pi}{2} - \alpha_e \right) \right] - \frac{\theta_c + \alpha_e - \pi}{\tilde{e}} \sin\theta_c + \cos\theta_c \right\}$$

and the set of final values $X_A^{t_*} = \left(0, \tilde{H}_a\right) \times \left(1-\tilde{e}_2, 1-\tilde{e}_1\right)$.

According to the considerations presented in section 4.2.2, $\tilde{l}(\tilde{t}) \in \left(0, \tilde{H}_a\right)$ for any $\tilde{l}_0 \in \left(0, \tilde{l}_*(0)\right)$.

In order to show that $\tilde{r}_c(\tilde{t}) \in \left[1-\tilde{e}_2, 1-\tilde{e}_1\right]$ it can be remarked that, according to statement 4.2 (section 4.2.3) $i(\tilde{t}) \in I$ assures the existence of a concave meniscus. This implies $\frac{\partial \psi}{\partial \tilde{r}_c}(\tilde{r}_c, i) < 0$ which proves that $\tilde{r}_c(\tilde{t}) \notin \left[1-\tilde{e}_2, 1-\tilde{e}_1\right]$. Therefore, the system (4.72) is practically unstable with respect to X_A^0, $X_A^{t_*}$, I defined above.

Remark: If $\left(-La_h^m - La_{hyd}\right)$ is negligible with respect to La then $\Delta\tilde{P} = La$ and $La = Bo\left[\tilde{H}_a - \tilde{l}\right] + i(\tilde{t})$. Therefore the pressure difference La has to satisfy:

$$Bo\left[\tilde{H}_a - \left(\tilde{l} + \tilde{h}\right) + \tilde{e}_2 \tan\left(\frac{\pi}{2} - \alpha_e \right) \right] - \frac{\theta_c + \alpha_e - \pi}{\tilde{e}_2} \sin\theta_c + \cos\theta_c < La$$
$$< Bo\left[\tilde{H}_a - \left(\tilde{l} + \tilde{h}\right) \right] - \frac{\theta_c + \alpha_e - \pi}{\tilde{e}_1} \sin\alpha_e - \frac{1}{1-\tilde{e}_1} \cos\alpha_e. \quad (4.74)$$

This means that during the growth, the pressure difference La has to be maintained between the limits given by the above inequalities.

4.2.5. Numerical illustration of the practical stability and practical instability

In order to illustrate numerically the practical stability of the system (4.72) describing the crystal radius and the melt-solid interface evolution, first the function $\psi(\tilde{r}_c, i)$ is determined on the basis of the steps described in section 4.2.3 (see also [Balint 2011-2]):

Case I: $\theta_c + \alpha_e > 180°$

- for *InSb*

$$\psi(\tilde{r}_c, i) = 9.155 - 15.567 \cdot \tilde{r}_c + 1.711 \cdot i + 7.632 \cdot \tilde{r}_c^2 + 9.87 \cdot 10^{-5} \cdot i^2 - 1.707 \cdot \tilde{r}_c \cdot i$$

with $\tilde{r}_c \in [1-\tilde{e}_2, 1-\tilde{e}_1] = [0.982, 0.9982]$, $i \in [E_1, E_2] = [-17.32, -3.21]$ (the pressure range which assure a convex meniscus);

- for *GaSb*

$$\psi(\tilde{r}_c, i) = 69.6 - 139.926 \cdot \tilde{r}_c + 1.525 \cdot i + 71.552 \cdot \tilde{r}_c^2 + 6.63 \cdot 10^{-9} \cdot i^2 - 1.522 \cdot \tilde{r}_c \cdot i$$

with $\tilde{r}_c \in [1-\tilde{e}_2, 1-\tilde{e}_1] = [0.982, 0.9982]$, $i \in [E_1, E_2] = [-36.97, -6.59]$.

Then, the system (4.72) is solved numerically for the following input function:

$i(\tilde{t}) = (E_1 + E_2)/2 + A \cdot \sin(\omega t)$, with $0 < A < (E_2 - E_1)/2$ and $f = \omega / 2\pi$, the input oscillations frequency.

The computed $\tilde{l}(\tilde{t})$, $i(\tilde{t})$, $\Delta\tilde{P}(\tilde{t})$, respectively $\tilde{r}_c(\tilde{t})$, for *InSb* in the case of $\tilde{l}_0 = 0.367$, $A = 4 \in (0; 7.055)$, are presented in Figure 4.2.5 for ω equal to 0.005 s^{-1}.

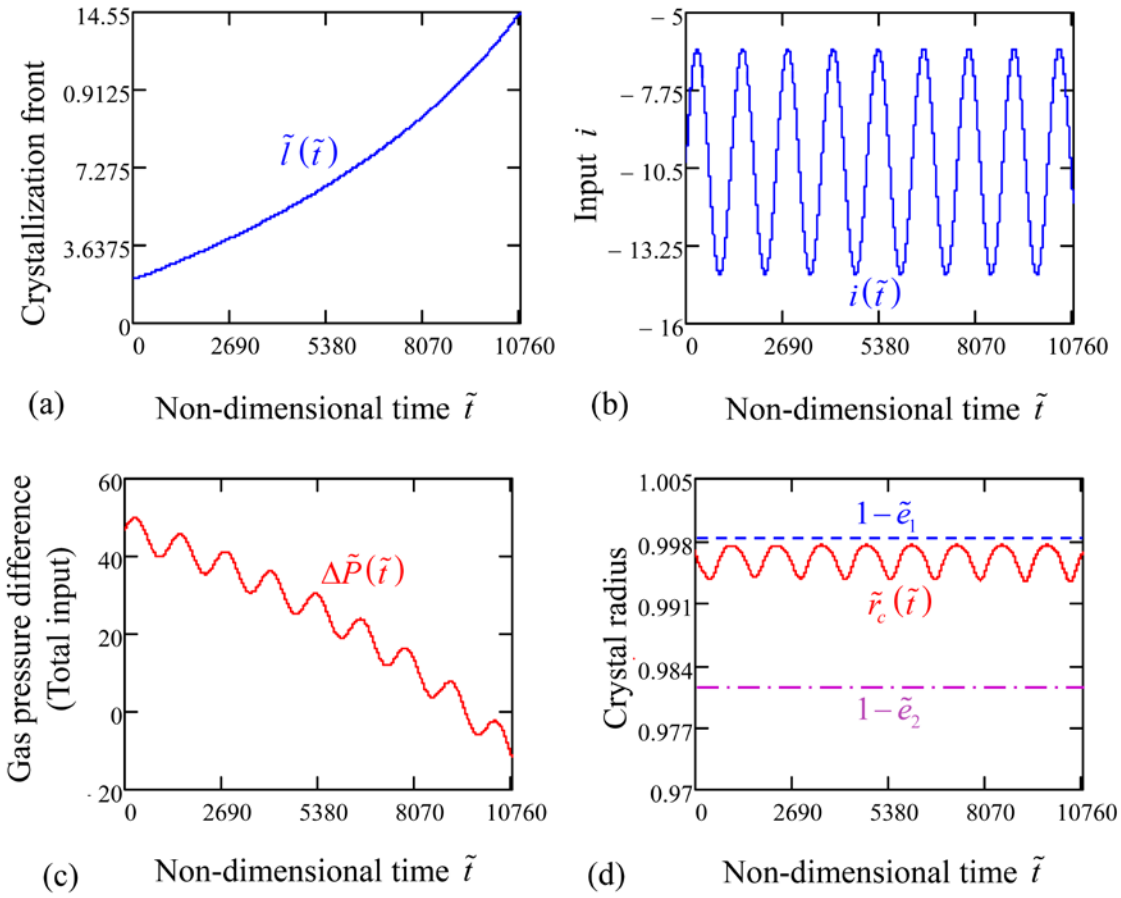

Figure 4.2.5 Computed $\tilde{l}(\tilde{t})$, $i(\tilde{t})$, $\Delta\tilde{P}(\tilde{t})$ showing the practical stability of the system for *InSb* crystals.

For *GaSb*, the computed $\tilde{l}(\tilde{t})$, $i(\tilde{t})$, $\Delta\tilde{P}(\tilde{t})$, respectively $\tilde{r}_c(\tilde{t})$, in the case of $\tilde{l}_0 = 1.458$, $A = 8 \in (0;15.19)$, are presented in Figure 4.2.6 for ω equal to 0.005 s^{-1}.

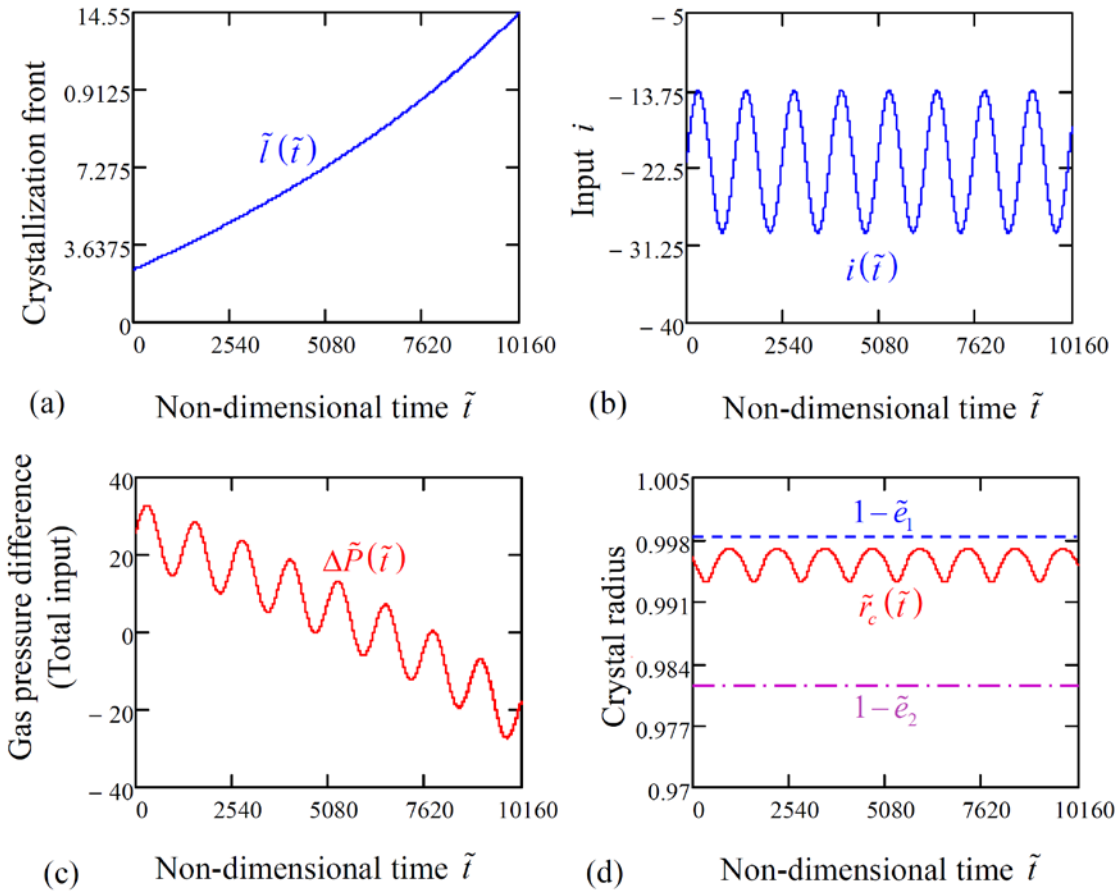

Figure 4.2.6 Computed $\tilde{l}(\tilde{t})$, $i(\tilde{t})$, $\Delta\tilde{P}(\tilde{t})$ showing the practical stability of the system for *GaSb* crystals.

Figures 4.2.5 and 4.2.6 show that for harmonic inputs $i(\tilde{t})$ of different frequencies having the amplitude in the prescribed range, the computed crystal radius fluctuates between the limits $1-\tilde{e}_2$ and $1-\tilde{e}_1$. This means that during the whole process, dewetting takes place, i.e., the gap thickness fluctuates between $\tilde{e}_1$ and $\tilde{e}_2$.

The computed $\tilde{l}(\tilde{t})$, $i(\tilde{t})$, $\Delta\tilde{P}(\tilde{t})$, respectively $\tilde{r}_c(\tilde{t})$, for *InSb* in the case of $\tilde{l}_0 = 0.367$, $A = 9 \notin (0; 7.055)$, are presented in Figure 4.2.7 for ω equal to 0.005 s^{-1}.

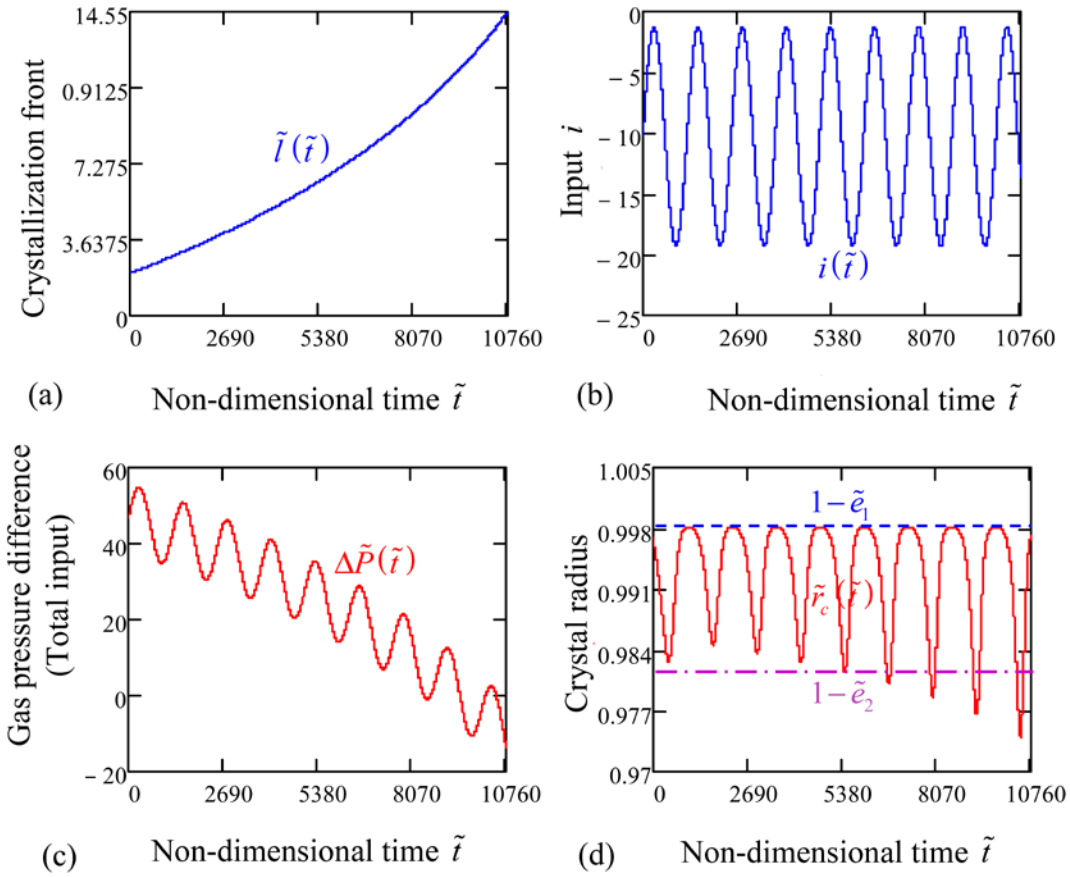

Figure 4.2.7 Computed $\tilde{l}(\tilde{t})$, $i(\tilde{t})$, $\Delta\tilde{P}(\tilde{t})$ showing the practical instability of the system for *InSb* crystals.

For *GaSb*, the computed $\tilde{l}(\tilde{t})$, $i(\tilde{t})$, $\Delta\tilde{P}(\tilde{t})$, respectively $\tilde{r}_c(\tilde{t})$, in the case of $\tilde{l}_0 = 1.458$, $A = 18 \notin (0;15.19)$, are presented in Figure 4.2.8 for ω equal to 0.005 s^{-1}.

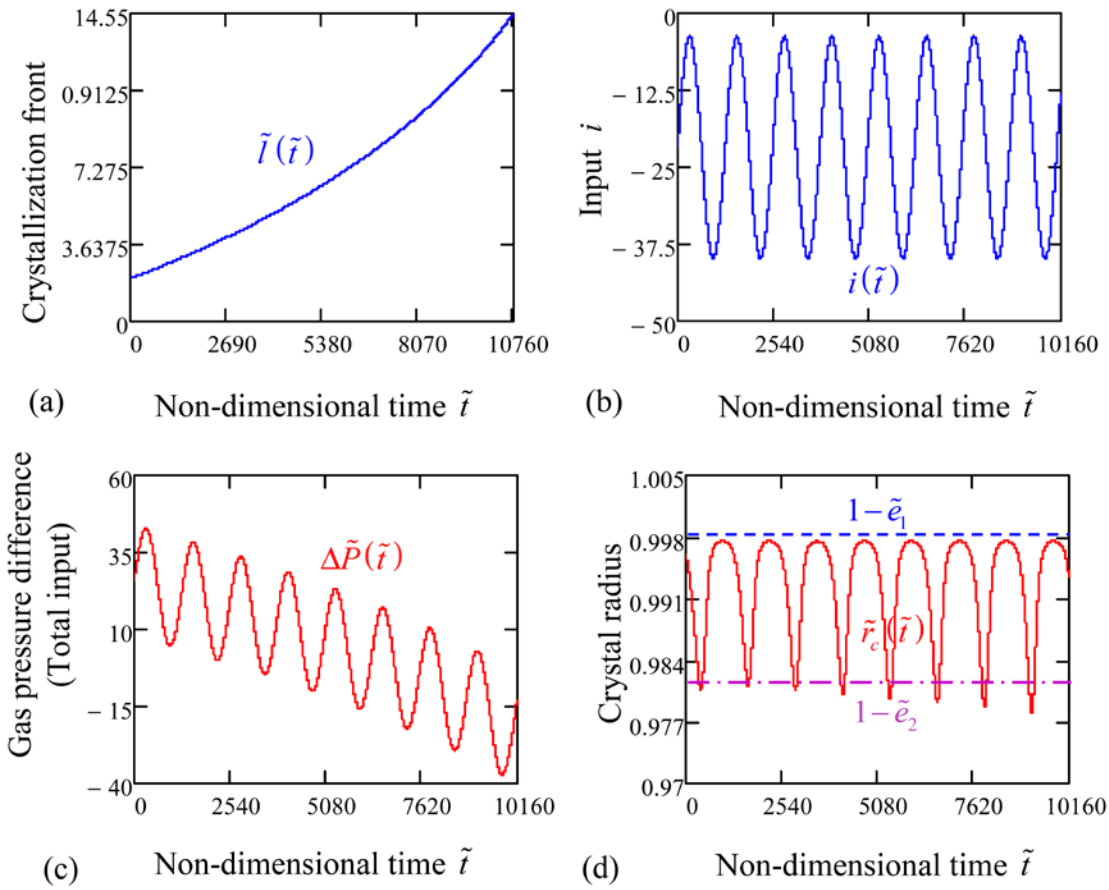

Figure 4.2.8 Computed $\tilde{l}(\tilde{t})$, $i(\tilde{t})$, $\Delta\tilde{P}(\tilde{t})$ showing the practical instability of the system for *GaSb* crystals.

Figures 4.2.7 and 4.2.8 show that for harmonic inputs with amplitudes not included in the prescribed range, the crystal radius fluctuations cross over the interval $[1-\tilde{e}_2, 1-\tilde{e}_1]$, i.e., the crystal grows with increasing fluctuations.

Case II: $\theta_c + \alpha_e < 180°$

- for *InSb*

$$\psi(\tilde{r}_c, i) = 9545.151 - 19238.492 \cdot \tilde{r}_c + 2.365 \cdot i + 9694.029 \cdot \tilde{r}_c^2 + 6.66 \cdot 10^{-6} \cdot i^2 - 2.369 \cdot \tilde{r}_c \cdot i$$

with $\tilde{r}_c \in [1-\tilde{e}_2, 1-\tilde{e}_1] = [0.9909, 0.9985]$, $i \in [E_1, E_2] = [76.16, 217.058]$ (the pressure range which assure a concave meniscus);

- for *GaSb*

$$\psi\left(\tilde{r}_c, i\right) = 657.742 - 1325.308 \cdot \tilde{r}_c + 2.302 \cdot i + 667.883 \cdot \tilde{r}_c^2 + 1.38 \cdot 10^{-6} \cdot i^2 - 2.302 \cdot \tilde{r}_c \cdot i$$

with $\tilde{r}_c \in \left[1-\tilde{e}_2, 1-\tilde{e}_1\right] = \left[0.9909, 0.9985\right]$, $i \in \left[E_1, E_2\right] = \left[45.56, 172.12\right]$.

Then, the system (4.72) was solved numerically for the following input function:

$i(\tilde{t}) = \left(E_1 + E_2\right)/2 + A \cdot \sin(\omega t)$, with $0 < A < \left(E_2 - E_1\right)/2$ and $f = \omega / 2\pi$, the input oscillations frequency.

The computed $\tilde{l}\left(\tilde{t}\right)$, $i\left(\tilde{t}\right)$, $\Delta\tilde{P}\left(\tilde{t}\right)$, respectively $\tilde{r}_c\left(\tilde{t}\right)$, for *InSb* in the case of $\tilde{l}_0 = 0.5$, $A = 30 \in \left(0; 70.449\right)$, are presented in Figure 4.2.9 for ω equal to 0.005 s^{-1}.

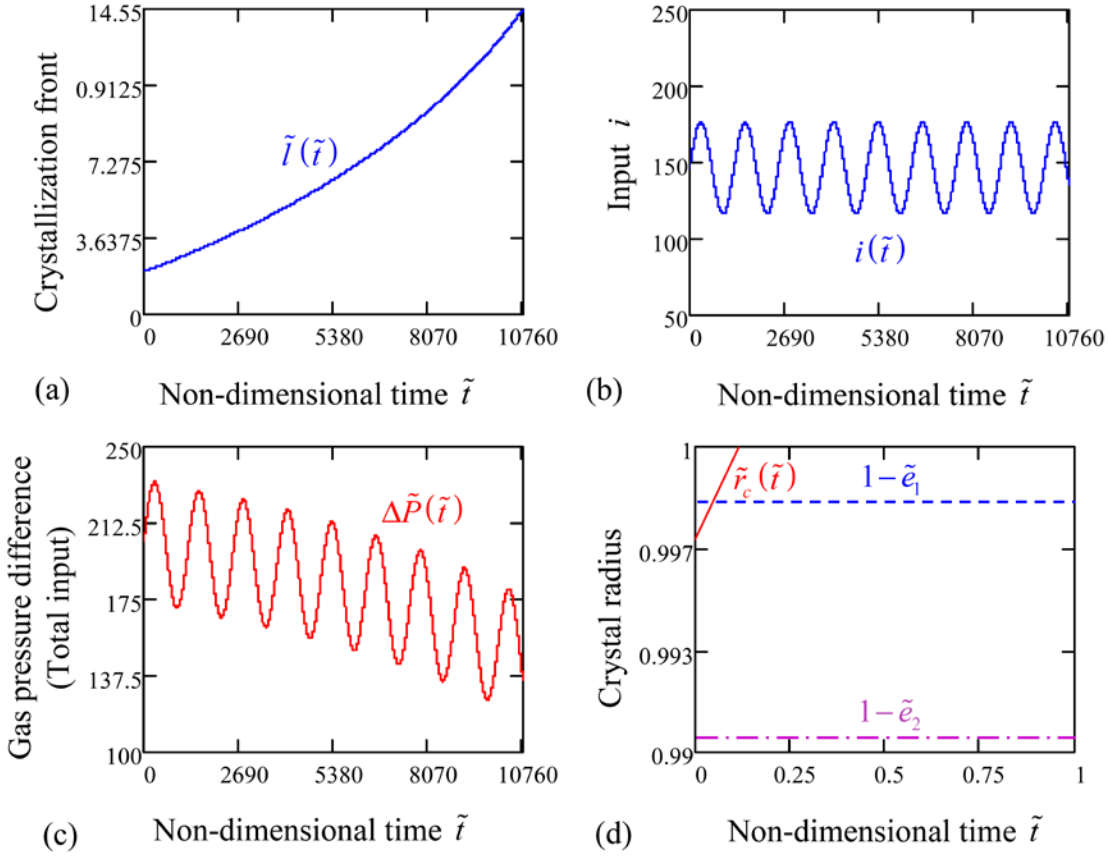

Figure 4.2.9 Computed $\tilde{l}\left(\tilde{t}\right)$, $i\left(\tilde{t}\right)$, $\Delta\tilde{P}\left(\tilde{t}\right)$ showing the practical instability of the system for *InSb* crystals, case $\theta_c + \alpha_e < 180°$.

For *GaSb*, the computed $\tilde{l}(\tilde{t})$, $i(\tilde{t})$, $\Delta\tilde{P}(\tilde{t})$, respectively $\tilde{r}_c(\tilde{t})$, in the case of $\tilde{l}_0 = 0.5$, $A = 20 \in (0; 63.28)$, are presented in Figure 4.2.9 for ω equal to 0.005 s^{-1}.

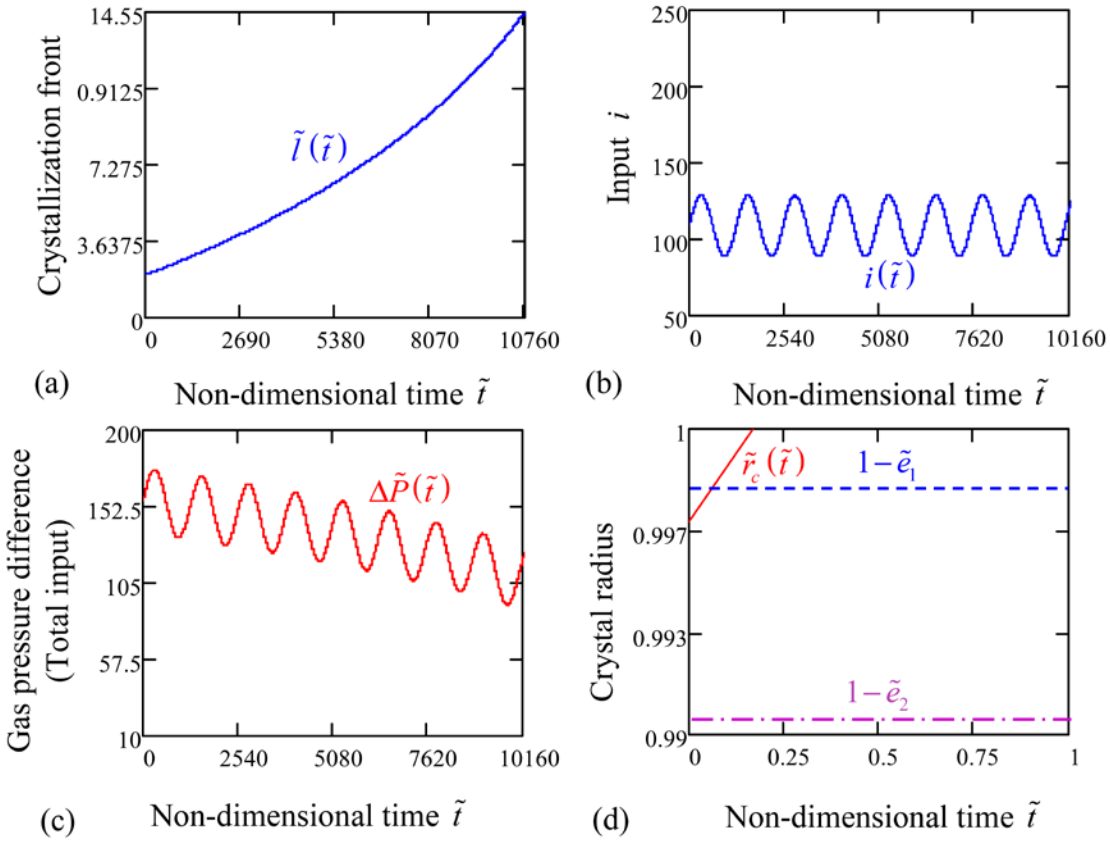

Figure 4.2.10 Computed $\tilde{l}(\tilde{t})$, $i(\tilde{t})$, $\Delta\tilde{P}(\tilde{t})$ showing the practical instability of the system for *GaSb* crystals, case $\theta_c + \alpha_e < 180°$.

Figures 4.2.9 and 4.2.10 show that the crystal radius fluctuations cross over the interval $[1-\tilde{e}_2, 1-\tilde{e}_1]$, i.e., the crystal grows attached to the ampoule wall.

Summary

In the first part of this chapter, different concepts of Lyapunov stability which can occur in shaped crystal growth: classical, uniform, asymptotic, and exponential Lyapunov stabilities of a steady-state; partial Lyapunov stability of a steady-state; and the same types of Lyapunov

stabilities for time-dependent regimes were presented. Applying these concepts for the dewetted Bridgman growth process permitted to conclude as in [Balint 2011-1] the followings:

(i) From mathematical point of view the capillary stability of a steady-state regime means partial Lyapunov stability of the regime with respect to the crystal radius, $\tilde{r}_c$.

(ii) Lyapunov stability of a steady-state regime implies partial stability with respect to all variables, in particular, implies capillary stability. The inverse of the above statement is not valid.

(iii) In the model which describes the dewetted Bridgman crystal growth in zero gravity conditions, the growth regime is time dependent. It is exponentially stable what is more than Lyapunov or capillary stability. This shows and explains, in agreement with the experiments, that the dewetting is always stable in zero gravity.

Further, in order to study the stability of the dewetted Bridgman process on the Earth, the concept of practical stability over a bounded time period was introduced. Analytical and numerical investigations of the practical stability over a bounded time period of the nonlinear system of differential equations describing the melt-solid interface displacement and the gap thickness evolution for dewetted Bridgman crystals grown in terrestrial conditions were developed. Explicit formulas were established for the limits of the range of the pressure difference in order to have practical stability of the system and the gap thickness in a prescribed range. According to these studies, in the case $\theta_c + \alpha_e > 180°$*, for a convex meniscus the system is practically stable and in the case* $\theta_c + \alpha_e < 180°$*, for a concave meniscus, the system is not practically stable. The practical stability of the convexo-concave meniscus was not studied here, as limitations of the gas pressure difference were not established analytically.*

GENERAL CONCLUSIONS AND PERSPECTIVES

The aim of this thesis was to bring information concerning the dewetted Bridgman technique by detailed theoretical results and numerical simulations, on the basis of mathematical models able to better reflect the real phenomena appearing during the growth. The dewetted Bridgman technique represents an exciting recent development for the growth of bulk single-crystals from the melt because it reduces the crystal defects due to the absence of crucible wall-crystal interaction.

The experiments performed under microgravity conditions have shown that the dewetting phenomenon is intrinsically stable with the formation of a constant crystal-crucible gap ($\approx 10\,\text{to}\,100\,\mu\text{m}$) along several centimetres.

The experimental observations under normal gravity conditions confirmed also the existence of a liquid meniscus linking the crucible-melt-gas and crystal-melt-gas triple points and its control by manipulating the gas pressure in the crucible. It generally leads to the apparition of a constant gap thickness between the grown crystal and the inner crucible walls. The experiments showed that an important characteristic of dewetting in normal gravity is the self-stabilizing gas pressure difference.

From the existent stability analysis presented in the bibliographic study it was concluded that the main parameter for stability is certainly a high wetting angle and the growth angle must be different from 0°. In practice two different cases, $\theta_c + \alpha_e < 180°$ and $\theta_c + \alpha_e \geq 180°$, should be considered, as they lead to different behavior.

According to this bibliographic survey, the present thesis work mainly consists in analytical and numerical studies of the dewetted Bridgman process including capillarity, heat transfer and stability problems.

- Capillarity problems

The capillarity problem is governed by Young-Laplace's equation that relates the pressure inside and outside the liquid to the normal curvature of the liquid surface, called meniscus. Firstly, the mathematical formulation of the capillarity problem was presented and the Young-Laplace

equation was expressed using the principal normal curvatures of a surface instead of using the radius of curvature (frequently used in crystal growth).

Analytical and numerical studies of the axi-symmetric Young-Laplace equation describing the meniscus shape were performed and the dependence of the meniscus shape and size, on the pressure difference between the cold and hot sides of the sample, was established in zero and normal gravity conditions. In the case of normal gravity conditions, qualitative studies for the meniscus shape were performed using Taylor polynomial approximation and also, without approximation using the properties obtained from Young-Laplace equation and the growth angle criterion. Explicit formulas for prescribing a pressure difference range and the corresponding meniscus shapes for which dewetting can be obtained were established analytically. These formulas can be used for a rough initial design of the growth process.

Further, in order to establish the dependence of the crystal-crucible gap thickness on the relevant parameters of the dewetted Bridgman process, a parametric study was performed for the two different cases: $\theta_c + \alpha_e < 180°$ and $\theta_c + \alpha_e \geq 180°$. It has been shown that optimal parameters exist that enhance dewetting and can be easily obtained from the physical properties of the material and characteristics of the process.

These results give a good understanding of the physics of the dewetting process and are basic reference tools for the practical crystal growers working with a given equipment and given materials and also for the equipment designers.

On the mathematical point of view, it was a good opportunity to show how some concepts from differential geometry of surfaces or the Taylor series can be applied for describing some phenomena occurring in crystal growth.

- Heat transfer problems

A simplified configuration of the dewetted Bridgman process with adiabatic lateral crucible walls was treated for modeling the heat transfer in the process. Analytical expressions of the temperature distribution and the temperature gradients in the melt and in the solid were established by solving analytically the non-stationary one-dimensional heat transfer equation by neglecting the latent heat release (quasi steady-state approximation). The melt-solid interface displacement differential equation was also derived from the thermal energy balance at the level

of the interface and relevant properties concerning the solution of this equation were established. The solution was found by solving numerically its ordinary differential equation. This approximation has been checked by comparison with the results obtained by solving numerically with COMSOL Multiphysics 3.5 the heat transfer problem that takes into account an averaged value of the latent heat released all along the process.

By using the Fourier series in order to find the analytical expressions of the thermal gradients in the solid and liquid, it was proven once again the importance and the utility of the mathematical tools for describing some phenomena during the crystal growth process.

Further, the effect of the crystal-crucible gap on the deflection of the solid-liquid interface has been studied for a set of non-dimensional parameters representative of classical semiconductor crystal growth. An analytical expression for the interface deflection, based on simple heat fluxes arguments was found. It shows that the solid-liquid interface deflection can be adjusted by the thickness of the gap: the deflection of the interface decreases when the crystal-crucible gap increases. Another interesting result is that, for a large enough gap, the curvature of the interface may be reversed. Therefore, the Bridgman crystal grower has now a new degree of freedom for the improvement of crystal quality. By adjusting the gap thickness in the dewetted mode, it is possible to modify the interface deflection. In order to get more precise values of interface deflection it is anyhow necessary to use numerical simulation and to take into account more realistic parameters, including the furnace design.

- Stability of the coupled capillarity and heat transfer problems

Different concepts of Lyapunov stability which can occur in shaped crystal growth were presented and applied for the dewetted Bridgman growth process. It was concluded that from the mathematical point of view the capillary stability of a steady-state regime means partial Lyapunov stability of the regime with respect to the crystal radius. In the model which describes the dewetted Bridgman crystal growth in zero gravity conditions, the growth regime is time dependent and is exponentially stable what is more than the Lyapunov or capillary stability. This shows and explains, in agreement with the experiments, that the dewetting is always stable in zero gravity.

For studying the dynamic stability of the dewetted Bridgman process in normal gravity conditions, the concept of practical stability over a bounded time period was introduced.

Analytical and numerical investigations of the practical stability over a bounded time period of the nonlinear system of differential equations describing the melt-solid interface displacement and the gap thickness evolution were developed. Explicit formulas were established for the limits of the fluctuations range of the pressure difference in order to obtain the gap thickness in a prescribed range leading to the practical stability of the system. According to these studies, the system is practically stable for a convex meniscus ($\theta_c + \alpha_e \geq 180°$).

Concerning the crystal-crucible gap thickness under microgravity conditions, it has been already demonstrated that its stability is a pure geometrical problem and is ascertained as far as the meniscus exists. This is independent of the time representation of the process, infinite or finite. However the problem is much more complicated under normal gravity conditions, where the meniscus shape, then the gap thickness, does depend on the solid-liquid interface position hence on the heat transfer. In this case the practical stability approach should absolutely be used in order to study the stability of the process.

It should be noticed that there is still one obscure point, the practical stability of a convexo-concave meniscus (so-called "S-shape meniscus"). For such meniscus shape, the mathematical tools developed in the present work did not lead to a limitation of the gas pressure difference needed for the analytical study of the practical stability. Only some numerical studies for the case of *InSb* and *GaSb* crystals were performed, without leading to a general conclusion concerning the practical stability of the system in the case of a convexo-concave meniscus.

These results show that the "practical stability" approach has a clear interest for the study of bounded time processes. For the industrial production, the stable conditions of the process (i.e. $\theta_c + \alpha_e \geq 180°$) should be chosen but it is not easy to find an ideal crucible. In this case, it is necessary to work with instable conditions (i.e. $\theta_c + \alpha_e < 180°$) and therefore to implement a control device.

For the development of a robust process control system it is important to understand the relation of the process dynamics with the different operating conditions and the important process characteristics such as gradients, process physics, system design, and materials characteristics and also the characteristic time for relaxation of the perturbations.

An overview of important process modeling and control issues, as well as mathematical modeling for analysis and controller design are provided in [Winkler 2010]. Winkler and co-

authors present many of the critical concepts and practices needed to design and implement modern control for the Czochralski process and these can be useful for dewetted Bridgman process.

On the practical point of view, the thermal field control in crystal growth is so well developed that in any case, stable or not, the thermal field, hence the solid-liquid interface position versus time, is under control. In order to implement a control process for dewetted Bridgman crystal growth in the case of a concave meniscus ($\theta_c + \alpha_e < 180°$) which was proven that it is practically unstable, a good understanding of the physics (capilarity and heat transfer) that describes the phenomena occuring in the growth process is necessary. The crystal-crucible gap thickness should be measured in order to control the gas pressure difference in the sample. It is also important to study the reaction of the system to an input change during the growth and to measure the characteristic relaxation time.

The results obtained in this thesis work, will be useful for the implementation of the automatic control of the dewetted Bridgman processes because informations about the reaction of the system to different fluctuations of the temperature gradients and of the gas pressure difference were provided. It will constitute premises for the elaboration of new production technologies and control processes for the improvement of the quality of the crystals. After such developments we can hope that the dewetted Bridgman process, now studied only in two or three laboratories in the world, would be used at the industrial scale.

Concluding, the objectives were mainly accomplished and robust tools (analytical and numerical) for studying the dewetted Bridgman process were developed. The obtained results show the importance of a careful calculation of the meniscus shapes for the optimization of the dewetted Bridgman process. In general terms, the understanding gained from the successful modeling will lead to better process operation and design, ultimately yielding better quality crystals at higher production rates and lower costs.

Acknowledgements

This work has been supported in part by the European Space Agency (Map-CdTe program), the French-Romanian PHC Brancusi program and the Romanian National University Research Council (Grant PN II- Idei).

REFERENCES

[Adornato 1987] Adornato P. M. and Brown R. A., "*Convection and segregation in directional solidification of dilute and non-dilute binary alloys: Effects of ampoule and furnace design*" J. Crystal Growth 80 (1987) 155-190.

[Ayasoufi 2009] Ayasoufi A., Rahmani R. K., Keith T. G.,"*Stefan Number-InsensitiveNumerical Simulation of the Enthalpy Method for Stefan Problems Using the Space-Time CE/SE Method*", Numerical Heat Transfer, Part B: Fundamentals 55 (2009) 257-272.

[Balikci 2004] Balikci E., Deal A., Abbaschian R., "*Detached crystal growth from melt by the axial heat processing technique*", J. Crystal Growth 271 (2004) 37-45.

[Balint 2008-1] Balint S., Braescu L., Kaslik E., Chapter 3 In: "*Regions of attraction and applications to control theory*", Cambridge Scientific Publishers (2008) 9-52.

[Balint 2008-2] Balint S., Braescu L., Sylla L., Epure S. and Duffar T, "*Dependence of the meniscus shape on the pressure difference in the dewetted Bridgman process*" J. Crystal Growth 310 (2008) 1564-1570.

[Balint 2008-3] Balint St., Balint A. M., Tanasie L., "*The effect of the pressure on the static meniscus shape in the case of tube growth by edge-defined film-fed growth (E.F.G.) method*", J. Crystal Growth 310 (2008) 382-390.

[Balint 2008-4] Balint St., Balint A. M., "*The effect of the pressure difference across the free surface on the static meniscus shape in the case of ribbon growth by edge-defined film-fed growth (E.F.G.) method*", J. Crystal Growth 311 (2008) 32-37.

[Balint 2010] Balint A.M., Balint S., "*Dynamics and control of the shape and size of a sitting drop-like meniscus, occurring in single-crystal growth*", Journal of Franklin Institute 347 (2010) 30-52.

[Balint 2010-1] Balint St., Balint A. M., "*Inequalities for single crystal rod growth by edge-defined film-fed growth (E.F.G.) technique*", J. of Mathematical Analysis and Applications 362 (2010) 231-240.

[Balint 2010-2] Balint St., Tanasie L., "*A procedure for the determination of the angles* $\tilde{\alpha}_e(r_e, h; p_e)$ *and* $\tilde{\alpha}_i(r_i, h; p_i)$ *which appears in the nonlinear system of differential equations describing the dynamics of the outer and inner radius of a tube, grown by the edge-defined film-fed growth (EFG) technique*", Nonlinear Analysis: Real World Applications (2010) *in press*.

[Balint 2011-1] Balint S., Epure S., "*Non-Lyapunov type stability occurring in the dewetted Bridgman crystal growth under zero gravity conditions*", submitted to Microgravity-Science and Technology.

[Balint 2011-2] Balint S., Epure S., Braescu L. and Duffar T., "*Dewetted Bridgman crystal growth: practical stability over a bounded time period in a forced regime*", accepted for publication in J. of Engineering Mathematics.

[Barat 1998] Barat C., Duffar T., Garandet J. P., "*Estimation of the curvature of the solid–liquid interface during Bridgman crystal growth*"J. Crystal Growth 194 (1998) 149-155.

[Bernfeld 1980] Bernfeld Stephen R. and Lakshmikantham V., "*Practical Stability and Lyapunov Functions*", Tôhoku Math. Journ. 32 (1980) 607-613.

[Bizet 2004] Bizet L., Duffar T., "*Contribution to the stability analysis of the dewetted Bridgman growth under microgravity conditions*", Cryst. Res. Techno. 39/6 (2004) 491-500.

[Braescu 2008] Braescu L. "*Shape of menisci in terrestrial dewetted Bridgman growth*", J. Colloid and Interface Science 319 (2008) 309-315.

[Braescu 2009-1] Braescu L. "*Static stability of the menisci in the case of semiconductor crystals grown by dewetted Bridgman technique,*" in SPIE-Optics and Photonics (2009), (San Diego, California, USA, 2009), Proceedings of the Society of Photo-Optical Instrumentation Engineers 7420, 742005-1-11.

[Braescu 2009-2] Braescu L., Epure S., Duffar T., "*Advances in Computational Modeling of Crystals Grown by the Dewetted Bridgman Process*" Proceedings of the XVth International Workshop on the Physics of Semiconductor Devices (Delhi, India) (2009) 36-41.

[Braescu 2010-1] Braescu L., "*On the pressure difference ranges which assure a specified gap size for semiconductor crystals grown in terrestrial dewetted Bridgman*" J. Crystal Growth 312 (2010) 1421-1424.

[Braescu 2010-2] Braescu L., Epure S., Duffar T., "*Mathematical and numerical analysis of capillarity problems and processes*" in Crystal growth processes based on capillarity: Czochralski, floating zone, shaping and crucible techniques, edited by Th. Duffar, John Wiley & Sons Ltd ISBN 978-0-470-71244-3 (2010) 465-524.

[Chang 1983] Chang C. J., Brown R. A., "*Radial segregation induced by natural convection and melt/solid interface shape in vertical Bridgman growth*" J. Crystal Growth 63 (1983) 343-364.

[Chang 1974] Chang C. E., Wilcox W. R., "*Control of interface shape in the vertical bridgman-stockbarger technique*" J. Crystal Growth, 21 (1974) 135-140.

[Chetaev 1961] Chetaev N.G., "*Stability of Motion*", Pergamon Press, Oxford, 1961, (cited in [Balint 2011-2]).

[Chevalier 2004] Chevalier N., Dusserre P., Garandet J-P., Duffar T., "*Dewetting application to CdTe single crystal growth on earth*" J. Crystal Growth 261 (2004) 590-594.

[Clanet 2002] Clanet C., Quere D., "*Onset of menisci*" J. Fluid Mechanics 460 (2002) 131-149.

[Coddington 1955] Coddington S. A., Levinson N., "*Theory of Ordinary Differential Equations*", McGraw-Hill, New York (1955) 91-97 and 314-344.

[Crochet 1989] Crochet M .J., Dupret F., Ryckmans Y., Geyling F. T., Monberg E. M., "*Numerical simulation of crystal growth in a vertical Bridgman furnace*" J. Crystal Growth 97 (1989) 173-185.

[Dobre 2007] Dobre T. G. and Sanchez Marcano J. G., "*Chemical Engineering. Modelling, Simulation and Similitude*", Wiley-VCH, Weinheim, ISBN: 978-3-527-30607-7 (2007) 465-475.

[Duffar 1990] Duffar T., Harter I., Dusserre P., "*Crucible de-wetting during bridgman growth of semiconductors in microgravity*" J. Crystal Growth 100 (1990) 171-184.

[Duffar 1995] Duffar T., Dusserre P., Abadie J., "*Crucible-semiconductor interactions during crystal growth from the melt in space*", Advances in Space Research 16 (1995) 199-203.

[Duffar 1996] Duffar T., Abadie J., "*Wetting of InSb melts on crucibles in weightlessness – Results of the TEXUS 32/TEM 01-4 Experiment*", Int. J. Microgravity Science and Technology IX/1 (1996) 35-39.

[Duffar 1997] Duffar T., Boiton P., Dusserre P., Abadie J., "*Crucible de-wetting during Bridgman growth in microgravity, II. Smooth crucibles*" J. Crystal Growth, 179 (1997) 397-409.

[Duffar 1998] Duffar T., Serrano M.D., Moore C.D., Camassel J., Contreras S., Dusserre P., Rivoallant A., Tanner B.K., "*Bridgman solidification of GaSb in space*", J. Crystal Growth 192 (1998) 63-72.

[Duffar 2000] Duffar T., Dusserre P., Picca F., Lacroix S., Giacometti N., "*Bridgman growth without crucible contact using the dewetting phenomenon*", J. Crystal Growth 211 (2000) 434-440.

[Duffar 2001-1] Duffar T., Dusserre P., Giacometti N., "*Growth of GaSb single crystals by an improved dewetting process*", J. Crystal Growth 223 (2001) 69-72.

[Duffar 2001-2] Duffar T., Dusserre P., Giacometti N., Benz K.W., Fiederle M., Launay J.C., Dieguez E., Roosen G., "*Dewetted growth and characterization of high-resisitivity CdTe*", Acta Astronautica 48 2-3 (2001) 157-161.

[Duffar 2001-3] Duffar T., Dusserre P., Giacometti N., "*Crystal growth apparatus and method*" PCT Int. Appl. (2001) 17 pp WO 0168956.

[Duffar 2004] Duffar T. "*Bulk Crystal Growth under microgravity conditions*" Chapter 17 in "Bulk crystal growth of Electronic, Optical and Optoelectronic Materials", P. Capper Editor, John Wiley and sons, ISBN 0-470-85142-2 (2004) 477-524.

[Duffar 2010] Duffar T., Sylla L., "*Vertical Bridgman and dewetting*", in Crystal growth processes based on capillarity: Czochralski, floating zone, shaping and crucible techniques, edited by Th. Duffar, John Wiley & Sons Ltd ISBN 978-0-470-71244-3 (2010) 355-408.

[Duhanian 1997] Duhanian N., Martin C., Abadie J., Chaudet M., Dieguez E., Duffar T., "*Chemical segregation and crystal crucible interaction during the growth of $Ga_{0.8}In_{0.2}Sb$ in space*", Microgravity Science and Technology X/4 (1997) 187-193.

[Epure 2008] Epure Simona, Duffar Thierry, Braescu Liliana, "*Comparison between analytical and numeric determination of the interface curvature during dewetted Bridgman crystal growth*" J. Crystal Growth 310 (2008) 1559-1563.

[Epure 2010-1] Epure S., "*Analytical and numerical studies of the meniscus equation in the case of crystals grown in zero gravity conditions by the dewetted Bridgman technique*", International Journal of Mathematical Models and Methods in Applied Sciences 4 (2010) 50-57.

[Epure 2010-2] Epure Simona, Duffar Thierry, Braescu Liliana "*Parametric study for dewetted Bridgman method: crystal-crucible gap dependence on the Bond and Laplace numbers and on contact angle*" J. Materials Science 45 (2010) 2239-2245.

[Epure 2010-3] Epure Simona, Duffar Thierry, Braescu Liliana, "*On the capillary stability of the crystal-crucible gap during dewetted Bridgman process*" J. Crystal Growth 312 (2010) 1416 - 1420.

[Eustathopoulos 2010] Eustathopoulos N., Drevet B., Brandon S., Virozub A. "*Basic Principles of Capillarity in Relation with Crystal Growth*" in Crystal growth processes based on capillarity: Czochralski, floating zone, shaping and crucible techniques, edited by Th. Duffar, John Wiley & Sons Ltd ISBN 978-0-470-71244-3 (2010) 1-50.

[Fergola 1970] Fergola P. and Moauro V., "*On partial stability*", Ricerche Mat., 19 (1970) 185-207 (cited in [Balint 2011-1]).

[Fiederle 2004-1] Fiederle M., Duffar T., Babentsov V., Benz K.W., Dusserre P., Corregidor V., Dieguez E., Delaye P., Roosen G., Chevrier V., Launay J.C., "*Dewetted growth of CdTe in microgravity (STS-95)*" Crystal Research and Technology 39-6 (2004) 481-490.

[Fiederle 2004-2] Fiederle M., Duffar T., Garandet J.P., Babentsov V., Fauler A., Benz K.W., Dusserre P., Corregidor V., Dieguez E., Delaye P., Roosen G., Chevrier V., Launay J.C.,

"*Dewetted growth and characterization of high-resistivity CdTe*", J. Crystal Growth 267 (2004) 429-435.

[Finn 1986] Finn R., "*Equilibrium capillary surfaces*", Springer-Verlag New York Inc. ISBN 0-387-96174-7 (1986) 1-16.

[Frolov 2005] Frolov A. M., "*Optimal shape of slowly rising gas bubbles*", Can. J. Phys. 83 (2005) 761-766.

[Fu 1981] Fu Ta-Wei and Wilcox W. R., "*Rate change transients in Bridgman-Stockbarger growth*", J. Crystal Growth 51 (2001) 557-567.

[Grujic 1973] Grujic Lj. T., "*On Practical Stability*", Internat. J. Control 17 (1973) 881-887 (cited in [Balint 2011-2]).

[Gruyitch 2004] Gruyitch L., Richard J. P., Borne P., Gentina J. C.. "*Stability Domains (Nonlinear Systems in Aviation, Aerospace, Aeronautics and Astronautics)*". Chapman & Hall/CRC, London (2004) 1-19.

[Halanay 1966] Halanay A., "*Differential Equations*", Academic Press, New York (1966) 19-128.

[Harter 1993] Harter I., Dusserre P., Duffar T., Nabot J.Ph., Eustathopoulos N., "*Wetting of III-V melts on crucible materials*", J. Crystal Growth 131 (1993) 157-164.

[Hauksbee 1709] Hauksbee F., "*Physico-mechanical experiments on various subjects*", London (1709) 139-169.

[Huh 1969] Huh C., Scriven L. E., "*Shapes of axisymmetric fluid interfaces of unboanded extent*" J. Colloid and Interface Science 30 (1969) 323-337.

[Kaiser 2001] Kaiser N., Cröll A., Szofran F.R., Cobb S.D., Benz K.W., "*Wetting angle and surface tension of germanium melts on different substrate materials*" J. Crystal Growth 231 (2001) 448-457.

[Lakshmikantham 1990] Lakshmikantham V., Leela S. and Martynyuk A. A., "*Practical Stability of Nonlinear Systems*", Singapore: World Scientific (1990).

[Laplace 1806] Laplace P.S., "*Traité de mécanique céleste* ; *suppléments au Livre X*", Œuvres Complètes Vol. 4, Gauthier-Villars, Paris (1806).

[La Salle 1961] La Salle J.P. and Lefschetz S., "*Stability by Lyapunov's Direct Method*", Academic Press, New York (1961).

[Michel 1970-1] Michel A. N. "*Stability, Transient Behaviour and Trajectory Bounds of Interconnected Systems*", Internat. J. Control 11 (1970) 703-715.

[Michel 1970-2] Michel A. N. "*Qualitative Analysis of Simple and Interconnected Systems: Stability, Boundedness and Trajectory Behaviour*", IEEE Trans. on Circuit Theory 17 (1970) 292–301.

[Ostrogorsky 2009] Ostrogorsky A. G., Marin C., Duffar T., Volz M., "*Initial transient in Zn-doped InSb grown in microgravity*", J. Crystal Growth 311 (2009) 3243-3248.

[Palosz 2005] Palosz W., Volz M. P., Cobb S., Motakef S., Szofran F. R., "*Detached growth of germanium by directional solidification*", J. Crystal Growth 277 (2005) 124-132.

[Pätzold 2005] Pätzold O., Jenkner K., Scholz S., Cröll A., "*Detached growth of 2-in germanium crystals*", J. Crystal Growth, 277 (2005) 37-43.

[Popov 1997] Popov D.I., Regel L.L., Wilcox W.R., "*Detached solidification. 2. Stability*" J. Mater.Synth. & Proc. 5 (1997) 298-312.

[Rouche 1977] Rouche N., Habets P., Laloy M., "*Stability Theory by Lyapunov's Direct Method*", Springer, New York (1977) 1-47.

[Roucke 1967] Roucke N., Peiffer K., "*Le theoreme de Lagrange-Dirichlet et la deuxieme method de Liapounoff "*, Ann Soc. Scient. Bruxelle., Ser. 1, Vol. 81, No.1 (1967).

[Rumyantsev 1957] Rumyantsev V. V., "*On stability of motion with respect to some of the variables*" (in Russian), Vestnik Moskov Gos. Univ., Ser. Mat. Mekh., Astron., Fiz., Khim, 4 (1957) (cited in [Balint 2011-1]).

[Schweizer 2002-1] Schweizer M., Cobb S.D., Volz M.P., Szoke J., Szofran F.R., "*Defect density characterization of detached-grown germanium crystals*" J. Crystal Growth 235 (2002) 161-166.

[Schweizer 2002-2] Schweizer M., Volz M.P., Cobb S.D., Vujisic L., Motakef S., Szoke J., Szofran F.R., "*Stability of detached-grown germanium single crystals*", J. Crystal Growth 237-239 (2002) 2107-2111.

[Stelian 2001] Stelian C., Duffar T., Santailler J. L., Barvinschi F., Nicoara I., Cryst. Res. Technol. 36/7 (2001) 663-673.

[Stelian 2009-1] Stelian C., Yeckel A. and Derby J. J. "*Influence of thermal phenomena on crystal reattachment during dewetted Bridgman growth*", J. Crystal Growth 311 (2009) 2572-2579.

[Stelian 2009-2] Stelian C., Volz M. P. and. Derby J. J "*On favorable thermal fields for detached Bridgman growth*", J. Crystal Growth 311 (2009) 3337-3346.

[Sylla, 2008-1] Sylla L., Duffar T., "*Effect of residual gaseous impurities on the dewetting of antimonide melts in fused silica crucibles in the case of bulk crystal growth*", Materials Science and Engineering A 495 (2008) 208–214.

[Sylla, 2008-2] Sylla L., "*Etude experimentale et thermodynamique du procédé de demouillage appliqué aux semiconducteurs*", Institut national Polytechnique de Grenoble, PhD Thesis (2008).

[Tatartchenko 1993] Tatarchenko Y. A., "*Shaped Crystal Growth*", Kluwer Academic Publishers, Dordrecht (1993) 19-167.

[Tatartchenko 2010] Tatartchenko V. A., "*Shape Stability in Capillary Crystal Growth as Possibility and Practical Realization of Shaped Crystals*" in Crystal growth processes based on

capillarity: Czochralski, floating zone, shaping and crucible techniques, edited by Th. Duffar, John Wiley & Sons Ltd ISBN 978-0-470-71244-3 (2010) 51-114.

[Vorotnikov 1998] Vorotnikov V. I., "*Partial Stability and Control*", Boston, Birkhaüser ISBN 0 8176 3917 9 (1998) 434.

[Young 1805] Young T., "*An essay on the cohesion of fluids*", Philos. Trans. Roy. Soc. London 95 (1805) 65 (internet resources).

[Landau 1971] Landau L.D., Lifchits E.M., "*Fluid Mechanics*", Pergamon Press Great Britain ISBN 0-08- 033933-6 (1987).

[Wilcox 1998] Wilcox W.R., Regel L.L., "*Detached solidification in Microgravity – A Review*" Microgravity Science and Technology XI/4 (1998) 25 pages. Also available at http://people.clarkson.edu/~lregel/detrev.pdf.

[Winkler 2010] Winkler J., Neubert M., Rudolph J., Duanmu, Gevelber M., "*Czochralski Process Dynamics and Control Design*" in Crystal growth processes based on capillarity: Czochralski, floating zone, shaping and crucible techniques, edited by Th. Duffar, John Wiley & Sons Ltd ISBN 978-0-470-71244-3 (2010) 115-202.

[Witt 1975] Witt A.F., Gatos H.C., Lichtensteiger M., Lavine M.C., Herman C.J., "*Crystal growth and steady-state segregation under zero gravity: InSb*" J. Electrochem.Soc., vol.122 (1975) 276-283.

[Witt 1978] Witt A.F., Gatos H.C., Lichtensteiger M., Lavine M.C., Herman C.J., "*Crystal growth and steady-state segregation under zero gravity: Ge*", J. Electrochem.Soc., vol.125 (1978) 1832-1840.

[Zemskov 1983] Zemskov V.S., Raukhman M.R., Barmin I.V., Senchenkov A.S., Shul'pina I.L., and Sorokin L.M., "*Special features of solidification of alloyed single crystals of indium antimonide in zero gravity conditions*", Fiz. Khim. Obrab. Mater. (in Russian) 17 (5) (1983) 56 (cited in [Duffar 2010]).

Analytical and numerical studies of the dewetted Bridgman process: capillarity, heat transfer and stability

The phenomenon of dewetting is characterized by the Vertical Bridgman growth of a crystal without contact with the walls of the crucible due to the existence of a liquid meniscus at the level of the solid-liquid interface which creates a gap between the crystal and the inner crucible walls. One of the immediate consequences of this phenomenon is the drastic improvement of the crystal quality. This improvement is essentially related to the absence of wall-crystal interaction, so that no grain or twin spurious nucleation can occur and no differential dilatation stresses exist, which could generate dislocations. In order to bring crucial information concerning dewetted phenomenon, detailed theoretical results and numerical simulations are necessary, on the basis of the mathematical models able to reflect better the real phenomenon which should include all essential processes appearing during the growth.

The main problem of the dewetting growth and the related improvements of the material quality is the stability of the growth process. In this context, the main purpose of the present work is to perform analytical and numerical studies for capillarity, heat transfer and stability problems of the dewetted Bridgman process.

Firstly, the mathematical formulation of the capillary problem governed by the Young-Laplace equation has been presented, followed by analytical and numerical studies for the meniscus equation for the cases of zero and normal terrestrial gravity. Secondly, the heat transfer problems have been treated. Thus, in order to find analytical expressions of the temperature distribution and the temperature gradients in the melt and in the solid, analytical and numerical studies for the non-stationary one-dimensional heat transfer equation have been performed. The melt-solid interface displacement equation was also derived from the thermal energy balance at the level of the interface. Further, for studying the effect of the crystal-crucible gap on the curvature of the solid-liquid interface for a set of non-dimensional parameters representative of classical semiconductor crystal growth, an analytical expression for the interface deflection, based on simple heat fluxes arguments was found. In order to check the accuracy of the obtained analytical formula and to identify its limits of validity, the heat transfer equation was solved numerically in 2D axial symmetry, stationary case, using the finite elements code COMSOL Multiphysics 3.3.

Further, the stability analysis has been developed. Different concepts of Lyapunov stability which can occur in shaped crystal growth: classical, uniform, asymptotic, and exponential Lyapunov stabilities of a steady-state; partial Lyapunov stability of a steady-state; and the same types of Lyapunov stabilities for time-dependent regimes, have been presented. In what follows, after the concept of practical stability over a bounded time period has been introduced, analytical and numerical investigations of the practical stability over a bounded time period of the nonlinear system of differential equations describing the melt-solid interface displacement and the gap thickness evolution for dewetted Bridgman crystals grown in terrestrial conditions have been performed.

Keywords: Meniscus shape (Numerical simulation), Stability, Dewetted Bridgman (Crystal growth)

Etudes analytiques et numériques du procédé de Bridgman démouillage: capillarité, transfert de chaleur et stabilité

L'objectif principal de cette thèse est de réaliser des études analytiques et numériques pour des problèmes de capillarité, de transfert de chaleur et de stabilité du procédé Bridgman démouillage. Pour le calcul de la forme du ménisque, sa surface sera donnée par l'équation de Young-Laplace décrivant l'équilibre sous la pression. Cette équation sera transformée en un système non linéaire d'équations différentielles. A partir d'études qualitatives et quantitatives de la solution, la dépendance de la forme du ménisque (convexe, concave, convexe-concave), de la différence de pression et d'autres paramètres du procédé, sera déterminée. Pour étudier la stabilité dynamique du système, l'épaisseur de l'espacement cristal-creuset et la position de l'interface liquide-solide sont des variables du problème et donc deux équations seront nécessaires, précisément, l'équation de Young-Laplace et le bilan thermique à l'interface liquide-solide.

Par conséquence, ce travail est organisé comme suit:

Des contributions récentes à la modélisation de certains problèmes de capillarité sont présentées dans le deuxième chapitre, à commencer par la formulation mathématique du problème capillaire régie par l'équation de Young-Laplace. Des études analytiques et numériques pour l'équation du ménisque sont élaborées pour le démouillage en microgravité et sur terre.

Le troisième chapitre traite des contributions à la modélisation des problèmes de transfert de chaleur. Ainsi, les études analytiques et numériques pour l'équation non stationnaire de transfert de chaleur à une dimension sont effectuées afin de trouver des expressions analytiques de la distribution de la température et des gradients de température dans le liquide et dans le solide. L'équation de déplacement de l'interface liquide-solide est également obtenue du bilan énergétique à l'interface.

Après quoi, l'effet de l'espacement cristal-creuset sur la courbure de l'interface liquide-solide est étudié pour un ensemble de paramètres représentatifs non-dimensionnels de la croissance de cristaux semi-conducteurs classiques. Une expression analytique pour la déflexion de l'interface, basée sur la théorie du flux de chaleur est rapportée. Afin de vérifier l'exactitude de la formule obtenue analytiquement et d'identifier ses limites de validité, l'équation de transfert de chaleur est résolue numériquement dans une symétrie axiale en 2D, pour un cas stationnaire et en utilisant le code d'éléments finis COMSOL Multiphysics 3.3.

Le dernier chapitre est entièrement consacré à l'analyse de la stabilité. Tout d'abord, différents concepts de stabilité de Lyapunov qui peuvent survenir dans la croissance des cristaux: classique, uniforme, asymptotique et exponentielle d'un état d'équilibre; stabilité partielle de Lyapunov d'un état d'équilibre, et les mêmes types de stabilités de Lyapunov pour la solution temporelle sont présentés. Dans ce qui suit, après l'introduction de la notion de stabilité pratique sur une période de temps limitée, des études analytiques et numériques de la stabilité pratique sur une période de temps limitée du système non linéaire, des équations différentielles décrivant le déplacement d'interface liquide-solide et

l'évolution de l'espacement cristal-creuset, pour des cristaux élaborés par le procédé Bridgman démouillage sous conditions terrestres sont développés.
Enfin, les conclusions générales et perspectives de ce travail sont exposées.

Studii analitice si numerice ale procesului dewetted Bridgmann: capilaritate, transfer de caldura si stabilitate

Scopul principal al acestei teze este studiul analitic si numeric al capilaritatii, al transferului de caldura si al stabilitatii dinamice a procesului de crestere a cristalelor cu metoda dewetted Bridgman. Pentru determinarea formei meniscului, suprafata sa $z = z(x, y)$ este descrisa de ecuatia Young-Laplace a unei suprafete capilare in echilibru. Aceasta ecuatie neliniara de ordinul doi a fost transformata intr-un sistem neliniar de ecuatii diferentiale de ordinul intai. In urma studiilor calitative si numerice ale solutiei sistemului, a fost determinata dependenta formei meniscului (global convex, global concav, convex-concav) de diferenta de presiune de gaz si de ceilalti parametrii relevanti ai procesului. Pentru studiul stabilitatii dinamice a sistemului, dimensiunea gap-ului (spatiul dintre cristal si peretii interiori ai creuzetului) si pozitia interfetei solid-lichid sunt doua variabile ale problemei, ceea ce inseamna ca sunt necesare doua ecuatii si anume, ecuatia Young-Laplace si ecuatia bilantului de energie la nivelul interfetei solid-lichid.

In acest context, teza a fost organizata astfel:

Contributii recente la modelarea problemelor de capilaritate au fost prezentate in capitolul 2, incepand cu formularea matematica a problemei capilaritatii guvernata de ecuatia Young-Laplace. Studii analitice si numerice au fost realizate atat pentru cazul gravitatiei nule cat si pentru gravitatie normala.

In al treilea capitol au fost prezntate contributii la modelarea problemelor de transfer de caldura. Asadar, studii analitice si numerice ale ecuatiei nestationare unidimensionale a caldurii au fost realizat pentru a determina expresiile analitice ale distributiei temperaturii si a gradientilor de temperatura in solid si in topitura. De asemenea, din ecuatia bilantului de energie la nivelul interfetei a fost dedusa si ecuatia care descrie deplasarea frontului de cristalizare.

Apoi a fost studiat efectul gap-ului cristal-creuzet asupra formei interfetei solid-lichid, pentru un set de parametrii adimensionali, reprezentativi in cresterea cristalelor semiconductoare. Pornind de la teoria fluxului de caldura s-a determinat expresia analitica a curburii interfetei. Pentru a verifica precizia acestei formule analitice si pentru a stabili limitele sale de validitate, s-a rezolvat numeric ecuatia caldurii in 2D axi-simetric, cazul stationar, folosind metoda elementelor finite propusa de soft-ul COMSOL Multiphysics 3.3.

Ultimul capitol este dedicat in totalitate analizei stabilitatii. Mai intai au fost prezentate diferite concepte de stabilitate in sens Lyapunov, intalnite adesea in cresterea cristalelor profilate: stabilitatea clasica, uniforma, asimptotica si exponentiala a unei solutii stationare , in sensul lui Lyapunov; stabilitatea partiala in sens Lyapunov a unei stari stationare; si aceleasi tipuri de stabilitate in regim dependent de timp. Dupa introducerea conceptului de stabilitate practica peste un interval de timp finit, s-a investigat analitic si numeric stabilitatea practica in timp finit a sistemului neliniar de ecuatii diferentiale care descrie deplasarea frontului de cristalizare si evolutia dimensiunii gap-ului pentru cristalele crescute cu metoda dewetted Bridgman in conditii terestre.

La final, au fost expuse concluziile generale si perspectivele acestor studii desfasurate pe parcursul tezei.

ABSTRACT

The phenomenon of dewetting is characterized by the Vertical Bridgman growth of a crystal without contact with the crucible wall due to the existence of a liquid meniscus at the level of the solid-liquid interface which creates a gap between the grown crystal and the inner crucible wall. One of the immediate consequences of this phenomenon is the drastic improvement of the crystal quality. In order to bring crucial information concerning dewetted phenomenon, detailed theoretical results and numerical simulations are necessary, on the basis of the mathematical models able to reflect better the real phenomenon which should include all essential processes appearing during the growth.

The main problem of the dewetting growth and the related improvements of the material quality is the stability of the growth process. In this context, the goal of the present work is to perform analytical and numerical studies for capillarity, heat transfer and stability problems of the dewetted Bridgman process.

Keywords: Meniscus shape (Numerical simulation), Stability, Dewetted Bridgman (Crystal growth).

RESUME

Le phénomène de démouillage est caractérisé par la croissance d'un cristal sans contact avec la paroi du creuset due à l'existence d'un ménisque liquide au niveau de l'interface solide-liquide. Ceci crée un espace de quelques dizaines de micromètres entre le cristal et le creuset dans lequel il est élaboré et une des conséquences immédiates de ce phénomène est la nette amélioration de la qualité du cristal.

Dans le cas du démouillage, la forme du ménisque est décrite par l'équation de Young-Laplace à partir de laquelle on a pu établir le système des équations différentielles non-linéaires qui décrivent l'évolution du rayon du cristal et de la hauteur du ménisque en fonction de diverses perturbations. L'intérêt réside dans la possibilité d'étudier numériquement, à partir de ces équations, les solutions stationnaires, leur stabilité, statique et dynamique, et d'effectuer une étude de la sensibilité des solutions vis-à-vis des paramètres du procédé et des conditions initiales.

Mots clés: Ménisque (simulation numérique), Stabilité, Bridgman démouillage (croissance cristalline).